

Electronic Thesis and Dissertation Repository

12-17-2020 2:00 PM

Hemithioindigo-based Photoswitchable Self- Complementary Hydrogen Bond Arrays


Suendues Noori, *The University of Western Ontario*

Supervisor: Wisner, James A., *The University of Western Ontario*

A thesis submitted in partial fulfillment of the requirements for the Master of Science degree in Chemistry

© Suendues Noori 2020

Follow this and additional works at: <https://ir.lib.uwo.ca/etd>

 Part of the [Materials Chemistry Commons](#), [Organic Chemistry Commons](#), and the [Physical Chemistry Commons](#)

Recommended Citation

Noori, Suendues, "Hemithioindigo-based Photoswitchable Self- Complementary Hydrogen Bond Arrays" (2020). *Electronic Thesis and Dissertation Repository*. 7572.
<https://ir.lib.uwo.ca/etd/7572>

This Dissertation/Thesis is brought to you for free and open access by Scholarship@Western. It has been accepted for inclusion in Electronic Thesis and Dissertation Repository by an authorized administrator of Scholarship@Western. For more information, please contact wlsadmin@uwo.ca.

ABSTRACT

Hydrogen bonded materials are slowly conquering grounds in the literature because of their dynamic features which stem from their reversible interactions. Incorporating the ability for light to chemically modify these interactions provides a unique template for innovative, efficient and self-healing materials. This thesis explores the design, synthesis, and characterization of nine derivatives of a well-known organic compound – hemithioindigo – with dual function; as a photoswitch and a novel self-complementary hydrogen bond array.

The supramolecular complexes formed moderate to strong associations (63 M^{-1} to 1100 M^{-1}) with spontaneous Gibbs free energy values (-10.3 kJ/mol to -17.3 kJ/mol) to infer the effect of strong electron-withdrawing and electron-donating additions on each framework. Solid state complexation (via Single-Crystal X-Ray Crystallography) further confirmed the dimer structures of each photoarray. Photochemical and photophysical properties of these dynamic arrays were explored using UV-Vis and NMR spectroscopy with photostationary state (PSS) conversions to the *E* isomers from 12% to 82%.

Keywords

Thioindigo, hemithioindigo, *Z/E* isomers, urea, photoswitch, photoisomerization, photochemistry, hydrogen bonds, ^1H NMR dilution curve, self-complementary complexes

SUMMARY FOR LAY AUDIENCE

Materials that have the potential to cycle between one or more metastable states have a promising future. When these metastable isomers absorb at different wavelengths of visible light and possess a higher or lower activity rate towards a target substrate, their productivity can be externally controlled. Molecular switches are molecules which can be controlled by a change in pH, temperature, enzymatic activity, or an electric current between its highly stable isomers. Photoswitches allow researchers to manipulate the properties of a molecule (through its structure) and thus its function by a non-invasive external handle: light.

In contrast to traditional electronics, dynamic smart materials respond directly with their environment. Monomeric units are first synthesized and are then held together by non-covalent interactions. Unlike dipole-dipole interactions, ion-dipole interactions and van der Waals forces, hydrogen bonds have been documented to form durable bonds. Hydrogen bonds are reversible, transient interactions between a hydrogen atom and an electronegative atom (fluorine, oxygen, nitrogen) with the hydrogen bond donor (HBD) forming a bond with a hydrogen bond acceptor atom (HBA).

Hydrogen bond arrays exist in two forms; complementary and self-complementary. Complementary hydrogen bond arrays contain either consecutive HBAs or HBDs whereas self-complementary arrays contain alternating HBAs and HBDs atoms to create the resulting complex.

This thesis seeks to evaluate the photoefficiency and complexation strength of a hemithioindigo self-complementary hydrogen bond array in solvents of varying polarity. The thermodynamic most stable product (*Z* isomer) is irradiated with visible light (410-660 nm) converting it to the other isomer (*E*). The specific wavelength of visible light causes a physical rearrangement in the structure capable of an overall electronic shuffling contributing to the weaker or stronger hydrogen bond interactions of the isomer with identical neighboring molecules. The photochemical and photophysical properties will be discussed along with the dimerization constant (K_d); a value that designates the strength of the hydrogen bond interactions. Overall, a library of nine urea-based hydrogen bond arrays were synthesized with the highest K_d value of 1100 M^{-1} . The stability of these hydrogen bond arrays as the *Z* isomer proved to be adequate for biomedical and materials-based applications.

DECLARATION OF CO-AUTHORSHIP

I. Co-Authorship Declaration

I hereby declare that this dissertation incorporates material that is a result of joint research. All crystal structures were solved and refined by Dr. Paul D. Boyle (X-Ray Facility Manager). Mass spectra were collected by Doug Hairsine (Former Mass Spec Facility Manager). This thesis incorporates the outcome of the research undertaken in Dr. James A. Wisner's research group. It contains joint research with Yichun Zhao, Noura Nachar and Amna Muhammad under the supervision of Dr. James A. Wisner as follows.

Chapter 2 contains research collaborated with Yichun Zhao for the synthesis of 2,3,6,7-tetrahydro-1H,5H-pyrido[3,2,1-ij]quinoline (**10**) and 2,3,6,7-tetrahydro-1H,5H-pyrido[3,2,1-ij]quinoline-9-carbaldehyde (**11**). Noura Nachar is credited for the development of a similar synthetic pathway as the one shown in Figure 2.3.1. Amna Muhammad is credited for the synthesis of (*Z*)-1-hexyl-3-(3-oxo-2-(2-oxoacenaphthylen-1(2*H*)-ylidene)-2,3-dihydrobenzo[*b*]thiophen-5-yl)urea (**2b**). Dr. James A. Wisner edited the corresponding content within this thesis.

I am aware of the University of Western Ontario Senate Policy on Authorship, and I certify that I have properly acknowledged the contribution of other researchers to my dissertation and have obtained written permission from each of the co-author(s) to include the above material(s) in this document. I certify that, with the above qualification, this dissertation, and the research to which it refers, is the product of my own work.

DEDICATION

This thesis is dedicated to my family-both immediate and past.

ACKNOWLEDGEMENTS

Being a part of a research group instills motivation, commitment and improves communication skills whilst strengthening teamwork and problem-solving skills amongst members. Joining the Wisner research group has been a rewarding experience as a graduate student as I can attest to the above statement. I am glad to have worked for two years with past and present members of the Wisner research group during the completion of this thesis.

Firstly, I would like to acknowledge my P.I., James, who saw potential in me and accepted me as a student in his lab. I am so grateful to have James as my supervisor and my mentor during my graduate degree. During the initial start of my graduate career, there were ups and downs and he was always there advising and encouraging me to overcome the rough points of the research process. I figured out quite quickly that research takes a lot of patience and perseverance. He took blocks of his time to teach me both as a student and a fellow colleague whether it was differentiating multiplets in a crude NMR spectrum, how to setup a Kugelrohr distillation or providing various conditions for optimization experiments. James, I am so appreciative for all the times that you managed to come into the lab despite your tightly scheduled and often back-to-back meeting days.

Secondly, many grad students in this Chemistry Department have provided a friendly, and supportive environment for me to come to everyday. Members of the Workentin, Gilroy, Gilles, Luyt, Blacquiere, Kerr, Pagenkopf, Ragona, Huang, Hudson, and Baines research groups have been a part of my graduate experience in various aspects within my two years. Amid the courses that we took, the trips that we had to relax and

take our minds off lab work, hours of laughter, learning, talking or bearing the TAing or proctoring hours have been an adventure and a long list of memorable moments.

Thirdly, I can't forget the undergraduate and visiting students in my lab that I mentored. Remembering my starting point last year in the lab and setting my mind to that perspective helped me to welcome and transition my mentees into the organic synthetic lab. Not only were they learning from me, but I was learning from them. Some days were hectic but at least we managed to fix everything and put everything "back to normal" for the night. They made the lab a brighter place with their energetic personality and wholesome conversations. Outside the lab, they helped me destress and wind down and I am very lucky to call them my friends. We had endless laughable and silly moments that I'll always remember.

All the support and assistance on my project has been made possible because of the outstanding research personnel and staff in the Chemistry Department as follows; Paul D. Boyle (X-Ray Facility Manager), Mathew Willans (NMR Facility Manager), Doug Hairsine (Mass Spec Facility Manager), and to Darlene McDonald, Clara Fernandes, and Anna Vandendries-Barr for their assistance in my graduate degree progression. I would like to acknowledge the staff at the ChemBioStores who helped me every time I was there. I want to thank Sandra Zakaria Holtslag for providing the training (prior to each session) for the undergrad labs.

I would not be here at Western or even in London if it wasn't for my strong backbone- my family. No matter how loud, outrageous and at times hilarious, they are also loving and understanding. Even through the hard and sometimes difficult times, they will always be my family. I was fortunate to meet many of my relatives in the Middle

East; many of whom I will never meet again. Even though I was very young when I first met them and I don't recall meeting them, they welcomed me into their homes and provided me with so much hospitality and gratitude. I hope to gain the same diligence and strength as they have had over the years.

My spiritual beliefs have been guiding me throughout my life but especially within the last two years. *Allah* has given me the strength to accomplish so much in my life. Not only have I received so many blessings, I have lost a considerable amount as well. The reason that I keep breathing and continue to do my best in life is to please

Almighty God. *إِنَّا لِلَّهِ وَإِنَّا إِلَيْهِ رَاجِعُونَ*

TABLE OF CONTENTS

Abstract	ii
Summary for Lay Audience.....	iii
Declaration of Co-Authorship.....	v
I. Co-Authorship Declaration.....	v
Dedication	vi
Acknowledgements.....	vii
Table of Contents	x
List of Tables	xiv
List of Figures	xv
List of Schemes.....	xxvii
List of Abbreviations/Symbols	xxviii
Chapter 1	
1 Introduction.....	2
1.1 Supramolecular chemistry	2
1.2 Nanocarriers, Molecular Machines and Biological Recognition.....	4
1.3 Photoresponsivity, Photoisomerization and Photochemistry.....	6
1.4 Molecular switch.....	8
1.4.1 Photoswitch.....	9
1.4.1.1 Types of Photoswitches	11
1.5 Hemithioindigo photoswitches	15
1.6 Photostationary state (PSS).....	19
1.6.1 Excessive UV-Vis Irradiation Outcomes.....	21

1.7 Nanotechnology and Smart materials	24
1.7.1 Polymers	24
1.7.2 Supramolecular Polymers	25
1.8 Non-covalent bonding interactions	29
1.9 Hydrogen Bond.....	31
1.9.1 Hydrogen Bond Distinction	34
1.9.2 Hydrogen Bond Strength	36
1.10 Known supramolecular hydrogen bond arrays	40
1.10.1 H-bond donors/acceptors within supramolecular complexes	40
1.10.2 The Effect of the Functionalization of Substituents	42
1.10.3 The Number of Hydrogen Bond Sites	45
1.10.4 The Sequence of Hydrogen Bond Arrays	47
1.10.5 Tautomerization	50
1.11 Design of Self-Complementary Hydrogen Bond Arrays.....	52
1.12 Subject and Scope of Thesis	54
1.13 References.....	56
Chapter 2	
2 Synthesis and Characterization of Photoswitchable	
Self-Complementary DD•AAA Hydrogen Bond Arrays.....	62
2.1 Introduction.....	62
2.2 Design	63
2.3 Synthesis of Self-complementary Hydrogen bond Arrays	69
2.4 ¹ H NMR Characterization of DDAA• AADD/DDAAA• AAADD	
arrays.....	72

2.5 Assessing the Dimer Stability of the Arrays by Solution Characterization	
Methods.....	79
2.5.1 ¹ H NMR dilution studies.....	83
2.6 X-ray Structural Analysis of DDAA•AADD Arrays.....	93
2.6.1 X-ray Structural Analysis of Z-1c Array	94
2.6.2 X-ray Structural Analysis of Z-2a Array	99
2.6.3 X-ray Structural Analysis of Z-3b Array	102
2.7 Conclusion	104
2.8 Experimental Methodology	105
2.8.1 Synthetic Methods	107
2.8.2 Standard Operating Procedures (SOP).....	125
2.9 References.....	126

Chapter 3

3 Photochemistry of Self-Complementary **DD•AA/ DD•AAA**

Hydrogen Bond Arrays	129
3.1 Introduction.....	129
3.2 Results and Discussion	130
3.2.1 UV-Vis Characterization of 1a-c Hydrogen Bond Arrays	130
3.2.2 Photoisomerization Studies of 1a-c Hydrogen Bond Arrays.....	132
3.3 Qualitative Analysis of 2a-d, 3a,b Hydrogen Bond Arrays	133
3.3.1 UV-Vis Characterization of 2a-d, 3a,b Hydrogen Bond Arrays.....	133
3.3.2 Photoisomerization Studies of 2a-c, 3a,b Hydrogen Bond Arrays Utilizing NMR and UV-Vis Techniques	136

3.3.3 <i>E</i> to <i>Z</i> Thermal Reversion Analysis of 2a and 2c Hydrogen Bond Arrays.....	143
3.4 Summary and Conclusions	147
3.5 Standard Operating Procedures (SOP).....	149
3.5.1 Generalities	149
3.5.2 NMR Photochemistry Experiments	149
3.5.2.1 PSS Experiments.....	149
3.5.2.2 ¹ H NMR Thermal Reversion Experiments	150
3.5.3 UV-Vis Thermal Experiments	151
3.5.4 UV-Vis Thermodynamic Reversion Experiments	151
3.6 References.....	152
 Chapter 4	
4 Conclusions/Future Work	155
4.1 Conclusions.....	154
4.2 Future Work	158
4.3 References.....	161
 A Appendices	
A.1 1D NMR Spectra (¹ H NMR Spectra).....	162
A.2 1D NMR Spectra (¹³ C NMR Spectra).....	173
A.3 2D NMR Spectra (^g COSY, HSQC, HMBC).....	183
A.4 ¹⁹ F NMR Spectra.....	207
A.5 Permission to Reproduce Material from the Literature	210
Curriculum Vitae	211

LIST OF TABLES

Chapter 1

Table 1.3 Various reactions that may take place after a photochemical event.....	6
Table 1.8 Summary of non-covalent forces and their characteristics.....	30
Table 1.9.1 Summary of H-bond properties and their characteristics.....	35
Table 1.10.2 Comparison of the electron-withdrawing ability of various derivatives on the association constant in CDCl ₃ at 298 K.....	45

Chapter 2

Table 2.5 The dimerization constants, Gibbs free energy and chemical shifts of monomer, dimer and the total change in chemical shift of all derivatives.....	93
Table 2.6.1 Crystallographic parameters for Z-1c crystals.....	96
Table 2.6.2 Hydrogen bond distances and angles of Z-1c crystals obtained from single X-ray crystal structure data.....	98
Table 2.6.3 Crystallographic parameters for Z-2a crystals.....	100
Table 2.6.4 Hydrogen bond distances and angles of Z-2a dimer obtained from single crystal X-ray structure data.....	101
Table 2.6.5 Crystallographic parameters for Z-3b crystals.....	103
Table 2.6.6 Hydrogen bond distances and angles of Z-3b dimer obtained from single X-ray crystal structure data.....	104

Chapter 3

Table 3.2.1 UV-Vis data characterization of Z-1a-c Hydrogen Bond Arrays in chloroform and DMSO at 298 K.....	131
Table 3.3 Physical and Photophysical properties of 2a-d, 3a,b Hydrogen Bond Arrays in various solvents at 298 K.....	135
Table 3.3.1 Physical and Photophysical properties of <i>Z/E</i> isomers of 2a-d, 3a,b Hydrogen Bond Arrays in various solvents at 298 K.....	142

LIST OF FIGURES

Chapter 1

- Figure 1.1** An image depicting a) a circular helicate synthesized by Lehn and co-workers pre-organized in this spatial arrangement enclosing a C1 atom in the center;²² and b) the structure of an isomorphous analogue to pyridine (hydrazone) where spontaneous pre-assembly promotes the formation of helical shapes ²³3
- Figure 1.2** A crystal structure of a rotaxane beneficial for targeted drug delivery within the human body ²⁹5
- Figure 1.4** Three crown ethers shown in consecutive sizes; 12-crown-4 binds Li ions, 15-crown-5 binds Na and K ions and 18-crown-6 binds K ions most effectively.....9
- Figure 1.4.1.1** A schematic displaying the use of photoswitchable polymers intended for targeted drug delivery within the human body ²⁶10
- Figure 1.4.1.5** Different types of photoswitches derived from hemithioindigo and stilbene ⁷⁶15
- Figure 1.5.1** The Jablonski diagram depicting transitions between S₀, S₁, S₂ and T₁ in a given photoreversible system where A= absorbance; F= fluorescence; ISC= Intersystem crossing; P = phosphorescence; T = triplet state. ⁸¹ (Image reproduced with permission; license #4842731145861).....16
- Figure 1.6.1** In a given photoreversible system A and B have distinct absorption spectra which defines their absorptivity and λ_{max}20
- Figure 1.6.3** A graph displaying the fatigue resistance of a photoswitch (black line) and a fatigue system (dotted red line) upon successive switching between its isomers. ⁸⁴23
- Figure 1.7.2.1** The relationship shown between the K_a and the rate of formation of supramolecular polymers ⁵¹26
- Figure 1.7.2.3** Three structures depicting various supramolecular complexes in order of increasing K_a : triple, quadruple, and sextuple hydrogen bonded arrays. Image modified from reference [50].....28
- Figure 1.9.2** Six different geometries and angles at which hydrogen bonds can form.....36
- Figure 1.10** Nucleotide base pairs; adenine (A), thymine (T), guanine (G), and cytosine (C), which engage in two hydrogen bond interactions (A, T) and three hydrogen bond interactions (G, C) to form the 3-D double helical DNA

structure.....	40
Figure 1.10.1 Various supramolecular complexes containing different geometries of hydrogen bond arrays studied in CDCl ₃ at 298 K by Zerbetto et al. ⁶⁸	41
Figure 1.10.2 Two triply hydrogen bonded heterodimers studied by Wilson <i>et al.</i> where they substituted various electron-donating and electron-withdrawing functional groups at X and Y in CDCl ₃ at 298 K.....	44
Figure 1.10.3 Various supramolecular complexes containing two and three donor and acceptor arrays in all possible arrangements studied by Zimmerman and Murray. ⁶ Quadruple hydrogen bond arrays studied by Wienand et al. ⁷³ All constants measured in CDCl ₃ at 298 K.....	46
Figure 1.10.4 Various supramolecular complexes containing two and three donor/acceptor arrays as displayed by Zimmerman and Murray ⁹	48
Figure 1.10.4.1 Various rearrangements involving a self-complementary hydrogen bond complex and their bonding interactions.....	50
Figure 1.10.5 The tautomers of acetone comprising the <i>keto</i> and the <i>enol</i> form.....	51
Figure 1.10.5.1 A complementary hydrogen bond complex displaying tautomerism as studied by Zimmerman and Murray in CDCl ₃ at 298 K.....	52
Figure 1.11 Self-complementary hydrogen bond network proposed by Gong <i>et al.</i> in 1999 with an ADAD• DADA sequence where the acceptors are in red and the donors are bolded ¹³	53
Figure 1.11.1 Hydrogen bonding interactions between (<i>Z</i>)/(<i>E</i>)-6,6'-diethoxy-3H,3'H-[2,2'-bibenzo[b]thiophenylidene]-3,3'-dione and donors ¹²	54
Figure 1.12 Electron-rich compounds utilized in the synthesis of the proposed photoswitches mentioned in this thesis.....	55
Chapter 2	
Figure 2.2 Self-complementary hydrogen bond network examined by Gong et al. in 1999 with an ADAD• DADA sequence. Acceptors are in red and the donors are bold in black	64
Figure 2.2.1 Complementary hydrogen bond design studied previously by Wisner and coworkers undergoing <i>E/Z</i> photoisomerization where Acceptor = A and Donor = D	65
Figure 2.2.3 The first generic self-complementary hydrogen bond array proposed	

displaying the <i>E/Z</i> photoisomerization where Acceptor = A and Donor = D	66
Figure 2.2.4 Self-complementary hydrogen bond arrays studied in this dissertation with derivatives 1a-c in a DDAAA • AAADD sequence whereas 2a-d , and 3a-b show a DDAA • AADD where Donor = D ; Acceptor = A	67
Figure 2.3 Synthesis of self-complementary hydrogen bond arrays 1a-c , 2a-d and 3a,b . 8a , 9a refer to the hexyl group at R ₁ , 8b , 9b refer to the 2-ethyl hexyl group at R ₁ , and 8c refer to the 3,5-bis(trifluoromethyl)phenyl group at R ₁	69
Figure 2.3.1 Alternate synthesis of selective self-complementary hydrogen bond arrays to yield derivatives 1c , 2c and 3b with strong electron withdrawing R ₁ 's...70	
Figure 2.4.1 ¹ H NMR spectrum of Z-1a in DMSO- <i>d</i> ₆ at 298 K.....	72
Figure 2.4.2 ¹ H NMR spectrum of Z-1b in DMSO- <i>d</i> ₆ at 298 K.....	73
Figure 2.4.3 ¹ H NMR spectrum of Z-1c in DMSO- <i>d</i> ₆ at 298 K.....	74
Figure 2.4.4 ¹ H NMR spectrum of (<i>Z</i>)-1-(2-(4-(tert-butyl)benzylidene)-3-oxo-2,3-dihydrobenzo[<i>b</i>]thiophen-5-yl)-3-hexylurea (Z-2a) in CDCl ₃ at 298 K.....	75
Figure 2.4.5 ¹ H NMR spectrum of (<i>E</i>)-1-(2-(4-(tert-butyl)benzylidene)-3-oxo-2,3-dihydrobenzo[<i>b</i>]thiophen-5-yl)-3-hexylurea (E-2a) in CDCl ₃ at 298 K.....	75
Figure 2.4.6 ¹ H NMR spectrum of Z-2b in CDCl ₃ at 298 K.....	77
Figure 2.4.7 ¹ H NMR spectrum of a mixture of Z/E-2b in CDCl ₃ at 298 K where the red, orange arrows correspond to the <i>Z</i> , <i>E</i> isomers respectively.....	78
Figure 2.5.1 The anticipated dimer of Z-2a occurring in solution with increasing monomer concentration.....	84
Figure 2.5.2 The NMR of Z-2a at three concentrations a) 0.172 mM, b) 1.69 mM and c) 5.49 mM.....	85
Figure 2.5.3 Calculated binding isotherm (black curve) and ¹ H NMR dilution data of Z-2a in CDCl ₃ at 298 K upon additions of a 4.81mM solution of Z-2a to 0.5 mL of CDCl ₃ . The chemical shift of NH _k was plotted vs. concentration of Z-2a . The red, blue and green data points correspond to the first, second and third dilutions respectively.....	86
Figure 2.5.4 Calculated binding isotherm (black curve) and ¹ H NMR dilution	

- data of **Z-2b** in CDCl_3 at 298 K upon additions of a 7.3 mM solution of **Z-2b** to 0.5 mL of CDCl_3 . The chemical shift of NH_k was plotted vs. concentration of **Z-2b**. The red, blue and green data points correspond to the first, second and third dilutions respectively.....86
- Figure 2.5.5** Calculated binding isotherm (black curve) and ^1H NMR dilution data of **Z-2b** in toluene- d_8 at 298 K upon additions of a 7.3 mM solution of **Z-2b** to 0.5 mL of toluene- d_8 . The chemical shift of NH_k was plotted vs. concentration of **Z-2b**. The red, blue and green data points correspond to the first, second and third dilutions respectively.....87
- Figure 2.5.6** Calculated binding isotherm and ^1H NMR dilution data of **Z-2b** in a mixture of **Z/E-2b** in CDCl_3 at 298 K upon additions of a 7.7 mM solution mixture of **Z/E-2b** to 0.5 mL of CDCl_3 . The chemical shift of NH_k was plotted vs. concentration of **Z-2b**. The blue and orange data points correspond to the first and second separate dilutions respectively. The black line is the average isotherm of the two data sets. The red line denotes the average isotherm of three separate dilution experiments of the lone Z isomer.....88
- Figure 2.5.7** Calculated binding isotherm and ^1H NMR dilution data of **E-2b** in a mixture of **Z/E-2b** in CDCl_3 at 298 K upon additions of a 7.7 mM solution mixture of **Z/E-2b** to 0.5 mL of CDCl_3 . The chemical shift of NH_k was plotted vs. concentration of **E-2b**. The red and green data points correspond to the first and second separate dilutions respectively. The black line is the average isotherm.....89
- Figure 2.5.8** Calculated binding isotherm (black curve) and ^1H NMR dilution data of **Z-2c** in CDCl_3 at 298 K upon additions of a 2.6 mM solution of **Z-2c** to 0.5 mL of CDCl_3 . The chemical shift of NH_k was plotted vs. concentration of **Z-2b**.....90
- Figure 2.5.9** Calculated binding isotherm and ^1H NMR dilution data of **Z-3a** in CDCl_3 at 298 K upon additions of a 10 mM solution of **Z-3a** to 0.5 mL of CDCl_3 . The chemical shift of NH_k was plotted vs. concentration of **Z-3a**. The red, blue and green data points correspond to the first, second and third dilutions respectively.....91
- Figure 2.5.10** Calculated binding isotherm (black curve) and ^1H NMR dilution data of **Z-3b** in CD_2Cl_2 at 298 K upon additions of a 10 mM solution of **Z-3b** to 0.5 mL of CD_2Cl_2 . The chemical shift of NH_k was plotted vs. concentration of **Z-3b**.....92
- Figure 2.6.1** The stick representation of the X-ray crystal structure of **Z-1c** hydrogen

bonding to a molecule of DMSO with intermolecular hydrogen bonds indicated (dashed green lines) and intramolecular hydrogen bonds indicated (dashed orange lines). Light grey, dark grey, red, blue, yellow and green correspond to carbon, hydrogen, oxygen, nitrogen, sulfur and fluorine atoms, respectively.....95

Figure 2.6.2 The stick representation of the X-ray crystal structure of **Z-1c** displaying planarity of the molecules via π -stacking and the slipped π -stacking perpendicular to the 0.690, -0.685 and 0.235 direction.....98

Figure 2.6.3 The stick representation of the X-ray crystal structure of **Z-2a** dimer with intermolecular hydrogen bonds indicated (dashed green lines). Light grey, dark grey, red, blue, and yellow correspond to carbon, hydrogen, oxygen, nitrogen and sulfur atoms, respectively.....101

Figure 2.6.4 The stick representation displaying the asymmetric unit of **Z-3b** hydrogen bonding to a molecule of DMSO. Hydrogen bonds are indicated as dashed green lines. Light grey, dark grey, red, blue, yellow and green correspond to carbon, hydrogen, oxygen, nitrogen, sulfur and fluorine atoms, respectively.....102

Chapter 3

Figure 3.2.1 UV-Vis absorption spectra of **Z-1a** (red; $c=3.7 \times 10^{-4}$ M, DMSO), **Z-1b** (violet; $c=1.2 \times 10^{-4}$ M, CHCl_3), and **Z-1c** (hot pink; $c=7.7 \times 10^{-5}$ M, CHCl_3) at 298 K.....130

Figure 3.2.2 The putative photoisomerization of self-complementary photoswitches **1a-1c** upon the irradiation of a specific wavelength of light and the reversion to the Z isomer upon a different wavelength of light or the addition of heat.....132

Figure 3.2.3 UV-Vis absorption spectra of **Z-1c** ($c=7.7 \times 10^{-5}$ M) in CHCl_3 at 298 K; where hot pink = lone Z isomer; orange = irradiation at 410 nm; blue = irradiation at 460 nm; green = irradiation at 490 nm; indigo = irradiation at 520 nm; and violet = irradiation at 660 nm. All irradiations lasted for 5 minutes.....133

Figure 3.3.1.1 UV-Vis absorption spectra of **2a-d** and **3a,b** ($c=7.7 \times 10^{-5} - 3 \times 10^{-3}$ M) in CHCl_3 at 298 K; where red = **Z-2a**; orange = **Z-2b**; yellow = **Z-2c**; brown = **Z-2d**; violet = **Z-3a** and indigo = **Z-3c**. Note: **Z-2d** and **Z-3c** are in DMSO.....134

Figure 3.3.2.1 Stacked plots of ^1H NMR spectra after irradiation of i) **Z-2a** in CDCl_3 at 298 K where the red NH chemical shifts = Z isomer and the orange NH chemical shifts = E isomer; ii) **Z-2b** in CDCl_3 at 298 K where the red NH

shifts = *Z* and the orange NH shifts = *E* isomer; iii) **Z-2c** in CD₂Cl₂ at 298K where the red aryl shifts = *Z* and the orange aryl shifts = *E* isomer; iv) **Z-3a** in DMSO-*d*₆ at 298K where the red alkene chemical shifts = *Z* and the orange aryl chemical shifts = the *E* isomer. For all spectra: a) pure *Z* isomer; b) pss at 410 nm; c) pss at 425 nm; d) pss at 440 nm; e) pss at 460 nm; f) pss at 490 nm; g) pss at 520 nm; h) pss at 590 nm; i) pss at 620 nm; j) pss at 660 nm.....139

Figure 3.3.2.2 UV-Vis absorption spectra of **Z-2a** after irradiation at 440 nm where red = pure *Z* and orange = a mixture of *E* and *Z* isomers in various solvents as follows; a) $c = 6.3 \times 10^{-5}$ M in CD₂Cl₂ at 298 K; b) $c = 6.3 \times 10^{-5}$ M in CHCl₃ at 298 K; c) $c = 2.3 \times 10^{-5}$ M in THF at 298 K; d) $c = 4.4 \times 10^{-5}$ M in acetone at 298 K; e) 5.5×10^{-5} M in DMSO at 298 K; f) 2.3×10^{-4} M in CH₃CN at 298 K; g) 6.2×10^{-6} M in MeOH at 298 K; h) 6.5×10^{-5} M in DMF at 298 K.....141

Figure 3.3.3.1 A first order kinetic analysis plot of the thermal reversion of **Z-2a** after irradiation at 440 nm to obtain a 56%*E* conversion in CDCl₃. The relative ratios were obtained from the integral values relative to concentration to give a linear first order rate equation.....144

Figure 3.3.3.2 Stacked plot of ¹H NMR spectra of the reversion of **E-2a** at select time intervals in CDCl₃ at 298 K. The red arrows = *Z* isomer; orange arrows = *E* isomer.....145

Figure 3.3.3.3 ¹H NMR spectra of the reversion of **E-2a** at select time intervals in CD₂Cl₂ at 298 K. The red arrows = *Z* isomer; orange arrows = *E* isomer.....146

Figure 3.3.3.4 UV-Vis absorption spectra displaying the *E* to *Z* thermal reversion of **E-2a** at room temp., where the red curve = pure *Z* isomer and the orange curve = irradiation at 440 nm in CHCl₃ at 298 K ($c = 1.1 \times 10^{-3}$ M). A spectrum was taken after 1 hour (green); 2 hours (violet); and four hours (blue).....146

Figure 3.3.3.5 A first order kinetic analysis plot of the thermal reversion of **Z-2c** after irradiation at 425 nm to obtain a 53%*E* conversion in CDCl₃. The relative ratios were obtained from the integral values relative to concentration to give a linear first order rate equation.....147

Chapter 4

Figure 4.1 Self-complementary hydrogen bond arrays and their dimerization constants (K_d) are illustrated demonstrating the hydrogen bond associations between identical units fashioned in an antiparallel arrangement.....157

Figure 4.2 Proposed self-complementary hydrogen bond arrays, A1, A2, and A3 with substitution of EDG at X and Y and EWG at R ₁	160
--	-----

Appendices

Figure A.1.1 ¹ H NMR spectrum of 2-((carboxymethyl)thio)-5-nitrobenzoic acid (5) in CDCl ₃ at 298 K.....	162
Figure A.1.2 ¹ H NMR spectrum of 6-nitrobenzo[b]thiophen-3-yl acetate (6) in CDCl ₃ at 298 K.....	162
Figure A.1.3 ¹ H NMR spectrum of 5-aminobenzo[b]thiophen-3-yl acetate (7) in CDCl ₃ at 298 K.....	163
Figure A.1.4 ¹ H NMR spectrum of 5-amino-2-(3,5-di-tert-butylbenzylidene)benzo[b]thiophen-3(2H)-one (7a) in CDCl ₃ at 298 K..	163
Figure A.1.5 ¹ H NMR spectrum of 5-(3-hexylureido)benzo[b]thiophen-3-yl acetate (8a) in CDCl ₃ at 298 K.....	164
Figure A.1.6 ¹ H NMR spectrum of 1-hexyl-3-(3-oxo-2,3-dihydrobenzo[b]thiophen-5-yl)urea (9a) in CDCl ₃ at 298 K.....	164
Figure A.1.7 ¹ H NMR spectrum of 5-(3-(2-ethylhexyl)ureido)benzo[b]thiophen-3-yl acetate (8b) in CDCl ₃ at 298 K.....	165
Figure A.1.8 ¹ H NMR spectrum of 5-(3-(3,5-bis(trifluoromethyl)phenyl)ureido)benzo[b]thiophen-3-yl acetate (8c) in CDCl ₃ at 298 K.....	165
Figure A.1.9 ¹ H NMR spectrum of 2,3,6,7-tetrahydro-1H,5H-pyrido[3,2,1-ij]quinoline (10) in CDCl ₃ at 298 K.....	166
Figure A.1.10 ¹ H NMR spectrum of 2,3,6,7-tetrahydro-1H,5H-pyrido[3,2,1-ij]quinoline-9-carbaldehyde (11) in CDCl ₃ at 298 K.....	166
Figure A.1.11 ¹ H NMR spectrum of 1-hexyl-3-phenylurea (13) in CDCl ₃ at 298 K.....	167
Figure A.1.12 ¹ H NMR spectrum of (<i>Z</i>)-1-hexyl-3-(3-oxo-2-(2-oxoacenaphthylen-1(2H)-ylidene)-2,3-dihydrobenzo[b]thiophen-5-yl)urea (Z-1a) in DMSO- <i>d</i> ₆ at 298 K.....	168
Figure A.1.13 ¹ H NMR spectrum of (<i>Z</i>)-1-(2-ethylhexyl)-3-(3-oxo-2-(2-oxoacenaphthylen-1(2H)-ylidene)-2,3-dihydrobenzo[b]thiophen-5-yl)urea (Z-1b) in DMSO- <i>d</i> ₆ at 298 K.....	168

Figure A.1.14 ^1H NMR spectrum of ((<i>Z</i>)-1-(3,5-bis(trifluoromethyl)phenyl)-3-(3-oxo-2-(2-oxoacenaphthylen-1(2H)-ylidene)-2,3-dihydrobenzo[<i>b</i>]thiophen-5-yl)urea (Z-1c) in $\text{DMSO-}d_6$ at 298 K.....	169
Figure A.1.15 ^1H NMR spectrum of (<i>Z</i>)-1-(2-(4-(tert-butyl)benzylidene)-3-oxo-2,3-dihydrobenzo[<i>b</i>]thiophen-5-yl)-3-hexylurea (Z-2a) in CDCl_3 at 298 K.....	169
Figure A.1.16 ^1H NMR spectrum of (<i>E</i>)-1-(2-(4-(tert-butyl)benzylidene)-3-oxo-2,3-dihydrobenzo[<i>b</i>]thiophen-5-yl)-3-hexylurea (E-2a) in CDCl_3 at 298 K.....	170
Figure A.1.17 ^1H NMR spectrum of (<i>Z</i>)-1-(2-(3,5-di-tert-butylbenzylidene)-3-oxo-2,3-dihydrobenzo[<i>b</i>]thiophen-5-yl)-3-hexylurea (Z-2b) in CDCl_3 at 298 K.....	170
Figure A.1.18 ^1H NMR spectrum of ((<i>Z</i>)-1-(3,5-bis(trifluoromethyl)phenyl)-3-(2-(3,5-di-tert-butylbenzylidene)-3-oxo-2,3-dihydrobenzo[<i>b</i>]thiophen-5-yl)urea (Z-2c) in CDCl_3 at 298 K.....	171
Figure A.1.19 ^1H NMR spectrum of (<i>Z</i>)-1-hexyl-3-(2-(4-hydroxybenzylidene)-3-oxo-2,3-dihydrobenzo[<i>b</i>]thiophen-5-yl)urea (Z-2d) in $\text{DMSO-}d_6$ at 298 K.....	171
Figure A.1.20 ^1H NMR spectrum of (<i>Z</i>)-1-hexyl-3-(3-oxo-2-((2,3,6,7-tetrahydro-1H, 5H-pyrido[3,2,1- <i>ij</i>]quinoline-9-yl)methylene)-2,3-dihydrobenzo[<i>b</i>]thiophen-5-yl)urea (Z-3a) in CDCl_3 at 298 K.....	172
Figure A.1.21 ^1H NMR spectrum of (<i>Z</i>)-1-(3,5-bis(trifluoromethyl)phenyl)-3-(3-oxo-2-((2,3,6,7-tetrahydro-1H,5H-pyrido[3,2,1- <i>ij</i>]quinolin-9-yl)methylene)-2,3-dihydrobenzo[<i>b</i>]thiophen-5-yl)urea (Z-3b) in CDCl_3 at 298 K.....	172
Figure A.2.1 ^{13}C NMR spectrum of 2-((carboxymethyl)thio)-5-nitrobenzoic acid (5) in CDCl_3 at 298 K.....	173
Figure A.2.2 ^{13}C NMR spectrum of 6-nitrobenzo[<i>b</i>]thiophen-3-yl acetate (6) in CDCl_3 at 298 K.....	173
Figure A.2.3 ^{13}C NMR spectrum of 5-aminobenzo[<i>b</i>]thiophen-3-yl acetate (7) in CDCl_3 at 298 K.....	174
Figure A.2.4 ^{13}C NMR spectrum of (<i>Z</i>)-5-amino-2-(3,5-di-tert-butylbenzylidene)benzo[<i>b</i>]thiophen-3(2H)-one (7a) in CDCl_3 at 298 K..	174
Figure A.2.5 ^{13}C NMR spectrum of 5-(3-hexylureido)benzo[<i>b</i>]thiophen-3-yl	

acetate (8a) in CDCl ₃ at 298 K.....	175
Figure A.2.6 ¹³ C NMR spectrum of 1-hexyl-3-(3-oxo-2,3-dihydrobenzo[b]thiophen-5-yl)urea (9a) in CDCl ₃ at 298 K.....	175
Figure A.2.7 ¹³ C NMR spectrum of 5-(3-(2-ethylhexyl)ureido)benzo[b]thiophen-3-yl acetate (8b) in CDCl ₃ at 298 K.....	176
Figure A.2.8 ¹³ C NMR spectrum of 5-(3-(3,5-bis(trifluoromethyl)phenyl)ureido)benzo[b]thiophen-3-yl acetate (8c) in CDCl ₃ at 298 K.....	176
Figure A.2.9 ¹³ C NMR spectrum of 2,3,6,7-tetrahydro-1H,5H-pyrido[3,2,1-ij]quinoline (10) in CDCl ₃ at 298 K.....	177
Figure A.2.10 ¹³ C NMR spectrum of 2,3,6,7-tetrahydro-1H,5H-pyrido[3,2,1-ij]quinoline-9-carbaldehyde (11) in CDCl ₃ at 298 K.....	177
Figure A.2.11 ¹³ C NMR spectrum of 1-hexyl-3-phenylurea (13) in CDCl ₃ at 298 K.....	178
Figure A.2.12 ¹³ C NMR spectrum of (Z)-1-(2-ethylhexyl)-3-(3-oxo-2-(2-oxoacenaphthylen-1(2H)-ylidene)-2,3-dihydrobenzo[b]thiophen-5-yl)urea (Z-1b) in DMSO- <i>d</i> ₆ at 298 K.....	179
Figure A.2.13 ¹³ C NMR spectrum of (Z)-1-(3,5-bis(trifluoromethyl)phenyl)-3-(3-oxo-2-(2-oxoacenaphthylen-1(2H)-ylidene)-2,3-dihydrobenzo[b]thiophen-5-yl)urea (Z-1c) in DMSO- <i>d</i> ₆ at 298 K.....	179
Figure A.2.14 ¹³ C NMR spectrum of (Z)-1-(2-(4-(tert-butyl)benzylidene)-3-oxo-2,3-dihydrobenzo[b]thiophen-5-yl)-3-hexylurea (Z-2a) in CDCl ₃ at 298 K.....	180
Figure A.2.15 ¹³ C NMR spectrum of (Z)-1-(2-(3,5-di-tert-butylbenzylidene)-3-oxo-2,3-dihydrobenzo[b]thiophen-5-yl)-3-hexylurea (Z-2b) in CDCl ₃ at 298 K.....	180
Figure A.2.16 ¹³ C NMR spectrum of ((Z)-1-(3,5-bis(trifluoromethyl)phenyl)-3-(2-(3,5-di-tert-butylbenzylidene)-3-oxo-2,3-dihydrobenzo[b]thiophen-5-yl)urea (Z-2c) in CDCl ₃ at 298 K.....	181
Figure A.2.17 ¹³ C NMR spectrum of (Z)-1-hexyl-3-(2-(4-hydroxybenzylidene)-3-oxo-2,3-dihydrobenzo[b]thiophen-5-yl)urea (Z-2d) in DMSO- <i>d</i> ₆ at 298 K...181	181
Figure A.2.18 ¹³ C NMR spectrum of (Z)-1-hexyl-3-(3-oxo-2-((2,3,6,7-	

tetrahydro-1H, 5H-pyrido[3,2,1-ij]quinoline-9-yl)methylene)-2,3-dihydrobenzo[b]thiophen-5-yl)urea (Z-3a) at 298 K.....	182
Figure A.2.19 ^{13}C NMR spectrum of (<i>Z</i>)-1-(3,5-bis(trifluoromethyl)phenyl)-3-(3-oxo-2-((2,3,6,7-tetrahydro-1H,5H-pyrido[3,2,1-ij]quinolin-9-yl)methylene)-2,3-dihydrobenzo[b]thiophen-5-yl)urea (Z-3b) at 298 K.....	182
Figure A.3.1 gCOSY NMR spectrum of (<i>Z</i>)-1-(2-ethylhexyl)-3-(3-oxo-2-(2-oxoacenaphthylen-1(2H)-ylidene)-2,3-dihydrobenzo[b]thiophen-5-yl)urea (Z-1b) in DMSO- d_6 at 298 K.....	183
Figure A.3.2 HSQC NMR spectrum of (<i>Z</i>)-1-(2-ethylhexyl)-3-(3-oxo-2-(2-oxoacenaphthylen-1(2H)-ylidene)-2,3-dihydrobenzo[b]thiophen-5-yl)urea (Z-1b) in DMSO- d_6 at 298 K.....	184
Figure A.3.3 HMBC NMR spectrum of (<i>Z</i>)-1-(2-ethylhexyl)-3-(3-oxo-2-(2-oxoacenaphthylen-1(2H)-ylidene)-2,3-dihydrobenzo[b]thiophen-5-yl)urea (Z-1b) in DMSO- d_6 at 298 K.....	185
Figure A.3.4 gCOSY NMR spectrum of (<i>Z</i>)-1-(3,5-bis(trifluoromethyl)phenyl)-3-(3-oxo-2-(2-oxoacenaphthylen-1(2H)-ylidene)-2,3-dihydrobenzo[b]thiophen-5-yl)urea (Z-1c) in DMSO- d_6 at 298 K.....	186
Figure A.3.5 HSQC NMR spectrum of (<i>Z</i>)-1-(3,5-bis(trifluoromethyl)phenyl)-3-(3-oxo-2-(2-oxoacenaphthylen-1(2H)-ylidene)-2,3-dihydrobenzo[b]thiophen-5-yl)urea (Z-1c) in DMSO- d_6 at 298 K.....	187
Figure A.3.6 HMBC NMR spectrum of (<i>Z</i>)-1-(3,5-bis(trifluoromethyl)phenyl)-3-(3-oxo-2-(2-oxoacenaphthylen-1(2H)-ylidene)-2,3-dihydrobenzo[b]thiophen-5-yl)urea (Z-1c) in DMSO- d_6 at 298 K.....	188
Figure A.3.7 gCOSY NMR spectrum of (<i>Z</i>)-1-(2-(4-(tert-butyl)benzylidene)-3-oxo-2,3-dihydrobenzo[b]thiophen-5-yl)-3-hexylurea (Z-2a) in CDCl $_3$ at 298 K.....	189
Figure A.3.8 HSQC NMR spectrum of (<i>Z</i>)-1-(2-(4-(tert-butyl)benzylidene)-3-oxo-2,3-dihydrobenzo[b]thiophen-5-yl)-3-hexylurea (Z-2a) in CDCl $_3$ at 298 K.....	190
Figure A.3.9 HMBC NMR spectrum of (<i>Z</i>)-1-(2-(4-(tert-butyl)benzylidene)-3-oxo-2,3-dihydrobenzo[b]thiophen-5-yl)-3-hexylurea (Z-2a) in CDCl $_3$ at 298 K.....	191
Figure A.3.10 gCOSY NMR spectrum of (<i>Z</i>)-1-(2-(3,5-di-tert-butylbenzylidene)-3-oxo-2,3-dihydrobenzo[b]thiophen-5-yl)-3-hexylurea (Z-2b) in CDCl $_3$ at	

298 K.....	192
Figure A.3.11 HSQC NMR spectrum of (Z)-1-(2-(3,5-di-tert-butylbenzylidene)-3-oxo-2,3-dihydrobenzo[b]thiophen-5-yl)-3-hexylurea (Z-2b) in CDCl ₃ at 298 K.....	193
Figure A.3.12 HMBC NMR spectrum of (Z)-1-(2-(3,5-di-tert-butylbenzylidene)-3-oxo-2,3-dihydrobenzo[b]thiophen-5-yl)-3-hexylurea (Z-2b) in CDCl ₃ at 298 K.....	194
Figure A.3.13 gCOSY NMR spectrum of (Z)-1-(3,5-bis(trifluoromethyl)phenyl)-3-(2-(3,5-di-tert-butylbenzylidene)-3-oxo-2,3-dihydrobenzo[b]thiophen-5-yl)urea (Z-2c) in CDCl ₃ at 298 K.....	195
Figure A.3.14 HSQC NMR spectrum of (Z)-1-(3,5-bis(trifluoromethyl)phenyl)-3-(2-(3,5-di-tert-butylbenzylidene)-3-oxo-2,3-dihydrobenzo[b]thiophen-5-yl)urea (Z-2c) in CDCl ₃ at 298 K.....	196
Figure A.3.15 HMBC NMR spectrum of (Z)-1-(3,5-bis(trifluoromethyl)phenyl)-3-(2-(3,5-di-tert-butylbenzylidene)-3-oxo-2,3-dihydrobenzo[b]thiophen-5-yl)urea (Z-2c) in CDCl ₃ at 298 K.....	197
Figure A.3.16 gCOSY NMR spectrum of (Z)-1-hexyl-3-(2-(4-hydroxybenzylidene)-3-oxo-2,3-dihydrobenzo[b]thiophen-5-yl)urea (Z-2d) in DMSO- <i>d</i> ₆ at 298 K.....	198
Figure A.3.17 HSQC NMR spectrum of (Z)-1-hexyl-3-(2-(4-hydroxybenzylidene)-3-oxo-2,3-dihydrobenzo[b]thiophen-5-yl)urea (Z-2d) in DMSO- <i>d</i> ₆ at 298 K.....	199
Figure A.3.18 HMBC NMR spectrum of (Z)-1-hexyl-3-(2-(4-hydroxybenzylidene)-3-oxo-2,3-dihydrobenzo[b]thiophen-5-yl)urea (Z-2d) in DMSO- <i>d</i> ₆ at 298 K.....	200
Figure A.3.19 gCOSY NMR spectrum of (Z)-1-hexyl-3-(3-oxo-2-((2,3,6,7-tetrahydro-1H, 5H-pyrido[3,2,1-ij]quinoline-9-yl)methylene)-2,3-dihydrobenzo[b]thiophen-5-yl)urea (Z-3a) in CDCl ₃ at 298 K.....	201
Figure A.3.20 HSQC NMR spectrum of (Z)-1-hexyl-3-(3-oxo-2-((2,3,6,7-tetrahydro-1H, 5H-pyrido[3,2,1-ij]quinoline-9-yl)methylene)-2,3-dihydrobenzo[b]thiophen-5-yl)urea (Z-3a) in CDCl ₃ at 298 K.....	202
Figure A.3.21 HMBC NMR spectrum of (Z)-1-hexyl-3-(3-oxo-2-((2,3,6,7-tetrahydro-1H, 5H-pyrido[3,2,1-ij]quinoline-9-yl)methylene)-2,3-dihydrobenzo[b]thiophen-5-yl)urea (Z-3a) in CDCl ₃ at 298 K.....	203

Figure A.3.22 gCOSY NMR spectrum of (Z)-1-(3,5- bis(trifluoromethyl)phenyl)-3-(3-oxo-2-((2,3,6,7-tetrahydro-1H, 5H-pyrido[3,2,1-ij]quinolin-9-yl)methylene)-2,3- dihydrobenzo[b]thiophen-5-yl)urea (Z-3b) in DMSO- <i>d</i> ₆ at 298 K.....	204
Figure A.3.23 HSQC NMR spectrum of (Z)-1-(3,5- bis(trifluoromethyl)phenyl)-3-(3-oxo-2-((2,3,6,7-tetrahydro-1H, 5H-pyrido[3,2,1-ij]quinolin-9-yl)methylene)-2,3- dihydrobenzo[b]thiophen-5-yl)urea (Z-3b) in DMSO- <i>d</i> ₆ at 298 K.....	205
Figure A.3.24 HMBC NMR spectrum of (Z)-1-(3,5- bis(trifluoromethyl)phenyl)-3-(3-oxo-2-((2,3,6,7-tetrahydro-1H, 5H-pyrido[3,2,1-ij]quinolin-9-yl)methylene)-2,3- dihydrobenzo[b]thiophen-5-yl)urea (Z-3b) in DMSO- <i>d</i> ₆ at 298 K.....	206
Figure A.4.1 ¹⁹ F NMR spectrum of 5-(3-(3,5- bis(trifluoromethyl)phenyl)ureido)benzo[b]thiophen-3-yl acetate (8c) in CDCl ₃ at 298 K.....	207
Figure A.4.2 ¹⁹ F NMR spectrum of (Z)-1-(3,5-bis(trifluoromethyl)phenyl)-3-(3-oxo-2-(2-oxoacenaphthylen-1(2H)-ylidene)-2,3- dihydrobenzo[b]thiophen-5-yl)urea (Z-1c) in CDCl ₃ at 298 K.....	208
Figure A.4.3 ¹⁹ F NMR spectrum of (Z)-1-(3,5-bis(trifluoromethyl)phenyl)-3-(2-(3,5-di-tert-butylbenzylidene)-3-oxo-2,3-dihydrobenzo[b]thiophen-5-yl)urea (Z-2c) in CDCl ₃ at 298 K.....	208
Figure A.4.4 ¹⁹ F NMR spectrum of (Z)-1-(3,5-bis(trifluoromethyl)phenyl)-3-(3-oxo-2-((2,3,6,7-tetrahydro-1H, 5H-pyrido[3,2,1-ij]quinolin-9-yl)methylene)-2,3-dihydrobenzo[b]thiophen-5-yl)urea (Z-3b) in CDCl ₃ at 298 K.....	209

LIST OF SCHEMES

Chapter 1

Scheme 1.4.1.1	Isomerization of azobenzene upon irradiation with Ultraviolet-Visible (UV-Vis) light.....	11
Scheme 1.4.1.2	Isomerization of 6-nitrospiropyran between the spiropyran (SP) and the merocyanine form (MC) upon irradiation with UV-Vis light.....	12
Scheme 1.4.1.3	Isomerization of Z-stilbene upon irradiation with UV light to yield 3 unique derivatives.....	13
Scheme 1.4.1.4	Isomerization of thioindigo upon irradiation with visible light.....	14
Scheme 1.5	Isomerization of hemithioindigo upon irradiation with visible light.....	15
Scheme 1.6	In a given photoreversible system A and B interconvert interchangeably at the PSS in the presence of light.....	19
Scheme 1.6.2	The photodegradation process of a select few photochromic compounds after being subjected to excessive UV-Vis irradiation ^{26, 47}	22
Scheme 1.7.2.2	Two representative diagrams reflecting the formation of supramolecular polymers between complementary monomers, a , and self-complementary monomers, b . Image modified from reference [3].....	27
Scheme 1.9	The hydrogen bond interaction given by IUPAC.....	32
Scheme 1.9.2.1	Resonance stabilized hydrogen bond formation of <i>o</i> -nitrophenol.....	37
Scheme 1.9.2.2	A HBA, A, and a HBD, D, are surrounded by solvent molecules (blue circle). Upon H-bond formation between A and D, the resulting complex becomes solvated. The potential for H-bond formation is dependent on the solvent's polarity.....	39

LIST OF ABBREVIATIONS/SYMBOLS

A/HBA hydrogen bond acceptor

ATPase a group of enzymes that catalyze the reaction of ATP to form ADP

ATR attenuated total reflection

α alpha

Ac₂O acetic anhydride

Å Ångström

β beta

BHLYP Becke 3-term functional; Lee, Yang, Parr exchange

CV coefficient of variation

°C degree Celsius

ca. circa

calc. calculated

CTC charge transfer character

cm centimeter

C1 complex 1

C2 complex 2

C3 complex 3

[Z] concentration of trans monomer

[Z•Z] concentration of trans complex

[Z]₀ total concentration of complex

° degrees

D/HBD hydrogen bond donor

DNA deoxyribonucleic acid

Δ heat

d doublet

dd doublet of doublets

DCM dichloromethane

DFS double focusing sector

δ chemical shift

δ_d chemical shift of dimer

δ_{free} chemical shift of free array

ΔG Gibbs free energy

$\Delta\Delta G$ Gibbs free energy difference

δ_m chemical shift of monomer

$\Delta\delta$ change in chemical shift

$\Delta\delta_{\text{max}}$ maximum change in chemical shift

DNA deoxyribonucleic acid

δ_{obs} observed chemical shift

δ_c chemical shift of cis complex

δ_t chemical shift of trans complex

DHP 4a,4b-dihydrophenanthrene

DFT Density-functional theory

DZP Double Zeta-Polarization

3D three-dimensional

E entgegen or *trans*

ϵ molar extinction or absorptivity constant

EI-HRMS Electron Impact Ionization High Resolution Mass Spectrometry

eq. equivalent

et al. and others

etc. et cetera

F fluorescence

γ gamma

g gram

HMBC Heteronuclear Multiple-Bond Correlation Spectroscopy

HSQC Heteronuclear Signal Quantum Coherence Spectroscopy

HRMS high resolution mass spectroscopy

h hour

h ν wavelength

hz Hertz

HOMO highest occupied molecular orbital

HTI hemithioindigo

HI hemiindigo

HOI hemioxindigo or aurone

H-bond hydrogen bond

IR Infrared

IUPAC International Union of Pure and Applied Chemistry

ISC intersystem/interstitial crossing

ITC Isothermal Calorimetry

in. inch

J coupling constant

J Joule

J/g Joule per gram

K rate of reaction

K Kelvin

K_a association constant

K_d dimerization constant

K_{c-c} cis-cis dimerization constant

kcal kiloCalories

kcal/mol kiloCalorie per mole

kJ kiloJoules

K_{t-t} trans-trans complexation constant

kHz kilohertz

λ wavelength

λ_{max} wavelength of maximum absorption

LED light-emitting diode

LUMO lowest unoccupied molecular orbital

ln logarithm to the base *e*

L liter

meta 1,3 positions

m multiplet

m.p. melting point

M⁻¹ (mole/liter)⁻¹

(Mcm)⁻¹ per centimeter per mole

min minute

mL milliliter

mmol millimole

mM millimolar

mol⁻¹ /mole

mg milligram

MC merocyanine

Me methyl

N/A not available/not applicable

number

nm nanometer

MHz megahertz

NMR Nuclear Magnetic Resonance Spectroscopy

¹H NMR Proton Nuclear Magnetic Resonance

¹³C NMR Carbon Nuclear Magnetic Resonance

NOESY Nuclear Overhauser Effect Spectroscopy

n non-bonding molecular orbital

O ortho (1,2 positions)

π pi

π* pi-star antibonding molecular orbital

p para, (1,4 positions)

pH $-\log[\text{H}^+]$

ppm part per million

PSS Photostationary State

P phosphorescence

PC-CLT photochemical crystal-liquid transition

ϕ quantum yield

σ_p hammett substituent constant at *para*-position

σ_m hammett substituent constant at *meta*-position

q quartet

R ideal gas constant, $8.3145 \text{ J}(\text{mol}\cdot\text{K})^{-1}$

RHO Rhodopsin

R.T. room temperature

R substituent group

RNA ribonucleic acid

RS relaxed state

ΔS entropic change

s singlet

sec second

SP spiropyran

SOP standard operating procedure

Σ sum

S₀ ground singlet state

S₁ excited singlet state

S₂ second excited singlet state

σ Hammett substituent constant

σ_m substituent constant at meta-position

TMS tetramethylsilane

theor. theoretical

t triplet

T_m melting temperature

TLC thin layer chromatography

tris-bpy ligand Tris(bipyridine)ruthenium(II) chloride

T₁ triplet state

temp., T temperature

t-butyl/tert-butyl tertiary butyl

μL microliter

UV ultraviolet

UV-Vis Ultraviolet Visible Spectroscopy

V volume

VDW van der Waals forces

Vis visible light

$\tilde{\nu}$ wavenumber

vs. versus

v/v volume per volume

VT-NMR Variable Temperature Nuclear Magnetic Resonance Spectroscopy

Wh/kg Watt-hour per kilogram

w weak

Z zusammen or *cis*

Chapter 1

1 Introduction

1.1 Supramolecular chemistry

Supramolecular chemistry has attracted the interest of many scientists in the last few decades and thus has acquired many definitions. Amongst various interpretations, Ariga and Kunitake published a book in 2006 where they described this relatively new field as “the chemistry beyond the molecule”.²¹ Although this definition is vague and less apparent than many, it encompasses the idea that chemical entities act as supermolecules. This term invented by Jean-Marie Lehn—who laid the foundation for the field of supramolecular chemistry²¹—refers to an organized, complex entity that results from the association of two or more chemical species held together by additive and often cooperative intermolecular forces. These forces may include hydrogen bonding, electrostatic interactions, hydrophobic interactions and/or metal-ligand coordination.

Many nanomaterials and technologies are based on the vast field of supramolecular chemistry with designs incorporating combinations of supramolecular polymers with beneficial functional entities and/or inorganic components. Future technology focuses on synthesizing materials that incorporate the electronic properties of both rubber-like materials and the conductive nature of copper-like electronics. Lehn and co-workers revolutionized this field upon synthesizing a circular helicate from five tris-bpy ligand strands and five equivalents of FeCl_2 ²² and later by discovering a hydrazone-based foldamer (see Figure 1.1).²³

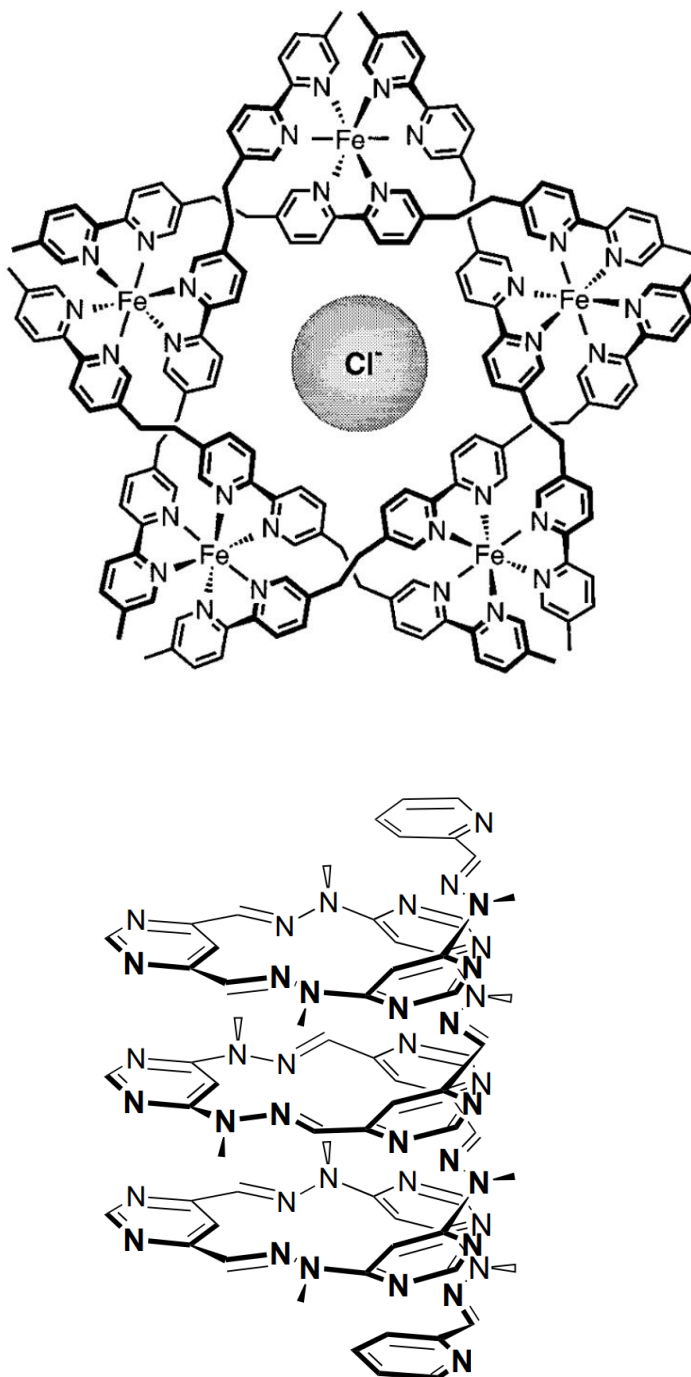


Figure 1.1 An image depicting *a*) a circular helicate synthesized by Lehn and co-workers pre-organized in this spatial arrangement enclosing a Cl⁻ atom in the center;²² and *b*) the structure of an isomorphous analogue to pyridine (hydrazone) where spontaneous pre-assembly promotes the formation of helical shapes.²³

Both complexes mentioned above exist as supermolecules - that is the intermolecular (noncovalent) binding interactions within these arrays are cooperatively adding - to create a powerful yet dynamic coherent system.

1.2 Nanocarriers, Molecular Machines and Biological Recognition

Observed in all of nature's extraordinary molecular machinery is the biological concept of mutualistic symbiosis: ²⁵ many dynamic parts working together to make a functional whole. The idea that more than one organism (or component) has a specific task (beneficial to all) and the sum of all parts is crucial to the proper functioning of the overall unit was oftentimes overlooked within the physical sciences until the development of supramolecular chemistry.

A blood cell has highly specific antigens on its surface allowing it to bind with high affinity to antibodies. An insulin molecule can only activate the insulin receptor triggering a cascade of reactions to uptake excess glucose from the blood stream. Morphine, an opiate, is a drug commonly used to treat chronic diarrhea, persistent cough, post-operative pain and some types of cancer. These molecular agents act in a similar manner as ligands- molecules that form a complex with a biomolecule. As such, opiates bind to precise molecular regions, called recognition sites, on receptor macromolecules.²⁷ Scientists must consider the body's immune response to the particulate as well as the pathway that the neurotransmitter or drug will take to reach its target. Assessing every aspect of the system and how each piece functions and interacts cooperatively is the key to understanding supramolecular chemistry. This process is vital in designing vaccines, effective medicines, prosthetic limbs and organ transplants.

A light-sensitive receptor protein found in the eukaryotic eye, rhodopsin, consists of a main protein and a cofactor. In the presence of light, this protein undergoes a series of electrochemical processes which ultimately causes a *cis* to *trans* isomerization allowing us to see every day. Rotaxanes are complexes which consist of two or more mechanically interlocked molecular species²⁵; usually a linear molecule intersecting a cyclic moiety as shown in Figure 1. The first attempt at synthesizing one was performed in 1967 and since then, many have been tuned to change conformation in the presence of an external stimulus thereby releasing its cargo (drug, antibiotic, protein or enzyme)^{24,85,86}. Due to their low cytotoxicity, versatility and controlled size, they can be incorporated within polymers and function as drug nanocarriers and “nanovalves” or prodrugs.

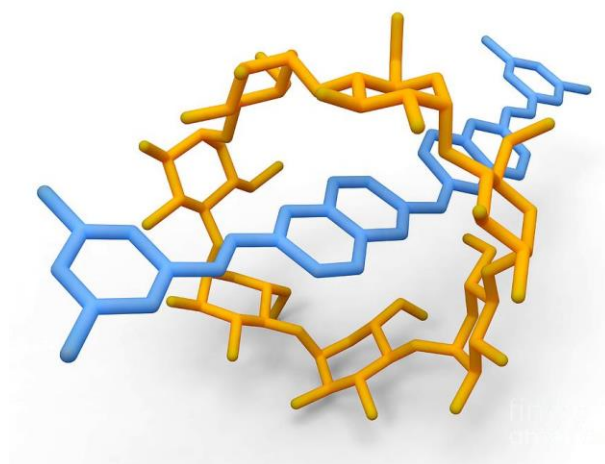


Figure 1.2 A crystal structure of a rotaxane beneficial for targeted drug delivery within the human body.²⁹

In 2018, Feringa, Stoddart and Sauvage were awarded the Noble prize in Chemistry for the design and synthesis of molecular motors. A molecular motor composed of a tricyclic complex demonstrated unidirectional rotation upon photoactivation between its several metastable states. Feringa published a paper in the *Proceedings of the National Academy of Sciences* where he states that the “inspiration [for this nanomachine is taken]

from the fascinating dynamic and motor function observed in biological systems.”²⁴

When investigating natural molecular motors within multicellular organisms; ATPase and bacterial flagella, are two of the most formidable architectures observed.

1.3 Photoresponsivity, Photoisomerization and Photochemistry

Photochemistry happens around us everyday. Plants convert light energy into chemical energy, solar-powered calculators convert light energy into electrical energy and photoreceptor cells in the retina convert light energy into electrical impulses.

Photochemistry directly translates into “light chemistry” and is a term used to describe all light-induced physical and chemical reactions.³³ There are several photoreactions that can occur upon the irradiation of light as shown in Table 1.3.

Table 1.3 Various reactions that may take place after a photochemical event

Type of reaction	Reaction scheme
Dissociation	$AB^* \rightarrow A + B$
Ionization	$AB^* \rightarrow AB^+ + e^-$
Reaction	$AB^* + C \rightarrow AC + B$ (or ABC)
Energy Transfer (intermolecular)	$AB^* + DE \rightarrow AB + DE^*$
Physical Quenching	$AB^* + M \rightarrow AB + M$
Energy Transfer (intramolecular)	$A^*B \rightarrow AB^*$
Luminescence	$AB^* \rightarrow AB + h\nu$
Isomerization	$AB^* \rightarrow BA$

When light is shone on a molecule, an electron absorbs some energy and creates an excited species in a higher energy state. The excited species can then undergo several reactions such as dissociation, ionization, luminescence or isomerization. During a photoisomerization, energy that is absorbed cleaves a bond (often a double bond) within the molecule. Rearrangement and reformation of the bond leads to a new molecular entity. Usually, irradiation of light leads to an excited species which can withstand physical and chemical changes. In some instances, the excited species is not stable and will undergo photodegradation. This latter process is not beneficial for materials-based designs.

The first law of photochemistry was formulated by Grotthus and Draper in 1800 whereby they proved that light absorbed by a specific molecule will produce a photochemical change in that molecule.^{33,87} A molecule can absorb multiple wavelengths of light. However; there is one wavelength unique to each substance where the absorbance is the highest or at a maximum. This wavelength is referred to as λ_{\max} and is important in distinguishing the wavelengths of light pertaining to each isomer in a photoisomerization. Later, Stark and Einstein developed the theory that only one photon can be absorbed at a time. This means that there is a 1:1 ratio of photon to excited species. The amount of light that is absorbed by a molecule will be used to determine the photoefficiency. This is a term used to quantify the amount of light absorbed in relation to the isomer conversion. The photoefficiency is oftentimes measured in terms of the quantum yield (ϕ);^{34,88}

$$\phi = \frac{\# \text{ of photons causing photo change}}{\# \text{ of photons absorbed}} \quad \text{Equation 1}$$

where a value of 1 reflects 100% efficiency. The nature of substituents on the photochrome can have a powerful effect on the quantum yield. Electron-donating substituents generally lead to a bathochromic shift in the absorbance whereas electron-withdrawing substituents lead to a hypsochromic shift. The absorbance of a lower or higher energy wavelength can inadvertently affect the stability of the surrounding functional groups within the photochrome. Quantum yield is independent of instrument settings making it a reliable and universal measurement. For a fluorophore, the quantum yield would describe how efficiently it converts the subjected wavelength of light into fluorescence. For a photoswitch (*vide infra*), the quantum yield would describe how efficiently the wavelength of light converts the *Z* into its counterpart; the *E* isomer. A photoswitch that can undergo a continued cycle of switches between isomers is quantified in terms of photocycles. Generally, the greater the number of photocycles achieved by the photoswitch, the better the photochromic abilities and the greater the lifespan.

1.4 Molecular switch

Rhodopsin, functionalized rotaxanes and Feringa *et al.*'s molecular motor all contain or act as molecular switches. A molecular switch is a single molecule which can reversibly shift between two or more metastable states in the presence of an external stimulus like pH, electric or magnetic field, temperature or light.³³ Crown ethers are cyclic, flexible organic compounds which bind very strongly to positive ions like Na⁺, Li⁺ or K⁺. Crown ethers are tailored to bind to specific ions based on their size and can be implemented to work as switches in the influence of a trigger such as light, or a pH change. This external trigger causes a deformity in the structure which affects the affinity

to certain ions thereby acting as a selective ion exchange carrier (shown in Figure 1.3). On another note, rotaxanes solely function based on the free translocation of the cyclic molecule between two or more binding sites along the length of the chain which is set at a thermally controlled speed. The binding sites of rotaxanes can be chemically modified to increase stability at one site at a time. This way, an electric current or a pH change can either activate or deactivate the binding site thereby shifting the position of the inner molecule like a switch.²⁸ Despite the enticing properties of rotaxane molecular switches, they are non-ideal as their efficiency is on the order of kHz, have low stability over long periods of time and consecutive switches must be placed a distance from one another to prevent interference.

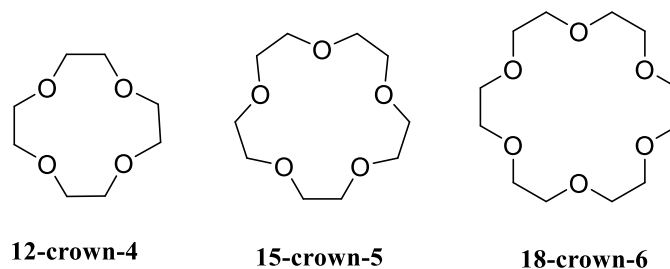


Figure 1.4 Three crown ethers shown in consecutive sizes; 12-crown-4 binds Li ions, 15-crown-5 binds Na⁺ and K⁺ ions and 18-crown-6 binds K⁺ ions most effectively.

1.4.1 Photoswitch

Molecules that change in configuration and thus function in the presence of light are referred to as photochromic compounds or photoswitches. Unlike rotaxanes, photoswitches have been researched as the most prevalent molecular switches in the literature due to their generally high molecular stability, high thermal isomerization energies, and significantly diverse isomer properties. As such, photoswitches belong to

the class of photochromism. In general, photochromism is “a reversible transformation of a chemical species induced in one or both directions by absorption of electromagnetic radiation between two forms, A and B, [each] having different absorption spectra.”²⁵ The discovery of photochromic compounds was brought to light in 1867, when Fritzsche reported the loss of color of a solution of tetracene in the daylight yet when the compound was subjected to a thermal stimulus in the dark, there was a return of the orange color.

In 2018, Boyd *et al.* synthesized and analyzed various derivatives of azobenzenes, spiropyrans, diarylethenes, and other promising photoswitchable molecules, including hemithioindigos, donor–acceptor Stenhouse adducts, and hexaarylbiimidazoles.²⁶ They were able to incorporate these photoswitches as a protective cap over a cross-section of the nanocarriers and upon visible and near-infrared light irradiation, the photoswitches isomerized and in turn cleaved as their properties and binding affinity changed. Figure 1.4.1.1 demonstrates the mechanism described above.

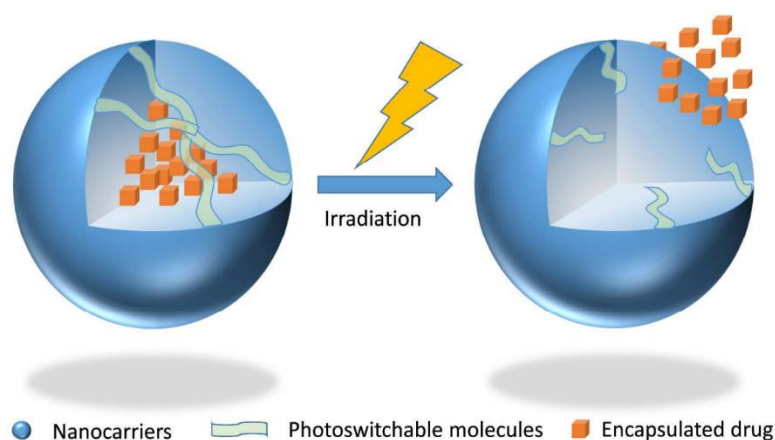
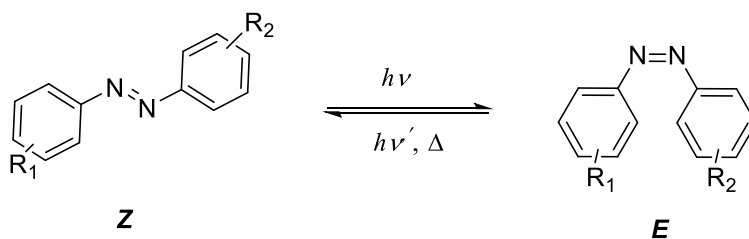


Figure 1.4.1.1 A schematic displaying the use of photoswitchable polymers intended for targeted drug delivery within the human body.²⁶

1.4.1.1 Types of Photoswitches

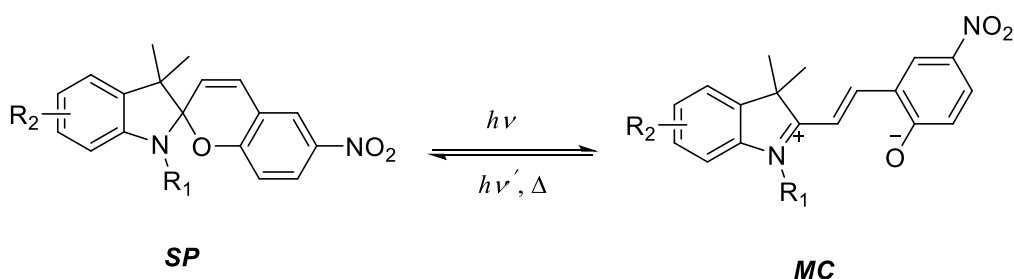
One of the traditional photoswitches studied intensively in the literature is azobenzene, an organic molecule involving two aromatic rings linked by an azo group ($R_1-N=N-R_2$). Before the analysis of azobenzenes (shown in Figure 1.4.1.1) as molecular switches, they were commonly utilized as dyes in the food industry for many years.³⁰ They are known to exist in two forms, the *cis* (*E*) and *trans* (*Z*) isomers, which can interconvert both photochemically and thermally. Irradiation of light between 320-350 nm causes reversible isomerization of the *Z* to the *E* form. Recovery of the dominant form is established by heat or irradiation of light at a different wavelength; 400-450 nm.³⁰ Derivatives of azobenzenes have been synthesized by various research groups with specific functionalities tailored toward a desired use.



Scheme 1.4.1.1 Isomerization of azobenzene upon irradiation with Ultraviolet-Visible (UV-Vis) light.

Azobenzenes are remarkable in that the photochemical conversion between the two isomers occurs on the scale of picoseconds, while thermal relaxation of the *E* to the *Z* isomer occurs from milliseconds to days. Additionally, the photoinduced isomerization leads to a change in absorption spectrum, photochemical properties and dipole moment.

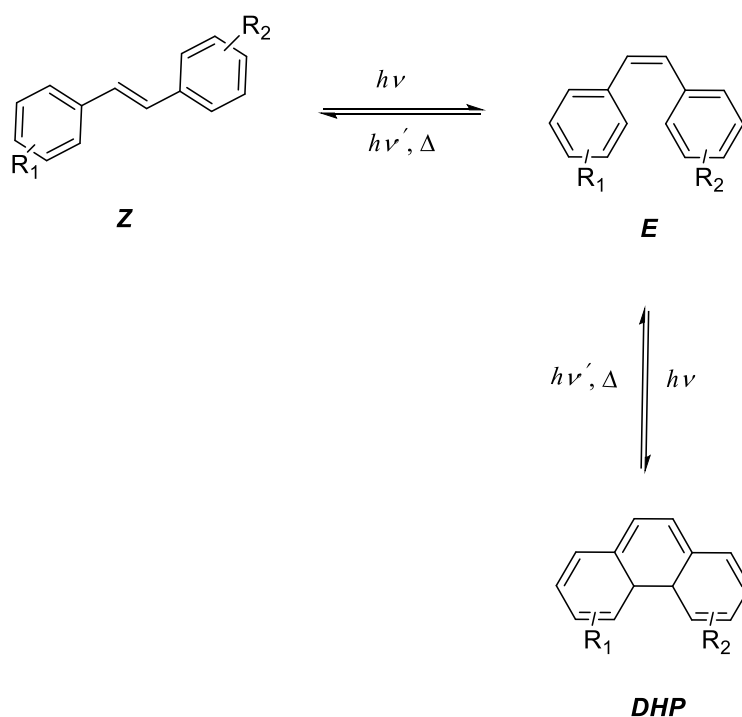
Spiropyrans are another type of photoswitch that, when irradiated, isomerize by intramolecular electrocyclic rearrangement. The spiropyran molecule consists of two functional groups - indoline and chromene - as shown in Figure 1.4.1.2. Due to the extended π -electron system of spiropyrans, their isomers have contrasting characteristics including but not limited to color, geometric planarity and polarity. These magnificent properties make them suitable for use in temperature sensors, reversible fluorescence quenchers and small molecule chelators.³¹ The mechanism of the photoconversion between the spiropyran (*SP*) and the merocyanine (*MC*) form is remarkable. When *SP* is subjected to ultraviolet light, it converts to the zwitterionic, colored *MC* via an electron



Scheme 1.4.1.2 Isomerization of 6-nitrospiropyran between the spiropyran (*SP*) and the merocyanine form (*MC*) upon irradiation with UV-Vis light.

transfer to the electron-rich phenolate oxygen atom. This oxygen atom then serves as a binding site whilst contributing to the overall stability of the molecule. Unfortunately, the equilibrium between *SP* and *MC* is non-specific, that is, it can be controlled by light, polarity and/or temperature or a combination of them. Photofatigue, insufficient selectivity and the lack of sensitivity³² are prominent downfalls of spiropyrans causing scientists to turn to other photoswitches.

Stilbenes are isoelectronic to azobenzenes^{37,89} and they mimic a similar *cis-trans* isomerization upon irradiation at 300 nm. Unlike azobenzenes, stilbenes are thermally stable at room temperature and its isomers can be isolated without any extensive procedures. Reversion of *cis* stilbenes happens upon irradiation at 280 nm. If *cis* stilbenes are subjected to excessive UV light, they will undergo an addition pathway involving ring closure and transform into 4a, 4b-dihydrophenanthrene (*DHP*) shown in Figure 1.4.1.3.

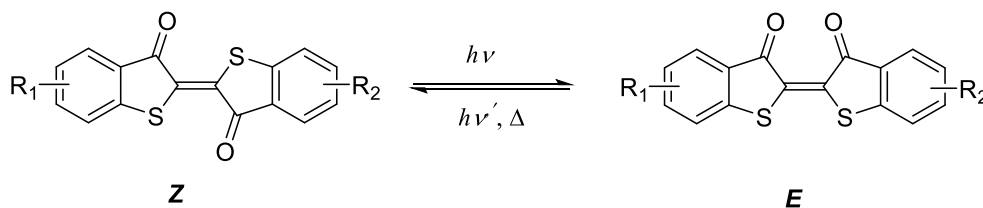


Scheme 1.4.1.3 Isomerization of *Z*-stilbene upon irradiation with UV light to yield 3 unique derivatives.

In 2007, Allen and Sauer experimentally discovered that 70% of excited *cis* isomers convert to the *trans* and the remaining 30% converts to *DHP*. This is due to the electron reshuffling between the LUMO and the HOMO orbitals upon excitation with UV light.³⁹

DHP can be converted back into its *cis* counterpart, however; because of their low stabilities (in the presence of oxygen) *DHP* will undergo irreversible oxidation in a process called photocyclodehydrogenation. There are two indicated theories of isomerization pathways that stilbenes may proceed by: the “one bond flip” or the “hula twist”.³⁸ The former refers to rotation around the double bond in the presence of UV light which would lead to the two phenyl groups lying on perpendicular planes to each other. Likewise, the “hula twist” mechanism isomerizes by rotation around the central double bond but does so via a low-energy intermediate by keeping the phenyl groups at planes parallel to one another. Regardless of either mechanism of action, the involuntary conversion of *cis* stilbene to *DHP*, when excited, greatly reduces its maximum efficiency and potential as a photoswitch.

Thioindigo photochromes have been known in the literature as an interesting class of photochromic compounds due to their ability to engage in reversible, yet robust isomerization upon being subjected to light. Derivatives of thioindigos (shown in Figure 1.4.1.4) have been explored as molecular motors, fluorescent probes and molecular switches due to their high conversion isomerization yields.¹⁶ Substitution of various electron donating and electron withdrawing groups to the thioindigo ring either enhance or decrease the association constants (K_a) between potential substrates. However, thioindigos have been documented to possess very low solubility at room temperature.¹⁶



Scheme 1.4.1.4 Isomerization of thioindigo upon irradiation with visible light.

Hemithioindigos (HTI), possessing both a thioindigo and a stilbene fragment, have been researched as emerging photoswitches over the last decade.^{7,11} Hemiindigos, and hemioxindigos where the pentone ring is functionalized with nitrogen and oxygen respectively (Figure 1.4.1.5) have also been examined as molecular switches.

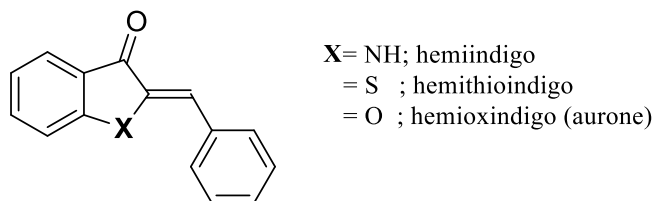
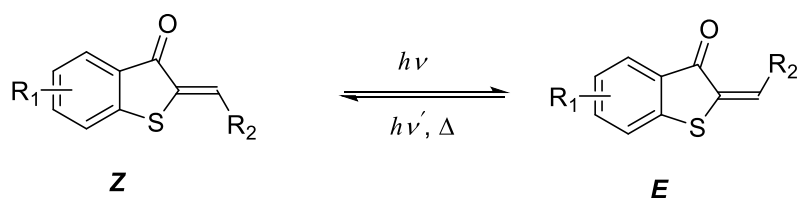


Figure 1.4.1.5 Different types of photoswitches derived from hemithioindigo and stilbene.⁷⁶

1.5 Hemithioindigo photoswitches

Given that these photochromes can rapidly switch upon the presence of visible light allows for non-invasive control and tuning. Hemithioindigos often switch from the usually more thermodynamically stable *Z* isomer to the *E* isomer upon visible light irradiation between 410-660 nm.



Scheme 1.5 Isomerization of hemithioindigo upon irradiation with visible light.

The photoisomerization occurs rapidly (on the order of picoseconds). Quantum chemical computational methods (DFT/BHLYP/DZP) of the HTI moiety confirm that the *Z* isomer is lower in energy (~ ca. 17.6 kcal/mol)⁴² at the electronic ground state in comparison to

its *E* counterpart. While the *Z* form is favoured in the electronic ground state, both isomers are nearly degenerate in the first excited state (S_1) with the *E* being slightly more stable. Usually, both hemithioindigo isomers are planar and the thermal stabilities at room temperature are relatively high with the *E/Z* isomerization possessing a transition energy barrier greater than 27 kcal/mol.⁴⁰ In comparison to conventional photoswitches, researchers have shown HTI photoswitches to hold high resistance against photofatigue and to withstand thousands of photocycles.³⁷

In general, the absorption of visible light results in four processes of decay: fluorescence, phosphorescence, internal conversion and intersystem conversion or crossing shown in Figure 1.5.1.

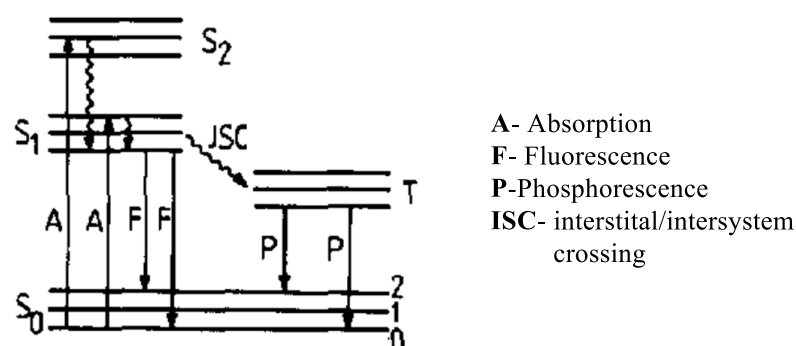


Figure 1.5.1 The Jablonski diagram depicting transitions between S_0 , S_1 , S_2 and T_1 in a given photoreversible system where A= absorbance; F= fluorescence; ISC= Intersystem crossing; P = phosphorescence; T = triplet state.⁸¹
(Image reproduced with permission; license #4842731145861)

Jablonski proposed a model where he described the processes involved with each transition. After absorption of light (A), the photon is now in the excited singlet state (S_1). There it can be released as fluorescence (F) back to the ground state or relax as internal conversion and remain in the same energy level. If intersystem crossing (ISC) occurs, the

photon enters the triplet state (T_1) and is classified as a “forbidden transition”. Relaxation from the triplet state can occur in a process called phosphorescence.

In terms of their absorption spectra, the *trans* isomer of HTI displays three maxima; the absorption at the shortest wavelength corresponds to the symmetry allowed $\pi \rightarrow \pi^*$ transition representing the first singlet state (S_1), the second absorption near 500-550 nm is characteristic of the subordinate symmetry allowed $\pi \rightarrow \pi^*$ transition denoting the second singlet state (S_2) and lastly the most bathochromic shift denotes the $n \rightarrow \pi^*$ energy level band yielding the triplet excited state (T_1). After irradiation of the *trans* isomer, the *cis* possesses one maximum around 300-500 nm due to the coincident absorption of both $\pi \rightarrow \pi^*$ transitions. The hypsochromic shift of the $n \rightarrow \pi^*$ energy level band is characteristic of the *cis*.

Liu and coworkers examined the nonadiabatic molecular dynamic stimulations of unsubstituted HTI bonded with stilbene across the double bond to better understand the photoisomerization mechanism in polar vs non-polar solvents. In cyclohexane solvent, small barrier energy, 5.97 kcal/mol, allows for double bond rearrangement and 6.34 kcal/mol promotes single bond rotation in DMSO solvent.⁴⁰ They measured the dihedral angles between the carbonyl oxygen of HTI and the hydrogen atom of DMSO and found constant values of 0° in the ground and excited state. The electrostatic potential map defined areas of high steric repulsion during the double bond rotation in DMSO and the single bond rotation in cyclohexane. Thus, single bond rotation of the photoswitch is favoured in DMSO whereas double bond cleavage and formation is consistent in cyclohexane.

Zinth and coworkers reported other processes occurring upon excitation.⁸² Upon absorption of a photon within the visible light range, a large amount of excess energy is generated. This induces energy dissipation, photon relaxation and release of some energy into the solvent leading to a relaxed state (RS) in a matter of picoseconds. Afterwards, the central double bond begins to slightly deviate from the horizontal characteristic of a twisted species exhibiting charge-transfer character (CTC). The return of the twisted species to ground state is hindered by a transition barrier and thus continues to twist resulting in a completely twisted structure. Herein, the HTI favours a structure that is lower in energy thus the twisted structure transforms to the *E* isomer.

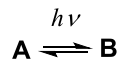
The mechanism of the *Z/E* photoisomerization process of HTI has gone through many debates over the years. The most accepted mechanism, aligned with Zinth and supported by Plötner⁴², comprises radiationless intersystem crossing from the singlet to the triplet state (states of different configuration). After the absorption of a photon (photoexcitation), an electron is excited to the S_1 energy state. The relaxation of the initial excited population state within the S_1 energy state supplies a small fraction of energy for some *Z* to isomerize to the ground state *E* form. The second decay of the *Z* isomer prompts a configurational change to the completely twisted state with substantial CTC. The excited twisted *Z* then decays back to the ground state where it transforms to the *E* and the rest is released as fluorescence.

The switching kinetics of HTI, the polarity and stability of its isomers, and other photophysical properties are greatly solvent and substituent dependant. Dube *et al.* investigated substituent effects on various hemithioindigo derivatives.⁴¹ Faster photoisomerization were achieved by stronger donor-acceptor frameworks. Looking at

the structure of HTI, the carbonyl group (C=O) serves as a hydrogen bond acceptor and substitution of R₂ with conjugated electron-donating groups on the stilbene fragment serves as the donor. Addition of electron-withdrawing groups on the thioindigo fragment and/or addition of electron-donating groups on the stilbene fragment positively increase the reaction kinetics of the HTI photoswitch.

1.6 Photostationary state (PSS)

The photostationary state (PSS) of a dynamic or living system is the equilibrium state wherein the rates of the forward reaction are equal in value to the rates of the reverse reaction for each of the participating species.⁴³ Therefore, we can conclude that in any photoreversible system, (in which A transforms to B),



Scheme 1.6 In a given photoreversible system A and B interconvert interchangeably at the PSS in the presence of light.

A and B are isomers where the quantum yield of $\text{A} \xrightarrow{h\nu} \text{B}$ is denoted by ϕ_{A} and the quantum yield of $\text{B} \xrightarrow{h\nu} \text{A}$ is denoted by ϕ_{B} with A, B denoting the concentrations of A, B respectively.

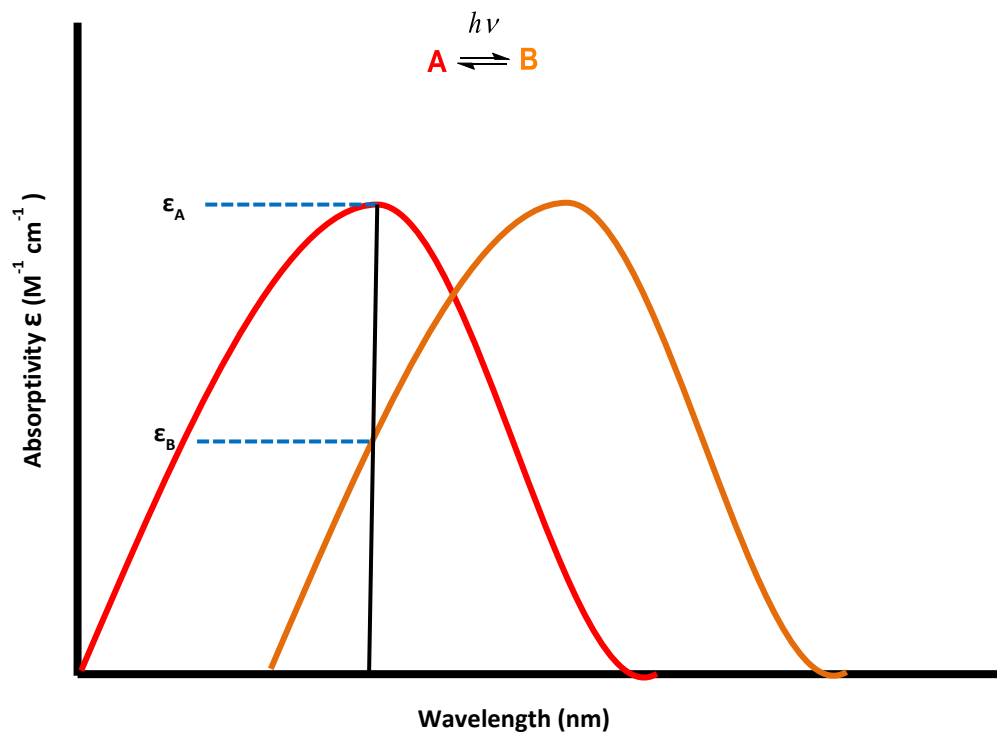


Figure 1.6.1 In a given photoreversible system A and B have distinct absorption spectra which defines their absorbivity and λ_{\max} .

Then the amount of B formed, η_B , is proportional to the absorbivity of A, ϵ_A , and the quantum yield of the photoconversion of $A \rightarrow B$, $\phi_{A \rightarrow B}$, shown by Equation 3.⁴⁵

$$\eta_A \propto \epsilon_B \cdot \phi_{B \rightarrow A} \quad \text{Equation 2}$$

$$\eta_B \propto \epsilon_A \cdot \phi_{A \rightarrow B} \quad \text{Equation 3}$$

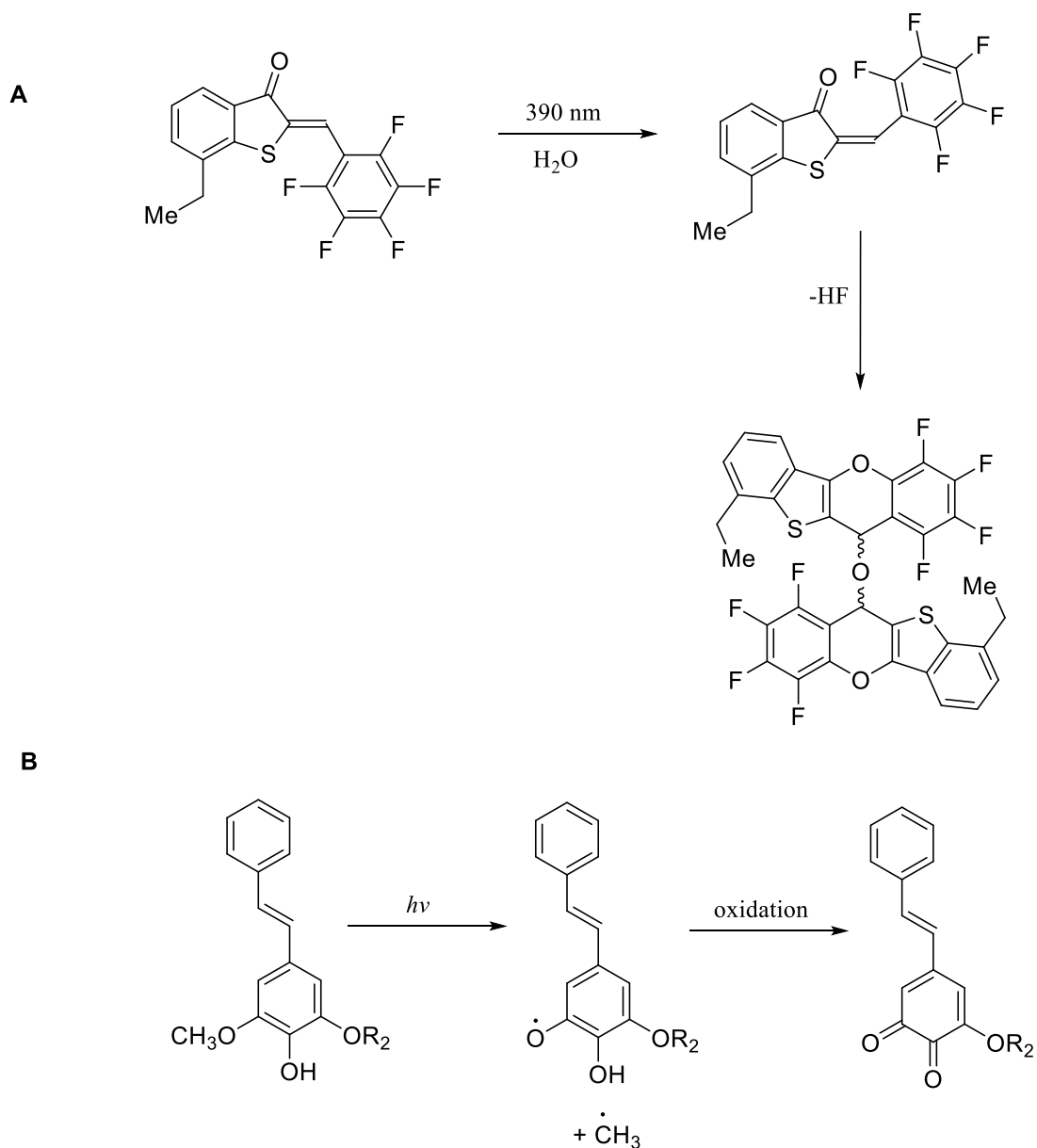
$$\frac{\eta_B}{\eta_A} = \frac{\epsilon_A \cdot \phi_{A \rightarrow B}}{\epsilon_B \cdot \phi_{B \rightarrow A}} \quad \text{Equation 4}$$

The reverse transformation is true for the amount of A formed, η_A , which is proportional to the absorbivity of B, ϵ_B , and the quantum yield of the photoconversion of $B \rightarrow A$,

$\phi_{B \rightarrow A}$, shown by Equation 2.⁴⁵ At the equilibrium state or the PSS, the ratio η_B / η_A is constant and can be rewritten as Equation 4. Interestingly, both isomers (A and B) produce close but varied absorption spectra suggesting that at a specific wavelength one isomer absorbs more strongly than the other giving rise to unique physical and chemical properties.

1.6.1 Excessive UV-Vis Irradiation Outcomes

Unfortunately, many photochromic material studies have shown that consistent irradiation of one isomer leads to a loss of reactivity and function and is referred to as fatigue in materials or more specifically photodegradation in photoresponsive materials.^{35,36} Excessive irradiation over time can promote the rise of side reactions or multiple excited species that may come together to form a dimer or excimer (excited dimer). These new products in solution can interfere with the interactive forces between native photoswitches thereby deteriorating the expected responses of the photosystem. Figure 1.6.1 displays the photodegradation process of a hemithioindigo (**A**), and a stilbene (**B**).



Scheme 1.6.2 The photodegradation process of a select few photochromic compounds after being subjected to excessive UV-Vis irradiation.^{26, 47}

Photodegradation is initiated by the formation of an excited state which reacts with a non-identical species in its environment. Molecular oxygen⁴⁸ is the most common cause of photodegradation because of its ability to oxidize other chemical species.

Fatigue resistance is the ability of a material to withstand multiple rounds of stress or external stimuli without losing function over a prolonged period of time. In photochromic materials, this property is measured in terms of cycles of switching called photocycles as shown in Figure 1.6.1.1.

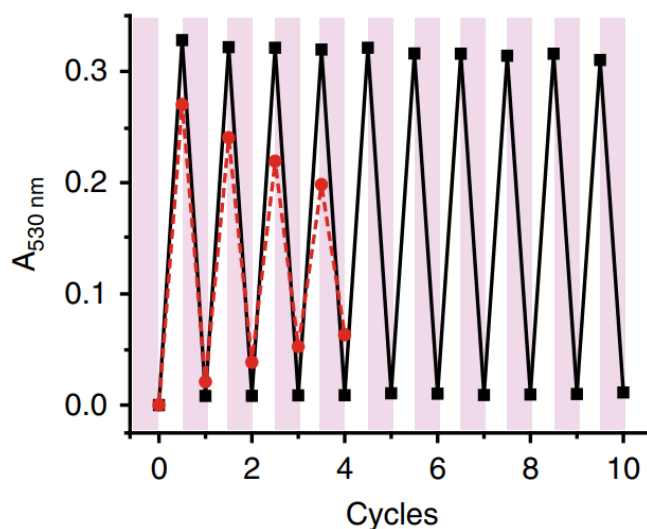


Figure 1.6.3 A graph displaying the fatigue resistance of a photoswitch (black line) and a fatigue system (dotted red line) upon successive switching between its isomers.⁸⁴

In a typical photocycle, the photoswitch is irradiated at specific wavelengths characteristic of each of its isomers to achieve the greatest conversion. The photoswitch is then converted repeatedly between its isomers over numerous cycles and acts as an “on” and “off” switch. The irradiation of the black line is consistent with a strong and efficient photoswitch whereas the red dotted line is decreasing in magnitude and intensity; signs of a weak photoswitch.

1.7 Nanotechnology and Smart materials

Lendlein et al., explain that “smart materials” are “able to respond to changes in their environment in a predetermined way” due to the ability of their “functional groups to accommodate a fascinating range of stimulation modes.”⁴ In addition, the large-scale manufacture of adhesives, inks, cosmetics and personal-care products have become more economic and require less processing costs with the use of supramolecular polymers.² Furthermore, environmentally safe yet robust and efficient materials have a very promising future in modern society.

1.7.1 Polymers

Conventional polymers have been synthesized by humans for more than 150 years with valuable roles in the automotive, medical, food, industrial and commercial sector. Advances in self-healing materials that involve rubber, protective coatings, adhesives, shape memory and electronic skins²⁵ have an underlying polymer backbone structure. Polymers are large macromolecules that are made up of many repeating units (called monomers) which are held together by intermolecular covalent interactions. Covalent bonds are a type of attraction where the distribution of electrons are shared between the atoms forming the bond.⁵⁴ Covalent bonds are irreversible, robust intermolecular forces that give a material strength, flexibility and contribute to its physical endurance. Polymers mainly stem from carbon and hydrogen atoms but can also contain sulfur, oxygen, nitrogen, chlorine and/or phosphorus atoms. Unfortunately, most polymeric-based materials like plastics lose value in the event of external damage (tear, rip, crack); a situation potentially solvable using supramolecular polymers.

1.7.2 Supramolecular Polymers

The idea that an external defect in a material can be fixed with little to no damage to the overall material sounds very promising, even a bit misleading. In practice, the broken non-covalent bonds can be reformed conserving most of the functionality and integrity of the material which is why they are often termed “living polymers”⁵¹. This is because supramolecular polymers share the same definition as polymers except that their monomers are linked together by reversible, often highly directional, non-covalent interactive forces, resulting in “polymeric properties in solution and in bulk”⁵⁰.

Supramolecular polymers are even responsive to external stimuli. Nicoletta *et al.* have recently discussed in an article the three categories of which stimuli-responsive polymer membranes can interact with their environment:⁴⁹

1. Direct or to a specific cue (pH, ion signals, membrane protein signals)
2. Indirect or a change in performance or activity (temp., increase/decrease in signal)
3. Field-induced (light, electric/magnetic field)

The stabilities of supramolecular complexes are often described in terms of association constants, K_a , for complementary arrays and more specifically dimerization constants for self-complementary arrays, denoted by K_d . There exists a logarithmic relationship between the K_a (or K_d) and the degree of polymerization for any given supramolecular polymer graphed as illustrated in Figure 1.7.2.1.

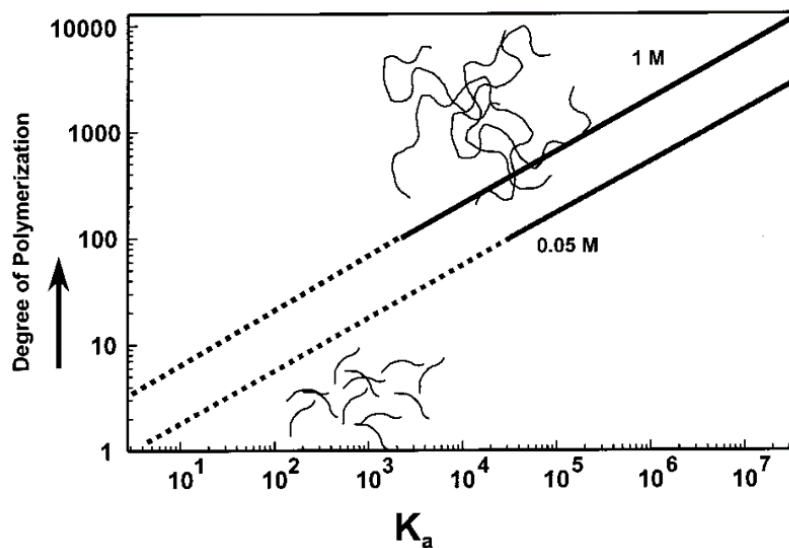
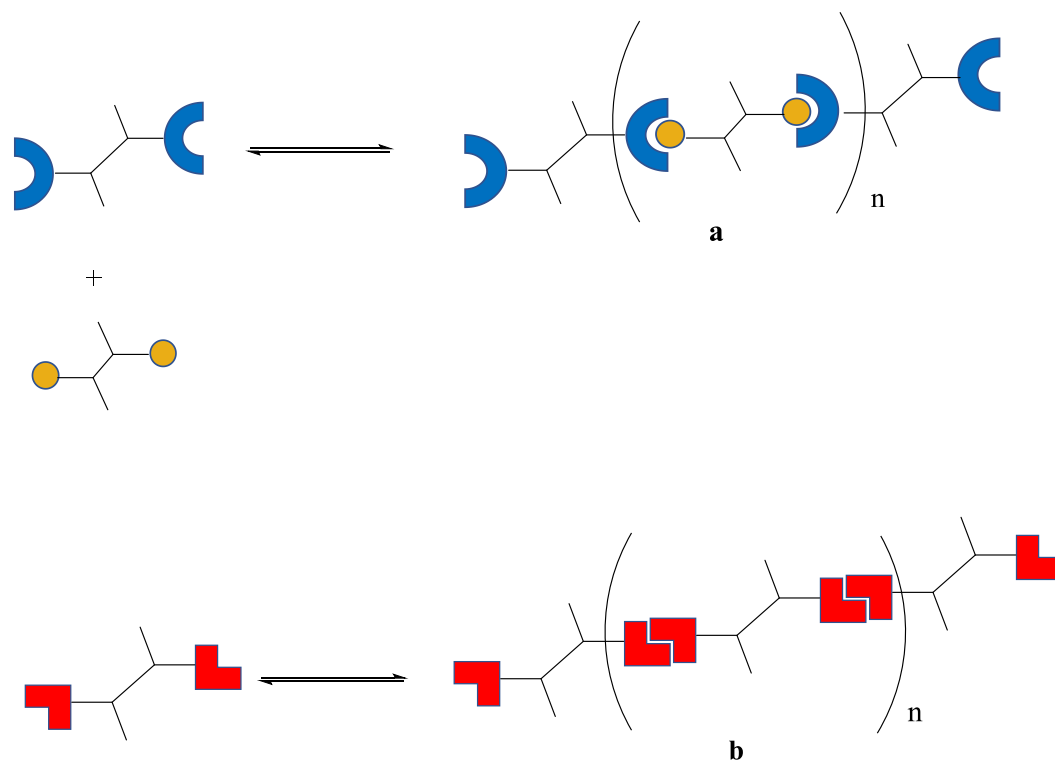


Figure 1.7.2.1 The relationship shown between the K_a and the rate of formation of supramolecular polymers.⁵¹

When exploring supramolecular geometries and binding strengths, there two basic arrangements to consider. Firstly, an interaction can form between complementary monomers (Figure 1.7.2.2 a) where one monomer binds strongly to a second non-identical monomer; similar to puzzle pieces. Secondly, self-complementary monomers (Figure 1.7.2.2 b) can interact with themselves due to the presence of complementary structures within each monomer unit.



Scheme 1.7.2.2 Two representative diagrams reflecting the formation of supramolecular polymers between complementary monomers, **a**, and self-complementary monomers, **b**. Image modified from reference [3].

In addition, Figure 1.7.2.3 presents a triple hydrogen bond complementary array with a K_a of 10^2 M^{-1} , a quadruple hydrogen bond self-complementary array with a K_a of 10^7 M^{-1} and a sextuple hydrogen bond complementary array with a K_a of 10^9 M^{-1} . Generally, the greater the number of hydrogen bond acceptor (HBA)/donor (HBD) pairs, the stronger the attraction between the two molecules, and the higher the association constant.

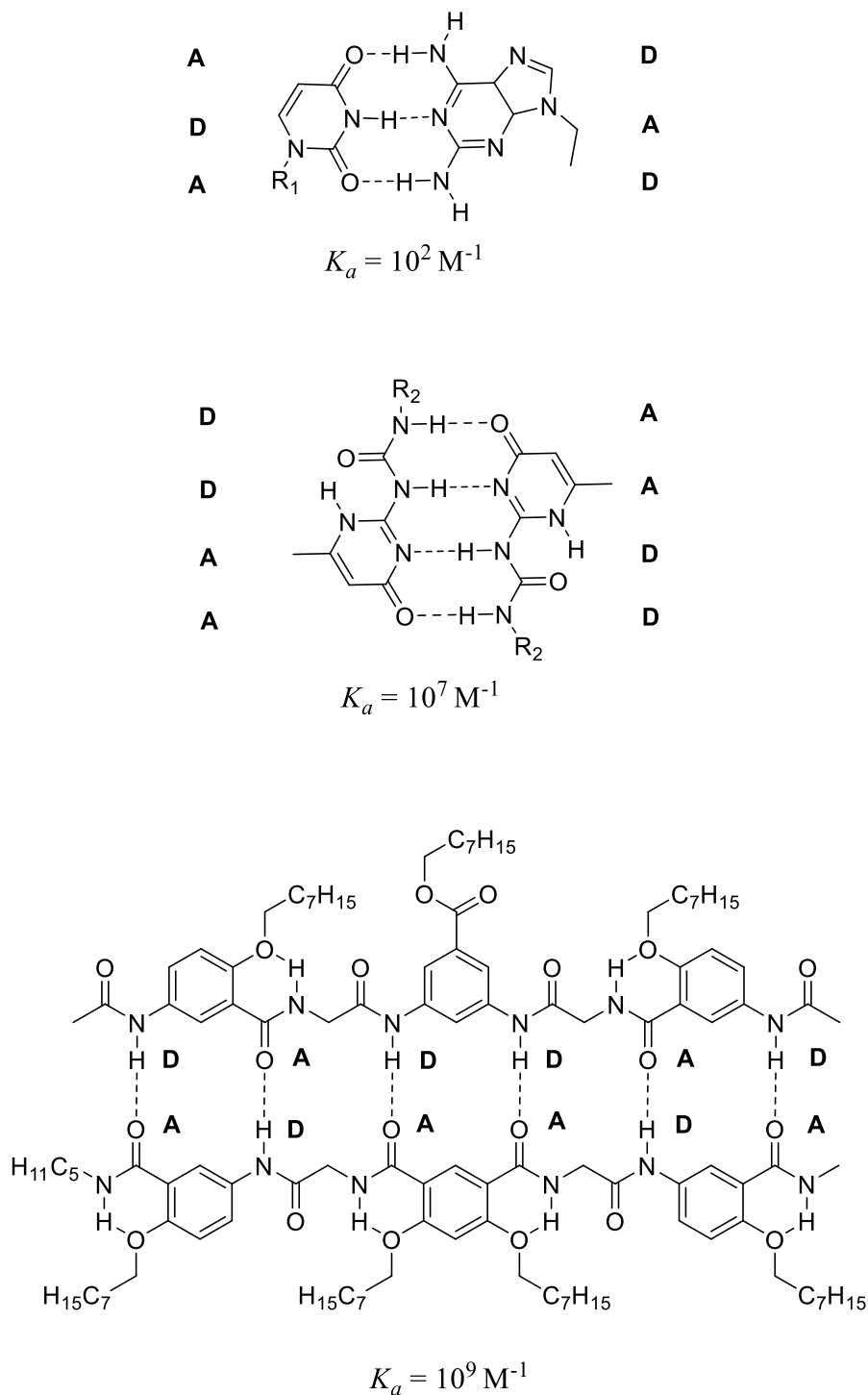


Figure 1.7.2.3 Three structures depicting various supramolecular complexes in order of increasing K_a : triple, quadruple, and sextuple hydrogen bonded arrays. Image modified from reference [50].

Of the two classes of supramolecular arrangements, five substantial combinations of supramolecular complexes can exist from these following monomers as outlined by Zhang *et al*: AA, AB, AA/BB, ABBA and aromatic-stacking (π - π stacking).⁵⁰ AA is composed of identical monomers to create a self-complementary dimer. AB and AA/BB types involve a complementary complex where AB monomers are assembled head to tail whereas AA/BB heterodimerize in an alternating manner. ABBA monomers coherently inhibit dimerization and cyclization which result in strong, linear arrays. Lastly, π - π stacking is mainly introduced by aromatic groups functionalized with electron donating/electron withdrawing groups to promote the rate of polymerization. The first case will be examined across several self-complementary hydrogen bond arrays.

1.8 Non-covalent bonding interactions

Covalent bonds have been the focus of most polymer designs due to their strength, thermal stability and high synthetic yields. However, the covalent nature of these polymers are short-range (ca. 2 Å), are usually unresponsive to external stimuli and result in materials that may be permanently damaged by breaking these bonds. Non-covalent interactions vary in strength and stability and include metal coordination, host-guest interactions, dipole-dipole, aromatic stacking and hydrogen bonding. Table 1.8 summarizes various non-covalent interactions and other properties such as the intermolecular force strength as a relation of distance. These interactive forces range from 0 kJ/mol to 300 kJ/mol and possess a variety of stabilities.

Table 1.8 Summary of non-covalent forces and their characteristics ⁵³

Non-covalent force	Strength (kJ/mol)	Relative Stability	Distance dependence	Example
Ion-ion	200-300	High	1/r	Tetrabutylammonium chloride
Ion-dipole	50-200	High	1/r ² , 1/r ⁴	Sodium [15]crown-5
Dipole-dipole	5-50	Low	1/r ³ , 1/r ⁶	Acetone
Hydrogen bond	4-120	Medium	See Table 1.7.1	H---F---H
Cation- π	5-80	Medium	1/r ² , 1/r ⁴	K ⁺ in benzene
π - π	0-50	Low	1/r ³ , 1/r ⁶	Benzene and graphite
van der Waals	<5	Low	1/r ⁶	Argon (crystals)
Hydrophobic	Dependent on solvent-solvent interaction	High	N/A	Cyclodextrin-related compounds

These intermolecular forces are largely responsible for a molecules' colligative properties like boiling point elevation and freezing point depression, etc. The energy associated with non-covalent interactions under ambient conditions are approximately equal to the average thermal energy of the kinetic motion of the molecules.⁵⁴ In other words, a single non-covalent bond, like an ion-ion bond, can be broken whereas a combination of several different types of interactive forces (electrostatic, dipole-dipole, hydrogen bond) creates a dynamic yet stable system.

Amongst the non-covalent interactions, hydrogen bonds (H-bond) stand out to natural science researchers. The role that hydrogen bonding plays in all aspects of

biological life is crucial to sustaining nature's miraculous nanomachines and biological processes. Hydrogen bonds can be as simple as the $\text{H}_2\text{O}\cdots\text{H-OH}$ interactions found in water or the intricate $\text{N-H}\cdots\text{O}$ interactions between complementary nucleotide base pairs found in DNA and thus, are often the main driving force for initiating supramolecular research studies. Hydrogen bonds are of utmost importance due to their participation in vital bodily functions such as protein folding, binding complementary nucleotide base pairs to form the 3D double helical structure of DNA and the remarkable properties of water as a solvent.

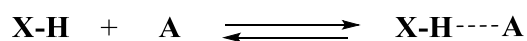
1.9 Hydrogen Bond

The definition of the hydrogen bond cannot be attributed to any one person as the official identification of hydrogen bonds was circulated and tweaked from a concept to a property to a non-covalent interactive force. Articulation of this novelty transpired in the early 1900s until the 1980s with revival of this non-covalent interaction in the 1990s. Early discussions in 1902 by Werner, Hantzsch and Pfeiffer denoting primary and secondary valences used the terms “nebenvalenz” and “innere komplexsalzbildung” to refer to intra- and intermolecular hydrogen bonds.⁵⁹ In 1912, Moore and Winmill introduced the “weak ion” terminology to describe the attractive force between an amine and a water molecule upon dissolution. Later in 1919, Huggins noticed that a hydrogen nucleus may be held between two oxygen atoms with octets in what looked like a “hydrogen bridge”.⁶⁰ It wasn't until the X-ray structure analysis was available (around 1930) that Linus Pauling called the interaction between a fluorine atom bound between two hydrogens, as the “hydrogen bond”. In his book “*The Nature of the Chemical Bond*”

(1939) he wrote, “an atom of hydrogen is attracted by....strong forces to two atoms, instead of one, so it may be considered.....a bond between them.”⁶⁰ In 1997, Jeffrey published a book, “*An Introduction to Hydrogen Bonding*” where he summarizes Pimental’s and McClellan’s (1960) definition as “a donor-acceptor interaction specifically involving hydrogen atoms”⁵⁸. This comes from the comparison that HBDs act as Lewis acids and HBAs as Lewis bases.

In 2011, IUPAC released an updated definition of a hydrogen bond encompassing most cases;⁶¹

“The hydrogen bond is an attractive interaction between a hydrogen atom from a molecule or a molecular fragment $X-H$ in which X is more electronegative than H , and an atom or a group of atoms in the same or a different molecule $[A]$, in which there is evidence of bond formation”.



Scheme 1.9 The hydrogen bond interaction given by IUPAC.

IUPAC took references from several sources, one of which was from 1960. During that time Pimentel and McClellan had their own definition of a hydrogen bond. Jeffrey and other scientists had limited interpretations and didn’t include non-conventional hydrogen interactions like $CH-\pi$. Pimental and McClellan’s was unique because of two additional criteria:⁶¹

- (i) evidence of bond formation (association or chelation)
- (ii) the new bond linking X-H and a group of atoms (A) involves existence of X-H formation prior to H-bond

The first requirement relies on three factors; geometry, the nature of the intermolecular forces involved and the method of experimental analysis. Whether the hydrogen bond forms via association with a HBA or occurs by a chelating agent, the directionality of the $\angle X-H \cdots A$ is one defining characteristic which can vary but is often linear or 180° . The H-bond also refers to the directionality of the bond in the presence of other intermolecular forces such as polarization and dispersion forces. Evidence of a hydrogen bond can be seen using multiple spectroscopy techniques such as IR or NMR to name two.

The terms acceptor and donor are central to understanding the hydrogen bond. In a hydrogen bond there are two groups: X-H; labelled as the hydrogen bond donor (HBD) and the receiving group of atom(s): A; labelled as the hydrogen bond acceptor (HBA). Typical donors are usually electronegative atoms with at least one attached hydrogen, but are not limited to oxygen, nitrogen, and sulfur. Typically, donors are Bronsted acids. These include any species capable of donating a H^+ . Equally, acceptors are Lewis bases- any species capable of donating a non-bonding electron pair. Acceptors range from electronegative atoms with lone electron pairs to the π - electrons of an unsaturated or aromatic system.

1.9.1 Hydrogen Bond Distinction

Hydrogen bond interactions between water molecules differ from those between ethanol molecules. They have distinct infrared vibrational stretching frequencies, bond energies and bond angles. Jeffrey classified hydrogen bonds based on their strength (strong, moderate, weak) as well as bond angle and bond energy amidst other parameters listed in Table 1.9.1.⁵⁸⁻⁶² Experimentally, hydrogen bonds can be proven to exist. The distance between X-A is less than the sum of the van der Waals radii of the two atoms X and A.⁶² Upon hydrogen bonding, there is an increase in the X-H distance, shifting the X-H stretching vibrational frequency to lower wavenumbers seen in an IR spectrum.⁵⁵ Another noticeable spectroscopic measure of hydrogen bonding is by Nuclear Magnetic Resonance Spectroscopy (NMR). Formation of the X-H...A bond causes the hydrogen atom to become electron deficient in the presence of the HBA, decreasing the magnetic shielding of the proton, shifting the chemical shift downfield or towards higher ppm. Studies have shown that the anisotropy of the proton magnetic shielding can be increased up to 22ppm.⁶²

Table 1.9.1 Summary of H-bond properties and their characteristics

H-bond parameters	Strong to Very Strong	Moderate to Strong	Weak
Interaction Type	Strongly Covalent	Mostly Electrostatic	Electrostatic/Dispersed
Bond Energy (kcal/mol)	60-170	15-60	<15
Bond Length (H...A[Å])	2.2-2.5	2.5-3.0	3.0-4.0
X-H vs H...A	X-H \approx H...A	X-H < H...A	X-H \ll H...A
Bond angle (°)	170-180	>130	>90
Relative IR shift	>25%	5-25%	<5%
Directionality	Strong	Moderate	Weak
Downfield ^1H chemical shift (ppm)	14-22	<14	Undifferentiable
Examples	[F...H...F] ⁻ [N...H...N] ⁻	(O – H...O=C) (N – H...O=C)	(C – H...O) (O – H... π)

Strong to very strong H-bonds exhibit attributes of covalent bonds which are considerably stronger than the weakest covalent bonds at energies of 60-170kcal/mol. Examples include hydrogen bonds formed between fluorine and nitrogen. Desiraju and Steiner organized hydrogen bonds as very strong, strong, moderate and weak whereas Jeffrey systematized them as strong, moderate and weak depending on the relevance and abundance of hydrogen bonds as they apply in specific applications. Nevertheless, they both agreed on one concept: the hydrogen bond is not a simple interaction.

1.9.2 Hydrogen Bond Strength

The strength of hydrogen bonds is dependent upon several factors. Some are contingent on the type of atoms involved or the orientation of the HBA and HBD. The spatial rearrangement of the hydrogen bond involving the four atoms X-H \cdots A-B (where B is a substituent) is conditional on the configuration of the lone pairs of the acceptor, the overall orientation and polarity of any neighboring substituents and the planarity of both molecules. Linear H-bonds are the strongest with the angle between the HBD and HBA being 180°; however, other geometries can exist as shown in Figure 1.9.2.^{63,64}

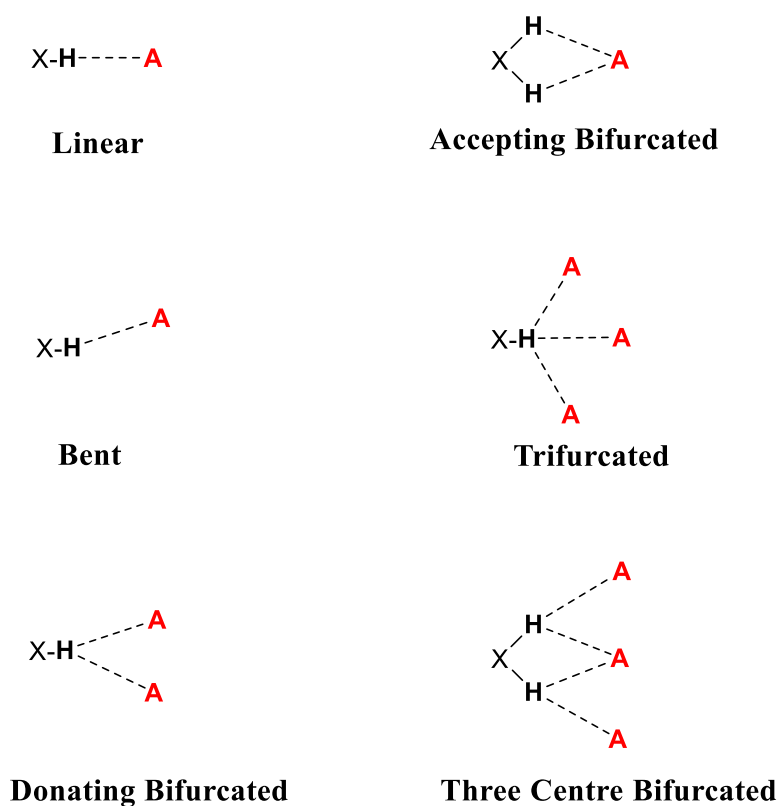
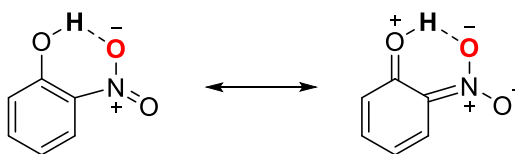


Figure 1.9.2 Six different geometries and angles at which hydrogen bonds can form.

H-bonds can form a variety of geometrical complexes such as accepting bifurcated, donating bifurcated and three centre bifurcated. In some cases where the two acceptors or two donors are a part of the same molecule, the term *chelated hydrogen bond* is used.⁶² The electrostatic origin (and therefore strength) of hydrogen bonds are affected by many factors as follows; electronegativity, resonance, polarization, and solvent effects. Each of these will be explored in further depth.

The electronegativity of the acceptor (A) as well as the atom covalently bonded to the hydrogen (X) affects the stability of the interaction. HBDs that exhibit a larger partial charge on the hydrogen atom tend to form robust H-bonds according to the trend HF > HCl > HBr > HI. Likewise, HBAs with a high δ^- charge pull electron density away from the hydrogen atom weakening the X-H bond whilst contributing to the H \cdots A bond.

In some cases, resonance stabilization greatly promotes the formation of the hydrogen bond. *O*-nitrophenol is known to engage in intramolecular hydrogen bonding as shown in Scheme 1.9.2.1. The nucleotide complementary base pairs within DNA engage in resonance-stabilized hydrogen bonding to a similar extent.



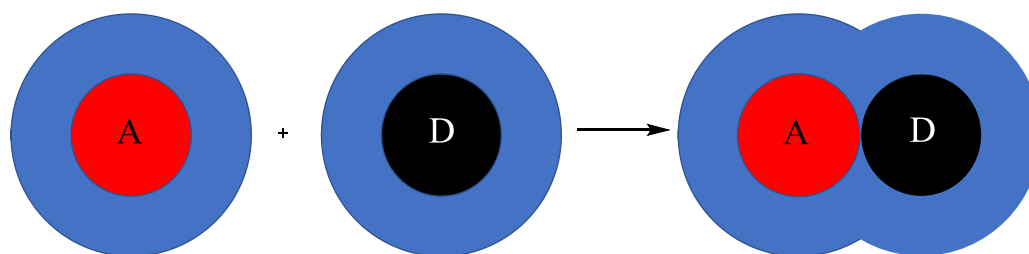
Scheme 1.9.2.1 Resonance stabilized hydrogen bond formation of *o*-nitrophenol.

When HBAs or HBDs on nearby molecular fragments increase or decrease the potential for its neighbour to form a hydrogen bond, it is a result of polarization.

Following the same illustration as resonance structures, a polarized interaction between

the hydrogen and the acceptor atom ($H^{\delta+}\cdots A^{\delta-}$) will contribute to a stronger H-bond. Crystal structures have confirmed bond energy increases upon cooperative or polarized hydrogen bonds binding three consecutive water molecules.⁵⁸ Thus, the microenvironment of hydrogen bonds is influenced by the proximity of other hydrogen bonds and their partial charges.

Most often hydrogen bonds are measured in solution. Thus, it is neglectful to ignore solvation effects on the strength and in turn the stability of H-bonds. Most HBAs and HBDs are solvated, that is, surrounded by water molecules prior to hydrogen bond interaction. In polar solvents, the hydrogen bond complexes are outnumbered by the solvent molecules hydrogen bonding to each unit. As such, they are competing for the hydrogen bond sites; these solvents would be termed competitive solvents. In non-polar solvents, the solvent molecules cannot form hydrogen bonds with the hydrogen complex resulting in a true and efficient measure of the hydrogen bonds; an advantage making them appear stronger. Solvation is the process where the solute is surrounded by a sphere of solvent molecules; called the solvent shell (shown in Figure 1.9.2.2). Vinter and coworkers conducted qualitative tests on hydrogen bonding interactions in a plethora of solvents and found that non-polar solvents such as carbon tetrachloride didn't interfere with hydrogen bond calculations as they showed little to no solvent competition.⁶⁷ According to Hunter, there always exists competition of sites between solute-solute, solvent-solvent and solute-solvent entities in solution.



Scheme 1.9.2.2 A HBA, A, and a HBD, D, are surrounded by solvent molecules (blue circle). Upon H-bond formation between A and D, the resulting complex becomes solvated. The potential for H-bond formation is dependent on the solvent's polarity.

Hunter investigated multiple trials of solute-solvent interactions with the following model equation depicting realistic results;^{65, 67}

$$\Delta G = -(\alpha - \alpha_s)(\beta - \beta_s) + 6kJmol^{-1} \quad \text{Equation 5}$$

α denotes the HBD constants whereas β denotes the HBA constants of the solute.

Likewise, α_s and β_s stand for the donor and acceptor constant properties of the solvent.

Considering a solute with neutral functional groups in solution, and if $\alpha_s > \alpha$, and if $\beta > \beta_s$, then favourable solvent-solvent donor interactions will dominate. If the solute's donor ability and the acceptor ability is higher than the solvent, ($\alpha_s < \alpha$, $\beta > \beta_s$) solute-solvent interactions will be in control giving a positive ΔG value. If the solvent has a high donor and acceptor capability, the same outcome is true. However, if the solute has a greater donor ability yet the solvent is a better acceptor ($\alpha_s < \alpha$, $\beta < \beta_s$), solute-solute interactions will prevail yielding a negative ΔG value. Therefore, a hydrogen bond array is favored if the solvent-solvent or the solute-solute interactions are greater than the solute-solvent interactions driving the formation of the H-bond.

1.10 Known supramolecular hydrogen bond arrays

Deoxyribonucleic acid (DNA) is one of the most universally recognized molecules understood as hydrogen bond complexes coiled intricately to form a spiral structure referred to as a double helix. The hydrogen bonded complexes are formed from the reversible interactions between nucleotide base pairs; adenine (A), guanine (G), cytosine (C) and thymine (T), where G and C form three hydrogen bonds with each other whereas A and T form two hydrogen bonds. Looking into the chemical structure of the nucleotide base pairs as shown in Figure 1.10, it is evident that the NH protons act as the donor and the carbonyl oxygen as the acceptor in the hydrogen bond interaction.

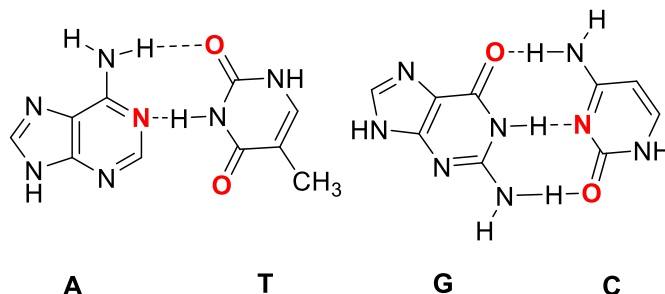


Figure 1.10 Nucleotide base pairs; adenine (A), thymine (T), guanine (G), and cytosine (C), which engage in two hydrogen bond interactions (A, T) and three hydrogen bond interactions (G, C) to form the 3-D double helical DNA structure.

1.10.1 H-bond donors/acceptors within supramolecular complexes

A hydrogen bonding monomer that participates in self-complementary binding, must contain at least one AD (where Hydrogen Bond Donor = D; Hydrogen Bond Aceptor = A) sequence whereas a monomer that engages in complementary binding needs only to contain a hydrogen bond acceptor as another monomer will contain a

hydrogen bond donor unit considering that the reverse is true. Figure 1.10.1 outlines some previously studied hydrogen bond supramolecular frameworks. The fact that these hydrogen bond arrays differ in magnitude is due in part to other factors that are not limited to steric hinderance, backbone rigidity, and competition of intramolecular binding sites.

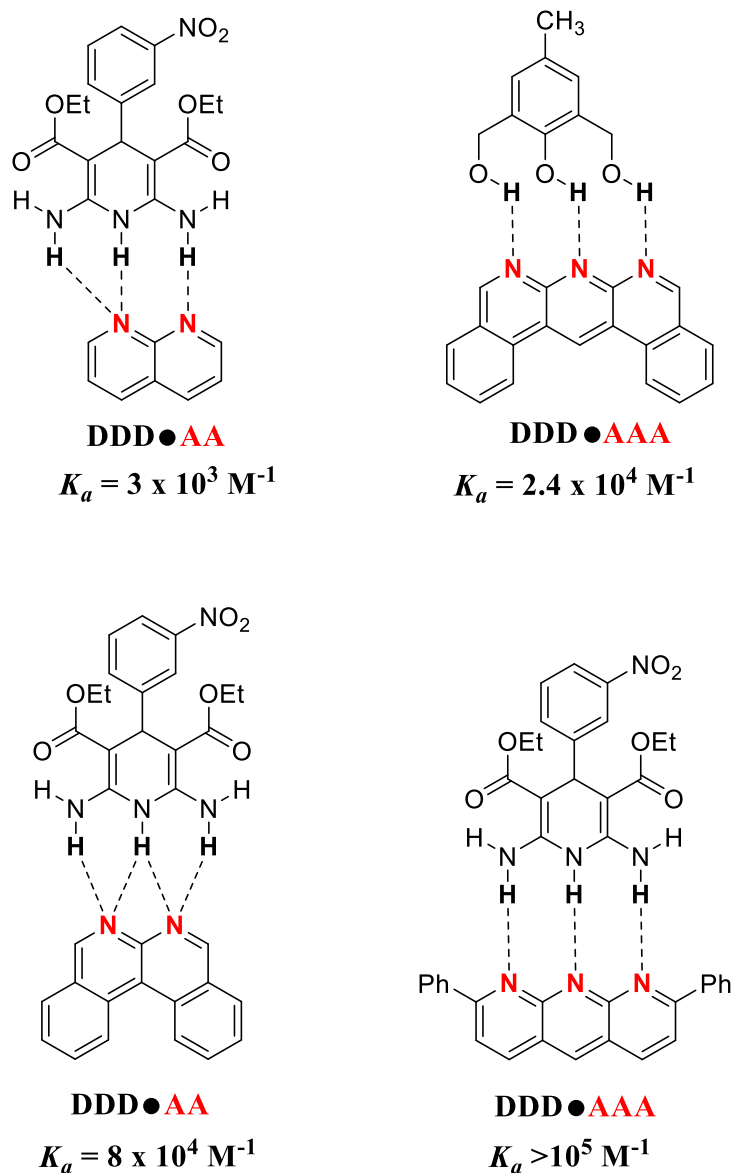


Figure 1.10.1 Various supramolecular complexes containing different geometries of hydrogen bond arrays studied in CDCl_3 at 298 K by Zerbetto et al.⁶⁸

When constructing a supramolecular hydrogen bond array, there are many approaches to consider. First most, a complex that has high thermal stability can withstand biological and environmental temperature fluctuations. Secondly, incorporating strong hydrogen bond donors and acceptors can be achieved by functionalizing substituents that possess high electron density on specific sites. This would lead to a robust yet dynamic supramolecular complex. In addition, the greater number of hydrogen bond sites, the greater the sum of the interactive forces and the stronger the overall array. Thirdly, the sequence of the hydrogen bond sites will rarely influence the primary interactive forces but will give rise to secondary repulsive forces diminishing the strength of the overall hydrogen bond composite. Some essential features defining the characteristics of excellent supramolecular hydrogen bond arrays will be explored in greater detail.

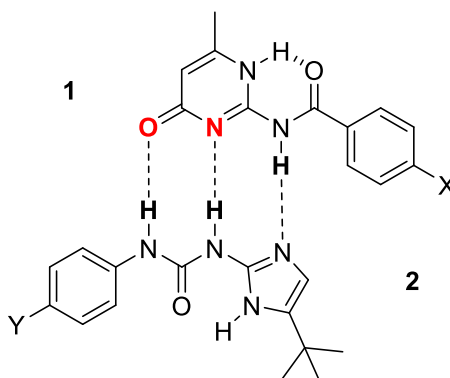
1.10.2 The Effect of the Functionalization of Substituents

Hydrogen bonds are formed between a hydrogen atom and an electron-rich atom like nitrogen, oxygen and/or fluorine. The greater the electronegativity of the hydrogen bond acceptor, the greater the electron affinity of the acceptor and the higher chance of forming a bond with hydrogen. On the other hand, the more electron poor the hydrogen atom is, the lower the electron affinity of the hydrogen and the greater potential for bond formation with the HBA. In 1995, a research group investigated the distribution of the electron density of C-H \cdots O bonds in comparison to O-H \cdots O.⁷¹ They concluded that charge density of the atoms within a H-bond should be used as a guide to delineate the rarer, overlooked cases of hydrogen bonding within biological systems. The difference in

polarization between the C-H bond vs the O-H bond resulted in a weaker hydrogen bond (calculated by quantum chemical computational methods) but nevertheless, a hydrogen bond.

In 2012, Wisner and coworkers studied the substituent effects of a complementary double-helical hydrogen bonded complex titrated with bis-pyridyl lutidine.⁷⁰ The hydrogen bond array was based on the diazonium salt of aniline functionalized with various substituents such as Br, CN, CO₂Et, CH₃ and the H substituted derivative as a native comparison. The installation of electron-withdrawing groups on the donor molecule (bis-indolyl-thiazine dioxide) increased the stability of the complexes as the developing partial charge on the nitrogen atom was minimized via electronic-resonance effects. Therefore, increasing the electron deficiency of the donor provided a site of low electron affinity for the acceptor to take advantage of. The K_a of the CN substituted derivative had a value of 1.1×10^5 in contrast to the native H derivative at 3.7×10^3 ; a 100-fold difference!

Wilson and coworkers established a similar analysis whereby they functionalized various electron-withdrawing and electron-donating units onto their hydrogen bond motifs.⁷² Their design consisted of two triple hydrogen bond heterodimers, amidoisocytosine (1) and ureidoimidazole (2), consisting of an AAD • DDA array as depicted in Figure 1.10.2.



AAD • DDA

Figure 1.10.2 Two triply hydrogen bonded heterodimers studied by Wilson *et al.* where they substituted various electron-donating and electron-withdrawing functional groups at X and Y in CDCl_3 at 298 K.

Amongst the derivatives, with methoxy being the most electron donating, and trifluoromethyl, being the most electron-withdrawing, the highest K_a value was $8.6 \times 10^4 \text{ M}^{-1}$. The same reasoning follows in that the methoxy group donates electron density into the resonance of the HBA strengthening its ability to attract an electropositive nucleus like hydrogen. The trifluoromethyl group pulls electron density away from nearby atoms and towards it due to the high electronegativity of the fluorine. With this push-pull system, the H-bond strengthens and with it, the stability of the supramolecular hydrogen bond array.

Table 1.10.2 Comparison of the electron-withdrawing ability of various derivatives on the association constant in CDCl_3 at 298K.⁷²

Identity	X	Y	K_a (M^{-1})
A	H	H	3.3×10^4
B	OMe	H	4.1×10^4
C	H	CO_2Et	8.4×10^4
D	Cl	H	1.8×10^4
E	CO_2Me	H	1.0×10^4
F	OMe	H	4.1×10^4
G	H	CF_3	8.6×10^4

1.10.3 The Number of Hydrogen Bond Sites

Two chemical bonds are stronger than one and three is stronger than two. The greater number of “bridges” or connections between two particles, the more force needs to be exerted to separate them. This statement holds true for hydrogen bonds as well. Figure 1.10.3 outlines double, triple and quadruple hydrogen bonded arrays with an increasing trend in the K_d or K_a . The greater the number of hydrogen bonds formed between two molecules, the higher the attraction between the two and the higher the K_a or K_d .

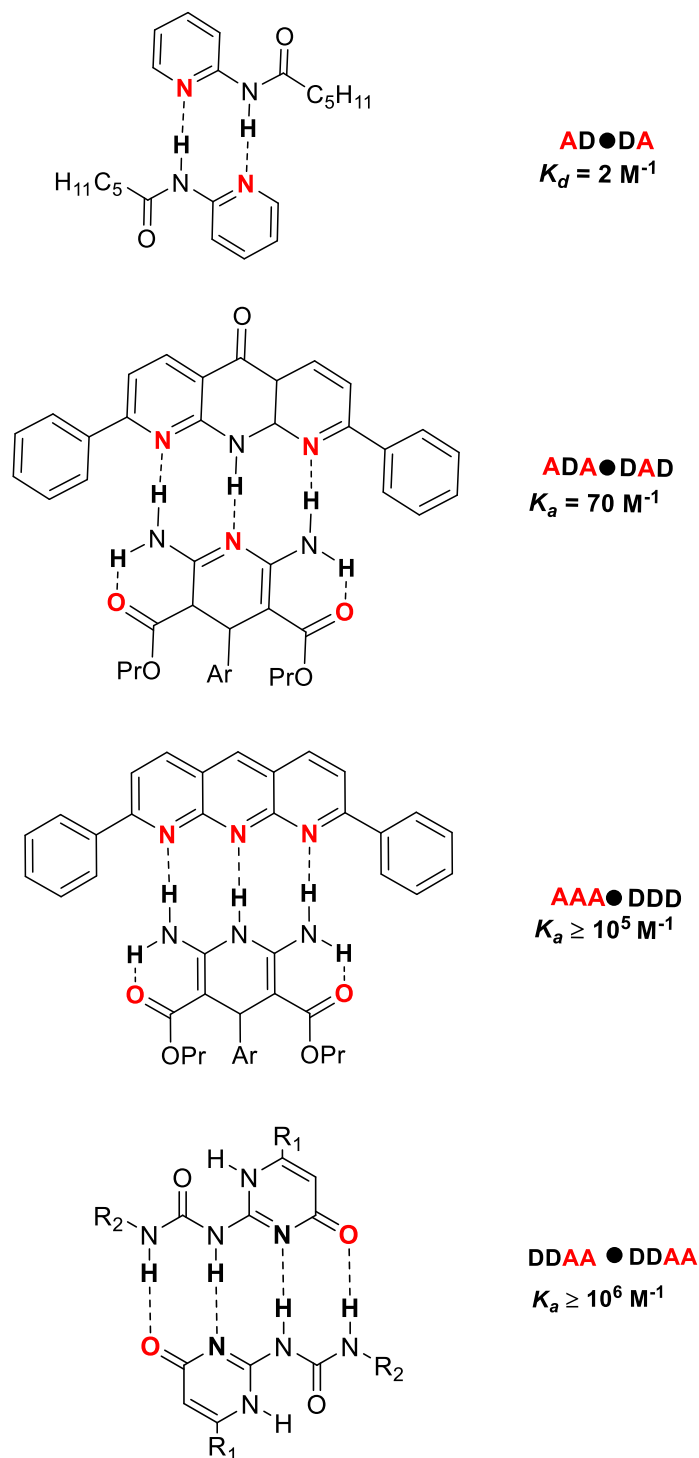


Figure 1.10.3 Various supramolecular complexes containing two and three donor and acceptor arrays in all possible arrangements studied by Zimmerman and Murray.⁶ Quadruple hydrogen bond arrays studied by Wienand et al.⁷³ All constants measured in CDCl_3 at 298 K.

Cooperativity, a term used to describe the binding properties of substrates in biochemistry, is the result of the binding of a second substrate molecule to the second subunit of the main enzyme or molecule wherein the main unit gains increased affinity towards a third or fourth substrate. This would be called positive cooperativity.

Negativity cooperativity would be the reverse where the binding of the first substrate decreases the affinity of the main unit from binding a successive substrate. When the first hydrogen bond forms, the adjoining sites are brought closer in proximity; thus, the affinity for the contiguous sites to form hydrogen bonds is energetically and sterically favored. As mentioned previously, crystal structures have confirmed the cooperative hydrogen binding energy upon addition of two and three water molecules.⁵⁸

1.10.4 The Sequence of Hydrogen Bond Arrays

The organization of hydrogen bond donor/acceptor sites into a regular array can greatly increase complexation strength by acting in a cooperative manner. The sequence of consecutive donors and/or acceptors within an array can either have a beneficial or unfavorable effect on the stability of a hydrogen bond complex because of the rise of secondary interactive forces. Figure 1.10.4 summarizes some typical recognition units involving two or three adjacent hydrogen bond donor and acceptor units in all possible arrangements.

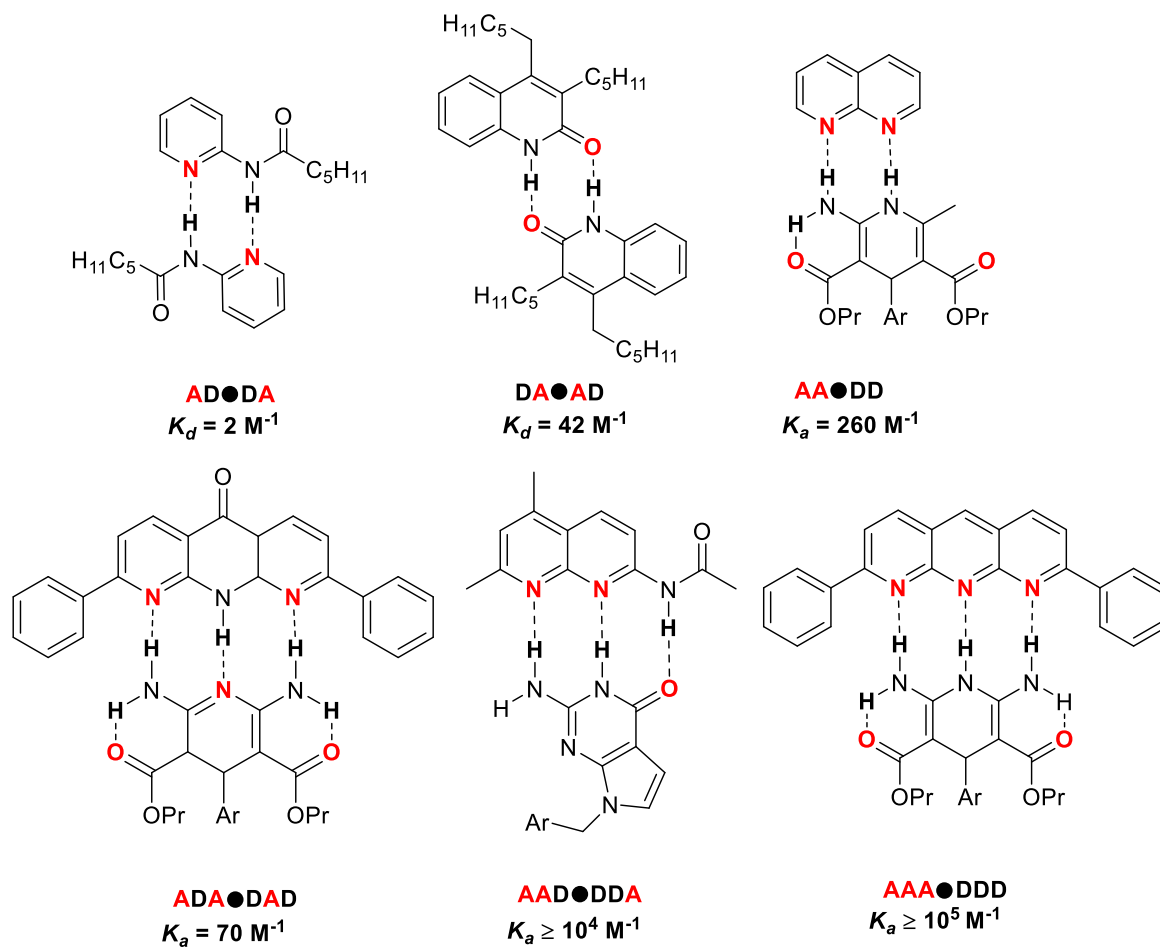
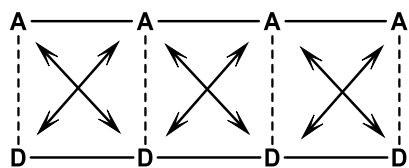


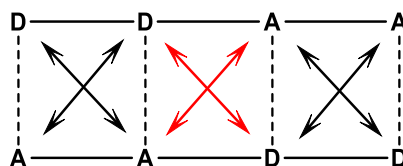
Figure 1.10.4 Various supramolecular complexes containing two and three donor/acceptor arrays as displayed by Zimmerman and Murray.⁹

The complexes shown above differ in K_a values drastically despite the identical number of acceptor and donor hydrogen bond sites. In the **AD•DA** motif, there exists two secondary repulsive interactions. The electron cloud of the nitrogen (as the acceptor) is within the vicinity of the opposing nitrogen (as the acceptor) creating a repulsive interaction between them and resulting in a very low K_a value; 2 M^{-1} . The same repulsive force is true for the donor atoms in this array. In the **DA•AD** we see a higher K_a , 42 M^{-1} due to the increased conjugation on either side. Lastly, the consecutive array, **AA•DD**

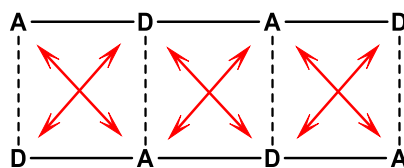
eliminates any secondary repulsive interactions and promotes secondary attractive interactions giving a higher K_a value of 260 M^{-1} . The same pattern is apparent in the triple hydrogen bonded heterodimers. The primary basis of the increase in association constant (K_a) for complementary systems or dimerization constant (K_d) for self-complementary systems is thought to be caused by the attractive and repulsive forces between neighboring acceptor and donor atoms. If the distance is within the van der Waals radii of bond formation relative to successive HBAs or HBDs, secondary intermolecular interactions begin to rise affecting the association constant. If the adjacent HBD is across from a neighboring HBA, the attraction is favorable. If the adjacent HBA is confronted with a like HBA, the secondary interaction becomes repulsive. Figure 1.10.4.1 summarizes some interactions regarding a four-bonding system.



C1



C2



C3

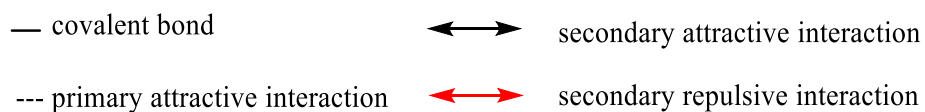


Figure 1.10.4.1 Various rearrangements involving a self-complementary hydrogen bond complex and their bonding interactions.

1.10.5 Tautomerization

Tautomerization is observed in strong hydrogen bonded systems and can often interfere with the complexation to a specific substrate in solution. Tautomerization refers to the intramolecular or intermolecular proton transfer between two atoms within a compound sometimes resulting in “structural isomerism with a low barrier to interconvert

between the isomers".^{74,90} Huggins recognized intramolecular hydrogen bonds as very stable;⁶⁰ in some cases so strong that an intramolecular proton transfer occurred. Thus, tautomerization involves the intramolecular transfer of a proton between two or more atoms. The most common example of two well-known tautomers are the *keto* and the *enol* form of carbonyl compounds, like acetone, shown in Figure 1.10.5.

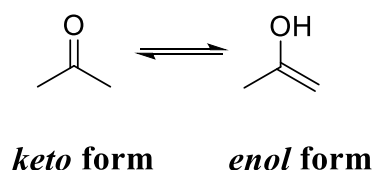


Figure 1.10.5 The tautomers of acetone comprising the *keto* and the *enol* form.

Tautomerization is observed in complementary hydrogen bonded arrays as the one shown in Figure 1.10.5.1 by Zimmerman and Murray. They noticed that (dipropyl 2,6-diamino-4-phenyl-1,4-dihydropyridine-3,5-dicarboxylate) **4** could undergo a tautomerization to its protomer, (1*Z*,1'*Z*)-(4-argio-2,6-diiminopiperidine-3,5-diylidene)bis(propoxymethanol) **4a** and still participate in hydrogen bonding with the substrate. Upon complexation of **4** with (2,8-diphenylpyrido[2,3-*b*][1,8]naphthyridine) **3**, only 15% of free **4** was detected when the concentration was ca. $2 \times 10^{-4} \text{ M}^{-1}$. Thus, they determined $K_a \geq 10^5$ due to the tautomeric ability of the supramolecular complex to switch between the two forms while hydrogen bonded to the resulting substrate.

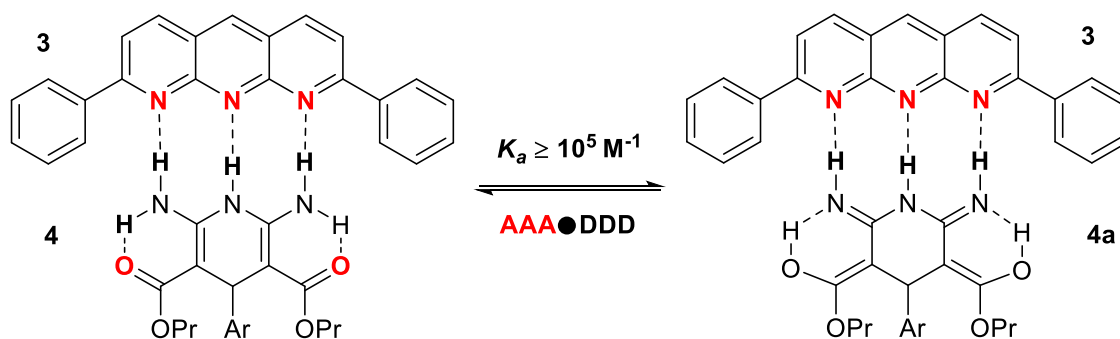


Figure 1.10.5.1 A complementary hydrogen bond complex displaying tautomerism as studied by Zimmerman and Murray in CDCl_3 at 298 K.

1.11 Design of Self-Complementary Hydrogen Bond Arrays

Among previously investigated self-complementary hydrogen bond arrays, the complexes introduced by Gong et al. in 1999 have interesting properties as shown in Figure 1.11.¹³ Gong and coworkers have successfully synthesized unique self-complementary hydrogen-bonding sequences consisting of **DADA** and **DDAA** arrays with a base consisting of N-(4-methoxyphenyl)acetamide units combined to form a dimerizable structure that engages in reversible yet dynamic hydrogen bond interactions.¹³ The dimerization constants of these derivatives ranged from $4.4 \times 10^4 \text{ M}^{-1}$ to $6.5 \times 10^4 \text{ M}^{-1}$ in CDCl_3 at room temperature proving to be an efficient hydrogen bonding system. Despite the substantial amount of free rotation, this unique structure is very stable and suggests insights into designing a new generation of supramolecular recognition sites with potential side chain tunability targeted toward a specific purpose.¹³

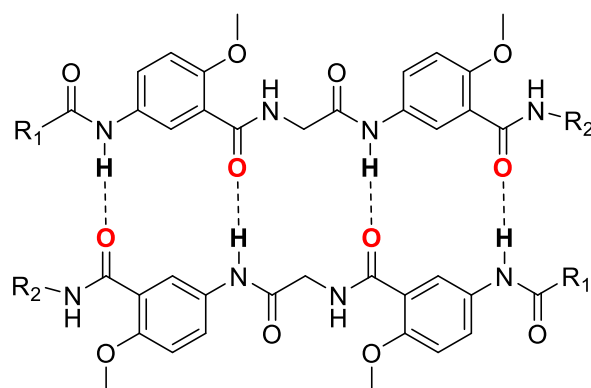


Figure 1.11 Self-complementary hydrogen bond network proposed by Gong *et al.* in 1999 with an **ADAD•DADA** sequence where the acceptors are in **red** and the donors are **bolded**.¹³

Recently, Wisner and coworkers have synthesized a hemithioindigo with an alkoxy thiophenone substituent and an acenaphthylenone group across a central double bond, assessed the photochemical properties and evaluated its interaction with various hydrogen bond donors. This hydrogen bond array proved to switch rapidly when subjected to ambient light from the more thermodynamically stable *trans* (*Z*) isomer to a mixture with the *cis* (*E*) isomer. To obtain the ratios of both isomers at the photostationary state (*ps*), a sample of pure *Z* isomer was irradiated with 520 nm light to obtain the *E* isomer and conversion back to the thermodynamic product was obtained at 450 nm. The hemithioindigo photoarray interconverts from the thermodynamically stable *trans* (*Z*) form to the *cis* (*E*) form by 180° rotation around a central double bond adopting an “*off*” and “*on*” state respectively. Of the complexes studied, the association constants (K_a) ranged from $7.0 \times 10^3 \text{ M}^{-1}$ to $>2.3 \times 10^5 \text{ M}^{-1}$.¹² This hydrogen bond array was part of a complementary system which is known to form strong hydrogen bond interactions and thus complexes as shown in Figure 1.11.1.

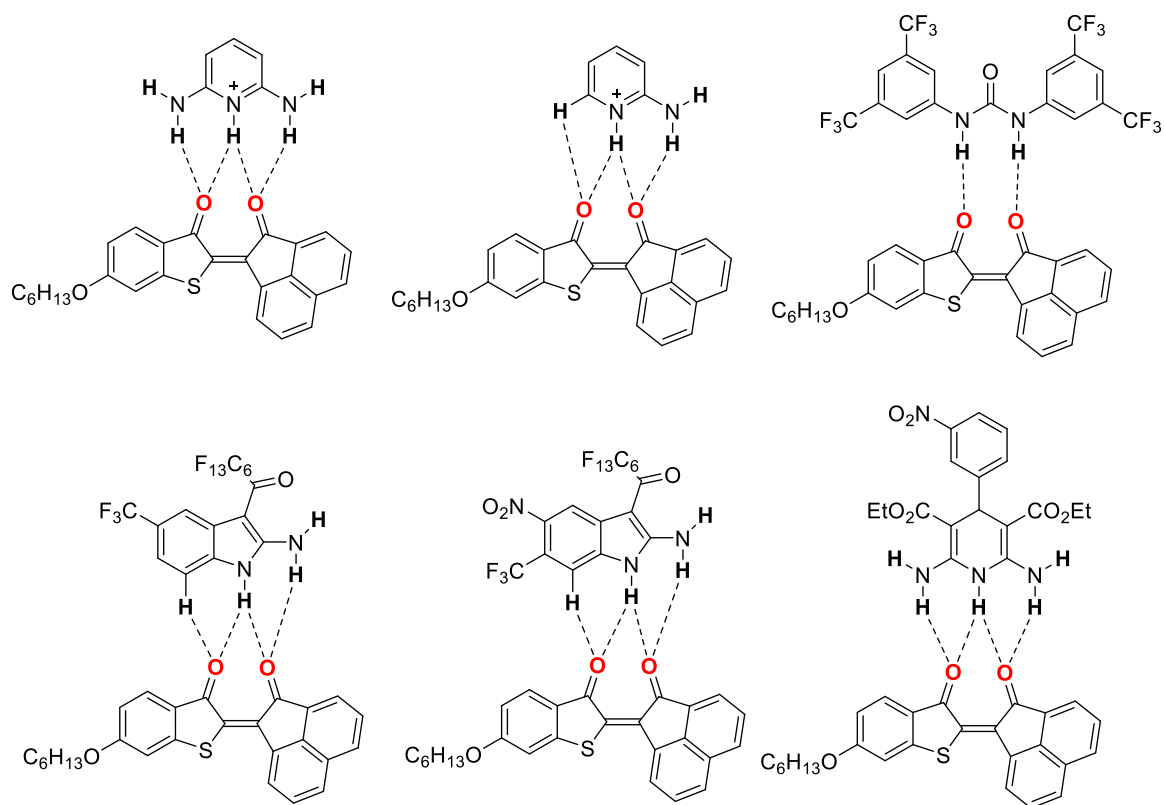


Figure 1.11.1 Hydrogen bonding interactions between (*Z*)/(*E*)-6,6'-diethoxy-3H,3'H-[2,2'-bibenzo[b]thiophenylidene]-3,3'-dione and donors.¹²

1.12 Subject and Scope of Thesis

This thesis will focus on the design, synthesis and characterization of the strength of the hydrogen bonding interaction between self-complementary hydrogen bond arrays intended for elaboration in supramolecular polymeric materials. The photoswitchable targets combine both donor and acceptor subunits and result in a self-complementary hydrogen bond array when present as the *Z* isomer. Given that they consist of a hemithioindigo and a urea group, it will engage in hydrogen bonding with itself as it contains both donors and acceptors in a **(DDAA • AADD)** complex. Additionally, substitution of the HTI arrays with different electron donating groups on the stilbene

portion enable stronger hydrogen bonding interactions between identical arrays. In principle, electron donating groups on the stilbene donate electron density into the π -conjugated system causing the carbonyl oxygen to become more basic as it becomes more electron dense. In addition to stilbene photochromes, a library of photoswitches will be synthesized including but not limited to acenaphthylenone, and julolidine photochromes (see Figure 1.12).

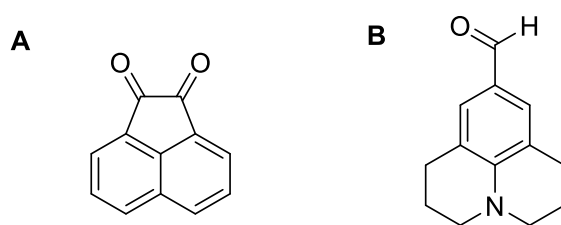


Figure 1.12 Electron-rich compounds utilized in the synthesis of the proposed photoswitches mentioned in this thesis.

Upon irradiation of visible light, the photoswitchable self-complementary arrays will reorganize and change configuration. Only one isomer is capable of binding strongly providing us with the ability to control the binding affinity of the photoswitch. In this sense, we are employing the photochemical properties of the hydrogen bond complexes as a non-invasive molecular tool turning their function “*on*” or “*off*”. This design incorporates both the arrangement of the Gong hydrogen bond donor/acceptor groups and hemithioindigo photochemistry to establish a photoreversible hydrogen bond array.

1.13 References

1. Lehn, Jean-Marie, *Polym. Int.*, **2002**, *51*, 825-839.
2. Greef de F.A Tom, Meijer, E.W. *Nature*, **2008**, *453*, 171-173.
3. Bouteiller, Laurent. *Advances in Polymer Science*, **2007**, *207*, 79–112.
4. Lendlein, Andreas; Feng, Yujun; Grijpma, Dirk W; Zhao, Yuanjin. *ChemPhysChem.*, **2018**, *19*, 16.
5. Laurent, Bous; Durr, Heinz. *Pure and Applied Chemistry*, **2001**, *73*, 639-665.
6. Zimmerman, S.C.; Murray, T.J. *Philos. Trans. R. Soc. London, Ser. A.*, **1993**, *345*, 49-56.
7. Wiedbrauk, Sandra; Dube, Henry. *Tetrahedron. Lett.*, **2015**, *56*, 4266-4274.
8. Morinaka A.; Yoshida, T.; Funakoshi, N. *Jpn. J. Appl. Phys.*, **1987**, *26*, 87.
9. Sadvovskii, O.; Beharry, A., A.; Zhang, F.; Woolley, A., G. *Angew. Chem. Int. Ed.*, **2009**, *48*, 1484-1486.
10. Toshiro, Tani; Itani, A.; Iino, Y.; Sakuda, M. *Jpn. J. Appl. Phys.*, **1987**, *26*, 77.
11. Zweig, E. J.; Newhouse, R. T. *J. Am. Chem. Soc.*, **2017**, *139*, 10956-10959.
12. Davoud, Fereshteh, "Thioindigo-Based Photoswitchable Hydrogen Bond Arrays", (2018), Electronic Thesis and Dissertation Repository. 5782.
13. Yan, Y.; Zeng, H.; Jankunn, S. E.; Kim, W. Y.; Zhu, J.; Ickes, H.; Gong, B. *J. Am. Chem. Soc.*, **1999**, *121*, 5607-5608.
14. Xu, W.; Chan, M. K.; Kool, T. E. *Nature Chem.*, **2017**, *11*, 1043-1055.
15. Steinle, W.; Rulck-Braun, K. *Org. Lett.*, **2003**, *5*, 141-144.
16. Koeppe, B.; Rompp, F. *Chem. Eur. J.*, **2018**, *24*, 14382-14386.
17. Shanker, N.; Dilek, O.; Mukherjee, K.; McGee, D.; Bane, S. *J. Fluoresc.*, **2011**, *21*, 2173-2184.
18. Hansch, C.; Leo, A.; Taft, W., R. *Chem. Rev.*, **1991**, *91*, 165-195.
19. Chen, J. S.; Shirts, R. B. *J. Phys. Chem.*, **1985**, *89*, 1643.

20. Orlandi, M.; Tosi, F.; Bonsignore, M.; Benaglia, M. *Org. Lett.*, **2015**, *17*, 3941–3943.
21. Katsuhiko Ariga, Toyoki Kunitake. *Supra. Chem. – Fund. and Appl.*, **2006**.
22. Hasenknopf, B.; Lehn, J. M.; Kneisel, O., B.; Baum, G.; Fenske, D., *Angew. Chem. Int. Ed. Engl.*, **1996**, *35 (16)*, 1838-1840.
23. Schmitta, J., L.; Stadlera, A. M.; Kyritsakasb, N.; Lehn, J. M., *Helvetica Chimica Acta.*, **2003**, *86*, 1598-1624.
24. Roke, D.; Stuckhardt, D.; Danowski, W.; Wezenberg, J., S.; Feringa, L., B., *Angew. Chem.*, **2018**, *57*, 10515.
25. Zhang, L.; Qiu, T.; Sun, X.; Guo, L.; He, L.; Ye, J.; Li, X., *Polymers*, **2020**, *12*, 989.
26. Jia, S.; Fong, W.-K.; Graham, B.; Boyd, B. J. *Chem. Mater.*, **2018**, *30*, 2873–2887.
27. Farinde, A., *Merck Sharp & Dohme Corp.*, **2020**. <<https://www.merckmanuals.com/professional/clinical-pharmacology/pharmacodynamics/drug%E2%80%93receptor-interactions>>
28. Soutter, W. *AZoNetwork*. **2020**. <<https://www.azonano.com/article.aspx?ArticleID=3051>>
29. Photo Researchers. *Science Source*. N.D. <<https://www.sciencesource.com/archive/Rotaxane--molecular-crystal-structure-SS2756311.html#/SearchResult&ITEMID=SS2756311>>
30. Merino, E.; Ribagorda, M., *Beilstein J. Org. Chem.*, **2012**, *8*, 1071–1090.
31. Brieke, C.; Heckel, A. *Chem. Eur. J.*, **2013**, *19*, 15726–1573.
32. Radua, A.; Byrne, R.; Alhashimya, N.; Fusaro, M.; Scarmagnani, S.; Diamond, D., *J. Photoch. Photobio. A.*, **2009**, *206*, 109–115.
33. Trentelman, K. *Photochemistry*, **2014**, *5*, 3337-3340.
34. Dongsansuk, A.; Lutz, C.; Neuner, G. *Photosynthetica*, **2013**, *51*, 13-21.
35. Baillet, G.; Giusti, G.; Guglielmetti, R. *J. Photochem. PhotobioL A: Chem.*, **1993**, *70*, 157.
36. Yoshida, T.; Morinaka, A. *J. Photochem. Photobiol. A: Chem.*, **1992**, *63*, 227.

37. V. Peddie, A.D. Abell, *J. Photochem. Photobiol. C: Photochem. Rev.*, **2019**, *40*, 1-20.
38. Schmidt, M., P.; Horn, K.; Dil, H., J.; Kampen, U., T., *Surface Science*, **2007**, 1775–1780.
39. Sauer, P.; Allen, E., R., *Chemical Physics Letters*, **2007**, *434*, 260–264.
40. Li, D.; Yang, Y.; Li, C.; Liu, Y., *Spectrochimica Acta Part A: Molecular and Biomolecular Spectroscopy*, **2018**, 1–9.
41. Maerz, B.; Wiedbrauk, S.; Oesterling, S.; Samoylova, E.; Nenov, A.; mayer, P.; Vivie-Riedle, D., R.; Zinth, W.; Dube, H., *Chem. Eur. J.* , **2014**, *20*, 13984–13992.
42. Plötner, J.; Dreuw, A., *J. Phys. Chem. A.*, **2009**, *113*, 11882-11887.
43. Scaiano, J. C., *CRC Handbook of Organic Photochemistry*. Boca Raton : CRC Press, **1989**.
44. Ludwig, E., E., *Stereochemistry of carbon compounds*. New York : McGraw-Hill, **1921**.
45. Fisher, E. *Journal of Physical Chemistry*, **1967**, *71*, 3704.
46. Crano, J. C.; Guglielmetti, R. J., *Organic Photochromic and Thermochromic Compounds*. New York : Plenum Press, **1999**.
47. Durbeej, B.; Eriksson, A., L., *J. Phys. Chem. A*, **2005**, *109*, 5677-5682.
48. Volman, H., D.; Hammond, S., G.; Neckers, C., D., *J. Photochem. Photobiol. A: Chem.*, **1993**, *70*, 197-200.
49. Pantuso, E.; De Flipo, G.; Nicoletta, P., F., *Adv. Optical Mater.*, **2019**, *7*, 1900253.
50. Yang, L.; Tan, X.; Wang, Z.; Zhang, X., *Chem. Rev.* **2015**, *115*, 7196–7239.
51. Brunsveld, B. J.; Folmer, B.; Meijer, E.W.; Sijbesma, R. P., *Chem. Rev.*, **2001**, *101*, 4071–4097.
52. Goshe, A. J.; Steele, I. M.; Ceccarelli, C.; Rheingold, A. L.; Bosnich, B. *Proc. Natl. Acad. Sci. U.S.A.*, **2002**, *99*, 4823-4829.
53. Steed, J. W., Turner, D. R. and Wallace, K. J. *Core concepts in Supramolecular Chemistry and Nanochemistry*. Chichester : John Wiley, **2007**.
54. Müller-Dethlefs, K.; Hobza, P. *Chem. Rev.*, **2000**, *100*, 143-168.

55. Arunan, E.; Desiraju, G. R.; Klein, R. A.; Sadlej, J.; Scheiner, S.; Alkorta, I.; Clary, D. C.; Crabtree, R. H.; Dannenberg, J. J.; Hobza, P.; Kjaergaard, H. G.; Legon, A. C.; Mennucci, B.; Nesbitt, D. *J. Pure Appl. Chem.*, **2011**, *83* (8), 1619.
56. Morokuma, K., *J. Chem. Phys.*, **1971**, *55*, 1236.
57. Umeyama, H.; Morokuma, K. *J. Am. Chem. Soc.*, **1977**, *99*, 1316.
58. Jeffrey, G. A. *An Introduction to Hydrogen Bonding*. New York : Oxford University Press, **1997**.
59. Steiner, T., *Angew. Chem. Int. Ed.*, **2002**, *41*, 48-76.
60. Prodic, K., B.; Molcanov, K., *Acta Chim. Slov.* **2008**, *55*, 692–708.
61. Smith, D. A. *In modeling the hydrogen bond*, Washington: ACS Symposium Series, American Chemical Society, **1994**.
62. Grabowski S. *Hydrogen Bonding - New Insights*. Dordrecht: Springer Netherlands; **2006**.
63. Taylor, R.; Kennard, O. *Acc. Chem. Res.*, **1984**, *17*, 320-326.
64. Taylor, R.; Kennard, O.; Versichel, W. *Acta Cryst.*, **1984**, *40*, 280-288.
65. Hunter, C. A.; *Angew. Chem. Int. Ed. Engl.*, **2004**, *43*, 5310.
66. Kamlet, M. J.; Abboud, J. L. M.; Abraham, M. H.; Taft, R. W.; *J. Org. Chem.*, **1983**, *48* (17), 2877.
67. Cook, J. L.; Hunter, C. A.; Low, C. M. R.; Perez-Velasco, A.; Vinter, J. G. *Angew. Chem. Int. Ed. Engl.*, **2007**, *46* (20), 3706.
68. Djurdjevic, S.; Leigh, A., D.; McNab, H.; Parsons, S.; Teobaldi, G.; Zerbetto, F., *J. Am. Chem. Soc.*, **2007**, *129*, 476-477.
69. Blight, B. A.; Camara-Campos, A.; Djurdjevic, S.; Kaller, M.; Leigh, D. A.; McMillan, F. M.; McNab, H.; Slawin, A. M. Z. *J. Am. Chem. Soc.*, **2009**, *131*, 14116.
70. Wang, H.-B.; Mudraboyina, P., B., *Chem. Eur. J.* **2012**, *18*, 1322 – 1327.
71. Koch, U.; Popelier, P. L. A., *J. Phys. Chem.* **1995**, *99*, 9747-9754.
72. Gooch, A.; McGhee, M., A.; Pellizzaro, L., M.; Lindsay, I., C.; Wilson, J., A., *Org. Lett.*, **2011**, *13*, 240-243.

73. Schmuck, C.; Wienand, W., *Angew. Chem. Int. Ed.*, **2001**, *40*, 4363-4369.
74. Jackman, L.M.; Sternhell, S., *Application of Nuclear Magnetic Spectroscopy in Organic Chemistry.*, Oxford: Pergamon Press., **1969**.
75. Murray, J., T.; Zimmerman, C., S., *J. Am. Chem. Soc.*, **1992**, *114*, 4010-4011.
76. Shanker, N.; Dilek, O.; Mukherjee, K.; McGee, W., D.; Bane, L., S., *J. Fluoresc.*, **2011**, *21*, 2173–2184.
77. Wyman, G. M.; Brode, W. R. *J. Am. Chem. Soc.*, **1951**, *73*, 1487-1493.
78. Rogers, D. A.; Margerum, J. D.; Wyman, G. M. *J. Am. Chem. Soc.*, **1957**, *79*, 2464-2468.
79. Gegiou, D.; Muszkat, A., K.; Fischer, E., *J. Am. Chem. Soc.*, **1968**, *90*, 3907-3918.
80. Maeda, Y.; Okada, T.; Mataga, N. *J. Phys. Chem.*, **1984**, *88*, 1117-1119.
81. Frackowiak, D., *J. Photochem. Photobiol. B: Biol.*, **1988**, *2*, 399-408.
82. Cordes, T.; Schadendorf, T.; Priewisch, B.; Braun-Ruick, K.; Zinth, W., *J. Phys. Chem.*, **2008**, *112*, 581-588.
83. Bonacic-Koutecky, V.; Koutecky, J.; Michl, J., *Angew. Chem. Int. Ed. Engl.*, **1987**, *26*, 170-189.
84. Zhang, Z.; Wang, W.; Jin, P.; Xue, J.; Sun, L.; Huang, J.; Zhang, J.; Tian, H., *Nat. Commun.*, **2019**, *10*, 1-9.
85. Pairault, N.; Barat, R.; Tranoy-Opalinski, I.; Renoux, B.; Thomas, M.; Papot, S., *Comptes Rendus Chimie*, **2016**, *19*, 103-112.
86. Stuckhardt, C.; Roke, D.; Danowski, W.; Otten, E.; Wezenberg, S.J.; Feringa, B. L. Beilstein, *J. Org. Chem.*, **2019**, *15*, 2767-2773.
87. Albin, A.; *Photochem. Photobiol. Sci.*, **2016**, *15*, 319-324.
88. Stranius, K.; Börjesson, K., *Sci. Rep.*, **2017**, *7*, 41145.
89. Jaffe, H., H.; Yeh, S-J.; Gardner, R.W., *J. Mol. Spectrosc.*, **1958**, *2*, 120-136.
90. Antonov, L., *Tautomerization: concepts and applications in science and technology.*, Wiley-VCH Verlag GmbH & Company KGaA, **2017**.

Chapter 2

2 Synthesis and Characterization of Photoswitchable Self-Complementary DD•AAA Hydrogen Bond Arrays

2.1 Introduction

There are many hydrogen bonding backbones to build upon varying from the complementary nucleotide base pairs in DNA to the linear fusion of anthridine.²⁶ They vary greatly in strength, binding properties, and solubility. When designing photochromic supramolecular hydrogen bond arrays, robust, fatigue-resistant compounds that can undergo multiple cycles of function yet conserve their hydrogen bonding affinity are advantageous. The reversibility of hydrogen bond interactions can endow designs for materials-based applications with self-healing and repairing properties.

Hydrogen bond arrays with contiguous placement of acceptors or donors to minimize secondary repulsive interactions have been found to possess the highest association constants.²⁵ Hydrogen bond acceptors that are surrounded by electron donor groups tend to participate in stronger hydrogen bonds. Conversely, hydrogen bond donors that are connected to groups which pull electron density away from the hydrogen tend to also participate in stronger hydrogen bonds. Incorporating heteroatoms into the backbone of the photoswitch will undoubtedly lead to increased complex stability due to the aforementioned effects. Lastly, addition of alkyl functional groups to the backbone of the complex allows some control of the solubility in non-polar solvents. Each of these factors will be considered when designing robust, yet dynamic self-complementary hydrogen bond arrays.

2.2 Design

Hemithioindigo (HTI) has been the focus of this project because of the desirable properties that drives this photoswitch. HTIs are appealing candidates for photochromic-based nanomaterials as a result of their less stable *E* isomer often being separable by chromatography, in addition to being photochemically robust. Furthermore, HTIs have been known to withstand thousands of photochemical cycles.³ The unsymmetrical structure of HTI allows us to modify the right side of the central double bond with varied substituents, like acenaphthylenone or julolidine.

We are looking for supramolecular complexes that, upon dissolution, form linear 180° hydrogen bonds with each other. Hydrogen bond arrays that are soluble in non-polar organic solvents can maximize possible hydrogen bond associations resulting in a larger K_a in these media. Moreover, the greater the number of hydrogen bonds, the stronger the hydrogen bond complex. Zimmerman and Murray explored the sequence of the acceptor and donor in the array as another underlying factor in complex stability.⁹ Putting these factors together into a resilient, yet dynamic system is a challenging process, but we can take previously published literature as a guide.

Reiterating the focus of the H-bond design, as mentioned in Section 1.11, where Gong and coworkers synthesized several self-complementary arrays (with one shown in Figure 2.2), they demonstrated the moderate to strong H-bond complexation between identical units. To prevent π -stacking and crystallization during the dilution NMR studies, unsymmetrical alkyl substituents were positioned at both ends of the duplex. The only arguable drawback with this framework is the lack of secondary interactions due to the distance between adjacent acceptors and donors. Despite this, they speculated that the

addition of extra hydrogen bonding sites (up to 8) would be manageable as alternative information-storage duplexes.

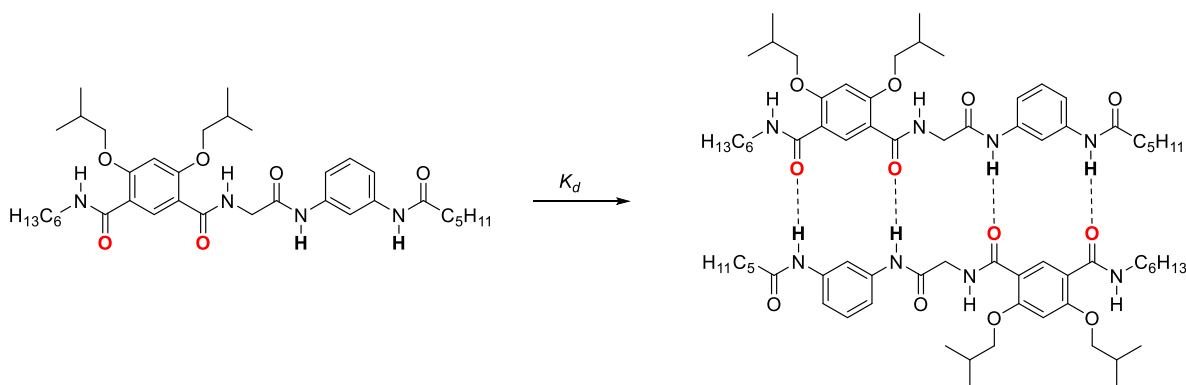


Figure 2.2 Self-complementary hydrogen bond network examined by Gong *et al.* in 1999 with an **ADAD•DADA** sequence. Acceptors are in **red** and the donors are **bold in black**.¹⁰

Secondly, a previous photoswitch synthesized by Wisner and co-workers containing a hemithioindigo moiety (*(E)*-6-(hexyloxy)benzo[b]thiophen-3(2H)-one) with an alkoxy substituent which when joined across a central double bond with acenaphthylen-1(2H)-one gave results ranging from a $K_a = 7.0 \times 10^3 \text{ M}^{-1}$ to $>2.3 \times 10^5 \text{ M}^{-1}$ with hydrogen bond donor arrays. This hydrogen bond array proved to not only be highly stable but could be synthesized in good synthetic yields in addition to being very soluble in common organic deuterated solvents, like CDCl_3 and CD_2Cl_2 . The photoswitch was fashioned as a **AAA** complementary design whereby the presence of a third “super site” is generated between the two carbonyls (refer to Figure 2.2.1) in the *E* isomeric form.

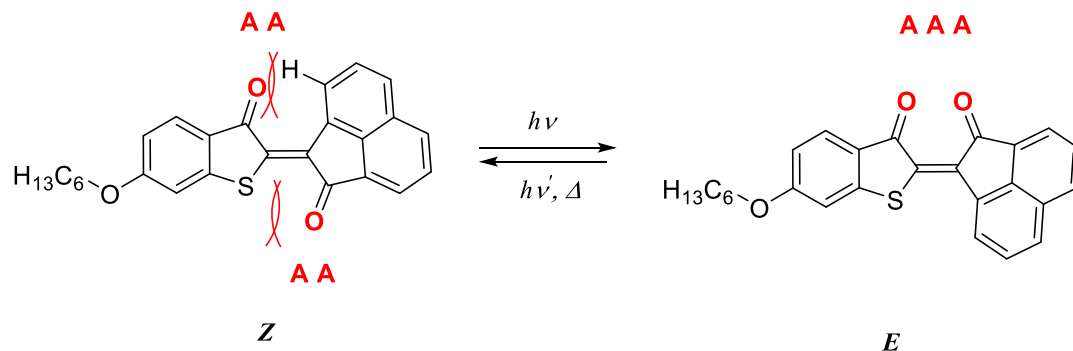


Figure 2.2.1 Complementary hydrogen bond design studied previously by Wisner and coworkers¹² undergoing *E/Z* photoisomerization where Aceptor = **A** and Donor = **D**.

The formation of this “super site” allows for the photoswitch to potentially hydrogen bond with three contiguous hydrogen bond donors as the *E* isomer. Importantly, the *Z* isomer displayed no measurable binding under similar conditions. Given this precedent, we decided to construct a self-complementary hydrogen bond array with acenaphthylen-1(2H)-one as the stilbenoid half of the photoswitch.

To construct a self-complementary hydrogen bond array, we need to synthesize a structure containing both acceptors and donors. The presence of both would inevitably lead to secondary repulsive interactions between adjacent crossover groups in the complex. To avoid this issue, we positioned the hemithioindigo moiety as a physical spacer between the donors and the acceptors. The donors comprise ureido substituents with varying alkyl chains and the carbonyls of the chromophore are the hydrogen bond acceptors (refer to Figure 2.3.2) similar in disposition to Gong and coworkers’ aryl amide designs.

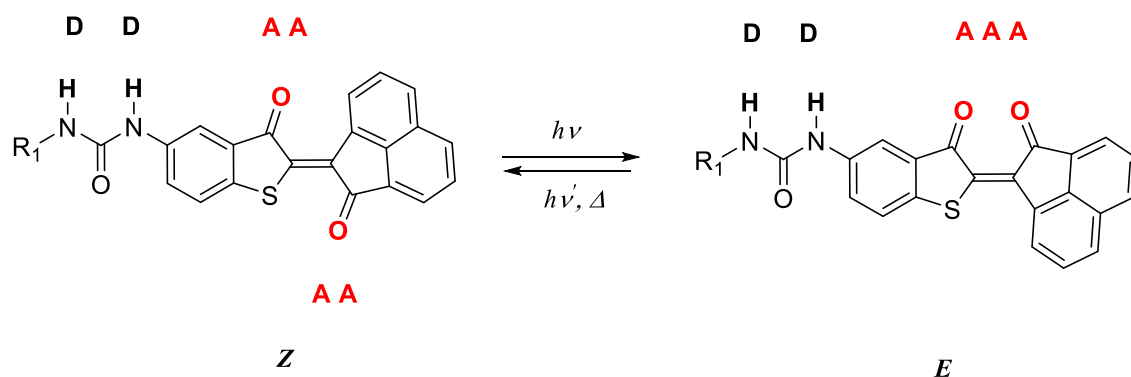
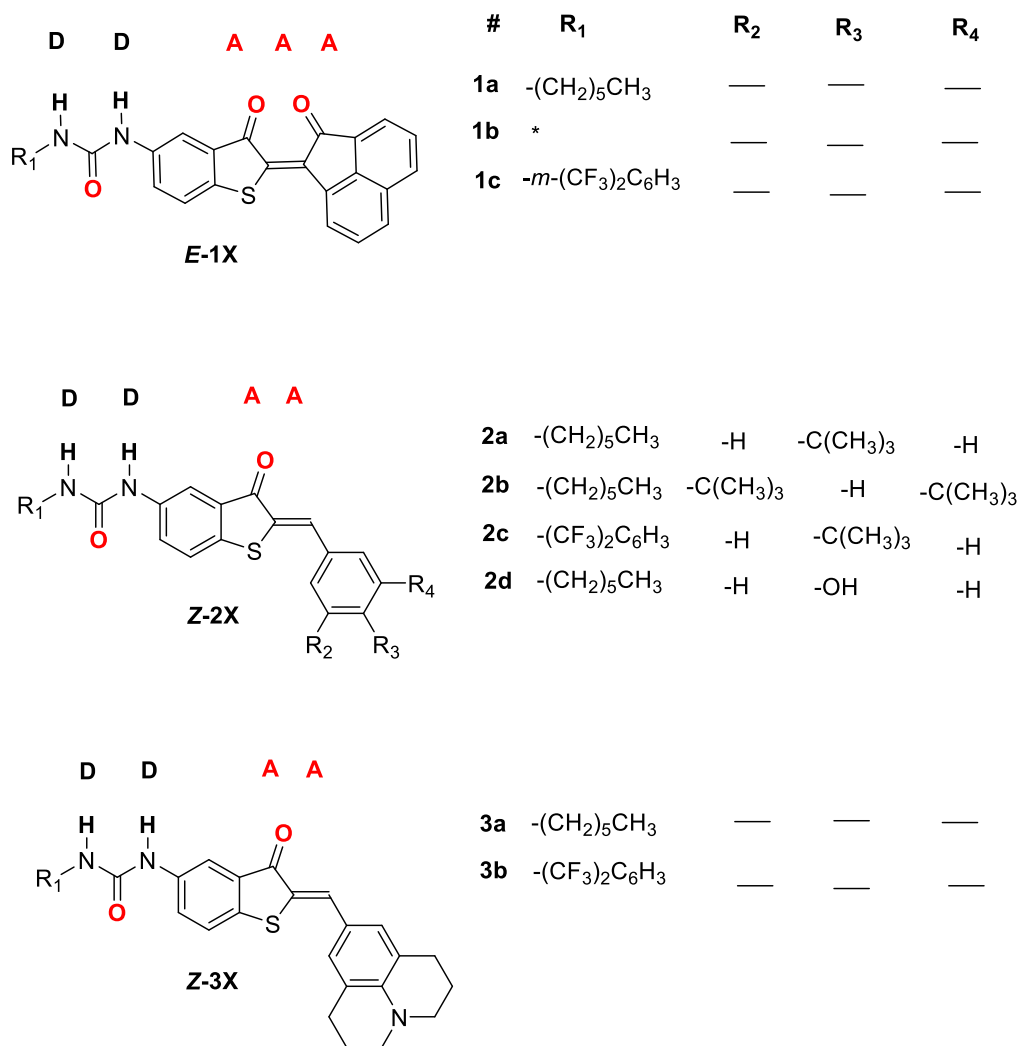


Figure 2.2.3 The first generic self-complementary hydrogen bond array proposed displaying the *E/Z* photoisomerization where Aceptor = **A** and Donor = **D**.

The first potentially photoswitchable hydrogen bond array (**1a**) considered was synthesized using an *n*-hexyl group as R_1 . This array, although robust and thermally stable, was insoluble in all traditional deuterated NMR solvents with DMSO being the only candidate and then only sparingly. Observing that **Z-1A** is only soluble in DMSO- d_6 , ^1H NMR dilution studies could not be performed as the solvent competes for binding with the hydrogen bond array moieties, saturating all hydrogen bonding sites and preventing any dimerization from occurring. Ideally, a non-polar solvent that dissolves the photoswitch would allow for dimerization and binding studies as there would be minimal solvent interference. We wished to preserve the acenaphthoquinone photochrome as the extra binding site provided by the carbonyls contribute to stronger dimerization in the *E* isomeric form. To potentially overcome the solubility issue, we synthesized an additional derivative (**1b**) with a branched side chain, which could likely inhibit π -stacking from occurring and possess a higher solubility in non-polar solvents. Figure 2.2.4 displays all self-complementary hydrogen bond derivatives studied.



* -(CH₂)CH(CH₂CH₃)(CH₂)₃CH₃

Figure 2.2.4 Self-complementary hydrogen bond arrays studied in this dissertation with derivatives **1a-c** in a DDAAA • AAADD sequence whereas **2a-d**, and **3a-b** show a DDAA • AADD where Donor = **D**; Aceptor = **A**.

To boost the hydrogen bonding donor ability of this original design, we decided to install a strong electron-withdrawing group (**1c**) with bulky trifluoromethyl groups off the urea.

The inductive nature of the fluorine groups will increase the donor ability of the NH protons by decreasing the surrounding electron density in proximity to the NHs.

We continued to expand the scope of our design to include **2a-d** and **3a-b** wherein the photochromic handle contained a stilbene only (i.e. no second C=O subgroup present). These photochromes should act to block the carbonyl binding site sterically when in the *E* isomeric form but not the *Z*. For **2a-c**, the stilbene was functionalized with bulky (bis)-*tert*-butyl groups. In this sense, upon visible light irradiation, the stilbene unit would flip over to the *E* form thereby blocking the lone carbonyl oxygen from participating in hydrogen bonding. Employing (branched) alkyl chains at R₁ allows us to again predispose the solubility of these compounds in a range of non-polar organic solvents. To further increase the solubility of **2a**, **2b** was synthesized with a second *t*-butyl group both now *meta* to the alkene connection. This improved the solubility greatly as **2b** was freely soluble in chloroform, dichloromethane and even more non-polar solvents like toluene and benzene. We decided to implement the same electron-withdrawing group - 3,5-bis(trifluoromethyl)phenyl- in this chromophore (**2c**) to presumably increase the solution-state dimerization stability and photophysical characteristics.

Lastly, a paper published by Dube and coworkers in 2018, reported several hemiindigo photoswitches with various stilbene derived photochromes. Surprisingly, the moiety containing the julolidine photochrome displayed *E/Z* isomer conversions up to 99% with half-lives up to a day. Furthermore, via resonance stabilization, the julolidine (**3a**) contributes to higher electron density on the oxygen atom of the carbonyl; improving the hydrogen bond donor character. The same concept was applied to **3c** to boost both the

hydrogen bond acceptor and donor ability by also functionalizing the urea group with 3,5-bis(trifluoromethyl)phenyl.

2.3 Synthesis of Self-complementary Hydrogen bond Arrays

All self-complementary hydrogen bond photoswitches synthesized started with commercially available, 2-chloro-5-nitrobenzoic acid (**4**), (Figure 2.3).

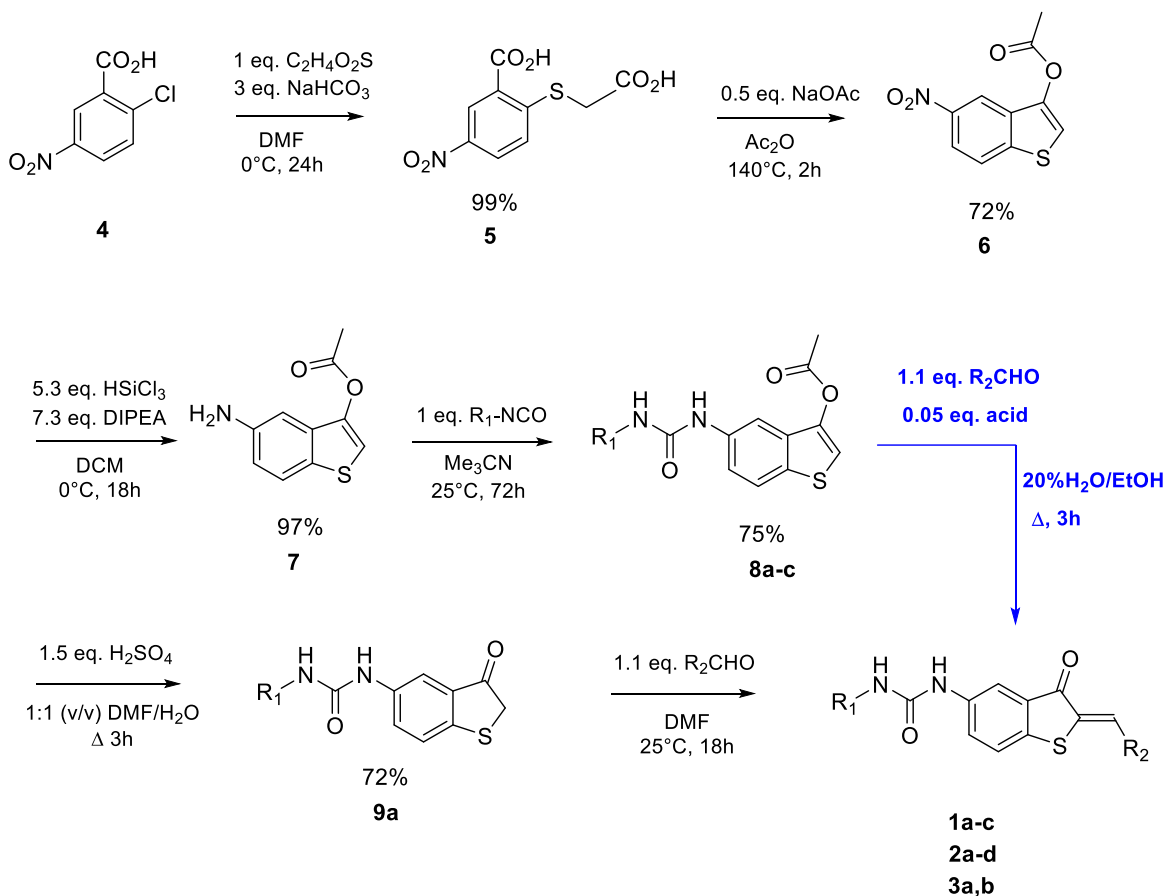


Figure 2.3 Synthesis of self-complementary hydrogen bond arrays **1a-c**, **2a-d** and **3a,b**. **8a**, **9a** refer to the hexyl group at R_1 , **8b**, **9b** refer to the 2-ethyl hexyl group at R_1 , and **8c** refer to the 3,5-bis(trifluoromethyl)phenyl group at R_1 .

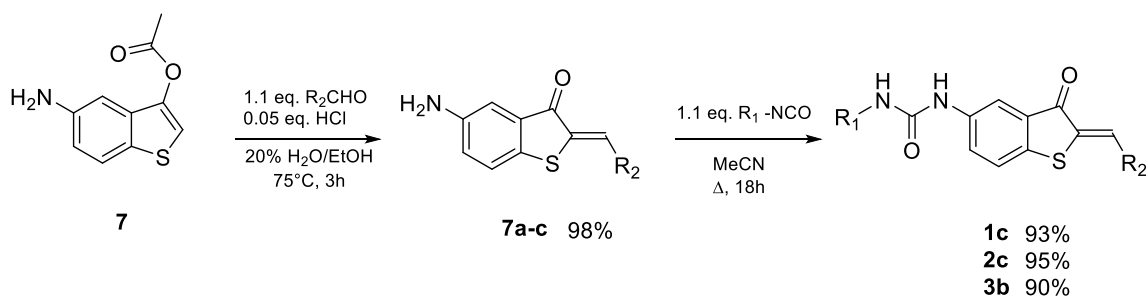


Figure 2.3.1 Alternate synthesis of selective self-complementary hydrogen bond arrays to yield derivatives **1c**, **2c** and **3b** with strong electron withdrawing R_1 's.

The synthesis of the hydrogen bond arrays were prepared in five to six steps. The commercially available precursor, **4**, was converted to **5** by replacement of the chlorine atom using thioglycolic acid in anhydrous DMF at 0°C to give the product in near quantitative yield ($\sim 99\%$).²¹ The intermediate was then decarboxylated and cyclized using a previously published method to yield **6** in 72% yield.¹¹ The nitro group was then reduced in anhydrous DCM, at 0°C with N,N-diisopropylethylamine and trichlorosilane¹² to produce the amine derivative **7** in high yield (97%). This intermediate was stirred with three different isocyanates in anhydrous acetonitrile to yield the hexyl (**8a**), 2-ethylhexyl (**8b**) and 3,5-bis(trifluoromethyl)phenyl (**8c**) derivatives in good yields (each 75%). The acetate functional group was hydrolyzed in acidic media to give the ketones, 1-hexyl-3-(3-oxo-2,3-dihydrobenzo[b]thiophen-5-yl)urea, **9a,b**, which were carried forward without purification in an aldol condensation with various aldehydes to synthesize the stilbene-based hemithioindigo photoswitches (**2a-d**, **3a,b**) in 50-95% yield. The tendency of **9a,b** to dimerize and/or decompose over time (3-7 days) gave us further motivation to pursue a shorter pathway (blue arrow) where **8a-c** is directly converted to the final hydrogen bond array by the one pot hydrolysis and condensation with the aldehyde of interest, in mildly acidic conditions. The yield over 2 steps was thus

increased to 95% in the case of in the case of **2c**. **8c** could not withstand the originally employed conditions to yield the ketone derivative (decomposition took place) and as such an alternative pathway was pursued (Figure 2.3.1). Using this shorter route allowed for the synthesis of **1c**, **2c**, **3b** derivatives without any unwanted reaction at the urea site; a limiting feature of the original hydrolysis conditions.

We demonstrated that the addition of the photochromic group (R_2CHO) is independent of R_1 . Starting from the amine derivative, **7**, we initially added the photochromic moiety in the presence of concentrated HCl under an inert atmosphere then proceeded with the substitution of the urea group with various isocyanates. This methodology allowed us to build photoswitches with strong electron withdrawing groups at R_1 with milder reaction conditions and better yields. Previously, hydrolyzing **8c** with the current acidic conditions gave yields lower than 20%. The milder approach greatly improved the yields and prevented any degradation of the 3,5-bis(trifluoromethyl)phenyl group.

Most of the products obtained from these reactions precipitated out after pouring the reaction mixture into distilled water and filtering off the solid under vacuum as **1a-c**, **2a-d** and **3a,b** were not water soluble. To obtain the pure hydrogen bond arrays, with a few exceptions, the compounds were separated from impurities using flash chromatography.

2.4 ^1H NMR Characterization of **DDAA**•**AADD/DDAAA**•**AAADD** arrays

Once the syntheses of the *Z* isomers of photoswitchable hydrogen bond arrays were complete, NMR spectroscopy was used to establish the structures and assign the resonances associated with each ^1H and ^{13}C atom using ^1H NMR, ^{13}C NMR, gCOSY, HSQC and HMBC experiments.

Figure 2.4.1 depicts the ^1H NMR spectrum of **Z-1a**, where H_a is the furthest downfield due to the intramolecular interaction with the carbonyl oxygen on the hemithioindigo ring. This anisotropic effect is not observed in the *E* isomeric form because of the different relationships between the proton (H_a) and the carbonyl group in that configuration. The attempted dissolution of **Z-1a**, a bright red solid, in common deuterated NMR solvents (CDCl_3 , CD_2Cl_2 , toluene- d_6 , etc.), was unsuccessful with $\text{DMSO-}d_6$ appearing to be the only viable candidate and then only sparingly.

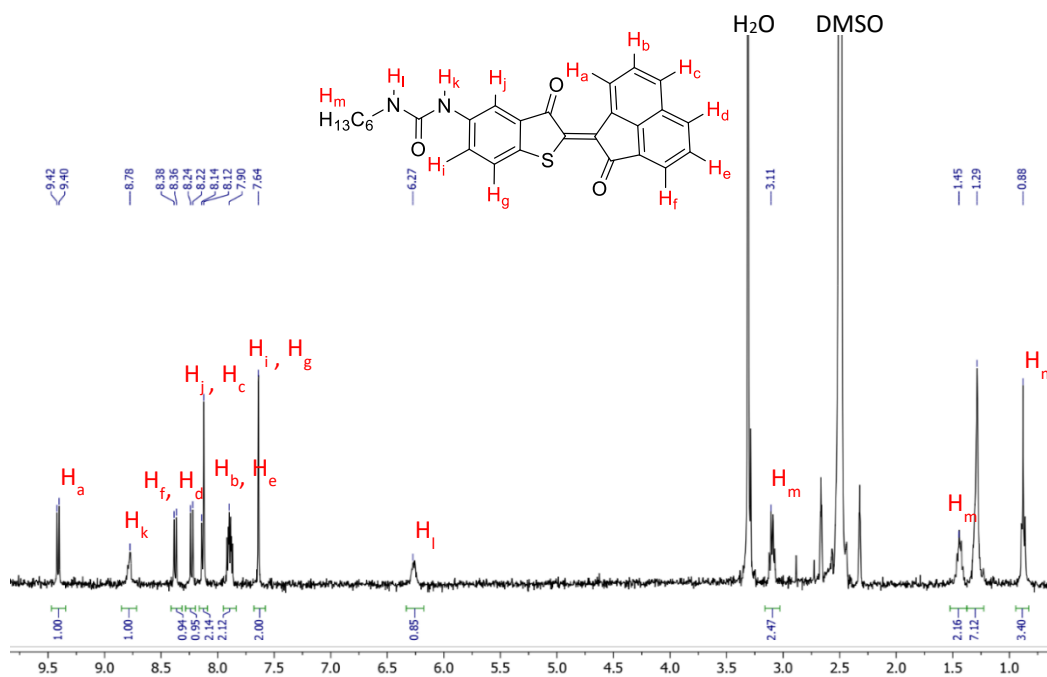


Figure 2.4.1 ^1H NMR spectrum of **Z-1a** in $\text{DMSO-}d_6$ at 298 K.

Unfortunately, due to the great insolubility of **Z-1a**, the *E* isomer could not be isolated. The *Z* form is the thermodynamically more stable isomer in this system confirmed by the X-ray structures¹⁶ of previous Wisner photoswitches which resembled **1a** and that of **Z-1c** (vide infra). The ¹H NMR spectrum of **1b** is similar to **1a** in that the most deshielded proton is the one in close proximity to the carbonyl oxygen of the hemithioindigo labelled as H_a in both cases. This anisotropic effect on the nearby proton is perceived in hydrogen bond arrays **2a-d**, and **3a,b** as well but to a lesser extent. **Z-1b**, a magenta solid, was soluble in chloroform with a lower solubility in dichloromethane but again maintained the greatest solubility in DMSO compared to its unbranched counterpart, **Z-1a**. The ¹H NMR spectra of **1a**, **1b** and **1c** are displayed in Figures 2.4.1, 2.4.2 and 2.4.3. Likewise, **Z-1c**, a vibrant pink solid possessed some solubility in DMSO but little to no solubility in CDCl₃ and CD₂Cl₂.

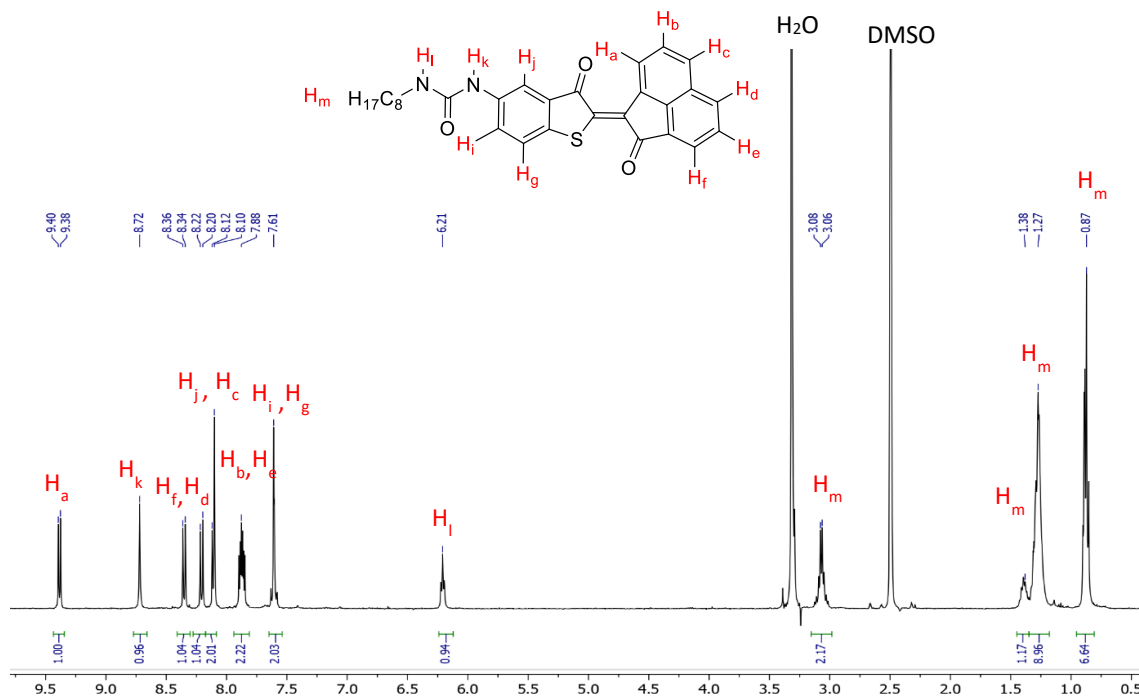


Figure 2.4.2 ¹H NMR spectrum of **Z-1b** in DMSO-*d*₆ at 298 K.

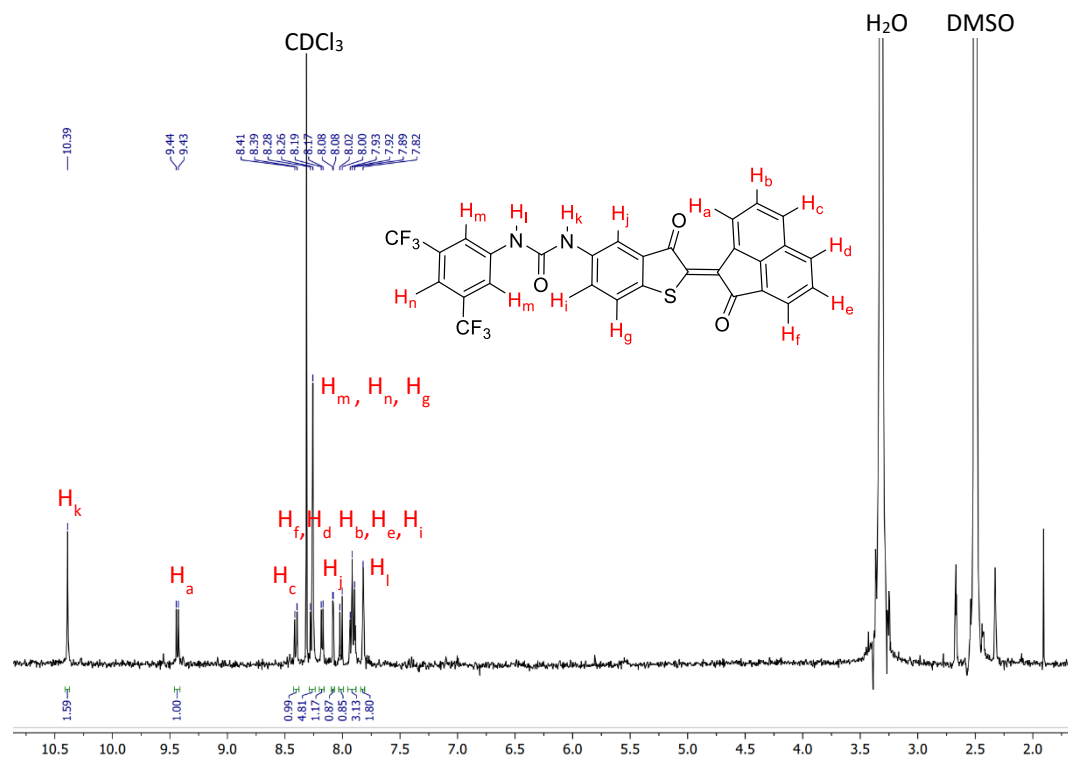


Figure 2.4.3 ^1H NMR spectrum of **Z-1c** in $\text{DMSO-}d_6$ at 298 K.

Moving forward to the simpler self-complementary design lead us to synthesize **Z-2a** (a bright red solid). This design allowed us to functionalize the chromophore more freely in order to increase the electron push-pull across the central double bond. This way, electron density could be deposited on the hemithioindigo carbonyl oxygen via resonance improving the acceptor character of this part of the array.

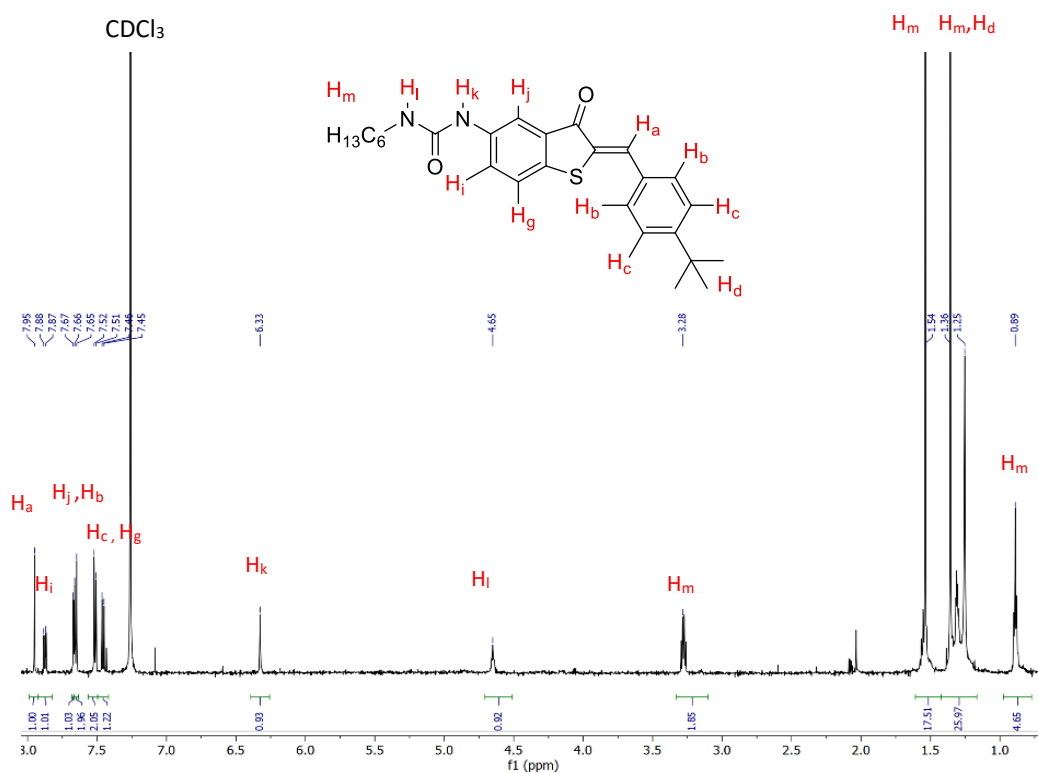


Figure 2.4.4 ^1H NMR spectrum of *(Z)*-1-(2-(4-(tert-butyl)benzylidene)-3-oxo-2,3-dihydrobenzo[*b*]thiophen-5-yl)-3-hexylurea (**Z-2a**) in CDCl_3 at 298 K.

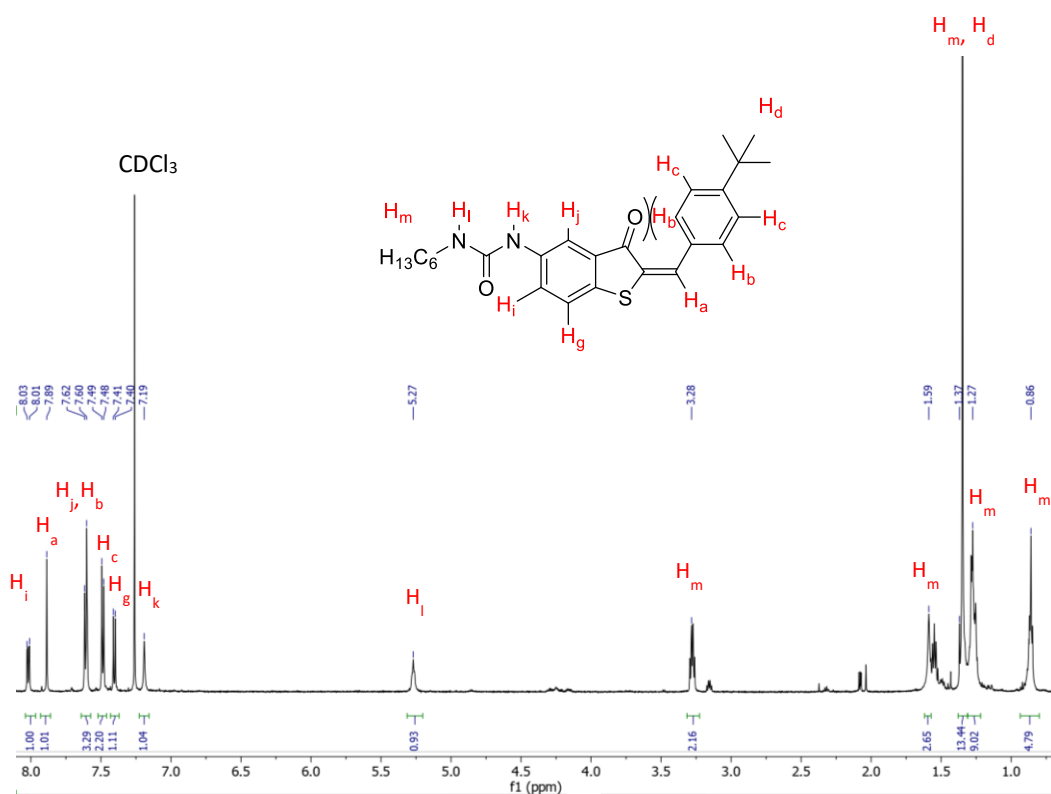


Figure 2.4.5 ^1H NMR spectrum of *(E)*-1-(2-(4-(tert-butyl)benzylidene)-3-oxo-2,3-dihydrobenzo[*b*]thiophen-5-yl)-3-hexylurea (**E-2a**) in CDCl_3 at 298 K.

Figure 2.4.4 pictures the ^1H NMR spectrum of **Z-2a** whereas Figure 2.4.5 depicts that of **E-2a**. The chemical shifts (in ppm) of protons associated with **E-2a** are upfield relative to **Z-2a**. The *E* isomer, a lighter red solid than the *Z*, is less polar and a small amount was isolated from a pure solution of *Z* after irradiation at 440 nm with a (3:1; v/v) mixture of chloroform and ether. **E-2a** has very low bistability as it starts to thermally revert to the *Z* isomer in 5 min. The protons (H_b) on the chromophore that occupy the same space as the carbonyl oxygen in the *E* form shift upfield by 0.06 ppm when compared to the *Z*. In a planar arrangement, where the phenyl ring lies in the same plane as the hemithioindigo fragment. The H_b protons should be significantly affected by the carbonyl oxygen atom as to their chemical shift. In this configuration, H_b should have a downfield chemical shift due to the deshielding effect of the oxygen. This is not observed since the experimental chemical shift of H_b lies essentially at the same value in both isomers, indicating that the aryl ring is likely twisted out of planarity. [More information discussed in 2.5].

We decided to increase the solubility of the molecular switch by placing an additional *t*-butyl functional group on the stilbene ring with an orientation *meta* to each other (**Z-2b**). Gratifyingly, this derivative (a bright red solid) was not only soluble in CDCl_3 and CD_2Cl_2 but also in more non-polar solvents like toluene and benzene. In a separation of both isomers, **E-2b** was a light red/orange colour (when viewed on a TLC plate) with a lower polarity than its *Z* counterpart. The low bistability of **E-2b**, like **E-2a**, prevented us from isolating this isomer alone and performing quantitative tests to confirm that in this design, the *Z* isomer is the sole hydrogen bonding array. [More information discussed in section 2.5].

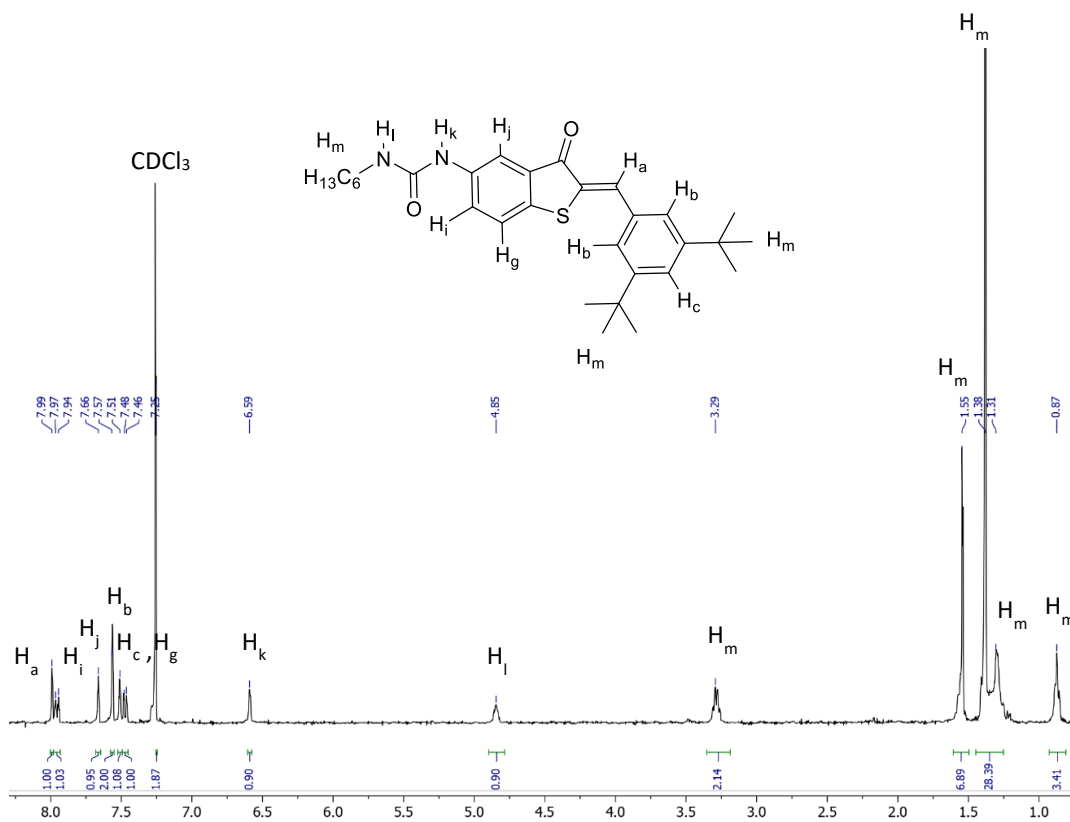


Figure 2.4.6 ^1H NMR spectrum of **Z-2b** in CDCl_3 at 298 K.

^1H NMR analysis of a mixture of both isomers of **2b** generated by irradiation at 425 nm yielded their superimposed spectra. Protons, H_b , don't shift as predicted again since the chemical shift in the *Z* form (Figure 2.4.7) is at 7.52 ppm and in the *E* form it moves upfield 0.05 ppm to 7.47 ppm. As discussed in the case of **2a**, the same conclusion is arrived for the solution structures of **2b**, where the stilbene-based ring must be twisted out of plane in the *E* form as indicated by the chemical shifts. This spatial disposition of the rings of the *E* form may allow participation in hydrogen bond dimerization and is further discussed in 2.5.

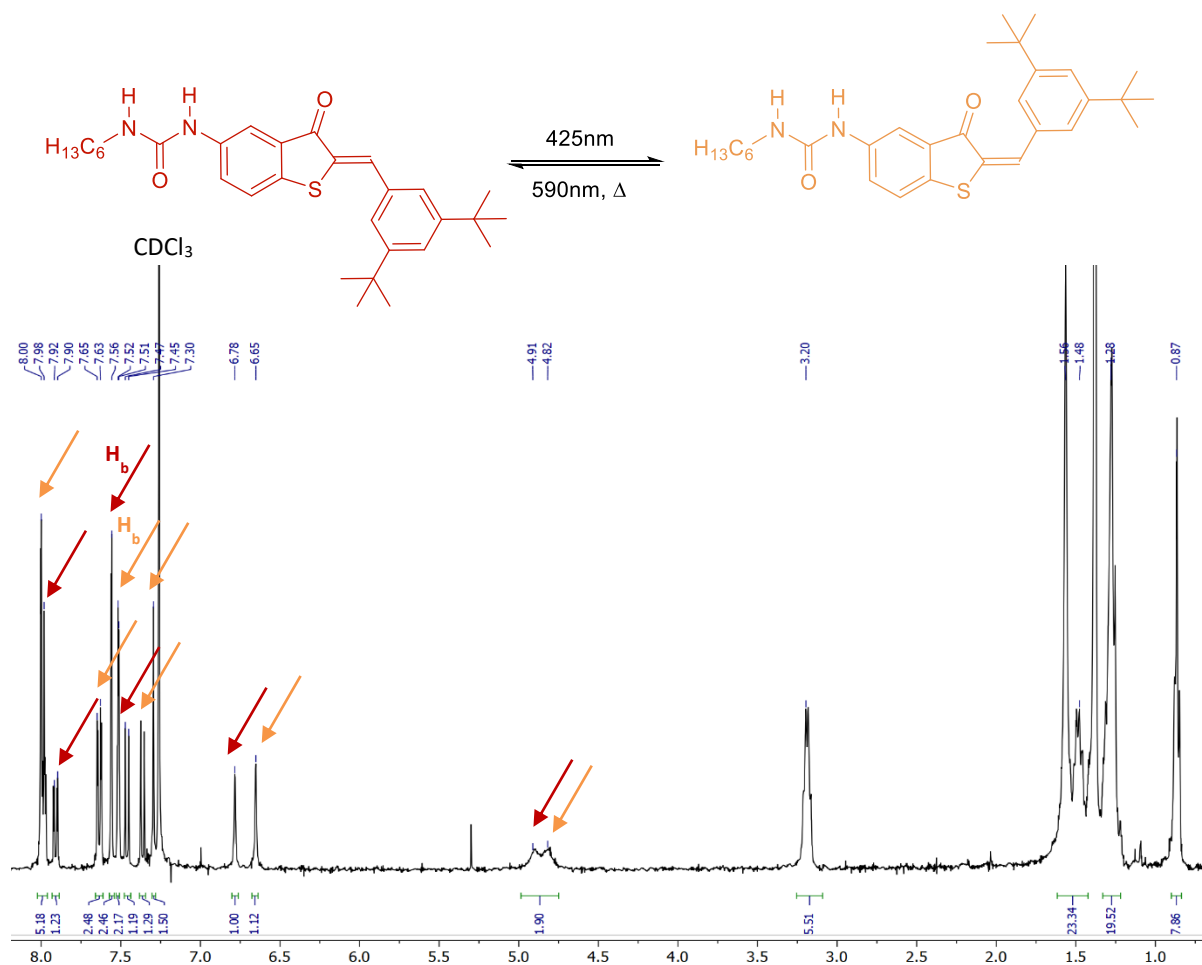


Figure 2.4.7 ^1H NMR spectrum of a mixture of *Z/E*-**2b** in CDCl_3 at 298K where the red, orange arrows correspond to the *Z*, *E* isomers respectively.

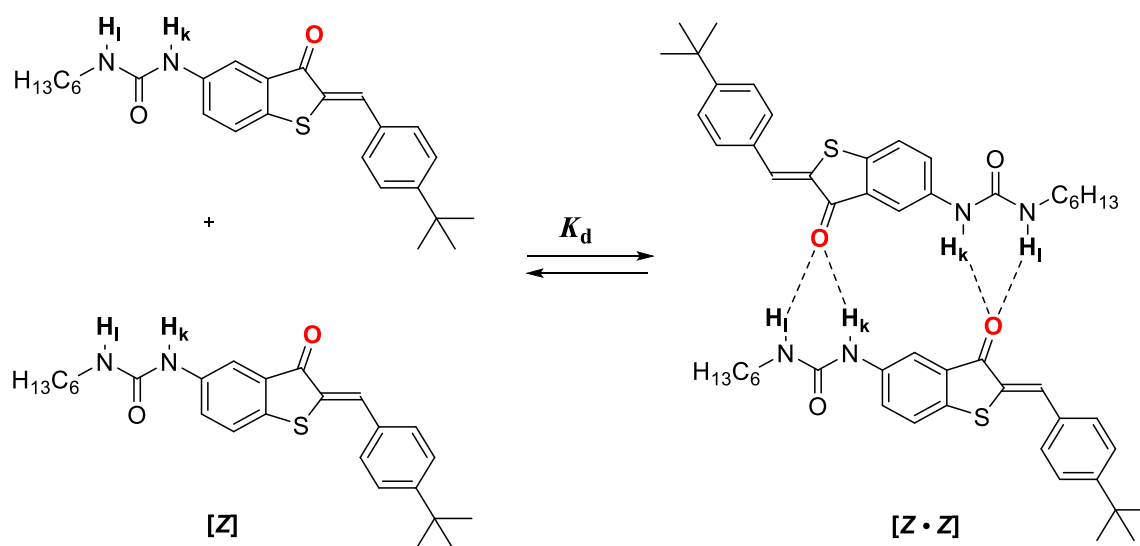
We decided to further increase the electron density of the overall photoswitch through conjugation on the stilbene by reaction of **9a** with 2,3,6,7-tetrahydro-1H,5H-pyrido[3,2,1-ij]quinoline-9-carbaldehyde (**11**) to yield a dark violet solid, **Z-3a**. This chromophore is a tricyclic molecule which contains a nitrogen atom enclosed in a resonance-stabilized structure. This derivative, like the previous, was greatly soluble in DMSO, but also possessed relatively good solubility in chloroform and dichloromethane. Trials to isolate the *E* isomer failed as the thermal reversion to the *Z* isomer was extremely fast at room temperature (on the scale of seconds).

The photoswitches (**1a**, **2a**, **2b**) involve a simple alkyl chain: a hexyl group at R₁. In an attempt to generate a stronger association between the hydrogen bond donors and acceptors in this system, we incorporated a strong electron withdrawing group using commercially available 3,5-bis(trifluoromethyl)phenyl isocyanate to give **1c**, **2c** and **3b**. **Z-1c**, after purified, was a neon pink solid with similarly low solubilities as **1a** and **1b** in chloroform. On the other hand, **Z-2c** was a yellow-orange solid and was soluble in chloroform, dichloromethane, acetone and methanol. **Z-3b** was a dark violet solid that precipitated directly from the reaction mixture. It had very low solubility in chloroform and dichloromethane. All *Z* isomer derivatives (**1b,c**, **2a-c**, **3a,b**) had high solubility in DMSO except for **Z-1a**. The next section will discuss the thermodynamics of hydrogen bond mediated dimerization of the arrays in non-polar solutions.

2.5 Assessing the Dimer Stability of the Arrays by Solution Characterization Methods

The stability of supramolecular complexation has been studied as a way of quantifying the interactions between host and guest compounds. There are several ways of determining complex stability, but the most common method is through titration or dilution studies, wherein we utilize the changes in chemical shift by NMR, UV-Vis absorption changes, quenching of fluorescence or the measurement of complexation enthalpy changes using Isothermal Calorimetry (ITC). Association (K_a) or dimerization (K_d) values as low as $1 \times 10^{-4} \text{ M}^{-1}$ to as high as $1 \times 10^5 \text{ M}^{-1}$ can be assessed on modern NMR instruments with good accuracy ($\pm 10\%$).¹³ For a typical NMR titration or dilution, the concentrations of the host and/or guest units are plotted against the chemical shifts (in ppm) of the species of interest. The data is then fitted to a stoichiometric binding model

using non-linear analysis software. Dimerization is a process wherein a molecule forms a complex with itself, usually in solution, resulting in a dimer with unique physical and chemical properties. For self-complementary complexes, the degree of dimerization is tracked with increasing/decreasing concentration and is referred to as a dilution as only one species is involved in the equilibrium. This process is defined by a quantity, called the dimerization constant (K_d), and can be measured by NMR spectroscopy. Figure 2.5 depicts the expected dimerization equilibrium for **Z-2a-d** and **Z-3a,b** in solution.



Scheme 2.5 The dimerization reaction scheme of **Z-2a** occurring in solution with complexation increasing with increasing concentration.

The dimerization constant is calculated from the equilibrium concentrations of the monomer and the dimer and are related by the equation;

$$K_d = \frac{[Z \cdot Z]}{[Z]^2} \quad \text{Equation 6}$$

where the monomer is denoted by Z , and the dimer is denoted by $Z \cdot Z$. Chemical shift changes of individual hydrogen bonded protons can be tracked in the ^1H NMR spectra.¹³ As a dimer is formed, the protons engaged in hydrogen bond interactions are “accepting” electrons from the acceptor causing them to become deshielded to the NMR magnetic field. These protons shift to a higher chemical shift in comparison to the monomer when observed in the NMR spectrum. In most cases, the individual protons engaged in hydrogen bonding are in fast exchange with their complexes; thus, only a single frequency is observed. The dilution data is then fitted to equation 7;¹⁸

$$\delta_{\text{obs}} = \delta_{\text{m}} \cdot \frac{[Z]}{[Z]_0} + \delta_{\text{d}} \cdot \frac{2 \cdot [Z \cdot Z]}{[Z]_0} \quad \text{Equation 7}$$

where,

$$[Z]_0 = [Z] + 2 \cdot [Z \cdot Z] \quad \text{Equation 8}$$

Equation 7 relates the observed chemical shift (δ_{obs}) to the chemical shift of the monomer (δ_{m}) and the chemical shift of the dimer (δ_{d}). $[Z]$, $[Z \cdot Z]$ and $[Z]_0$ represent the monomer, dimer and total concentration respectively. In almost all cases involving hydrogen bonding, absolute values don't need to be included in either equation since the resulting observed chemical shift from dimerization is positive due to $\delta_{\text{d}} > \delta_{\text{m}}$. Intuitively, increasing the overall concentration leads to an increase in dimer formation due to Le Chatelier's principle. Plotting the δ_{obs} against $[Z]_0$ leads to the determination of the K_d , δ_{m} , δ_{d} by fitting the data to a dimerization isotherm modelled by equation 9;

$$\delta_{\text{obs}} = \delta_{\text{m}} + (\delta_{\text{d}} - \delta_{\text{m}}) \cdot \frac{[1+8 \cdot K_{Z:Z} \cdot [Z]_o]^{1/2} - 1}{[1+8 \cdot K_{Z:Z} \cdot [Z]_o]^{1/2} + 1} \quad \text{Equation 9}$$

A dilution is concentration dependent on the monomer; as such, the range of data should provide a good representation of complex formation (a minimum of 10 points covering 80% of the isotherm). Weak association constants ($<10 \text{ M}^{-1}$) tend to have large $\Delta\delta_{\text{max}}$ extrapolation errors whereas very strong K_d constants on the order of 10^5 M^{-1} and greater often show small shift changes at detectable monomer concentrations. Lastly, the chemical shift between the monomer and the dimer ($\Delta\delta \geq 0.5 \text{ ppm}$) should be significant for the difference to be detectable in most modern NMR spectrometers. Once the K_d is computationally calculated, the Gibbs free energy can be obtained from equation 10;

$$\Delta G = -RT \ln(K) \quad \text{Equation 10}$$

where R is the ideal gas constant in units of $\text{J}(\text{mol}\cdot\text{K})^{-1}$, T is the temperature in kelvin, and \ln represents a logarithm to the base e .

The other most common method of assessing supramolecular complexes is by UV-Vis spectroscopy. The advantage in observing UV-Vis absorption changes is that binding constants of 1:1 systems as high as 10^9 M^{-1} can be evaluated with strongly absorbing chromophores.¹³ However, the concentrations chosen must lie within the region of both monomer and dimer while obeying the limits of the Beer-Lambert law;

$$A = \epsilon cl \quad \text{Equation 11}$$

where A=absorbance, ϵ = molar absorptivity constant, c= concentration, and l = path length.

Similarly, quantifying fluorescence changes upon the association of two or more molecules is a common instrumental technique. In the present case, none of the dimers display significant departures in an absorbance or fluorescence from the monomeric to dimeric species and these techniques were not pursued in this context.

2.5.1 ^1H NMR dilution studies

^1H NMR dilution studies were successfully carried out for **Z-2a**. The solvent first implemented was CD_2Cl_2 . However, at high concentrations, **Z-2a** began to visually precipitate from solution. The hydrogen bond array was then tested in CDCl_3 in which it was soluble without any observable precipitation. Thus, three trials were conducted in chloroform. The ureido protons, labelled as **H_I** and **H_k**, (refer to Figure 2.5.1) were observed at 16 concentrations.

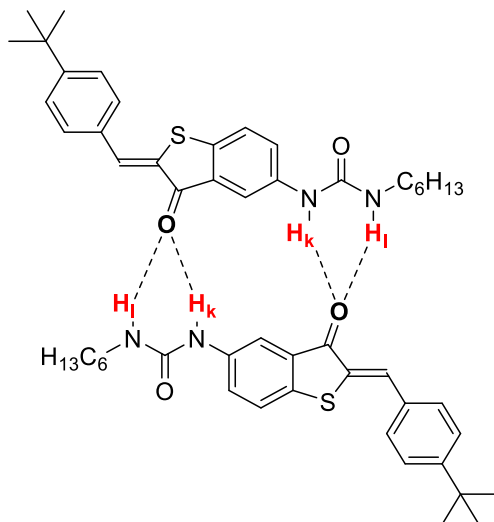


Figure 2.5.1 The anticipated dimer of **Z-2a** occurring in solution with increasing monomer concentration.

Figure 2.5.2 shows the concentration dependent behavior of the ureido protons upon addition of a concentrated CDCl_3 solution of **Z-2a** to an NMR tube containing 500 μL of pure solvent at room temperature at three of the sixteen concentrations. The chemical shift of the proton (H_k) moved from a calculated starting chemical shift of 6.08 in the monomer to 7.75 ppm in the dimer; a $\Delta\delta_{\text{max}} = 1.67$ ppm. From the calculated isotherm (Figure 2.5.3), the K_d value was determined to be 110 M^{-1} which is indicative of relatively weak self-association ($\Delta G = -11.4 \text{ kJ/mol}$).

In the case of **Z-2b**, the solvent that was chosen was CDCl_3 until it was proven soluble in toluene. A dilution was first performed in CDCl_3 to which the $K_d = 70 \text{ M}^{-1}$ with $\Delta G = -10.5 \text{ kJ/mol}$ (Figure 2.5.4). This was not the expected result as the change to two *meta* *t*-butyl groups was predicted to have a similar electronic contribution to the phenyl group ($2 \times \sigma_m = 2 \times 0.15 = 0.3$) as a *para* *t*-butyl substituent ($\sigma_p = 0.3$)²⁹. However, one reason might be because of the steric effects of the bulky *t*-butyl groups in the hemithioindigo dimer which may weaken the association of the dimer leading to a lower

K_d value. To compare the stability of dimerization in a more non-polar solvent, trials were performed in toluene (Figure 2.5.5). The dimer stability of **Z-2b** in toluene, to our surprise, decreased to a value of 63 M^{-1} ($\Delta G = -10.3 \text{ kJ/mol}$) but with a high $\Delta\delta_{\text{max}} = 4.99$. Typically, complexation in toluene would be expected to increase the stability by 3-6 kJ/mol on average.²⁸

In principle, the *E* isomeric form of **2b** should not participate in any dimerization equilibria due to the expected steric obstruction of the carbonyl oxygen as part of the design. We therefore decided to attempt a dilution with both

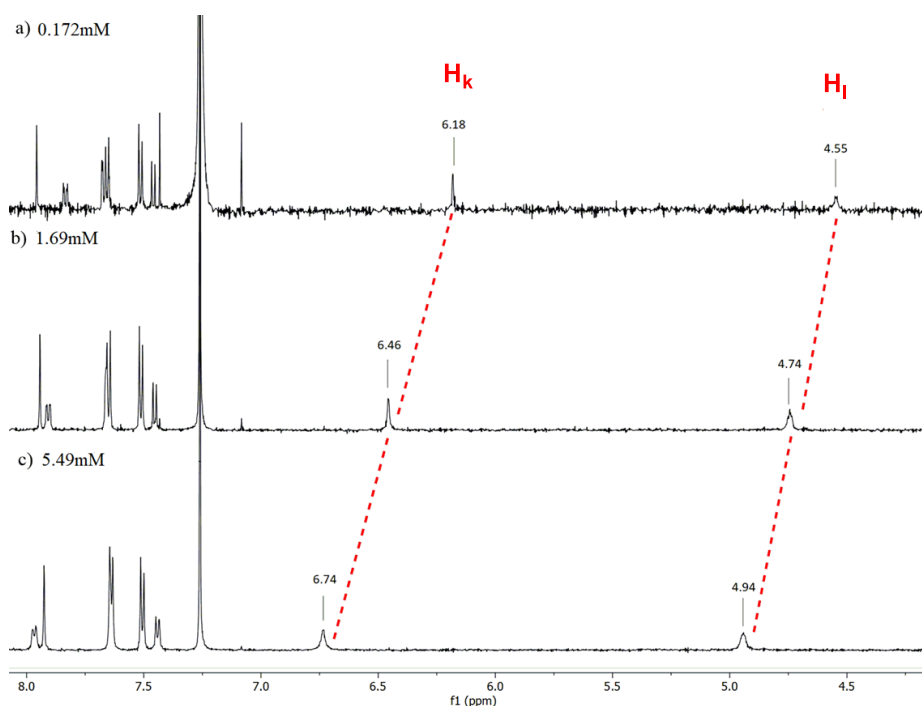


Figure 2.5.2 The Stacked ¹H NMR plot of **Z-2a** at three concentrations a) 0.172 mM, b) 1.69 mM and c) 5.49 mM at 298 K.

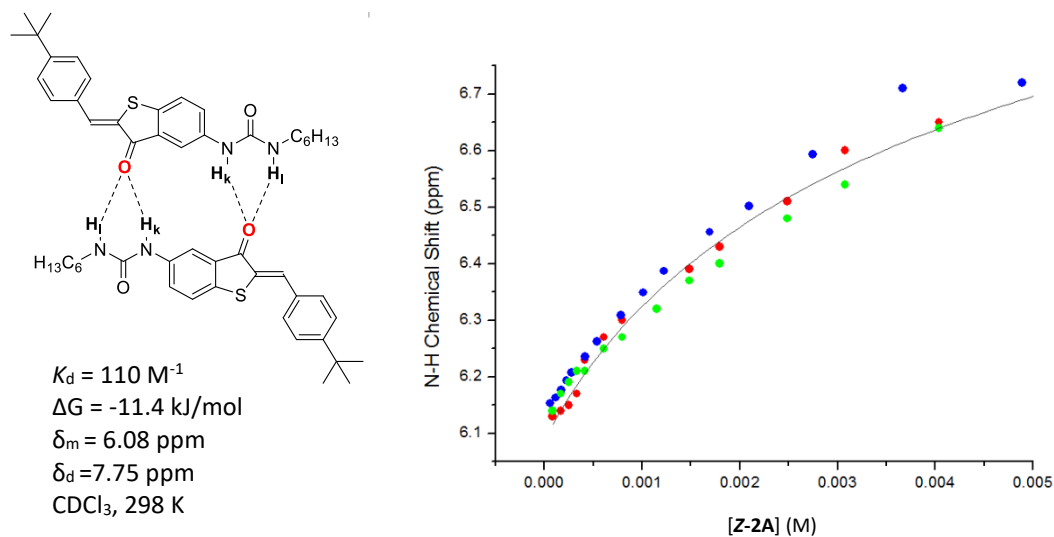


Figure 2.5.3 Calculated binding isotherm (black curve) and ^1H NMR dilution data of **Z-2a** in CDCl_3 at 298 K upon additions of a 4.81 mM solution of **Z-2a** to 0.5 mL of CDCl_3 . The chemical shift of NH_k was plotted vs. concentration of **Z-2a**. The red, blue and green data points correspond to the first, second and third dilutions respectively.

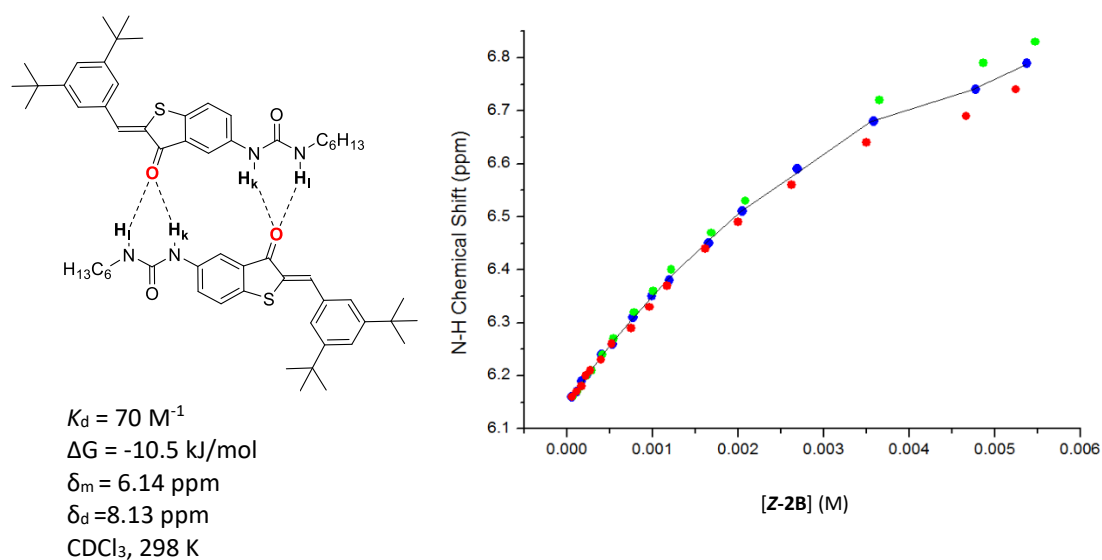


Figure 2.5.4 Calculated binding isotherm (black curve) and ^1H NMR dilution data of **Z-2b** in CDCl_3 at 298 K upon additions of a 7.3 mM solution of **Z-2b** to 0.5 mL of CDCl_3 . The chemical shift of NH_k was plotted vs. concentration of **Z-2b**. The red, blue and green data points correspond to the first, second and third dilutions respectively.

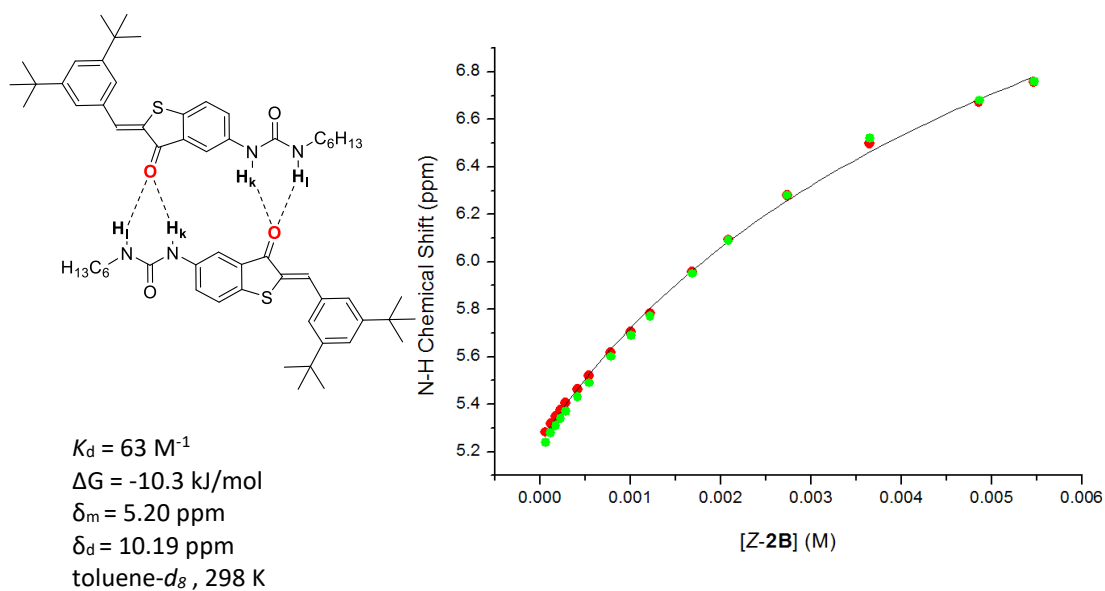


Figure 2.5.5 Calculated binding isotherm (black curve) and ^1H NMR dilution data of **Z-2b** in toluene- d_8 at 298 K upon additions of a 7.3 mM solution of **Z-2b** to 0.5 mL of toluene- d_8 . The chemical shift of NH_k was plotted vs. concentration of **Z-2b**. The red, blue and green data points correspond to the first, second and third dilutions respectively.

isomers of **2b** present in solution to observe whether the *E* isomer would interact with itself and/or the *Z* isomer. If the *E* isomer is only a spectator in the hydrogen bonding equilibria, the dilution data recorded for the *Z* isomer should be identical to that observed on its own. A solution with a known concentration of **Z•Z** was irradiated at 425 nm for 2 hours to generate a 30% conversion to **E-2b** (measured by integration). The solution was then used in the standard dilution procedure to observe the behavior of both isomers simultaneously (Figure 2.5.6 and Figure 2.6.7). The dilution was performed twice and there was no significant change in the isomer ratios over the course of the dilution. The dimerization of the *Z* isomer in solution in the presence of the *E* isomer is very similar to that determined alone ($\Delta K_d = 2 \text{ M}^{-1}$, $\delta_d = 0.29$). Figure 2.5.6 summarizes these findings with the blue and orange spots data points corresponding to the shift of NH_k in **Z-2b** from two separate dilutions of the mixed **Z•E** solutions. The black curve is the average

isotherm calculated from the data. The red line is the average isotherm calculated from three separate dilutions of lone **Z-2b**. The difference is minimal, and one can conclude that **Z-2b** is largely unaffected by complexation with **E-2b** in the mixed solution.

However, we observed, to our surprise that **E-2b** does in fact participate in hydrogen bonding in CDCl_3 . Figure 2.5.7 plots the data plots corresponding to the NH_k shift of **E-2b** in the mixed **Z/E-2b** solutions during dilution in CDCl_3 .

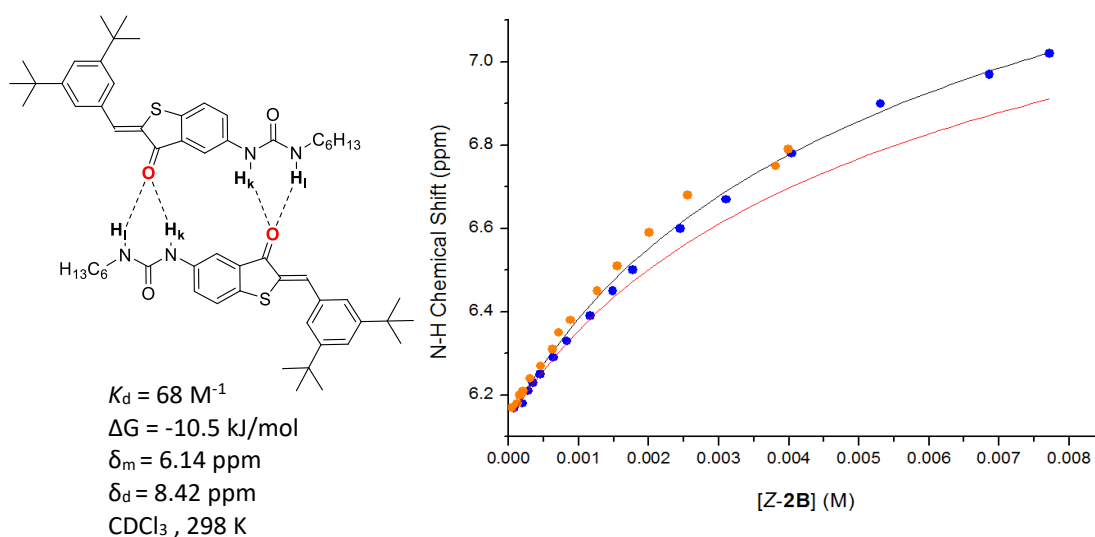


Figure 2.5.6 Calculated binding isotherm and ^1H NMR dilution data of **Z-2b** in a mixture of **Z/E-2b** in CDCl_3 at 298 K upon additions of a 7.7 mM solution mixture of **Z/E-2b** to 0.5 mL of CDCl_3 . The chemical shift of NH_k was plotted vs. concentration of **Z-2b**. The blue and orange data points correspond to the first and second separate dilutions respectively. The black line is the average isotherm of the two data sets. The red line denotes the average isotherm of three separate dilution experiments of the lone **Z** isomer.

Assuming minimal interference from complexation with **Z-2b**, the dimerization of **E-2b** was calculated to be 210 M^{-1} ; a 3-fold increase of that observed for the lone **Z-2b** in solution. We surmise that bond rotation of the bis(t-butyl)phenyl ring and a concomitant

loss of coplanarity (deduced by the lack of downfield shift of the two ortho protons, H_b , see section 2.4) with the carbonyl group allows for dimerization. The phenyl ring must then stabilize dimer formation in some way, perhaps through $N-H \cdots \pi$ interactions. Regardless of the origin of the effect, the hypothetical steric block of the carbonyl moiety by the phenyl substituent does not function as planned.

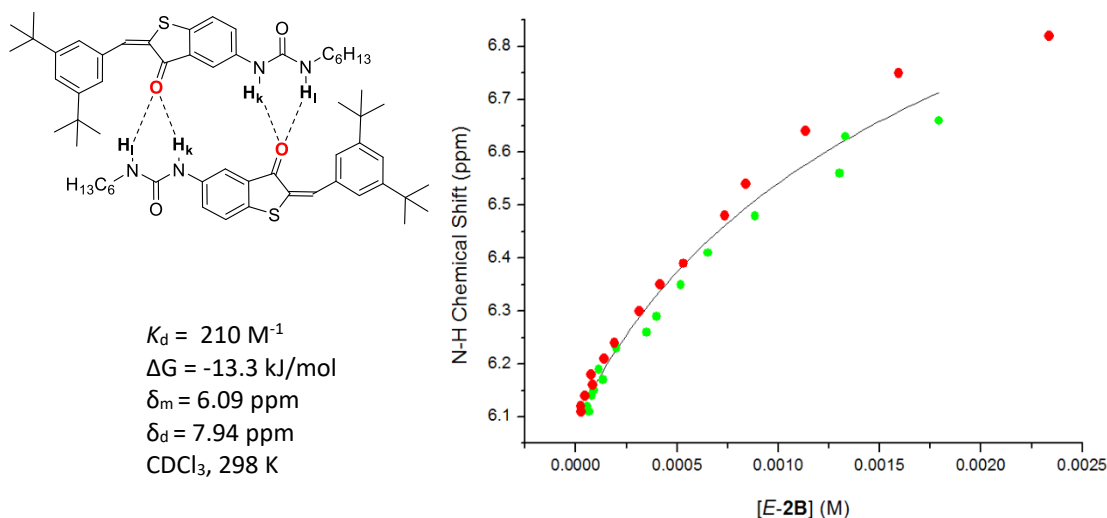


Figure 2.5.7 Calculated binding isotherm and ^1H NMR dilution data of **E-2b** in a mixture of **Z/E-2b** in CDCl_3 at 298 K upon additions of a 7.7 mM solution mixture of **Z/E-2b** to 0.5 mL of CDCl_3 . The chemical shift of NH_k was plotted vs. concentration of **E-2b**. The red and green data points correspond to the first and second separate dilutions respectively. The black line is the average isotherm.

The addition of the electron withdrawing group - 3,5-bis(trifluoromethyl)phenyl – (**Z-2c**) increased the K_d by a factor of *ca.* 3 ($K_d = 230 \text{ M}^{-1}$) from its alkyl counterpart (**Z-2b**). The Gibbs free energy was calculated to be -13.5 kJ/mol with $\Delta\delta_{\text{max}} = 1.06$. The urea protons of **Z-2c** are more acidic because of the inductive character of the trifluoromethyl groups, thus; the increase in dimerization constant is expected.

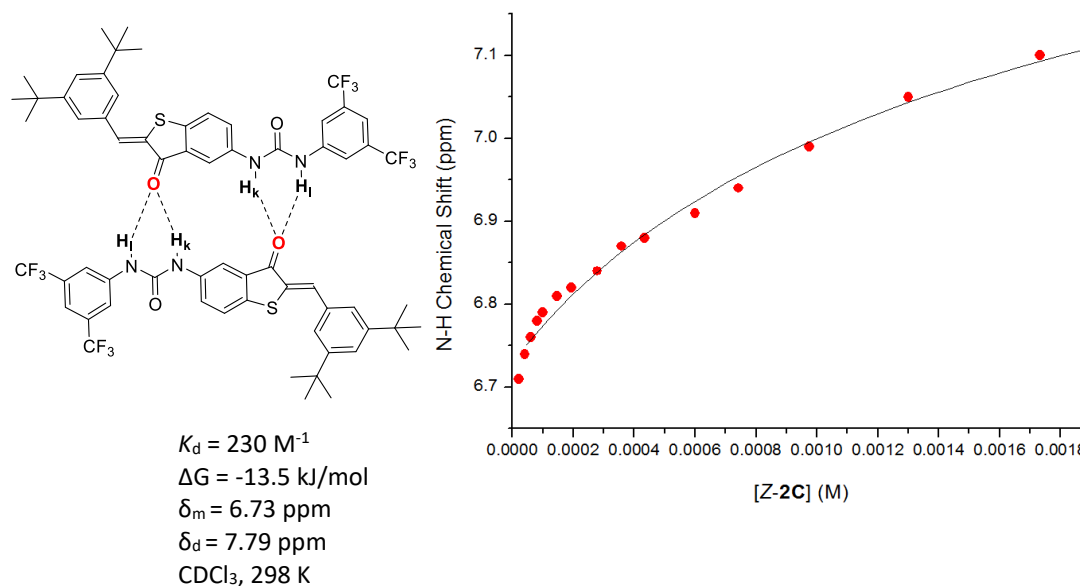


Figure 2.5.8 Calculated binding isotherm (black curve) and ^1H NMR dilution data of **Z-2c** in CDCl_3 at 298 K upon additions of a 2.6 mM solution of **Z-2c** to 0.5 mL of CDCl_3 . The chemical shift of NH_k was plotted vs. concentration of **Z-2b**.

The dilution of **Z-3a** in CDCl_3 , yielded a $K_d = 1100 \text{ M}^{-1}$ (a 10-fold difference compared to **Z-2a**) with a $\Delta G = -17.3 \text{ kJ/mol}$ and shifted a total of 1.03 ppm. This derivative (shown in Figure 2.5.4) has a julolidine substituent which through resonance and conjugation donates electron density to the carbonyl oxygen of the hemithioindigo. This in turn causes the carbonyl to transiently possess a partial negative charge which increases the electrostatic character of both atoms within the hydrogen bond. The 10-fold increase in the K_d illustrates that the ketone oxygen on the hemithioindigo is the acceptor participating in dimerization as substitution at the stilbene side of the molecule should have very little effect on the urea carbonyl group.

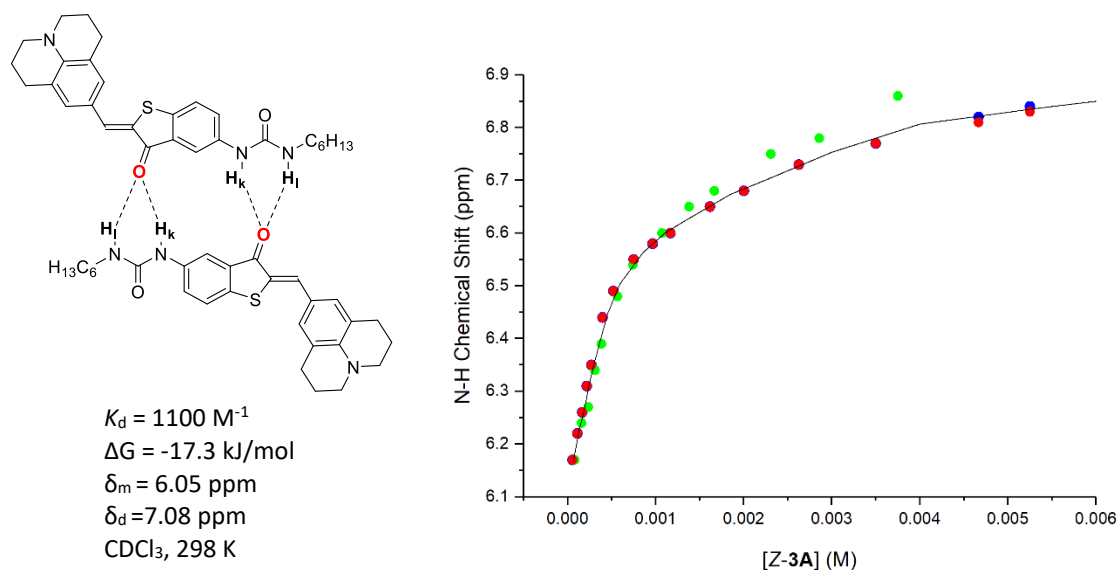


Figure 2.5.9 Calculated binding isotherm and ¹H NMR dilution data of **Z-3a** in CDCl₃ at 298 K upon additions of a 10 mM solution of **Z-3a** to 0.5 mL of CDCl₃. The chemical shift of NH_k was plotted vs. concentration of **Z-3a**. The red, blue and green data points correspond to the first, second and third dilutions respectively.

We expected the addition of the electron withdrawing group, 3,5-bis(trifluoromethyl)phenyl, in **Z-3b** to the julolidine design should increase the K_d from its alkyl counterpart (**Z-3a**). This prediction follows from the strong electron-withdrawing nature of the trifluoromethyl groups. In reality, the K_d of **Z-3b** is lower than **Z-3a** by approximately 10% ($K_d = 990 \text{ M}^{-1}$). The Gibbs free energy was calculated to be $\Delta G = -17.1 \text{ kJ/mol}$ with $\Delta\delta_{\text{max}} = 2.17$. One reason for the unpredicted result may be due to the steric interference between the trifluoromethyl groups and the alkyl groups on the julolidine substituent during dimerization (vide infra Figure 2.6.5).

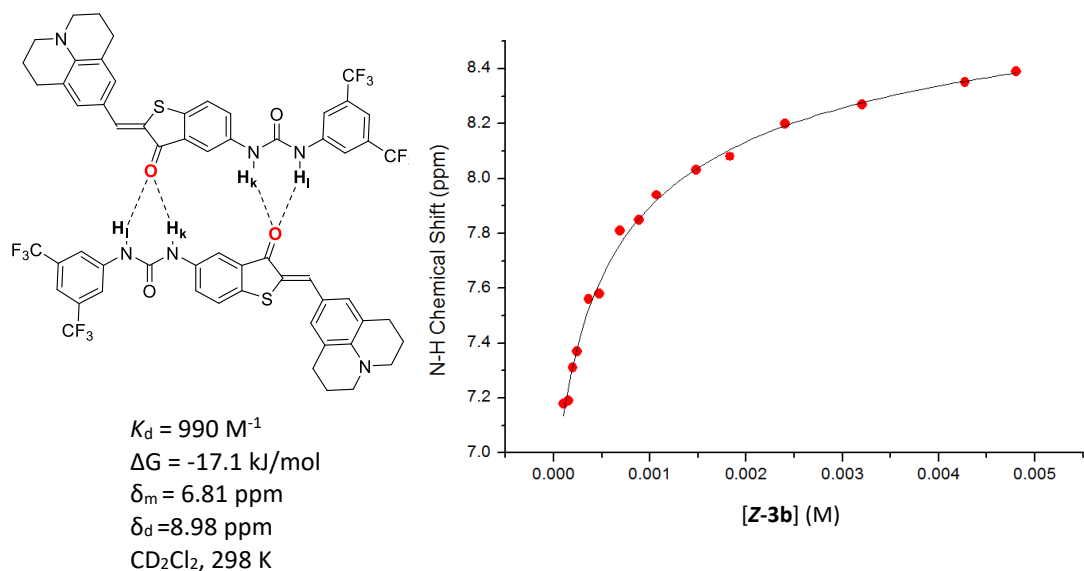


Figure 2.5.10 Calculated binding isotherm (black curve) and ^1H NMR dilution data of **Z-3b** in CDCl_2 at 298 K upon additions of a 10 mM solution of **Z-3b** to 0.5 mL of CDCl_2 . The chemical shift of NH_k was plotted vs. concentration of **Z-3b**.

Overall, the dimerization constants ranged from 63 to 1100 M^{-1} . The weakest dimerization isotherm was of **Z-2b** in toluene- d_8 and the strongest was of **Z-3b** in CDCl_3 . The combined results are tabulated in Table 2.5 below. The Gibbs free energy of the corresponding complexes varied from -10.3 kJ/mol to -17.3 kJ/mol implying that complex formation is indeed a spontaneous process. When comparing **Z-2b**, and **Z-2c**, the addition of the 3,5-bis(trifluoromethyl)phenyl group increased the ΔG of **Z-2c** by 161 kJ/mol. This implies that the hydrogen bond dimerization was stronger and had greater stability as the electron-withdrawing group pulled electron density away from the urea protons and the hemithioindigo ring. The Gibbs free energies were relatively the same for **Z-3a** and **Z-3b** ($\Delta G = -17 \text{ kJ/mol}$). The design of **2b** as a hypothetical steric block in the *E* form did not function as planned as **E-2b** was found to dimerize with a $K_d = 210 \text{ M}^{-1}$ in CDCl_3 and possessed a larger ΔG (-13.3 kJ/mol) than its *Z* counterpart. Nevertheless, in a

solution mixture of **Z/E-2b**, the isomers were found to have a greater affinity for complexation with themselves instead of **Z•E**.

Table 2.5 The dimerization constants, Gibbs free energy and chemical shifts of monomer, dimer and the total change in chemical shift of all derivatives

Derivative	K_d (M^{-1})	ΔG (kJ/mol)	δ_m (ppm)	δ_d (ppm)	δ_{max} (ppm)
Z-2a	$110 \pm 44^{a,d}$	-11.4 ^a	6.08 ^a	7.75 ^a	1.67 ^a
Z-2b	$70 \pm 11^{a,d}$ $63 \pm 8^{b,d}$	-10.5 ^a -10.3 ^b	6.14 ^a 5.20 ^b	8.13 ^a 10.19 ^b	1.99 ^a 4.99 ^b
E-2b	$210 \pm 100^{a,d}$	-13.3 ^a	6.09 ^a	7.94 ^a	1.21 ^a
Z-2c	230 ± 66^a	-13.5 ^a	6.73 ^a	7.79 ^a	1.06 ^a
Z-3a	$1100 \pm 282^{a,d}$	-17.3 ^a	6.05 ^a	7.08 ^a	1.03 ^a
Z-3b	990 ± 185^c	-17.1 ^c	6.81 ^c	8.98 ^c	2.17 ^c

^a Average values obtained using Equation 5 and three separate dilution experiments in $CDCl_3$. ^b Average values obtained using Equation 5 and three separate dilution experiments in toluene. ^c Average values obtained using Equation 5 and three separate dilution experiments in CD_2Cl_2 . ^d Errors calculated from two times the standard deviation to give a 95% confidence interval.¹³

2.6 X-ray Structural Analysis of **DDAA•AADD** Arrays

We attempted to crystallize all nine hydrogen bond arrays in order to investigate their solid state structure using single crystal X-ray diffraction. Suitable crystals of **Z-1c**, **Z-2a** and **Z-3b** were obtained. Crystals were grown either by slow evaporation or slow diffusion.

2.6.1 X-ray Structural Analysis of **Z-1c** Array

Array **Z-1c** was crystallized upon standing from a dark violet DMSO solution after one week in the dark at room temperature. A molecule of **Z-1c** and DMSO crystallized in the asymmetric, monoclinic unit space group; $C 2/c$. The two molecules were doubly hydrogen bonded (as shown in Figure 2.6.1) where the DMSO sulfoxide oxygen forms short contacts with the urea protons ($O1S \cdots H1N1 = 2.856 \text{ \AA}$, Table 2.6.2). In addition, there are no significant hydrogen bond interactions between individual **Z-1c** likely because of the competitive nature of the occluded DMSO solvent. There are further close intramolecular contacts between C-H groups and O2/O3 ($C4H4 \cdots O2 = 2.9796 \text{ \AA}$; $C20H20 \cdots O3 = 2.898 \text{ \AA}$; $C23H23 \cdots O3 = 2.890 \text{ \AA}$, Table 2.6.2) in **Z-1c** that serve to provide stability of the nearly planar conformation (no heavy (non-fluorine) atom deviating from the least squares plane, 0.0023 \AA). The **Z-1c** molecules align with each other via a slipped π -stacking antiparallel arrangement in planes normal to $0.690, -0.685, 0.235$ (Figure 2.6.2) with inversion symmetry relating neighboring molecules.

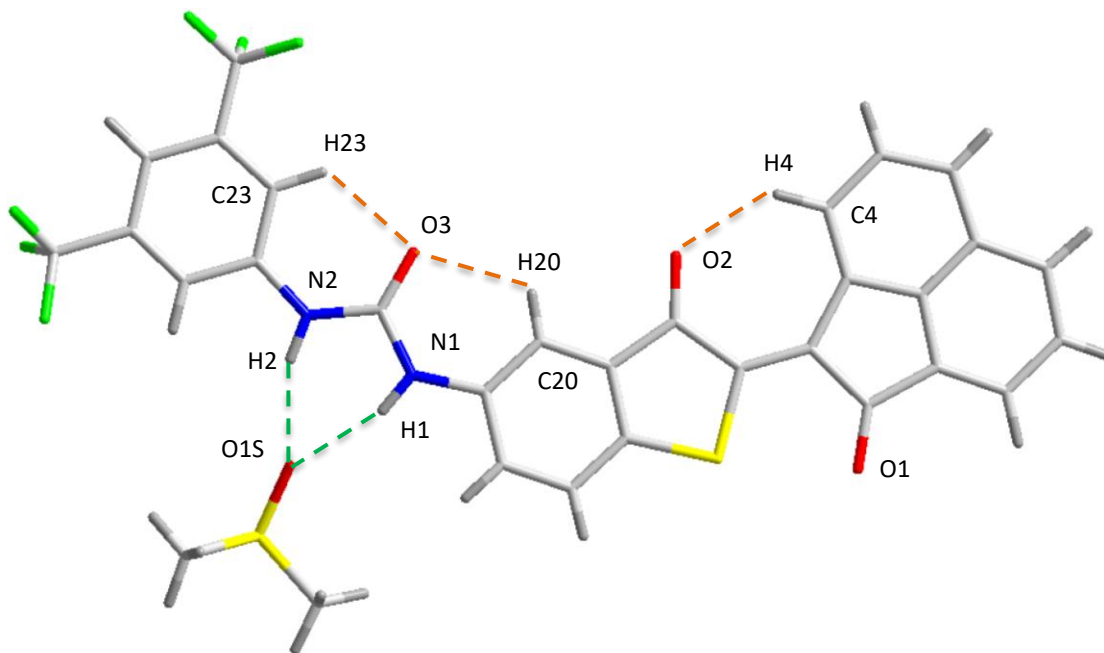


Figure 2.6.1 The stick representation of the asymmetric unit in the X-ray crystal structure of **Z-1c** hydrogen bonding to a molecule of DMSO. Intermolecular hydrogen bonds indicated (dashed green lines) and intramolecular close contacts are indicated (dashed orange lines). Light grey, dark grey, red, blue, yellow and green correspond to carbon, hydrogen, oxygen, nitrogen, sulfur and fluorine atoms, respectively.

Table 2.6.1 Crystallographic parameters for **Z-1c** crystals

Crystal Parameter	Z-1c
Chemical Formula	$C_{31}H_{20}F_6N_2O_4S_2$
Formula Weight ($\text{g}\cdot\text{mol}^{-1}$)	662.61
Crystal System	monoclinic
Space Group	$C 2/c$
a (Å)	30.160 (12)
b (Å)	9.662 (4)
c (Å)	19.613 (8)
α (°)	90
β (°)	103.232 (7)
V (Å ³)	5564 (4)
T (K)	110
Z	8
λ (Mo $K\alpha$) (Å)	0.71073
ρ_{calc} ($\text{g}\cdot\text{cm}^{-3}$)	1.582
γ (°)	90
μ (cm^{-1})	0.275
$F(000)$	2704
reflections collected	69789
unique reflections	4905
absorption correction	multi-scan
refinement on	F^2
parameters defined	496
$R(F_0)$ ($I > 2\sigma(I)$)	0.0369
$R_w(F_0^2)$ ($I > 2\sigma(I)$)	0.0818
$R(F_0)$ (all data)	0.0588
$R_w(F_0^2)$ (all data)	0.0918
GOF on F^2	1.022

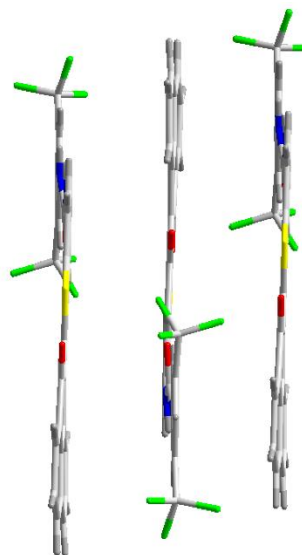


Figure 2.6.2 The stick representation of the X-ray crystal structure of **Z-1c** displaying planarity of the molecules via π -stacking and the slipped π -stacking perpendicular to the 0.690, -0.685 and 0.235 direction.

Table 2.6.2 Hydrogen bond distances and angles of **Z-1c** obtained from single crystal X-ray structure data

Bonds (D····A)	Distances <u>N</u>-<u>H</u>····<u>O</u> (Å)	Distances <u>N</u>-<u>H</u>····<u>O</u> (Å)	Angles (°) <u>N</u>-<u>H</u>····<u>O</u>
N1-H1····O1S	2.856(3)	2.03(3)	160(3)
N2-H2····O1S	2.842(3)	2.00(3)	159(3)
N2-H2O····O3	2.842(3)	2.00(3)	159(3)
C20-H2O····O3	2.898(3)	2.35(2)	119.3(18)
C23-H23····O3	2.890(3)	2.28(2)	121.0(18)
C4-H4····O2	2.9796(3)	2.2298(2)	121.3(18)

2.6.2 X-ray Structural Analysis of **Z-2a** Array

Bright red **Z-2a** crystallized in a triclinic space group; $P\bar{1}$ from dichloromethane. The crystals, once formed, did not occlude solvent and were air stable without loss of integrity. Two molecules occupy the asymmetric unit forming a hydrogen bonded dimer in an antiparallel manner (see Figure 2.6). The self-complementary arrays are largely planar with the two benzothiophenone rings canted with respect to each other at an angle of 33.47° (angle between mean planes of all heavy atoms in the backbone). The ureido moieties deviate from their respective benzothiophenones by 9.51° and 29.4° (angles of mean planes of atoms N1A,N2A,C20A,O2A and N1B,N2B,C20B, O2B respectively). Hydrogen bonds between urea donors and opposing ketone acceptors (N1A-H1A···· O1B = 2.12 Å; N2A-H2A···· O1B = 2.32 Å; N1B-H1B···· O1A = 2.25 Å; N2B-H2B···· O1A = 2.25 Å) stabilize the solid state structure of the dimer. It is also notable that the alkene proton is outside the distance limit for detection plus, the absence of an additional neighboring proton inhibits the use of correlation by a ^1H NMR NOESY experiment. The hydrogen bond angles are all less than ideal with the lowest (N2B-H2B····O1A = 132°) associated with the longest contact (refer to Table 2.6.1).

Table 2.6.3 Crystallographic parameters for **Z-2a** crystals

Crystal Parameter	Z-2a
Chemical Formula	C ₂₆ H ₃₂ N ₂ O ₂ S
Formula Weight (g.mol ⁻¹)	436.59
Crystal System	Triclinic
Space Group	<i>P</i> $\bar{1}$ (2)
<i>a</i> (Å)	9.9569(14)
<i>b</i> (Å)	12.8837(16)
<i>c</i> (Å)	19.373(3)
α (°)	108.964(6)
β (°)	102.633(6)
<i>V</i> (Å ³)	2285.39(60)
<i>T</i> (K)	110
<i>Z</i>	4
λ (Cu K α) (Å)	1.5478
ρ_{calc} (g·cm ⁻³)	1.26881
γ (°)	90.348(6)
μ (cm ⁻¹)	1.450
F (000)	936
reflections collected	31311
unique reflections	5146
absorption correction	multi-scan
refinement on	F ²
parameters refined	727
R (F ₀) (I > 2 σ (I))	0.0568
Rw(F ₀ ²) (I > 2 σ (I))	0.1536
R (F ₀) (all data)	0.0968
Rw(F ₀ ²) (all data)	0.1322
GOF on F ²	1.013

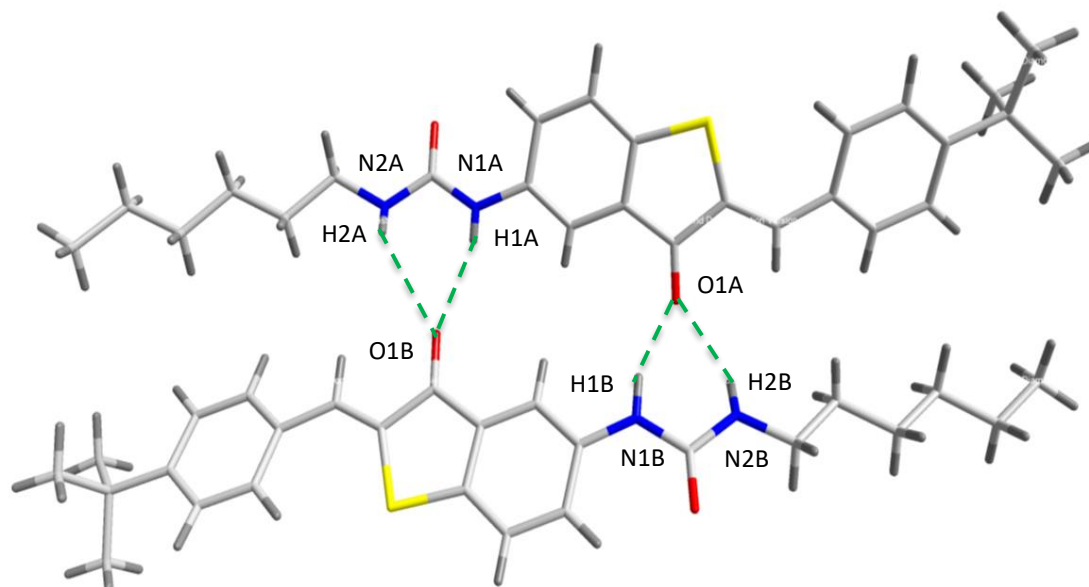


Figure 2.6.3 The stick representation of the X-ray crystal structure of **Z-2a** dimer with intermolecular hydrogen bonds indicated (dashed green lines). Light grey, dark grey, red, blue, and yellow correspond to carbon, hydrogen, oxygen, nitrogen and sulfur atoms, respectively.

The formation of a dimer in the solid state that conforms to our expected design for **Z-2a** supports the solution state dimerization in a similar manner.

Table 2.6.4 Hydrogen bond distances and angles of **Z-2a** dimer obtained from single crystal X-ray structure data

Bonds (D····A)	Distances <u>N</u>-<u>H</u>····<u>O</u> (Å)	Distances <u>N</u>-<u>H</u>····<u>O</u> (Å)	Angles (°) <u>N</u>-<u>H</u>····<u>O</u>
N2B-H2B····O1A	3.144(3)	2.591(3)	132(3)
N1B-H1B····O1A	2.939(3)	2.247(3)	161(3)
N1A-H1A····O1B	2.990(3)	2.122(4)	158(3)
N2A-H2A····O1B	3.016(3)	2.314(3)	154(3)

2.6.3 X-ray Structural Analysis of **Z-3b** Array

Dark violet crystals of **Z-3b** were obtained from DMSO upon standing in triclinic space group; $P\bar{1}$. The crystals are occluded by the DMSO solvent in the lattice, but the present array still exists in an extended, largely coplanar conformation. The 3,5-bis(trifluoromethyl)phenyl ring deviates from coplanarity with the benzothiophenone ring system by 21.38° . Similarly, the julolidine aryl ring deviates from coplanarity with the benzothiophenone ring system by 12.05° (calculated using the angle between least squares planes of all heavy atoms in the rings). The DMSO sulfoxide acceptor hydrogen bonds to the urea donors ($N2-H2 \cdots O1S = 2.09 \text{ \AA}$; $N3-H3 \cdots O1S = 1.98 \text{ \AA}$) as shown in Figure 2.6.4.

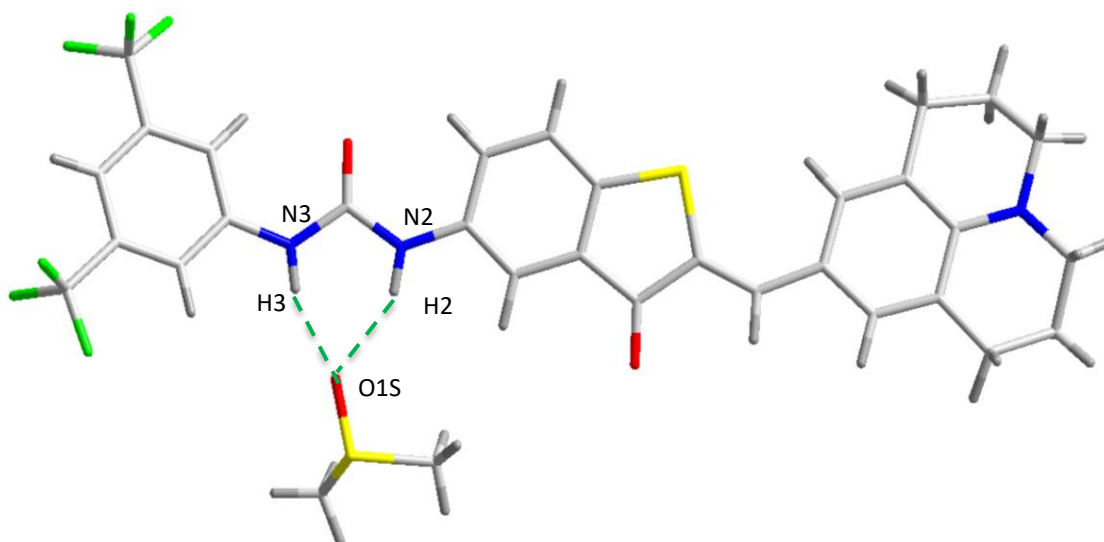


Figure 2.6.4 The stick representation displaying the asymmetric unit of **Z-3b** hydrogen bonding to a molecule of DMSO. Hydrogen bonds are indicated as dashed green lines. Light grey, dark grey, red, blue, yellow and green correspond to carbon, hydrogen, oxygen, nitrogen, sulfur and fluorine atoms, respectively.

Table 2.6.5 Crystallographic parameters for **Z-3b** crystals

Crystal Parameter	Z-3b
Chemical Formula	$C_{32}H_{29}F_6N_3O_3S_2$
Formula Weight ($\text{g}\cdot\text{mol}^{-1}$)	681.70
Crystal System	Triclinic
Space Group	$P\bar{1}$
a (Å)	8.9986(19)
b (Å)	9.330(2)
c (Å)	19.837(4)
α (°)	89.262(11)
β (°)	78.862(8)
V (Å ³)	1479.5(5)
T (K)	110
Z	2
λ (Mo K α) (Å)	0.71073
ρ_{calc} ($\text{g}\cdot\text{cm}^{-3}$)	1.530
γ (°)	65.241(14)
μ (cm^{-1})	0.259
F (000)	704
reflections collected	119170
unique reflections	15887
absorption correction	multi-scan
refinement on	F^2
parameters refined	531
R (F_0) ($I > 2\sigma(I)$)	0.0442
Rw(F_0^2) ($I > 2\sigma(I)$)	0.1149
R (F_0) (all data)	0.0649
Rw(F_0^2) (all data)	0.1255
GOF on F^2	1.047

Table 2.6.6 Hydrogen bond distances and angles of **Z-3b** obtained from single crystal X-ray structure data

Bonds (D···A)	Distances N-H···O (Å)	Distances N-H···O (Å)	Angles (°) N-H···O
N2-H2···O1S	2.9232(13)	2.095(15)	155.2(13)
N3-H3···O1S	2.7983(11)	1.976(18)	161.5(16)

2.7 Conclusion

Nine novel self-complementary hydrogen bond arrays (**1a-c**, **2a-d**, and **3a,b**) were designed, synthesized and their dimerization was examined. The arrays, **2a-d**, **3a,b** formed four hydrogen bonds in a bifurcated manner in both the solution and the solid state. The stability of the dimers varied depending on the substitution of the stilbene and urea fragments with values ranging from 63 M^{-1} to 1100 M^{-1} . The Gibbs free energy of the corresponding complexes varied from -10.3 kJ/mol to -17.3 kJ/mol implying that complex formation is indeed a spontaneous process. The model design for the complexes started with **1a**; however, because of insolubility issues, **1b** was synthesized.

Unfortunately, the solubility of **1b** did not improve greatly. To increase the acidity of the urea protons and further modify the solubility, a strong electron withdrawing group was substituted off the urea to give **1c** with similar insolubility. The design was modified to **2a** with 1-(*tert*-butyl)-4-methylbenzene as the chromophore to produce a $K_d = 110 \text{ M}^{-1}$ in CDCl_3 . Installation of a second *t*-butyl group *meta* to the first provided a similar donating factor to the stilbene as **2a**; however, the K_d decreased to 70 M^{-1} in chloroform and 63 M^{-1} in toluene, results that were not expected. Addition of an electron-withdrawing group in

2c lead to an increase in dimerization constant to 230 M^{-1} . Changing the stilbene fragment to julolidine (**3a**) further increased the K_d by 10-fold (1100 M^{-1}) and installing an electron withdrawing substituent at the urea subunit (**3b**) yielded a $K_d = 990 \text{ M}^{-1}$. The Gibbs free energies were relatively the same for **Z-3a** and **Z-3b** ($\Delta G = -17 \text{ kJ/mol}$). Overall, the Gibbs free energies varied from -10.3 kJ/mol to -17.3 kJ/mol confirming that complexation is spontaneous. The design of **2b** as a hypothetical steric block in the *E* form did not function as planned as **E-2b** was found to dimerize with a $K_d = 210 \text{ M}^{-1}$ in CDCl_3 and possessed a larger ΔG (-13.3 kJ/mol) than its *Z* counterpart. Nevertheless, in a solution mixture of **Z/E-2b**, the isomers were found to have a greater affinity for complexation with themselves instead of with each other (**Z•E**).

The X-ray crystal structures of **Z-2a** illustrate solid-state complexation adopting an antiparallel conformation with hydrogen bonds at slightly less than ideal angles with the lowest at 132° (N2B-H2B \cdots O1A), and the highest being 161° (N1B-H1B \cdots O1A). The solid state complexation of **Z-1c** and **Z-3c** were prevented by solvent competition in DMSO. Alterations and suggestions to improve the design and produce stronger complexes are discussed in Chapter 4.

2.8 Experimental Methodology

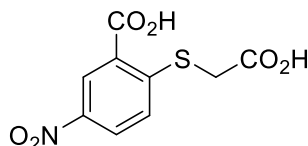
General Notes

All chemicals were purchased from commercial vendors: Sigma-Aldrich, Alfa Aesar, AK Scientific, and Oakwood Chemical and were used as received. Mass spectra were obtained on a Thermo Scientific Double Focusing Sector (DFS) mass spectrometer and samples were analyzed by Electron Impact or Chemical Ionization. Results are

reported in mass-to-charge units; m/z . In the case of inert atmosphere conditions, solvents were dried using an Innovative Technology Inc. Controlled Atmospheres Solvent Purification System that utilizes dual alumina columns (SPS-400-5) or purchased from Sigma-Aldrich and used as received. For reactions that require an oxygen-free environment, a nitrogen atmosphere using standard Schlenk line techniques was administered. Most of the synthetic manipulations and procedures were performed under ambient conditions unless otherwise stated. Photosensitive hydrogen bond arrays were dissolved in their respective NMR solvents then covered to avoid photoisomerization or photoreversion until an NMR experiment was run. To assign the chemical shifts of the *E* isomers, 2D NMR spectroscopy ($^2\text{COSY}$, HMBC, HSQC) was taken. Reactions were monitored by thin-layer chromatography (TLC) on pre-coated TLC-sheets POLYGRAM[®]SIL G/UV254. Column chromatography was performed with SiliCycle[®]SiliaFlash[®] F60, 40-63 μm 60 Å. Nuclear Magnetic Resonance (NMR) spectra were recorded on Bruker 400 MHz, Varian INOVA 400 MHz and Varian INOVA 600 MHz spectrometers (^1H = 400.08 MHz, 399.77 MHz and 599.32 MHz; ^{13}C {1H} = 100.52 MHz and 150.78 MHz respectively). ^1H and ^{13}C spectra were referenced relative to residual solvent signals. Solvents for NMR spectroscopy (chloroform-*d*, DMSO-*d*₆, methylene chloride-*d*₂ and toluene-*d*₈, benzene-*d*₆) were purchased from Cambridge Isotope Laboratories and Sigma-Aldrich which were referenced according to literature values for residual solvent protons.¹⁶ ^1H NMR dilution experiments were performed on INOVA 400 MHz and INOVA 600 MHz spectrometers. X-ray diffraction data was collected on a Bruker-Nonius Apex II diffractometer using graphite monochromatic Cu-

K_{α} radiation ($\gamma = 1.54178 \text{ \AA}$) or a Bruker Kappa Axis Apex II diffractometer using Mo- K_{α} radiation ($\gamma = 0.71073 \text{ \AA}$) and Kappa CCD detector at a temperature of 110K.

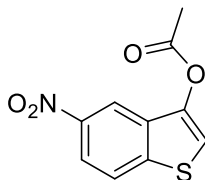
2.8.1 Synthetic Methods



2-((carboxymethyl)thio)-5-nitrobenzoic acid (**5**)

Synthetic procedure was taken from a previous published report with some modifications.²¹

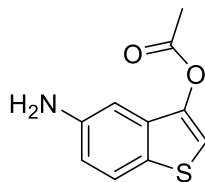
Under a nitrogen atmosphere, a 500 mL round bottom flask equipped with a stir bar and charged with 200 mL anhydrous dimethylformamide was added 2-chloro-5-nitrobenzoic acid (3.0g, 15mmol, 1eq.), sodium bicarbonate (3.8g, 45mmol, 3eq.) and thioglycolic acid (1.4g, 15mmol, 1eq.) at 0°C. The reaction was stirred overnight and allowed to come to room temperature. Once the reaction was complete, the suspension was poured into an ice-water mixture and acidified to pH 1 with concentrated HCl. The resulting precipitate was filtered to yield compound **5** as a pale-yellow solid. Yield: 1.4g, 99%. ¹H NMR (400 MHz, CDCl₃) δ (ppm): 8.83 (d, $J = 2.7\text{Hz}$, 1H), 8.28 (dd, $J = 2.8, 8.8\text{Hz}$, 1H), 8.06 (s, DMF), 7.66 (d, $J = 8.7\text{Hz}$, 1H), 2.98 (s, DMF), 2.90 (s, DMF), *the CH₂ is obstructed underneath the DMF signal*; ¹³C NMR (101 MHz, CDCl₃) δ (ppm): 165.3, 164.4, 162.9, 141.1, 132.4, 127.1, 126.8, 36.7; IR (Diamond ATR): $\tilde{\nu}$ (cm⁻¹) = 2750 (m), 1689 (m), 1685 (m), 1625 (s), 1590 (s), 1525 (s), 1370 (s), 1300 (s), 1248 (s); EI-HRMS: Calc. for C₉H₇NO₆S: 256.9994; Found: 256.9988.



6-nitrobenzo[*b*]thiophen-3-yl acetate (**6**)

Synthetic procedure was taken from a previous published report with some modifications.²¹

Under a nitrogen atmosphere, a 50 mL round bottom flask equipped with a stir bar and 20 mL of acetic anhydride was added **5** (3.0g, 12mmol, 1eq.), and sodium acetate (0.5g, 6.1mmol, 0.5eq.). The reaction was heated to 140°C and allowed to reflux for two hours. After the allotted time, the reaction mixture was poured into 50 mL of boiling water and allowed to cool to room temperature. The resulting precipitate was filtered to yield compound **6** as a pale brown solid. The product was used without any further purification in the following step. Yield: 1.9g, 72%. ¹H NMR (400 MHz, CDCl₃) δ (ppm): 8.62 (d, *J* = 2.1 Hz, 1H), 8.24 (d, *J* = 8.9 Hz, 1H), 7.92 (d, *J* = 8.9 Hz, 1H), 7.64 (s, 1H), 2.48 (s, 3H); ¹³C NMR (101 MHz, CDCl₃) δ (ppm): 21.1, 115.1, 116.7, 119.5, 123.6, 132.2, 141.2, 142.3, 145.6, 167.9; IR (Diamond ATR): $\tilde{\nu}$ (cm⁻¹) = 3370 (s), 2990 (s), 2880 (s), 2869 (s), 1750 (w), 1312 (m); EI-HRMS: Calc. for C₉H₇NO₄S: 237.0096; Found: 237.0093.

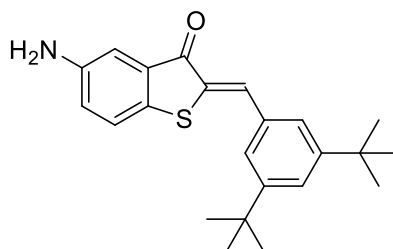


5-aminobenzo[*b*]thiophen-3-yl acetate (**7**)

Synthetic procedure was taken from a previous report with some modifications.¹⁸

Under a nitrogen atmosphere, a 250 mL round bottom flask equipped with a stir bar was added **6** (2.0g, 8.4mmol, 1eq.) and diisopropylethylamine (8.0g, 62mmol, 7.3eq.) in 100

mL of anhydrous dichloromethane. A solution of HSiCl_3 (6.0g, 44mmol, 5.3eq.) in 10 mL of dichloromethane was prepared separately under nitrogen and added dropwise to the first solution over 10 minutes at 0 °C. After stirring the reaction mixture for 18 h, 600 mL of a saturated solution of NaHCO_3 was added slowly and the biphasic mixture was stirred rapidly for 30 min. The crude mixture was extracted with dichloromethane (x3), washed with distilled water (x3), dried over Mg_2SO_4 , filtered and then dried under reduced pressure to afford the pure product, **7**. Yield: 1.7g, 97%. ^1H NMR (400 MHz, CDCl_3) δ (ppm): 7.55 (d, $J = 8.5$ Hz, 1H), 7.31 (s, 1H), 6.93 (s, 1H), 6.81 (d, $J = 8.7$ Hz, 1H), 3.75 (s, 2H), 2.37 (s, 3H); ^{13}C NMR (101 MHz, CDCl_3) δ (ppm): 168.3, 143.9, 139.9, 133.3, 127.5, 123.6, 115.8, 112.8, 104.8, 21.0; IR (Diamond ATR): $\tilde{\nu}$ (cm^{-1}) = 2980 (w), 1700 (m), 1188 (s); EI-HRMS: Calc. for $\text{C}_{10}\text{H}_9\text{NO}_2\text{S}$: 207.0354; Found: 207.0356.

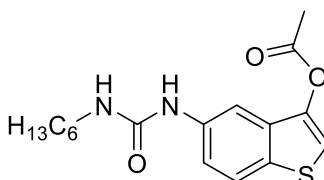


(Z)-5-amino-2-(3,5-di-tert-butylbenzylidene)benzo[b]thiophen-3(2H)-one (7a)

Under a nitrogen atmosphere, a 50 mL round bottom flask equipped with a stir bar and 20% deionized water in ethanol (total volume; 25mL) was added **7** (0.47g, 2.3mmol, 1eq.) and 3,5-di-tert-butylbenzaldehyde (0.54g, 2.5mmol, 1.1eq.) The reaction mixture was heated to 75°C at which point 3 mL of concentrated HCl was added, and the temperature was maintained for 3 hours under reflux. After the allotted time, the resulting solution was cooled and poured into a beaker of 100 mL of ice water. A saturated solution of NaHCO_3 was added dropwise whilst stirring to neutralize the solution. The crude red product was filtered and dried under vacuum. The crude material was then purified by flash chromatography using a solvent mixture 2:1 chloroform : ether as eluent to remove any residual 3,5-di-tert-butylbenzaldehyde. The solution was poured in a round bottom flask and dried under reduced pressure to yield the pure compound **Z-7a**. The

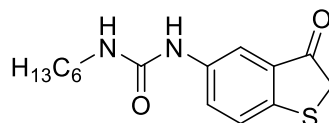
reaction as well as the purification was performed in the dark to give a dark red solid.

Yield: 0.81g, 98%. ^1H NMR (400 MHz, CDCl_3) δ (ppm): 7.98 (s, 1H), 7.57 (d, $J = 1.6$ Hz, 2H), 7.50 (t, $J = 1.7$ Hz, 1H), 7.29 (d, $J = 8.4$ Hz, 1H), 7.25 (d, $J = 2.4$ Hz, 1H), 6.96 (dd, $J = 8.3$ Hz, 2.5Hz, 1H), 3.84 (s, 2H), 1.39 (s, 18H); ^{13}C NMR (101 MHz, CDCl_3) δ (ppm): 188.7, 151.4, 144.6, 135.0, 134.3, 133.5, 131.4, 130.5, 125.3, 124.4, 124.1, 123.2, 111.7, 34.7, 31.2; IR (Diamond ATR): $\tilde{\nu}$ (cm^{-1}) = 3470 (w), 3411 (w), 3362 (m), 2953 (s), 1664 (s), 1625 (m), 1581 (s), 1561 (m), 1472 (s), 1448 (m), 1423 (m), 1392 (m), 1361 (m), 1315 (s), 1177 (s), 1067 (m), 1046 (s).



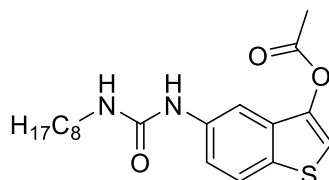
5-(3-hexylureido)benzo[b]thiophen-3-yl acetate (**8a**)

Under a nitrogen atmosphere, a 50mL round bottom flask equipped with a stir bar and 25mL of anhydrous acetonitrile was added **7** (1.0g, 4.8mmol, 1eq.) and hexyl isocyanate (0.92g, 7.2mmol, 1.5eq.) at room temperature. The reaction was monitored with Thin Layer Chromatography. Once the reaction was complete, the crude solid was filtered off and then stirred with petroleum ether for 30 minutes. The solid was filtered to yield the pure compound **8a** as a pale grey solid. Yield: 1.2g, 75%. ^1H NMR (400 MHz, CDCl_3) δ (ppm): 7.79 (d, $J = 2$ Hz, 1H), 7.72 (d, $J = 8.6$ Hz, 1H), 7.42 (s, 1H), 7.23 (dd, $J = 8.6$ Hz, 2Hz, 1H), 6.49 (s, 1H), 4.79 (s, 1H), 3.30-3.26 (m, 2H), 2.40 (s, 3H), 1.59-1.28 (m, 10H), 0.91 (s, 3H); ^{13}C NMR (101 MHz, CDCl_3) δ (ppm): 168.3, 155.8, 140.4, 135.5, 133.0, 132.7, 123.6, 120.4, 113.4, 113.2, 40.6, 31.5, 30.1, 26.6, 22.6, 21.1, 14.0; IR (Diamond ATR): $\tilde{\nu}$ (cm^{-1}) = 3312 (m), 2938 (m), 2880 (m), 2768 (m), 1760 (m), 1630 (s), 1570 (s), 1200 (s); EI-HRMS: Calc. for $\text{C}_{17}\text{H}_{22}\text{N}_2\text{O}_3\text{S}$: 334.1351; Found: 334.1358.



1-hexyl-3-(3-oxo-2,3-dihydrobenzo[*b*]thiophen-5-yl)urea (**9a**)

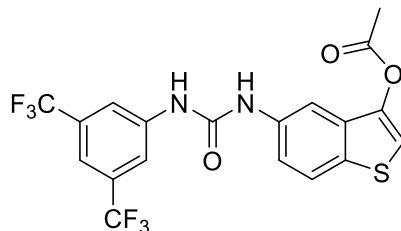
Under a nitrogen atmosphere, a 50 mL round bottom flask equipped with a stir bar and 10 mL of a 2:1 (v/v) mixture of dimethylformamide and water was added **8a** (1.0g, 2.9mmol, 1eq.) and concentrated sulfuric acid (0.44g, 4.5mmol, 1.5eq.) and refluxed for three hours at 153°C. The reaction was monitored with Thin Layer Chromatography. Once the reaction was complete, the reaction mixture was poured into 50 mL of distilled water and allowed to stir for 30 minutes until the resulting mixture cooled to room temperature. The resulting precipitate was filtered to yield compound **9a** as a pale green solid. The product was used without any further purification in the following step. Yield: 0.63g, 72%. ¹H NMR (400 MHz, CDCl₃) δ (ppm): 7.85 (dd, *J* = 8.6 Hz, 2.2 Hz, 1H), 7.43 (d, *J* = 2.1 Hz, 1H), 7.33 (d, *J* = 8.6 Hz, 1H), 6.82 (s, 1H), 5.01 (s, 1H), 3.80 (s, 2H), 3.25 (m, 2H), 1.52 -1.30 (m, 10H), 0.88 (s, 3H) ; ¹³C NMR (101 MHz, CDCl₃) δ (ppm): 200.3, 155.9, 148.3, 136.9, 131.4, 129.1, 125.0, 116.8, 40.6, 40.1, 31.7, 30.2, 26.7, 22.7, 14.2 ; IR (Diamond ATR): $\tilde{\nu}$ (cm⁻¹) = 3281 (w), 2895 (m), 2002 (m), 1675 (s), 1628 (s), 1572 (s), 1560 (s), 1455 (s) ;EI-HRMS: Calc. for C₁₇H₂₂N₂O₃S: 292.1245; Found: 292.1240.



5-(3-(2-ethylhexyl)ureido)benzo[*b*]thiophen-3-yl acetate (**8b**)

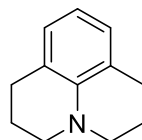
Under a nitrogen atmosphere, a 50mL round bottom flask equipped with a stir bar and 25mL of anhydrous acetonitrile was added **7** (1.0g, 4.8mmol, 1eq.) and 2-ethyl hexyl isocyanate (0.92g, 7.2mmol, 1.5eq.) at room temperature. The reaction was monitored

with Thin Layer Chromatography. Once the reaction was complete, the crude solid was then stirred with petroleum ether for 30 minutes. The resulting precipitate was filtered to yield the pure compound **8b** as a pale grey solid. Yield: 1.2g, 75%. ^1H NMR (400MHz, CDCl_3) δ (ppm): 7.73 (dd, $J = 8.6$ Hz, 2.2 Hz, 1H), 7.70 (d, $J = 2.2$ Hz, 1H), 7.41 (s, 1H), 7.20 (d, $J = 8.6$ Hz, 1H), 6.32 (s, 1H), 4.66 (s, 1H), 3.21 (m, 2H), 2.38 (s, 3H), 1.55 (s, 1H), 1.45-1.27 (m, 10H), 0.90 (s, 3H); ^{13}C NMR (101 MHz, CDCl_3) δ (ppm): 168.8, 156.6, 140.9, 136.1, 133.4, 132.8, 124.0, 120.5, 113.7, 113.1, 43.8, 40.1, 31.4, 29.3, 24.7, 23.5, 21.5, 14.5, 11.3; IR (Diamond ATR): $\tilde{\nu}$ (cm^{-1}) = 3364 (m), 2956 (w), 2924 (w), 2850 (w), 1665 (s), 1536 (s), 1590 (w), 1469 (m); EI-HRMS: Calc. for $\text{C}_{19}\text{H}_{26}\text{N}_2\text{O}_3\text{S}$: 362.1664; Found: 362.1652.



5-(3-(3,5-bis(trifluoromethyl)phenyl)ureido)benzo[b]thiophen-3-yl acetate (**8c**)

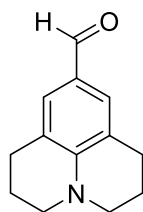
Under a nitrogen atmosphere, a 50 mL round bottom flask equipped with a stir bar and 25 mL of anhydrous acetonitrile was added **7** (1.0g, 4.8mmol, 1eq.) and 3,5-bis(trifluoromethyl)phenyl isocyanate (2.46g, 5.3mmol, 1.1eq.) at room temperature. The reaction was stirred for 3 days. Once the reaction was complete, the crude solid was then filtered under vacuum. The resulting precipitate was filtered to yield the pure compound **8c** as a pale grey solid. Yield: 1.7g, 75%. ^1H NMR (400MHz, CDCl_3) δ (ppm): 9.29 (s, 2H), 8.08 (d, $J = 8.5$ Hz, 1H), 7.95 (s, 3H), 7.81 (d, $J = 1.8$ Hz, 1H), 7.64 (s, 1H), 7.43 (dd, $J = 8.6$ Hz, 2.2 Hz, 1H), 2.39 (s, 3H); ^{13}C NMR (101 MHz, CDCl_3) δ (ppm): 167.8, 153.6, 140.4, 138.6, 138.3, 133.6, 132.5, 132.2, 131.5, 125.5, 125.3, 124.2, 121.8, 121.4, 120.2, 117.9, 115.0, 20.9, 0.85; IR (Diamond ATR): $\tilde{\nu}$ (cm^{-1}) = 3349 (w), 1749 (w), 1694 (w), 1650 (m), 1572 (m), 1505 (m), 1473 (m), 1443 (m), 1386 (m), 1311 (m), 1273 (s), 1129 (s).



2,3,6,7-tetrahydro-1H,5H-pyrido[3,2,1-ij]quinoline (**10**)

Synthetic procedure was taken from a previous published report with some modifications.²³

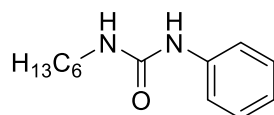
Under a nitrogen atmosphere, a 500 mL round bottom flask equipped with a stir bar and oven dried, was added aniline (9.3g, 1mmol, 1eq.), 1.3-bromochloropropane (236.2g, 1.5mol, 15eq.) and sodium carbonate (42.4g, 4mmol, 4eq.) at room temperature. A glass column equipped with sintered glass and by-passing column for vapor was placed between the reaction vessel and the condensor and packed with molecular sieves (4Å, 10g) a third of the length of the column. The round bottom flask containing the reaction mixture was heated by a gradual increase of the bath temperature (70°C/ 1hour, 100°C/ 2 hours, 160°C/ 12 hours). After the allotted time, the reaction mixture was slowly poured into a 1L beaker of 200 mL of glacial distilled water to which 100 mL of concentrated hydrochloric acid was added. The solution was allowed to stir until the presence of the two layers appeared clear. The aqueous layer of the residual solution was then extracted with dichloromethane (50 mL x 3). The acidic extracts were then basified with 150 mL of 10 M sodium hydroxide and then extracted with dichloromethane (50mL x 3), washed with distilled water (50 mL x 3), dried over Na₂SO₄, filtered and then dried under reduced pressure to afford the pure product as a pale pink oil, **10**. Yield: 13.54g, 78%. ¹H NMR (400MHz, CDCl₃) δ (ppm): 6.77 (d, *J* = 7.4Hz, 2H), 6.49 (t, *J* = 7.4 Hz, 1H), 3.13 (t, *J* = 5.7Hz, 4H), 2.76 (t, *J* = 6.5 Hz, 4H), 1.97 (m, *J* = 6.5 Hz, 4H) ; ¹³C NMR (101 MHz, CDCl₃) δ (ppm): 150.6, 127.1, 105.7, 81.1, 50.0, 34.1, 27.8.



2,3,6,7-tetrahydro-1H,5H-pyrido[3,2-ij]quinoline-9-carbaldehyde (**11**)

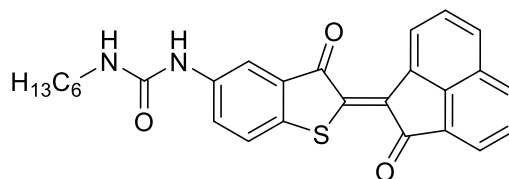
Synthetic procedure was taken from a previous published report with some modifications.²⁴

Under a nitrogen atmosphere, a 250 mL round bottom flask equipped with a stir bar and 50 mL of anhydrous dimethylformamide was added **10** (5.0g, 28.9mmol, 1eq.). In a separate 50 mL round bottom flask with 10 mL of anhydrous dimethylformamide was added phosphoryl chloride (4.4g, 28.9mmol, 1eq.) dropwise at 0 °C. The latter was then combined into the 250 mL round bottom flask and the resulting mixture was heated at 90°C for two hours. Once the reaction was complete, the reaction solution was cooled to room temperature and poured into a 100 mL beaker of glacial distilled water. The mixture was then neutralized to pH 6-8 by addition of saturated sodium acetate. The desired aldehyde precipitated out of solution as a green-brown solid. The solid was filtered, washed with water (25 mL) and hexanes (5 mL) and dried over potassium oxide to afford the pure aldehyde (**11**) as a brown solid. Yield: 4.94g, 85%. ¹H NMR (400MHz, CDCl₃) δ (ppm): 9.60 (s, 1H), 7.29 (s, 2H), 3.29 (t, *J* = 6.3Hz, 4H), 2.77 (t, *J* = 6.3 Hz, 4H), 1.96 (m, *J* = 6.1Hz, 4H) ; ¹³C NMR (101 MHz, CDCl₃) δ (ppm): 190.6, 148.3, 130.0, 124.5, 120.8, 50.5, 28.1, 21.7; IR (Diamond ATR): $\tilde{\nu}$ (cm⁻¹) = 2900 (m), 2100 (m), 1620 (s), 1590 (s), 1520 (s), 1510 (s), 1450 (s), 1370 (s), 1125 (s).



1-hexyl-3-phenylurea (**13**)

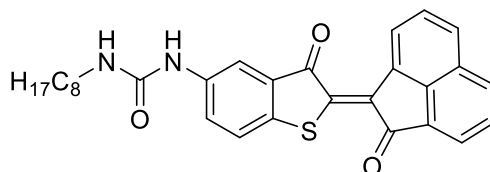
Under a nitrogen atmosphere, a 50 mL round bottom flask equipped with a stir bar and 25mL of anhydrous acetonitrile was added aniline (0.1g, 1.1mmol, 1eq.) and hexyl isocyanate (0.14g, 1.1mmol, 1eq.) at room temperature. The reaction was monitored with Thin Layer Chromatography. Once the reaction was complete, the crude solid was filtered off and washed with cold acetonitrile to yield the pure compound **13** as a white solid. Yield: 0.20g, 85%. ¹H NMR (400MHz, CDCl₃) δ (ppm): 7.37 – 7.28 (m, 4H), 7.10 (t, *J* = 7.0Hz, 1H), 6.28 (s, 1H), 4.73 (s, 1H), 3.24 (t, *J* = 8Hz, 2H), 1.59 – 1.29 (m, 8H), 0.88 (t, *J* = 8Hz, 3H); ¹³C NMR (101 MHz, CDCl₃) δ (ppm): 155.9, 138.6, 138.5, 129.0, 123.7, 123.4, 121.0, 120.7, 40.6, 40.2, 31.3, 30.0, 29.9, 26.4, 22.4, 13.8; IR (Diamond ATR): $\tilde{\nu}$ (cm⁻¹) = 3750 (m), 3569 (m), 2900 (s), 2985 (s), 2130 (s), 1625 (s), 1562 (s), 1499 (m), 1470 (m); EI-HRMS: Calc. for C₁₇H₂₂N₂O₃S: 334.1351; Found: 334.1358.



(*Z*)-1-hexyl-3-(3-oxo-2-(2-oxoacenaphthylen-1(2*H*)-ylidene)-2,3-dihydrobenzo[*b*]thiophen-5-yl)urea (**Z-1a**)

Under a nitrogen atmosphere, a 50 mL round bottom flask equipped with a stir bar and 25 mL of anhydrous dimethylformamide was added **9a** (0.63g, 2.2mmol, 1eq.), acenaphthylene-1,2-dione (0.35g, 2.2mmol, 1eq.) and potassium carbonate (0.20g, 1.5mmol, 0.3eq.) at room temperature. The reaction was protected from light. Once the reaction was deemed complete (after 24h), the resulting precipitate was filtered to yield the pure compound **Z-1a** as a red solid. Yield: 0.49g, 50%. ¹H NMR (400 MHz, DMSO-

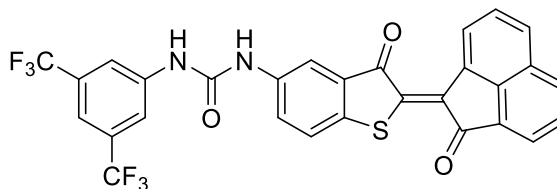
d_6) δ (ppm): 9.42 (d, $J = 6.0\text{Hz}$, 1H), 8.81 (s, 1H), 8.39 (d, $J = 9.6\text{Hz}$, 1H), 8.25 (d, $J = 12.0\text{Hz}$, 1H), 8.13 (s, 1H), 7.91 (d, $J = 6.9\text{Hz}$, 1H), 7.65 (s, 1H), 6.31 (s, 1H), 3.11 (m, 2H), 1.45-1.29 (m, 8H), 0.88 (s, 3H); *theor.* ^{13}C NMR (101 MHz, CDCl_3) δ (ppm): 146.3, 137.9, 187.0, 188.0, 136.3, 122.8, 134.5, 162.4, 127.5, 141.1, 130.1, 119.8, 133.6, 129.4, 131.9, 126.3, 134.8, 128.2, 127.9, 131.9, 154.3, 40.2, 29.5, 26.0, 31.5, 22.7, 14.1; EI-HRMS: Calc. for $\text{C}_{27}\text{H}_{24}\text{N}_2\text{O}_3\text{S}$: 456.1508; Found: 456.1499.



(Z)-1-(2-ethylhexyl)-3-(3-oxo-2-(2-oxoacenaphthylen-1(2H)-ylidene)-2,3-dihydrobenzo[b]thiophen-5-yl)urea (Z-1b)

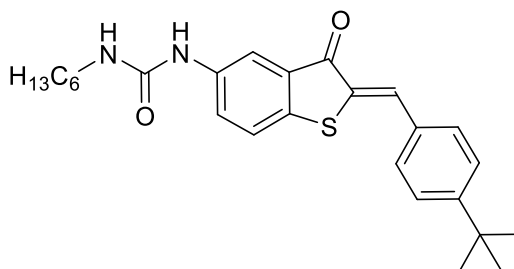
Under a nitrogen atmosphere, a 50 mL round bottom flask equipped with a stir bar and 20 mL of ethanol and 5 mL of distilled water was added **8b** (0.84g, 2.3mmol, 1eq.), acenaphthylene-1,2-dione (0.42g, 2.3mmol, 1eq.). The reaction mixture was heated to 75°C at which 3 mL of concentrated HCl was added, and the temperature was maintained for 3 hours under reflux. After the allotted time, the resulting solution was cooled and poured into a beaker of 100 mL of distilled water. The solid was filtered and dried under vacuum. The crude material was then purified by flash chromatography using a solvent mixture 2:1 chloroform : ether as eluent to remove any residual acenaphthylene-1,2-dione. The solution was poured in a round bottom flask and dried under reduced pressure to yield the pure compound **Z-1b**. The reaction as well as the purification was performed in the dark to give a dark magenta solid. Yield: 1.12g, 93%. ^1H NMR (400 MHz, $\text{DMSO-}d_6$) δ (ppm): 9.40 (d, $J = 7.3\text{Hz}$, 1H), 9.39 (s, 1H), 8.73 (d, $J = 8.1\text{Hz}$, 1H), 8.37 (d, $J = 8.20\text{Hz}$, 1H), 8.13 (s, 1H), 8.11 (d, $J = 7.0\text{Hz}$, 1H), 7.91 – 7.86 (m, 2H), 7.62 (m, 2H), 6.22 (s, 1H), 3.08 (m, 2H), 1.40 (m, 1H), 1.28 (m, 8H), 0.88 (s, 6H); ^{13}C NMR (101 MHz, CDCl_3) δ (ppm): 211.3, 192.7, 190.4, 159.1, 154.6, 139.4, 139.0, 137.8, 137.6, 132.0, 131.8, 130.8, 130.0, 129.6, 128.3, 128.2, 127.9, 125.7, 125.2, 124.0, 121.6, 113.7,

41.0, 29.8, 27.8, 23.0, 21.9, 13.4, 10.2; IR (Diamond ATR): $\tilde{\nu}$ (cm⁻¹) = 3313 (m), 2950 (s), 2130 (m), 1690 (s), 1630 (s), 1600 (s), 1580 (s), 1562 (s), 1495 (s), 1248 (s).



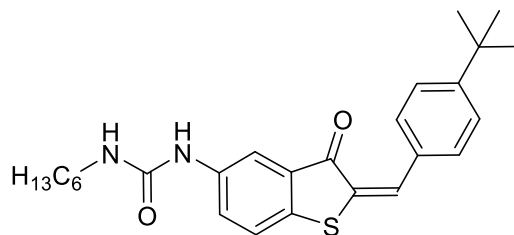
(Z)-1-(3,5-bis(trifluoromethyl)phenyl)-3-(3-oxo-2-(2-oxoacenaphthyl-1(2H)-ylidene)-2,3-dihydrobenzo[b]thiophen-5-yl)urea (Z-1c)

Under a nitrogen atmosphere, a 50 mL round bottom flask equipped with a stir bar and 20 mL of ethanol and 5 mL of distilled water was added **8c** (0.60g, 1.3mmol, 1eq.), acenaphthylene-1,2-dione (0.24g, 1.3mmol, 1eq.). The reaction mixture was heated to 75°C at which 3 mL of concentrated HCl was added, and the temperature was maintained for 3 hours under reflux. After the allotted time, the resulting solution was cooled and poured into a beaker of 100 mL of distilled water. The solid was filtered and dried under vacuum. The crude material was then purified by flash chromatography using a solvent mixture 2:1 chloroform : ether as eluent to remove any residual acenaphthylene-1,2-dione. The solution was poured in a round bottom flask and dried under reduced pressure to yield the pure compound **Z-1c**. The reaction as well as the purification was performed in the dark to give a pale purple solid. Yield: 1.12g, 93%. ¹H NMR (400 MHz, DMSO-*d*₆) δ (ppm): 10.40 (s, 2H), 9.44 (d, *J* = 7.4Hz, 1H), 8.41 (d, *J* = 8.1Hz, 1H), 8.32 (s, 2H), 8.29 (s, 1H), 8.27 (s, 3H), 8.18 (d, *J* = 6.7Hz, 1H), 8.09 (s, 1H), 8.02 (d, *J* = 8.3Hz, 1H), 7.92 (m, 3H), 7.83 (s, 1H); ¹³C NMR (101 MHz, DMSO-*d*₆) δ (ppm): 191.2, 182.6, 181.7, 161.5, 150.9, 148.0, 145.0, 144.5, 138.9, 131.2, 126.3, 111.6, 107.6, 102.3, 101.4, 98.9, 97.5, 87.2, 79.7, 77.1, 57.6, 51.4; IR (Diamond ATR): $\tilde{\nu}$ (cm⁻¹) = 2900 (s), 2878 (m), 2135 (m), 2129 (m), 1700 (s), 1550 (s), 1375 (s), 1270 (s), 1230 (s), 1160 (s), 1125 (s); EI-HRMS: Calc. for C₂₉H₁₄F₆N₂O₃S: 584.06.



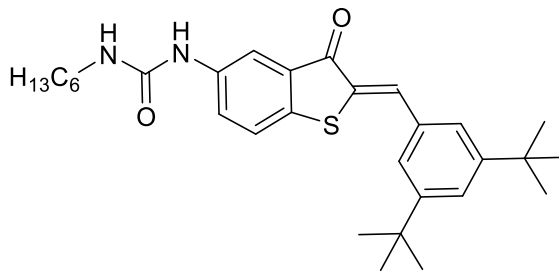
(Z)-1-(2-(4-(tert-butyl)benzylidene)-3-oxo-2,3-dihydrobenzo[*b*]thiophen-5-yl)-3-hexylurea (Z-2a)

Under a nitrogen atmosphere, a 50 mL round bottom flask equipped with a stir bar and 25 mL of anhydrous dimethylformamide was added **9a** (0.63g, 2.2mmol, 1eq.), 4-(tert-butyl)benzaldehyde (0.35g, 2.2mmol, 1eq.) and potassium carbonate (0.20g, 1.5mmol, 0.3eq.) at room temperature. The reaction was protected from light and monitored with Thin Layer Chromatography. Once the reaction was complete, the resulting solution was acidified with 0.1M HCl and subsequently extracted with dichloromethane (x3), washed with distilled water (x3), dried over Mg₂SO₄, filtered and then dried under reduced pressure. The crude material was then stirred in petroleum ether for 30 minutes to remove any residual 4-*tert*-butyl benzaldehyde to yield the pure compound **Z-2a**. The reaction as well as the purification was performed in the dark to give a red solid. Yield: 0.74g, 79%. ¹H NMR (599 MHz, CDCl₃) δ (ppm): 7.95 (dd, *J* = 8.6 Hz, 2.2 Hz, 1H), 7.93 (s, 1H), 7.64 (m, 3H), 7.51 (m, 2H), 7.44 (d, *J* = 8.5 Hz, 1H), 6.59 (s, 1H), 4.85 (s, 1H), 3.28 (m, 2H), 1.53 – 1.32 (m, 17H), 0.88 (s, 3H); ¹³C NMR (101 MHz, CDCl₃) δ (ppm): 218.1, 132.8, 132.0, 131.5, 130.8, 126.7, 41.3, 41.0, 35.5, 32.2, 31.4, 30.7, 27.2, 25.4, 23.2, 14.4, 1.3; IR (Diamond ATR): $\tilde{\nu}$ (cm⁻¹) = 3270 (w), 2940 (m), 2200 (w), 1900 (w), 1640 (m), 1626 (s), 1530 (s), 1505 (m), 1450 (s), 1300 (m), 1195 (s), 1183 (s), 1065 (s); EI-HRMS: Calc. for C₂₆H₃₂N₂O₂S: 436.2184; Found: 436.2184.



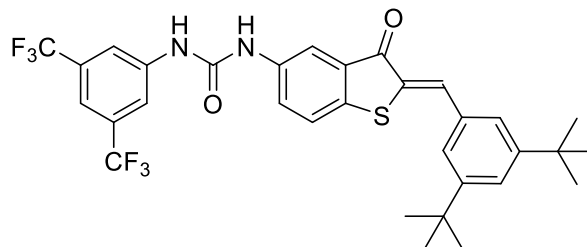
(E)-1-(2-(4-(tert-butyl)benzylidene)-3-oxo-2,3-dihydrobenzo[*b*]thiophen-5-yl)-3-hexylurea (*E*-2a)

In a clean and flame-dried vial, 50 mg of compound **Z-2a** was dissolved in 125 mL of dichloromethane and purged with nitrogen while it was under irradiation at 520 nm light at room temperature for approximately one hour. The conversion of *Z* to *E* isomer was monitored by ^1H NMR until it reached to the maximum amount of converted *E* possible (66%). The solvent was evaporated to 10 mL by blowing air into the flask. The solution was then loaded on a preparatory TLC plate and chloroform/ether (3:1) was used as eluent to yield a red/orange solid. After scraping the fraction off the TLC plate, the contents were stirred in diethyl ether and the solvent was filtered off under vacuum. The solvent was removed to yield **E-2a** as a red solid. The entire procedure was performed in the dark since ambient light can affect isomerization. Yield: 0.025g, 50%. ^1H NMR (599 MHz, CDCl_3) δ (ppm): 8.02 (dd, $J = 8.6$ Hz, 2.2 Hz, 1H), 7.89 (s, 1H), 7.61 (m, 3H), 7.48 (m, 2H), 7.41 (d, $J = 8.5$ Hz, 1H), 7.19 (s, 1H), 5.27 (s, 1H), 3.28 (m, 2H), 1.35 – 1.25 (m, 17H), 0.86 (s, 3H); ^{13}C NMR could not be obtained due to low bistability of *E* isomer in solution.



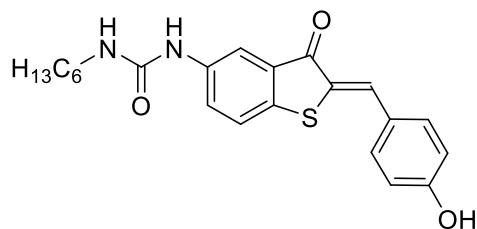
(Z)-1-(2-(3,5-di-tert-butylbenzylidene)-3-oxo-2,3-dihydrobenzo[b]thiophen-5-yl)-3-hexylurea (Z-2b)

Under a nitrogen atmosphere, a 50 mL round bottom flask equipped with a stir bar 20 mL of ethanol and 5 mL of distilled water was added **8a** (0.63g, 2.2mmol, 1eq.), 3,5-di-tert-butylbenzaldehyde (0.4708g, 2.2mmol, 1eq.) and 3 mL of conc. HCl at room temperature. The reaction mixture was heated to 75°C and the temperature was maintained for 3 hours under reflux. The reaction was protected from light during the whole procedure. Once the reaction was deemed complete (after 3h), the resulting solution was cooled and poured into a beaker of 100 mL of icy distilled water and allowed to cool for 15minutes. The solution was then filtered under vacuum to yield an orange solid. The crude material was then purified by flash chromatography using a solvent mixture of 66% chloroform in ether as eluent to remove any residual 3,5-di-tert-butylbenzaldehyde and to yield the pure compound **Z-2b** as a bright red solid. Yield: 1.34g, 80%; ¹H NMR (599 MHz, CDCl₃) δ (ppm): 7.99 (s, 1H), 7.95 (d, *J* = 7.4Hz, 1H), 7.66 (s, 1H), 7.57 (s, 2H), 7.5-7.46 (m, 2H), 6.59 (s, 1H), 4.85 (s, 1H), 3.29 (m, 2H), 1.55-1.31 (m, 26H), 0.87 (s, 3H); ¹³C NMR (101 MHz, CDCl₃) δ (ppm): 205.5, 198.0, 189.2, 155.8, 151.9, 140.3, 137.9, 135.7, 133.9, 133.6, 132.6, 131.1, 130.6, 128.4, 125.7, 125.3, 124.5, 117.1, 115.3, 104.6, 96.1, 81.4, 40.6, 35.1, 31.7, 31.5, 30.4, 26.8, 22.7, 14.2; IR (Diamond ATR): $\tilde{\nu}$ (cm⁻¹) = 3730 (m), 3600 (m), 3590 (m), 3260 (m), 2990 (s), 2940 (s), 2935 (s), 2920 (s), 2880 (s), 2490 (s), 2320 (s), 2310 (s), 2185 (s), 2130 (s), 2090 (s), 2005 (s), 1875 (s), 1630 (s), 1535 (s), 1465 (s), 1200 (s), 1163 (s), 1065 (s); EI-HRMS: Calc. for C₃₀H₄₀N₂O₂S: 492.2810; Found: 492.2796.



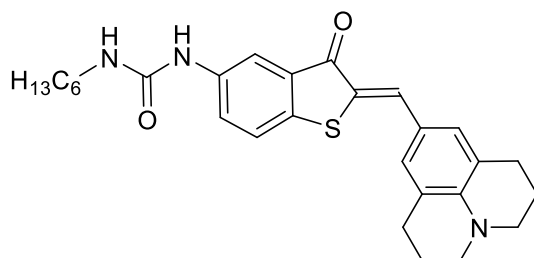
(Z)-1-(3,5-bis(trifluoromethyl)phenyl)-3-(2-(3,5-di-tert-butylbenzylidene)-3-oxo-2,3-dihydrobenzo[b]thiophen-5-yl)urea (Z-2c)

Under a nitrogen atmosphere, a 50 mL round bottom flask equipped with a stir bar and 25 mL of anhydrous acetonitrile was added **12** (81mg, 0.22mmol, 1eq.) and 3,5-bis(trifluoromethyl)phenyl isocyanate (62mg, 0.24mmol, 1.1eq.). The reaction mixture was heated to 80°C and temperature was maintained overnight under reflux. The reaction was protected from light during the whole procedure. Once the reaction was deemed complete by TLC, the resulting solution was cooled to 0°C whilst stirring for 15 minutes. The solution was then filtered under vacuum to yield **Z-2c** as a light orange solid. Yield: 0.13g, 95%. ¹H NMR (599 MHz, CDCl₃) δ (ppm): 8.08 (d, *J* = 8.5Hz, 1H), 8.02 (s, 1H), 7.95 (s, 1H), 7.89 (s, 1H), 7.84 (s, 1H), 7.76 (s, 1H), 7.56 – 7.52 (m, 4H), 7.36 (s, 1H), 1.38 (s, 18H); ¹³C NMR (101 MHz, CDCl₃) δ (ppm): 189.9, 153.0, 152.0, 147.5, 142.3, 140.3, 139.8, 137.6, 136.5, 133.2, 133.1, 132.9, 132.5, 132.3, 131.1, 130.5, 129.3, 127.6, 126.1, 125.9, 124.9, 124.6, 122.2, 121.9, 117.6, 114.3, 111.7, 111.7, 35.1, 31.5, 31.4, 1.2; IR (Diamond ATR): $\tilde{\nu}$ (cm⁻¹) = 3325 (w), 2164 (w), 1991 (w), 1664 (s), 1573 (s), 1471 (s), 1377 (s), 1270 (s), 1270 (s), 1173 (s), 1131 (s).



(Z)-1-hexyl-3-(2-(4-hydroxybenzylidene)-3-oxo-2,3-dihydrobenzo[b]thiophen-5-yl)urea (Z-2d)

Under a nitrogen atmosphere, a 50 mL round bottom flask equipped with a stir bar and 20 mL of ethanol and 5 mL of distilled water was added **8a** (0.51g, 1.7mmol, 1eq.), and 4-hydroxybenzaldehyde (0.23g, 1.9mmol, 1.1eq.). The reaction mixture was heated to 75°C at which 3 mL of concentrated HCl was added, and the temperature was maintained for 3 hours under reflux. After the allotted time, the resulting solution was cooled and poured into a beaker of 100 mL of cold distilled water. The solid was filtered and dried under vacuum. The crude material was then purified by flash chromatography using a solvent mixture 66% chloroform in ether as eluent to remove any residual 4-hydroxybenzaldehyde. The solution was poured in a round bottom flask and dried under reduced pressure to yield the pure compound **Z-2d**. The reaction as well as the purification was performed in the dark to give an orange/brown solid. Yield: 0.52g, 75%. ¹H NMR (599 MHz, DMSO-*d*₆) δ (ppm): 10.37 (s, 2H), 8.72 (s, 1H), 8.08 (s, 1H), 7.86 (s, 1H), 7.66 (m, 2H), 7.61 (m, 2H), 6.96 (m, 2H), 6.53 (s, 1H), 6.24 (s, 1H), 3.10 (m, 2H), 1.44 -1.29 (m, 8H), 0.88 (s, 3H); ¹³C NMR (101 MHz, CDCl₃) δ (ppm): 133.1, 133.0, 132.8, 126.6, 125.5, 124.6, 124.2, 116.2, 114.1, 113.6, 68.8, 66.7, 30.8, 29.5, 25.8, 21.9, 13.7.

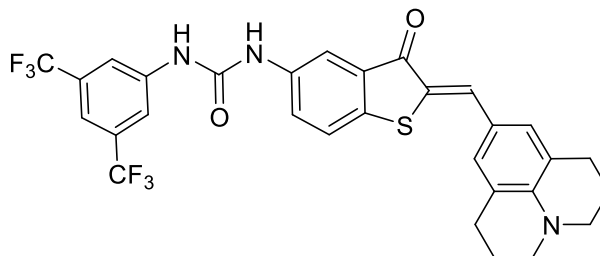


(Z)-1-hexyl-3-(3-oxo-2-((2,3,6,7-tetrahydro-1H, 5H-pyrido[3,2,1-*ij*]quinoline-9-yl)methylene)-2,3-dihydrobenzo[*b*]thiophen-5-yl)urea (Z-3a)

Synthetic procedure was taken from a previously published 1965 paper with some modifications.²²

Under a nitrogen atmosphere, a 50 mL round bottom flask equipped with a stir bar and 20 mL of ethanol and 5 mL of distilled water was added **8a** (0.50g, 1.5mmol, 1eq.), and 2,3,6,7-tetrahydro-1H, 5H-pyrido[3,2,1-*ij*]quinoline-9-carbaldehyde (**11**) (0.30g, 1.5mmol, 1eq.). The reaction mixture was heated to 75°C at which 3 mL of concentrated HCl was added, and the temperature was maintained for 3 hours under reflux. After the allotted time, the resulting solution was cooled and poured into a beaker of 100 mL of cold distilled water. The solid was filtered and dried under vacuum. The crude material was then purified by flash chromatography using a solvent mixture 66% chloroform in ether as eluent to remove any residual 2,3,6,7-tetrahydro-1H, 5H-pyrido[3,2,1-*ij*]quinoline-9-carbaldehyde. The solution was poured in a round bottom flask and dried under reduced pressure to yield the pure compound **Z-3a**. The reaction as well as the purification was performed in the dark to give a dark purple solid. Yield: 0.41g, 57%. ¹H NMR (599 MHz, CDCl₃) δ (ppm): 7.94 (d, *J* = 8.5 Hz, 1H), 7.84 (s, 1H), 7.61 (s, 1H), 7.45 (d, *J* = 8.7Hz, 1H), 7.19 (s, 2H), 6.73 (s, 1H), 5.01 (s, 1H), 3.30 (m, 6H), 2.79 (m, 4H) 1.99 (m, 4H), 1.53-1.26 (m, 8H), 0.88 (s, 3H) ; ¹³C NMR (101 MHz, CDCl₃) δ (ppm): 155.6, 131.2, 121.1, 108.3, 80.7, 76.8, 71.4, 65.7, 65.3, 49.9, 41.8, 41.4, 31.4, 30.1, 29.5, 27.6, 26.5, 22.4, 21.2, 15.1, 14.0, 13.9, 0.85; IR (Diamond ATR): $\tilde{\nu}$ (cm⁻¹) = 3360 (m), 3319 (m), 3063 (s), 2880 (m), 2230 (m), 2010 (m), 1675 (m), 1630 (m), 1580

(m), 1521 (s), 1500 (s), 1450 (s), 1390 (m), 1378 (s), 1313 (s), 1257 (m), 1210 (s), 1156 (s), 1132 (m), 1073 (s) ; EI-HRMS: Calc. for C₂₈H₃₃N₃O₂S: 475.2293; Found: 475.2299.



(Z)-1-(3,5-bis(trifluoromethyl)phenyl)-3-(3-oxo-2-((2,3,6,7-tetrahydro-1H, 5H-pyrido[3,2,1-ij]quinolin-9-yl)methylene)-2,3-dihydrobenzo[b]thiophen-5-yl)urea (Z-3b)

Synthetic procedure was taken from a previously published 1965 paper with some modifications.²²

Under a nitrogen atmosphere, a 50 mL round bottom flask equipped with a stir bar and 20 mL of ethanol and 5 mL of distilled water was added **8c** (0.24g, 0.52mmol, 1eq.), and 2,3,6,7-tetrahydro-1H, 5H-pyrido[3,2,1-ij]quinoline-9-carbaldehyde (**11**) (0.10g, 0.52mmol, 1eq.). The reaction mixture was heated to 75°C at which 3 mL of concentrated HCl was added, and the temperature was maintained for 3 hours under reflux. After the allotted time, the resulting solution was cooled and poured into a beaker of 100 mL of icy distilled water. The solid was filtered and dried under vacuum. The crude material was then purified by flash chromatography using a solvent mixture 2:1 chloroform : ether as eluent to remove any residual 2,3,6,7-tetrahydro-1H, 5H-pyrido[3,2,1-ij]quinoline-9-carbaldehyde. The solution was poured in a round bottom flask and dried under reduced pressure to yield the pure compound **Z-3b**. The reaction as well as the purification was performed in the dark to give a dark purple solid. Yield: 0.28g, 90%. ¹H NMR (400 MHz, DMSO-*d*₆) δ (ppm): 9.82 (s, 1H), 9.49 (s, 1H), 8.14 (m, 2H), 8.06 (s, 1H), 7.72 (s, 1H), 7.68 (s, 1H), 7.65 (s, 1H), 7.20 (s, 2H), 3.28 (m, 4H), 2.72 (m, 4H), 1.88 (m, 4H); ¹³C NMR (101 MHz, DMSO-*d*₆) δ (ppm): 186.5, 152.7, 145.5, 142.0, 137.9, 137.4, 135.3, 131.5, 131.1, 130.8, 126.0, 124.9, 124.6, 122.8, 122.2, 121.2, 119.9, 118.1, 115.4, 65.1,

49.5, 27.4, 21.0, 15.4 ; IR (Diamond ATR): $\tilde{\nu}$ (cm⁻¹) = 3174 (w), 3086 (w), 2948 (w), 2844 (w), 1721 (w), 1685 (m), 1622 (m), 1569 (m), 1507 (m), 1470 (m), 1436 (m), 1370 (m), 1310 (s), 1272 (m), 1171 (m), 1127 (s), 1090 (s) ; EI-HRMS: Calc. for C₃₀H₂₃F₆N₃O₂S: 603.14.

2.8.2 Standard Operating Procedures (SOP)

General Procedure for a Dilution Experiment

Preparation of solutions of (Z)-1-(2-(4-(tert-butyl)benzylidene)-3-oxo-2,3-dihydrobenzo[b]thiophen-5-yl)-3-hexylurea (**Z-2a**)

On a Sartorius Analytical Balance CPA124S, 9.4mg of (Z)-1-(2-(4-(tert-butyl)benzylidene)-3-oxo-2,3-dihydrobenzo[b]thiophen-5-yl)-3-hexylurea (**Z-2a**) was weighed in a clean and darkened dry vial. Immediately prior to the dilution procedure, 2.0 mL of deuterated solvent (CDCl₃, CD₂Cl₂ or toluene-*d*₈) was added to the darkened vial to dissolve **Z-2a**. The vial was covered and protected from ambient light throughout the whole dilution procedure.

Dilution Procedure

In a clean and dry eight-inch NMR tube, 0.5 mL of the selected deuterated solvent (CDCl₃, CD₂Cl₂ or toluene-*d*₈) was injected via syringe. A ¹H NMR spectrum was recorded in order to ensure the purity of the solvent. Aliquots of the prepared concentrated solution were added successively to the NMR tube with the selected deuterated solvent (4 μL x 5, 10 μL x 2, 20 μL x 3, 50 μL x 2, 100 μL, 200 μL, 500 μL x 2). The NMR tube was shaken after each addition and a ¹H NMR spectrum was recorded immediately. The chemical shifts of the N-H protons from **Z-2a** were identified and tracked during the experiment. The correlation between the concentration of **Z-2a** and the chemical shift of an NH proton was fitted satisfactorily to the dimerization model using Origin Data Analysis 7.0 Software. The dilution procedure was repeated twice more to ensure the reliability and reproducibility of the obtained values.

2.9 References

1. Pantuso, E.; De Filpo, G.; Nicoletta, P., F., *Adv. Optical Mater.*, **2019**, 7, 1-35.
2. Steinle, W.; Ruck-Braun, K., *Org. Lett.*, **2003**, 5, 141-144.
3. Eggers, K.; Fyles, M., T.; Montoya-Pelaez, J., P., *J. Org. Chem.*, **2001**, 66, 2966-2977.
4. Reamonn, L. S. S.; O'Sullivan, W. I. *J. Chem. Soc., Perkin Trans. 1*, **1977**, 1009-1012.
5. Yamaguchi, T.; Seki, T.; Tamaki, T.; Ichimura, K. *Bull. Chem. Soc. Jpn.* **1992**, 65, 649-656.
6. Seki, T.; Tamaki, T.; Yamaguchi, T.; Ichimura, K. *Bull. Chem. Soc. Jpn.*, **1992**, 65, 657-663.
7. Ichimura, K.; Seki, T.; Tamaki, T.; Yamaguchi, T. *Chem. Lett.*, **1990**, 1645-1646.
8. Yavari, I.; Khajeh-Khezri, A., *Georg Thieme Verlag Stuttgart*, **2018**, 50, 3947-3973.
9. Murray, J., T.; Zimmerman, C., S., *J. Am. Chem. Soc.*, **1992**, 114, 4010-4011.
10. Yan, Y.; Zeng, H.; Jankunn, S. E.; Kim, W. Y.; Zhu, J.; Ickes, H.; Gong, B. *J. Am. Chem. Soc.*, **1999**, 121, 5607-5608.
11. Toshiro, Tani; Itani, A.; Iino, Y.; Sakuda, M. *Jpn. J. Appl. Phys.*, **1987**, 26, 77.
12. Orlandi, M.; Tosi, F.; Bonsignore, M.; Benaglia, M. *Org. Lett.*, **2015**, 17, 3941-3943.
13. Thordarson, P. *Chem. Soc. Rev.*, **2011**, 40 (3), 1305.
14. Arunan, E.; Desiraju, G. R.; Klein, R. A.; Sadlej, J.; Scheiner, S.; Alkorta, I.; Clary, D. C.; Crabtree, R. H.; Dannenberg, J. J.; Hobza, P.; Kjaergaard, H. G.; Legon, A. C.; Mennucci, B.; Nesbitt, D. *J. Pure Appl. Chem.*, **2011**, 83 (8), 1637.
15. Baruah, K., P.; Gonnade, R.; phalgune, D., U.; Sanjayan, J., G. *J. Org. Chem.*, **2005**, 70, 6461-6467.
16. Davoud, Fereshteh, "Thioindigo-Based Photoswitchable Hydrogen Bond Arrays", (**2018**), Electronic Thesis and Dissertation Repository. 5782.
17. Schneider, H.-J., *Angew. Chem. Int. Engl.*, **1991**, 30, 1417-1436.
18. Chen, J. S.; Shirts, R. B. *J. Phys. Chem.*, **1985**, 89, 1643-1646.

19. Bisson, A. P.; Carver, F. J.; Eggleston, D. S.; Haltiwanger, R. C.; Hunter, C. A.; Livingstone, D. L.; McCabe, J. F.; Rotger, C.; Rowan, A. E. *J. Am. Chem. Soc.*, **2000**, *122* (37), 8856-8868.
20. Fielding, L. *Tetrahedron*, **2000**, *56* (34), 6151-6170.
21. Mostoslavski, M.A.; Ismailski, W.A; *J. Gen. Chem. USSR (Engl. Transl.)*, **1960**, *31*, 21.
22. Mostoslavski, M.A.; Ismailski, W.A; *J. Gen. Chem. USSR (Engl. Transl.)*, **1965**, *35*, 520.
23. Katayama, H.; Abe, E.; Kaneko, K., *J. Heterocyc. Chem.*, **1982**, *19*, 925-926.
24. Cai, G.; Bozhkova, N.; Odingo, J.; Berova, N.; Nakanishi, K., *J. Am. Chem. Soc.*, **1993**, *115*, 7192-7198.
25. Jorgensen, W. L.; Pranata, J., *J. Am. Chem. Soc.* **1990**, *112* (5), 2008-2010.
26. Caluwe, P.; Majewicz, T. G., *J. Org. Chem.*, **1977**, *42* (21), 3410-3413.
27. Bell, D. A.; Anslyn, E. V., *Tetrahedron*, **1995**, *51* (26), 7161-7172.
28. Mendez, L., J., I.; Pleizier, S., J.; Wang, H.-B.; Wisner, A., J., *J. Phys. Org. Chem.*, **2018**, *31*, 1-15.
29. Hansch, C.; Leo, A.; Taft, R., W., *Chem., Rev.*, **1991**, *97*, 165-195.
30. Jeffrey, G. A. *An Introduction to Hydrogen Bonding*. New York : Oxford University Press, 1997.

Chapter 3

3 Photochemistry of Self-Complementary DD●AA/ DD●AAA Hydrogen Bond Arrays

3.1 Introduction

Smart materials are gaining popularity as current research seeks to exploit novel compounds with efficient and self-repairing properties. Some smart materials contain or function as a molecular switch when activated by an external physical change such as pH, temperature, solvent system, substrate (enzyme), pressure, electric and magnetic fields and/or light. Amongst numerous promising designs are molecules that are stimulated by light and are generally categorized as field-induced stimuli. Light is a fascinating natural stimulus as its intensity, polarization, direction and wavelength can be modulated in a precise way.² Utilizing light as an external control provides scientists a simple handle for modifying cellular (and subcellular component) interactions microscopically leading to changes in macroscopic properties.

In the field of photochemistry, there are many photoswitches to choose from. They vary in strength, absorption spectrum, endurance and resistance to photofatigue.⁹⁻¹⁵ Hemithioindigo photoswitches possess many advantageous photochemical properties. First, they often have relatively simple and low-cost syntheses using inexpensive commercially available starting materials. Second, the light-induced changes are based on a reversible isomerization mechanism upon exposure to specific wavelengths of visible light to yield high conversions of photoisomerization. Third, hemithioindigo photoswitches have been known to possess high thermal bistability (>25 kcal/mol), high fatigue-resistant photoisomerization and moderate to strong absorptions in the visible

range.⁴ Here, we examine nine photoswitchable arrays with absorptions in the visible range.

3.2 Results and Discussion

3.2.1 UV-Vis Characterization of **1a-c** Hydrogen Bond Arrays

The absorption spectra of **1a-c** were obtained for the thermodynamically stable *Z* isomeric form at 10^{-4} to 10^{-5} M in chloroform or dimethylsulfoxide solutions. **1a-c** each showed three characteristic maxima absorptions as expected (shown in Figure 3.2.1). The first absorption at the highest energy corresponds to a $\pi \rightarrow \pi^*$ transition at (268 nm, 266 nm, 251 nm); denoted as *a*.

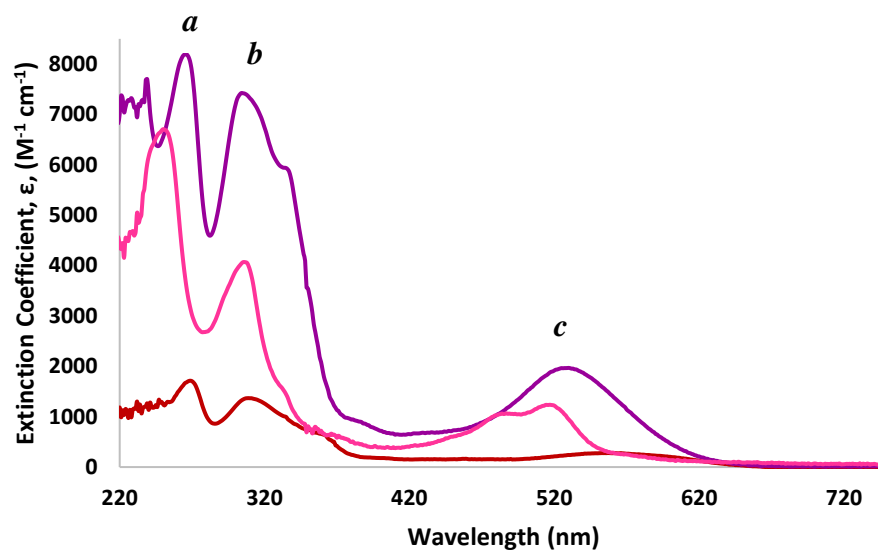


Figure 3.2.1 UV-Vis absorption spectra of **Z-1a** (red; $c=3.7 \times 10^{-4}$ M, DMSO), **Z-1b** (violet; $c=1.2 \times 10^{-4}$ M, CHCl_3), and **Z-1c** (hot pink; $c=7.7 \times 10^{-5}$ M, CHCl_3) at 298 K.

The second highest absorption maxima correspond to the second $\pi \rightarrow \pi^*$ transition at (312 nm, 305 nm, 308 nm); denoted as **b**. Lastly the absorptions within the visible region correspond to $n \rightarrow \pi^*$ transitions (557 nm, 544 nm, 515 nm) indicated as **c**. **1b** is shifted hypsochromically in comparison to **1c** by 29 nm (Table 3.2.1).

Table 3.2.1 UV-Vis data characterization of **Z-1a-c** Hydrogen Bond Arrays in chloroform and DMSO at 298K

Compound	R ₁	$n \rightarrow \pi^*$ transition		$\pi \rightarrow \pi^*$ transition	
		λ_{\max} (nm) (Z)	ϵ (M ⁻¹ cm ⁻¹) (Z)	λ_{\max} (nm) (Z)	ϵ (M ⁻¹ cm ⁻¹) (Z)
1a (DMSO)	hexyl	557	278	312, 268	1358, 1710
1b (CHCl ₃)	ethyl hexyl	544	1795	305, 266	7421, 8194
1c (CHCl ₃)	3,5-(CF ₃) ₂ Ph	517	1235	308, 251	4051, 6695

Due to solubility issues the analogous *E* isomers could not be isolated and characterized. In principle, when the *Z* isomers are irradiated at a unique wavelength, they are converted to their *E* counterpart (shown in Figure 3.2.2). The *E* isomer of the acenaphthylen-1(2H)-one hemithioindigo chromophore has been known to potentially display stable lifetimes as explored previously in our group.

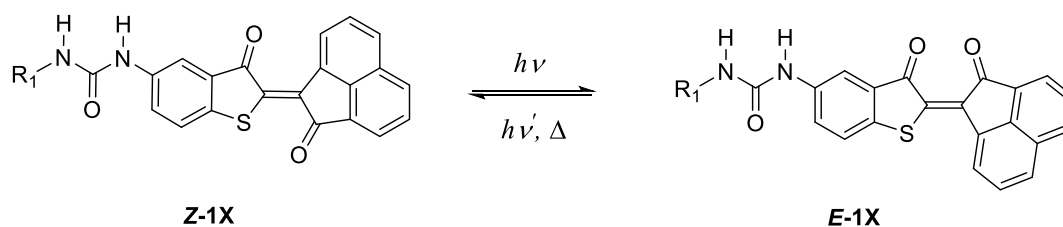


Figure 3.2.2 The putative photoisomerization of self-complementary photoswitches **1a-1c** upon the irradiation of a specific wavelength of light and the reversion to the Z isomer upon a different wavelength of light or the addition of heat.

3.2.2 Photoisomerization Studies of **1a-c** Hydrogen Bond Arrays

Photoisomerization of the self-complementary hydrogen bond arrays, **1a-c** were explored with NMR and UV-Vis spectroscopy techniques. The photoirradiation of **1a** and **1b** in DMSO yielded no observable change in absorption spectra nor presumed photoisomerization. At very low concentration (7.7×10^{-5} M), **Z-1c** was observed to undergo a presumed photoisomerization. Figure 3.2.3 displays the normalized absorption spectrum of **Z-1c** upon irradiation at 410 nm, 460 nm, 490 nm, 520 nm and 660 nm. The absorption of the *E* isomer exhibits an apparent hypsochromic shift ($\lambda_{\text{max}} = 477$ nm) as a result of the transformation ($\Delta\lambda_{\text{max}} = 37$ nm) where the *Z* isomer has a $\lambda_{\text{max}} = 514$ nm. Three isosbestic points are evident at 542, 478 and 337 nm greatly minimizing any potential degradation or byproduct formation during the photoisomerizations. The change reverses when heated at 60°C for 5 minutes in the dark to regenerate the original spectrum of **Z-1c**. Unfortunately, the solubility of **Z-1c** was too low to monitor the isomerization by ^1H NMR to verify the character of the light-inducing change we have assumed is a photoisomerization.

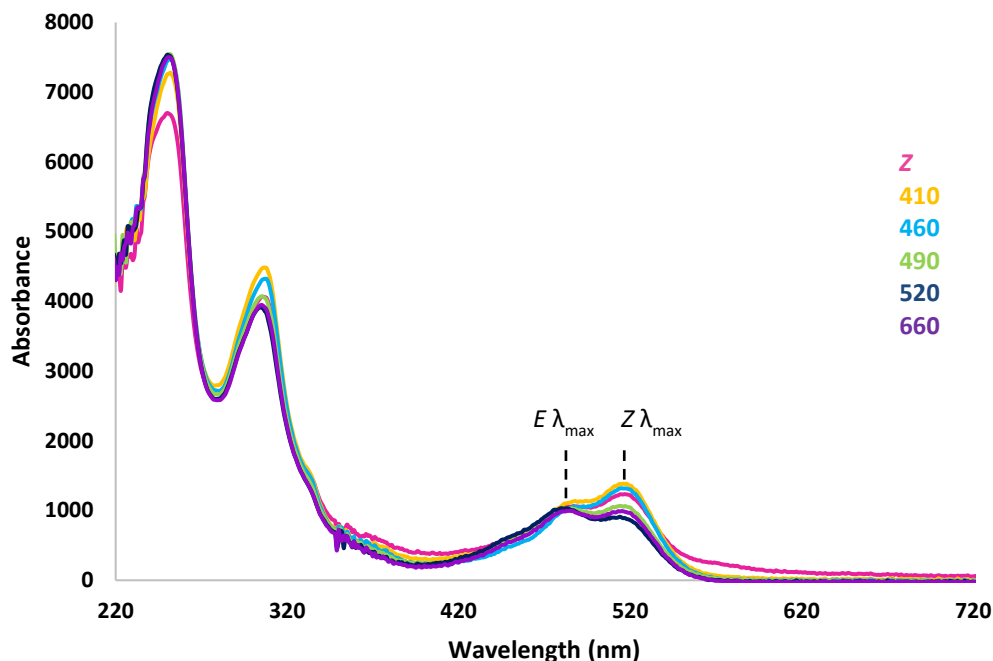


Figure 3.2.3 UV-Vis absorption spectra of **Z-1c** ($c=7.7 \times 10^{-5}$ M) in CHCl_3 at 298 K; where hot pink = lone *Z* isomer; orange = irradiation at 410 nm; blue = irradiation at 460 nm; green = irradiation at 490 nm; indigo = irradiation at 520 nm; and violet = irradiation at 660 nm. All irradiations lasted for 5 minutes.

3.3 Qualitative Analysis of **2a-d**, **3a,b** Hydrogen Bond Arrays

3.3.1 UV-Vis Characterization of **2a-d**, **3a,b** Hydrogen Bond Arrays

The absorption spectra of the *Z* isomeric forms of **2a-d** and **3a,b** were obtained in solutions of chloroform or DMSO at 298 K in varying concentrations (10^{-3} to 10^{-5} M). Figure 3.3.1.1 shows the absorption spectra of **2a-d** and **3a,b** with three distinct maxima; the absorption at the shortest wavelength (signified as *a*) corresponds to the symmetry allowed $\pi \rightarrow \pi^*$ transition representing the first singlet state (S_2)⁸, the second absorption labelled as *b* is characteristic of the subordinate allowed $\pi \rightarrow \pi^*$ transition denoting the

second singlet state (S_1)⁸ and lastly the most bathochromically shifted found in the visible region labelled as *c* is a result of the $n \rightarrow \pi^*$ excitation.

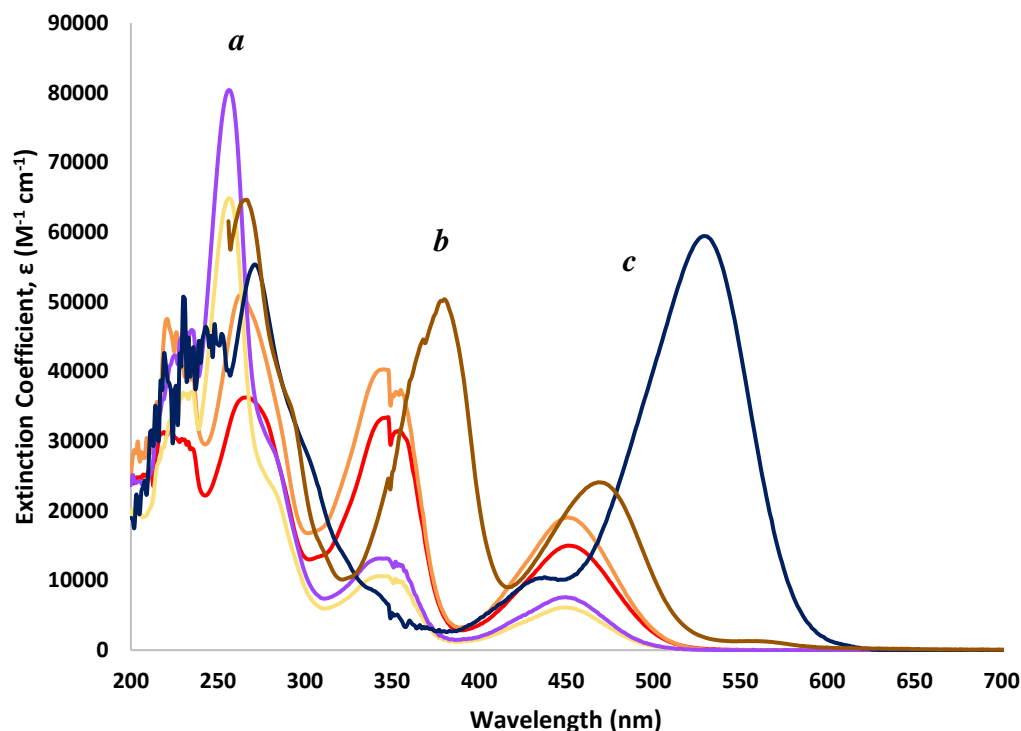


Figure 3.3.1.1 UV-Vis absorption spectra of **2a-d** and **3a,b** ($c=7.7 \times 10^{-5} - 3 \times 10^{-3}$ M) in CHCl_3 at 298 K; where red = **Z-2a**; orange = **Z-2b**; yellow = **Z-2c**; brown = **Z-2d**; violet = **Z-3a** and indigo = **Z-3b**. Note: **Z-2d** and **Z-3b** are in DMSO.

The maximum absorbances of each transition for each derivative are summarized in Table 3.3. **Z-2a** and **Z-2b** share similar $\pi \rightarrow \pi^*$ and $n \rightarrow \pi^*$ transitions. **Z-2c** displays a slight hypsochromic shift in comparison, whereas **Z-2d**, **Z-3a**, and **Z-3b** are at a bathochromic shift with **Z-3b** possessing the longest wavelength absorbance (529 nm). A mild trend is observed of solvent dependence in the $n \rightarrow \pi^*$ transitions. As polarity of the solvent increases, the lowest energy absorbance exhibits a hypsochromic shift for **Z-2a** and **Z-2b**; however, the reverse is true for

Table 3.3 Physical and Photophysical properties of **2a-d**, **3a,b** Hydrogen Bond Arrays in various solvents at 298K

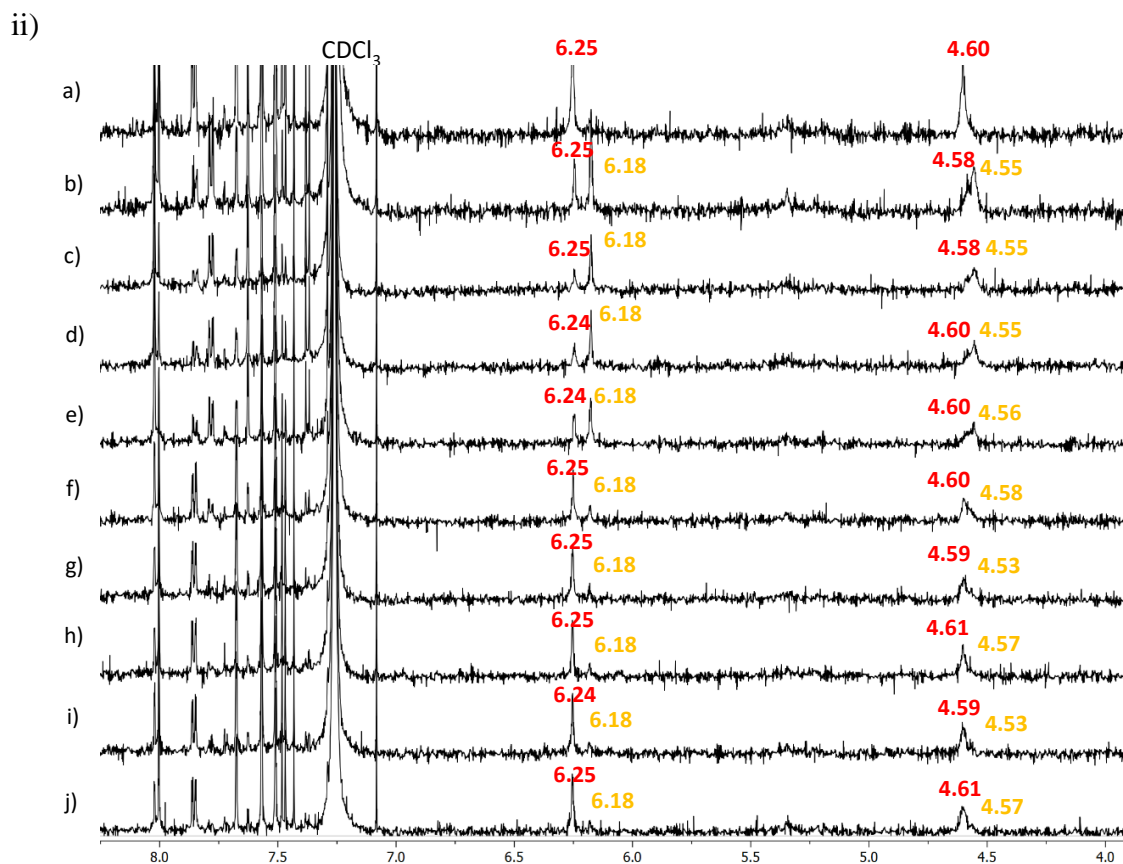
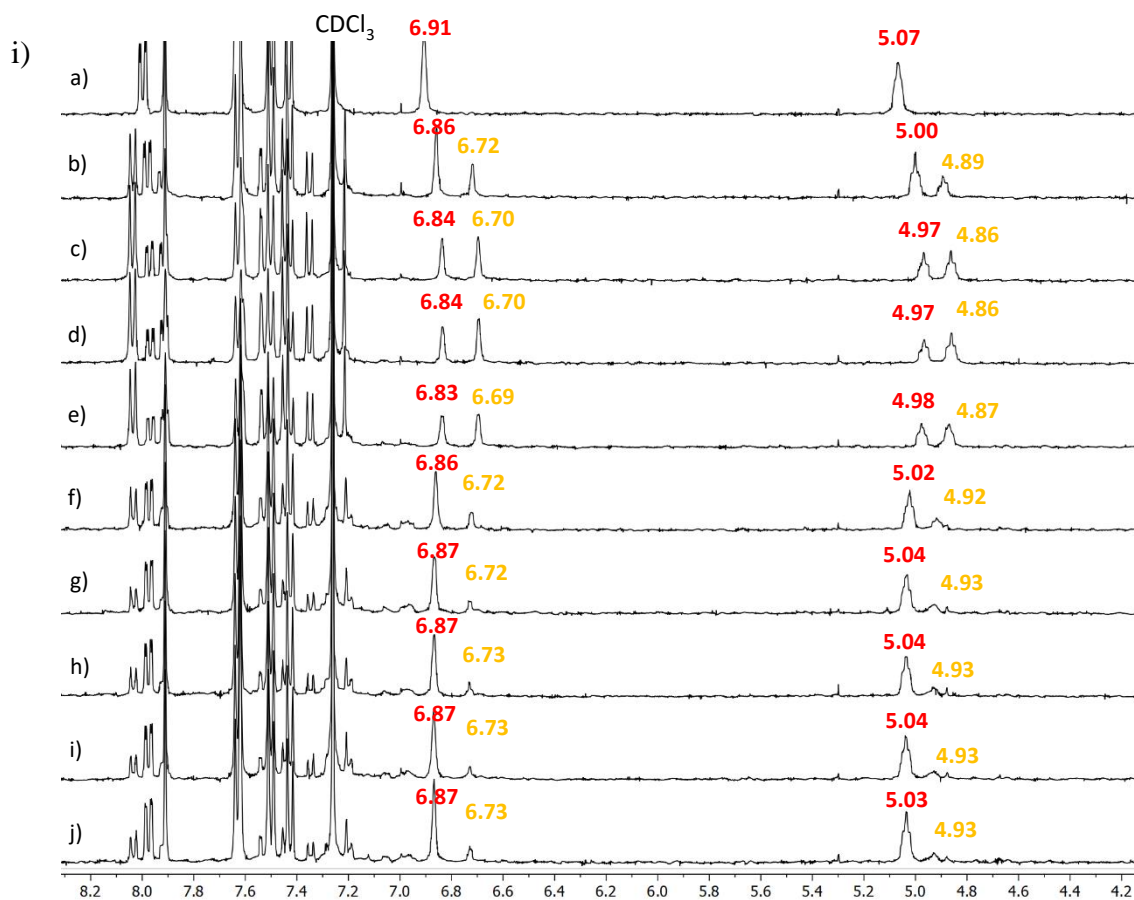
HTI	Solvent (<i>Non-polar to Polar</i>)	$n \rightarrow \pi^*$ transitions		$\pi \rightarrow \pi^*$ transitions	
		λ_{\max} (nm) (Z)	ϵ ($M^{-1} cm^{-1}$) (Z)	λ_{\max} (nm) (Z)	ϵ ($M^{-1} cm^{-1}$) (Z)
2a	CHCl ₃	453	2330	347, 276	5703, 5814
	DCM	453	2997	348, 270	7539, 9822
	THF	457	5599	356, 270	18650, 20296
	Acetone	462	5005	348, 314	16282, 16420
	CH ₃ CN	455	1250	348, 269	3602, 3981
	MeOH	455	20395	352, 263	64830, 69105
	DMF	462	2045	355, 265	6878, 7512
	DMSO	463	3425	356, 269	11352, 13325
2b	CHCl ₃	455	829	348, 262	2083, 2800
	DCM	452	390	348, 260	161, 224
	THF	462	5353	348, 253	17924, 36798
	Acetone	457	3546	353, 309	11747, 13253
	CH ₃ CN	456	1281	349, 260	3684, 7727
	MeOH	453	10924	350, 265	24127, 49252
	DMF	463	1330	358, 270	4403, 5858
	DMSO	470	806	357, 268	2833, 3531
2c	CHCl ₃	450	6138	348, 262	10573, 56134
	DCM	447	1934	344, 257	5066, 28060
	THF	450	4121	348, 265	9509, 77821
	Acetone	452	3920	353, 238	11292, 36336
	CH ₃ CN	450	-	342, 263	-
	MeOH	450	910	348, 265	2372, 15196
	DMF	456	2703	352, 267	7333, 43892
	DMSO	456	8474	349, 272	25934, 137498
2d	CHCl ₃	451	23540	359, 261	36802, 62200
	DMSO	469	24083	381, 267	50144, 64560
3a	CHCl ₃	524	37962	305, 255	11745, 23832
	DCM	522	-	304, 256	-
	THF	510	46003	304, 243	14922, 32576
	Acetone	511	5763019	322, 248	-
	CH ₃ CN	517	23385	305, 251	8362, 19573
	MeOH	533	2985504	298, 221	-
	DMF	521	82185	306, 267	26349, 47793
	DMSO	531	46626	308, 258	13934, 31800
3b	CHCl ₃	532	21705	345, 266	12302, 25276
	THF	-	-	-	-
	DMSO	529	88134	308, 269	36561, 84747

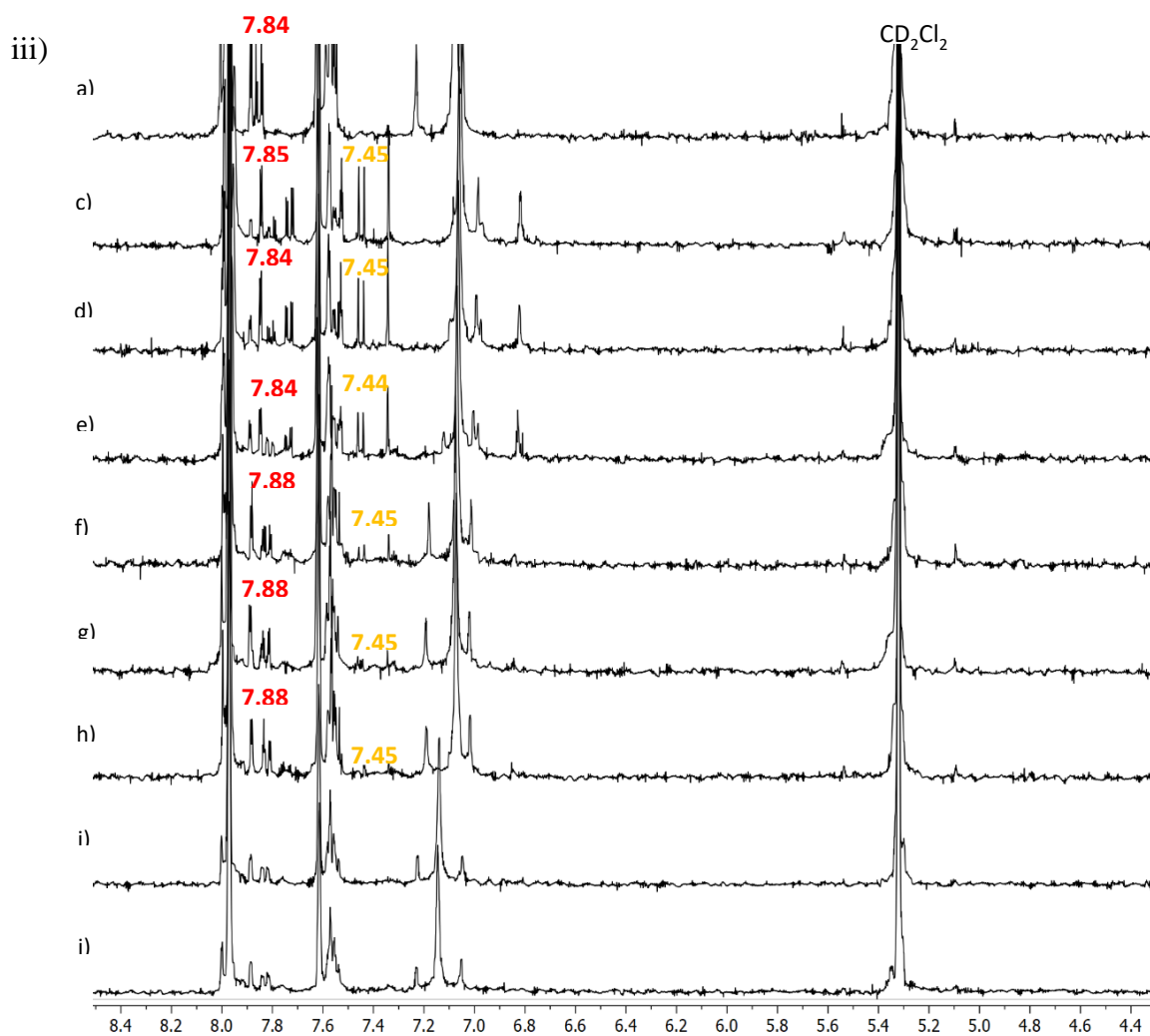
** = no conversion observed upon irradiation

Z-2d and **Z-3a**.

3.3.2 Photoisomerization Studies of **2a-c**, **3a,b** Hydrogen Bond Arrays Utilizing NMR and UV-Vis Techniques

The photoswitches, **Z-2a-c**, **Z-3a,b** were studied with ^1H NMR and UV-Vis spectroscopies to establish a quantitative analysis of conversion between the individual isomers. Fresh solutions of each *Z* isomer were weighed prior to the experiment, purged with nitrogen and covered to prevent any isomerization due to ambient light. The wavelength that yielded the highest %*E* conversion (in a mixture of *Z* and *E* isomers) was used for the remainder of the experiment for each derivative. To establish the wavelength of maximum absorption characteristic to each photoswitch, photostationary states (pss) were evaluated by irradiation with wavelengths from 410 – 660 nm. At first, the time required to induce photoisomerization in each derivative was explored. The photoswitches were irradiated at the following intervals; 30 sec, 1 min, 2 min, 4 min, 5 min, 15 min, 30 min and immediately afterward a ^1H NMR spectrum was taken. In general, the amount of *E* in the solution increased steadily until the 5min mark where the %*E* at further successive times remained constant. The results are tabulated in Table 3.3. Figure 3.3.2.1 *i-iv* illustrates the ^1H NMR spectra of **2a-c**, and **3a** after irradiation with the LEDs to establish the pss ratios of both isomers the resulting solution.





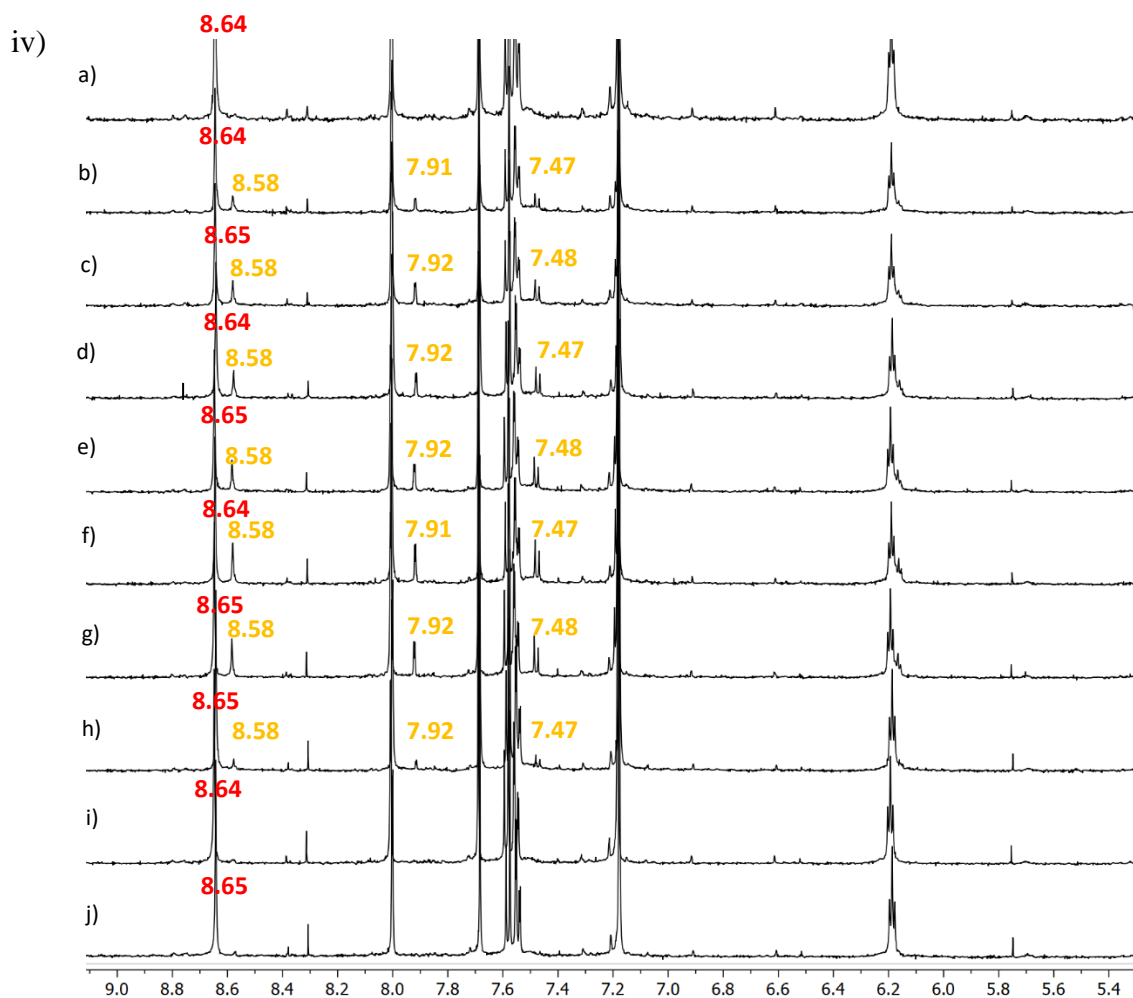


Figure 3.3.2.1 Stacked plots of ^1H NMR spectra after irradiation of *i)* **Z-2a** in CDCl_3 at 298 K where the red NH chemical shifts = *Z* isomer and the orange NH chemical shifts = *E* isomer; *ii)* **Z-2b** in CDCl_3 at 298 K where the red NH shifts = *Z* and the orange NH shifts = *E* isomer; *iii)* **Z-2c** in CD_2Cl_2 at 298 K where the red aryl shifts = *Z* and the orange aryl shifts = *E* isomer; *iv)* **Z-3a** in $\text{DMSO}-d_6$ at 298 K where the red alkene chemical shifts = *Z* and the orange aryl chemical shifts = the *E* isomer. For all spectra: a) pure *Z* isomer; b) pss at 410 nm; c) pss at 425 nm; d) pss at 440 nm; e) pss at 460 nm; f) pss at 490 nm; g) pss at 520 nm; h) pss at 590 nm; i) pss at 620 nm; j) pss at 660 nm.

UV-Vis absorption spectra were taken for each isomeric mixture at the pss in various solvents (shown in Table 3.3.1). The trend found in all photoisomerizations performed is a red-shifted absorption of the *E* isomer when compared to its *Z* counterpart. The

absorption maxima in solvents of varying polarity are very similar for each isomeric. The photoactivity of the photoarrays appears to be largely solvent independent. The *Z* to *E* photoconversions of these photoarrays were studied using NMR spectroscopy. **Z-2a** was converted 56% to the *E* isomer in CDCl₃ at the photostationary state but a greater conversion was reached in CD₂Cl₂ (66%). Likewise, when **Z-2b** was subjected to a 425 nm irradiation, 82% converted to the *E* isomer. Conversely, a higher *E* conversion was observed in CDCl₃ (61%) versus in CD₂Cl₂ (50%) for **Z-2c**. Since **Z-3a** was completely soluble in DMSO, photoirradiation was performed in this solvent but resulted in a 25% conversion to the *E* isomer at the PSS.

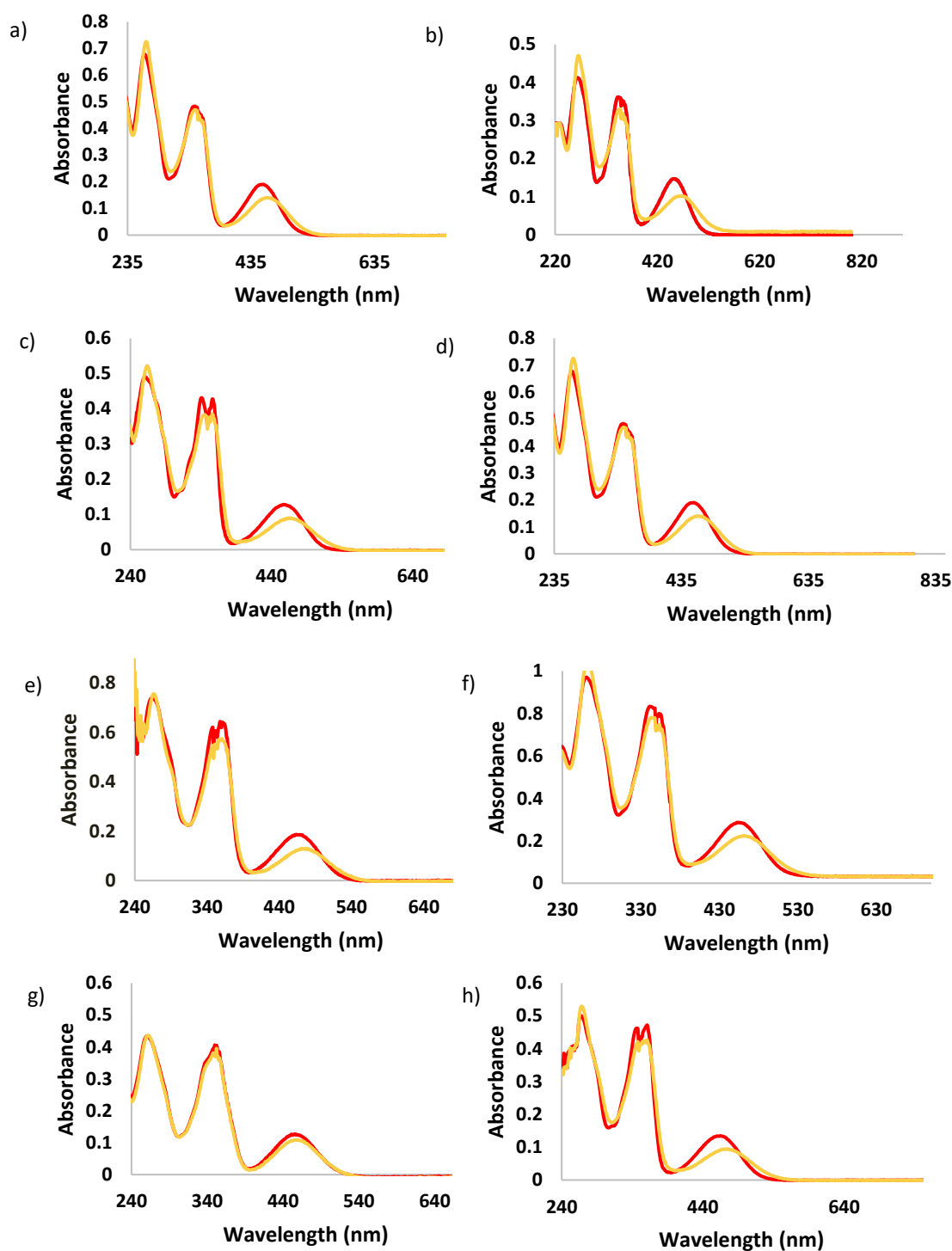


Figure 3.3.2.2 UV-Vis absorption spectra of **Z-2a** after irradiation at 440 nm where red = pure *Z* and orange = a mixture of *E* and *Z* isomers in various solvents as follows; a) $c = 6.3 \times 10^{-5}$ M in CD_2Cl_2 at 298 K; b) $c = 6.3 \times 10^{-5}$ M in CHCl_3 at 298 K; c) $c = 2.3 \times 10^{-5}$ M in THF at 298 K; d) $c = 4.4 \times 10^{-5}$ M in acetone at 298 K; e) 5.5×10^{-5} M in DMSO at 298 K; f) 2.3×10^{-4} M in CH_3CN at 298 K; g) 6.2×10^{-6} M in MeOH at 298 K; h) 6.5×10^{-5} M in DMF at 298 K.

Table 3.3.1 Physical and Photophysical properties of *Z/E* isomers of **2a-d**, **3a,b** Hydrogen Bond Arrays in various solvents at 298K

HTI	Solvent (<i>Non-polar to Polar</i>)	Isomer yield in the pss (% <i>E</i>)	Isosbestic point (s)
2a	CHCl ₃	56 (440)	478, 406, 369
	DCM	66 (440)	470, 395, 362
	THF	-	488, 397, 311
	Acetone	29 (440)	486, 399, 365
	CH ₃ CN	-	484, 397, 364
	MeOH	**	-
	DMF	-	494, 405, 370
	DMSO	18 (440)	504, 375, 374
	2b	Toluene	35 (425)
CHCl ₃		82 (425)	485, 392, 326
DCM		44 (425)	480, 391, 361
THF		-	494, 392, 363
Acetone		57 (425)	484, 384, 361
CH ₃ CN		48 (425)	471, 385, 287
MeOH		19 (425)	481, 381, 275
DMF		-	496, 396, 366
DMSO		12 (425)	492, 402, 372
2c	Toluene	65 (425)	-
	CHCl ₃	61 (425)	476, 388, 326
	DCM	50 (425)	445, 395, 272
	THF	-	482, 385, 365
	Acetone	82 (425)	475, 387, 355
	CH ₃ CN	**	478, 391, 362
	MeOH	-	480, 396, 327
	DMF	-	484, 394, 366
	DMSO	**	524, 432, 380
2d	CHCl ₃	-	517, 457, 417
	DMSO	60 (440)	-
3a	CHCl ₃	**	544, 447, 283
	DCM	19 (490)	535, 458, 223
	THF	-	527, 453, 279
	Acetone	-	525, 453, 268
	CH ₃ CN	44 (490)	538, 454, 274
	MeOH	-	-
	DMF	-	541, 459, 279
	DMSO	25 (490)	552, 464, 284
3b	CHCl ₃	-	614, 418, 242
	THF	-	-
	DMSO	-	551, 454, 417
** = no conversion observed upon		irradiation	

3.3.3 *E* to *Z* Thermal Reversion Analysis of **2a** and **2c** Hydrogen Bond Arrays

The *E* isomers of the photoswitches, **2a,b**, **3a,b**, were found to have low bistability at room temperature. ***E*-2a** begins noticeably reverting to the *Z* isomer immediately in solution and was tracked by ¹H NMR for a total of 4 hours (~ 250 min). The following day (~24 hours later), the solution consisted entirely of the *Z* isomer. The lifetime of the *E* is solvent dependent; where in dichloromethane, the %*E* isomer in solution decreased by a factor of 4 after 1 hour (Figure 3.3.3.2) but after 1 hour in CDCl₃, the %*E* decreased by a factor of 1.2. A thermal reversion was performed on a mixture of ***Z/E*-2a** in CDCl₃ wherein an initial ¹H NMR spectrum of the pure *Z* isomer was taken then irradiated at 440 nm to obtain a 56%*E* conversion in solution. The sample stayed in the NMR spectrometer for the remainder of the experiment and the amount of %*E* that was observed decreased in quantity over time. The natural log of the initial *E* concentration ($[E]_{t_0}$) over the *E* concentration at each respective time ($[E]_t$) was plotted as a function of time (in minutes) shown in Figure 3.3.3.1 with the slope equal to the rate constant; *k*. Since the thermal *E/Z* isomerization is a unimolecular first order reaction due to the following equation;

$$-\frac{d([E \text{ isomer}])}{dt} = \frac{d([Z \text{ isomer}])}{dt} = k[E \text{ isomer}] \quad \text{Equation 12}$$

we can say that the decrease of concentration of *E* is proportional to the increase of concentration of *Z* over time; having both ratios equal to the rate constant, *k*, multiplied by the concentration of the *E* isomer. Given the initial concentration of the *E* isomer,

($[E]_{t0}$) and the concentration of E at each respective time ($[E]_t$), they can be related relative to time by this equation;

$$k = \frac{\ln\left(\frac{[E \text{ isomer}]_{t0}}{[E \text{ isomer}]_t}\right)}{t} \quad \text{Equation 13}$$

in which a first order rate law can be determined. The first order analysis of **2a** closely matches with that of a first order rate law with a linear regression (R^2) value of 0.984 and a k value of $1.92 \times 10^{-2} \text{ s}^{-1}$.

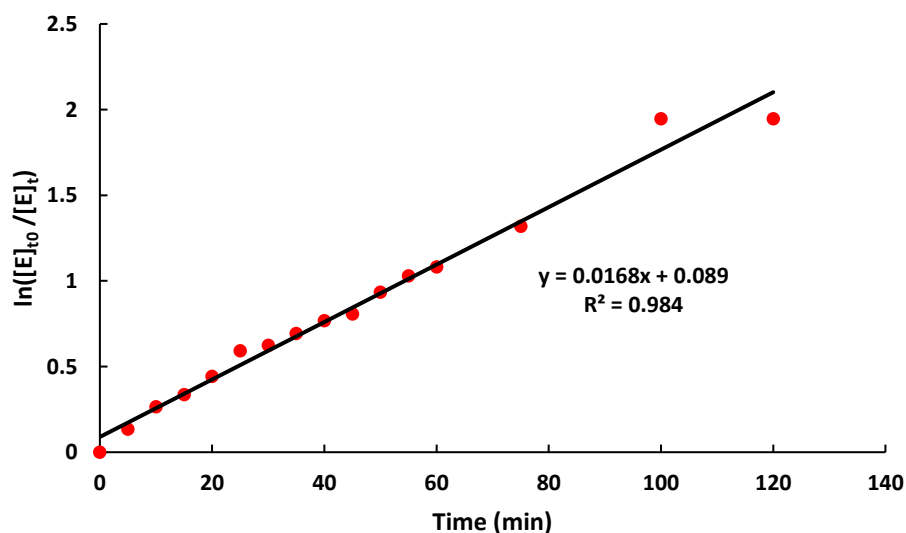


Figure 3.3.3.1 A first order kinetic analysis plot of the thermal reversion of **Z-2a** after irradiation at 440 nm to obtain a 56% E conversion in CDCl_3 at 298 K. The relative ratios were obtained from the integral values relative to concentration to give a linear first order rate equation.

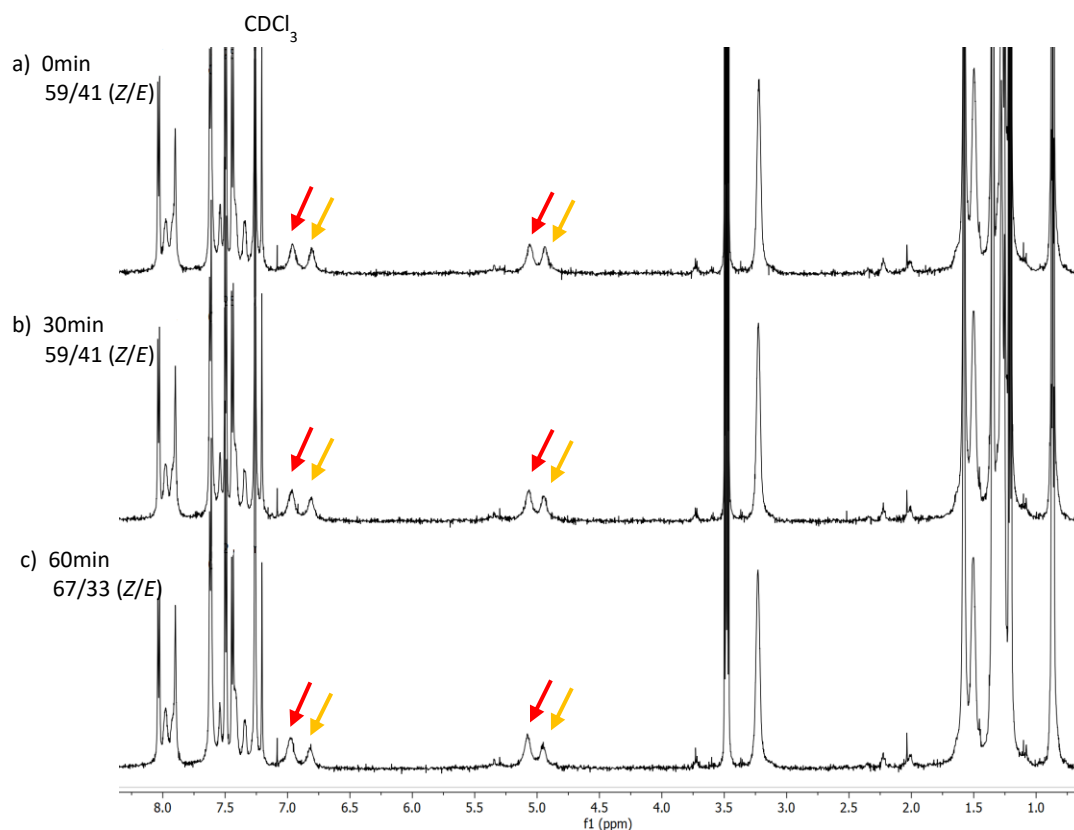


Figure 3.3.3.2 Stacked plot of ^1H NMR spectra of the reversion of *E-2a* at select time intervals in CDCl_3 at 298 K. The red arrows = *Z* isomer; orange arrows = *E* isomer.

UV-Vis absorption spectra following the change in *Z/E* ratios after irradiation yield different absorption maxima. Once the sample was irradiated at 440 nm, a spectrum was taken at each selected time interval and as expected the shift in λ_{max} aligns with that of the pure *Z* isomer (Figure 3.3.3.4). *E-2b* reverted thermally more slowly than *E-2a* in chloroform with a decrease of 4% after 1 hour. Examination of the solution after 1 day (~ 24 hours) yielded a 2-fold decrease in the amount of *E* present in solution. *E-2c* showed very little decrease in concentration after initial irradiation over the course of 90 min in CDCl_3 .

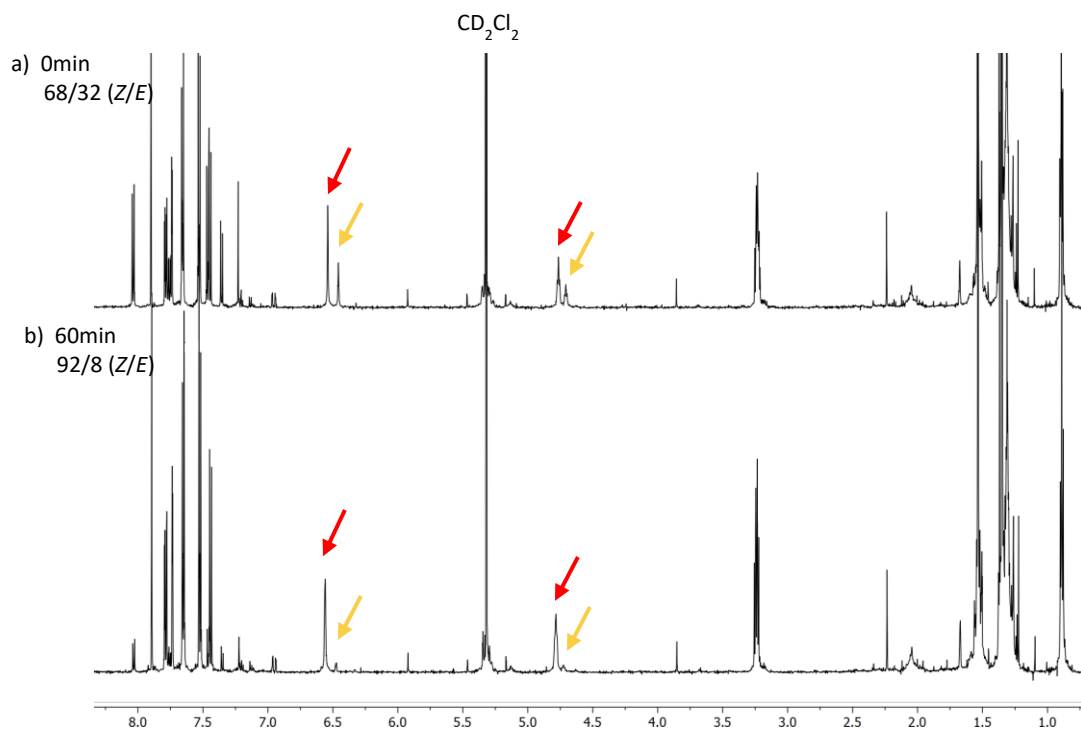


Figure 3.3.3.3 Stacked plot of ^1H NMR spectra illustrating the reversion of *E*-**2a** at select time intervals in CD_2Cl_2 at 298 K. The red arrows = *Z* isomer; orange arrows = *E* isomer.

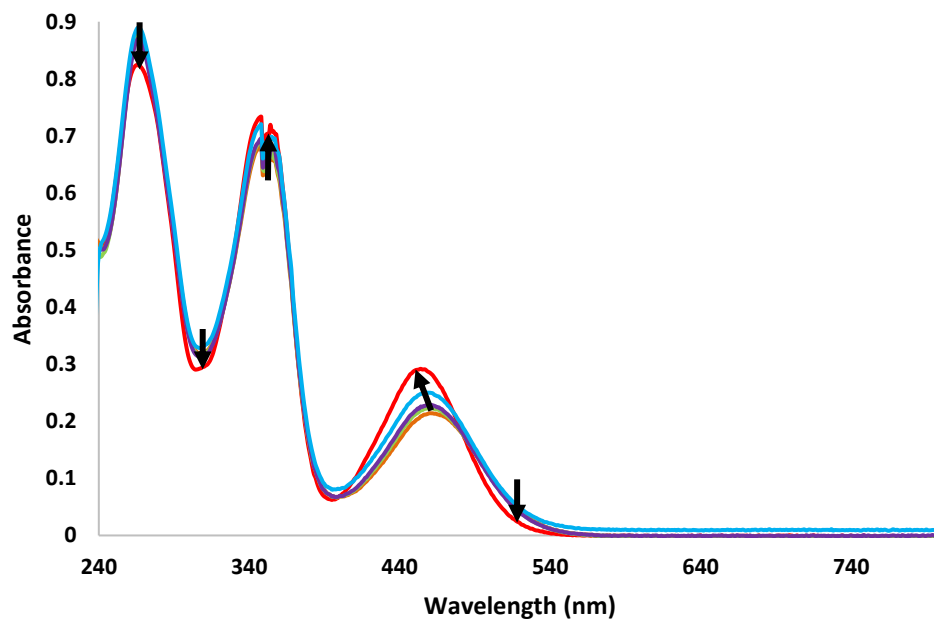


Figure 3.3.3.4 UV-Vis absorption spectra displaying the *E* to *Z* thermal reversion of *E*-**2a** at room temp., where the red curve = pure *Z* isomer and the orange curve = irradiation at 440 nm in CHCl_3 at 298 K ($c = 1.1 \times 10^{-3}$ M). A spectrum was taken after 1 hour (green); 2 hours (violet); and four hours (blue).

Similarly, the *E* to *Z* thermal reversion at room temperature (298 K) for **2c** follows a first order reaction model (Figure 3.3.3.5) with a linear regression value of 0.8984 and a lower *k* value of $3.99 \times 10^{-3} \text{ s}^{-1}$ in comparison to **E-2a**.

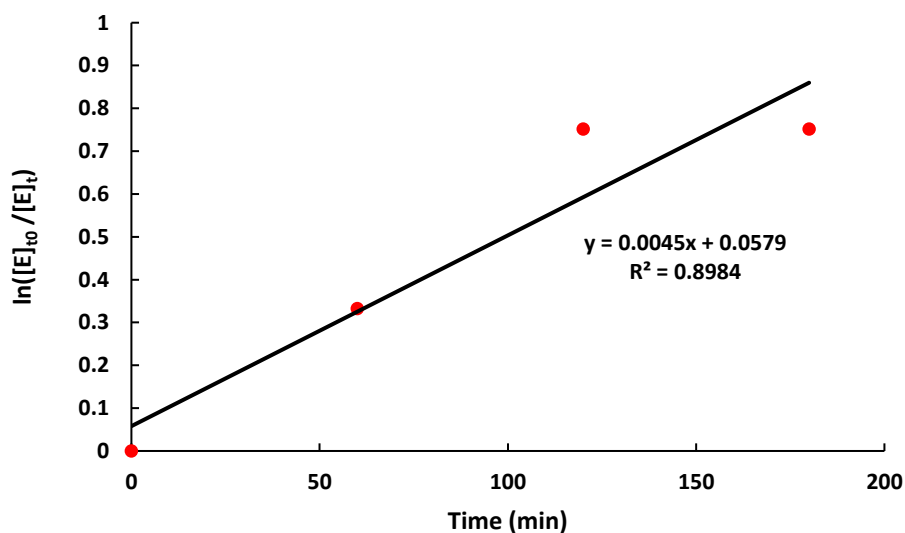


Figure 3.3.3.5 A first order kinetic analysis plot of the thermal reversion of **Z-2c** after irradiation at 425 nm to obtain a 53% *E* conversion in CDCl_3 . The relative ratios were obtained from the integral values relative to concentration to give a linear first order rate equation.

3.4 Summary and Conclusions

The photochemical and photophysical properties of the self-complementary photoswitches were investigated with NMR and UV-Vis spectroscopy techniques. Unfortunately, the photoirradiation of **1a,b** wasn't successful as their solubility prevented any physical change from occurring (even in DMSO). The photoisomerization of **Z-1c** could be induced by irradiation at low concentrations. **Z-2a** and **Z-2b** share similar $\pi \rightarrow \pi^*$ and $n \rightarrow \pi^*$ transitions whereas **Z-2c** is at a slight hypsochromic shift and **Z-2d**, **Z-3a**, **Z-3b** are at a bathochromic shift. The trend found in all photoisomerizations performed is

the apparent red-shifted absorption of the *E* isomer when compared to its *Z* counterpart leading to low energy absorptions. The PSS conversions to the *E* isomers varied from 12% to 82%. **Z-2b** in DMSO converted the least (at 12% *E* isomer) when irradiated at 490 nm whereas **Z-2b** in CDCl₃ and **Z-2c** in acetone-*d*₆ both showed the largest conversion (at 82% *E* isomer) when irradiated at 425 nm. The *E* isomers of the corresponding photoswitches (**2a,b**, **3a,b**) were found to have low metastability at room temperature. **E-2a** began noticeably reverting to the *Z* isomer after 10 min and was tracked for a total of 4 hours (~ 250 min). The reversion was tracked by ¹H NMR and the next day (~24 hours), the solution consisted entirely of the *Z* isomer. The photoswitches adopt a first order rate constant in regard to the *E* to *Z* thermal reversion rates with **E-2a** possessing a faster decay ($k = 1.92 \times 10^{-2} \text{ s}^{-1}$) with a linear regression (R^2) value of 0.984 and **E-2c** with a slower decay ($k = 3.99 \times 10^{-3} \text{ s}^{-1}$) with a linear regression value of 0.8984. In conclusion, the photoswitchable hydrogen bond arrays had moderate photoisomerizations; however, they lacked adequate thermal bistability for isolation and analysis of pure *E* isomeric forms in all cases.

3.5 Standard Operating Procedures (SOP)

3.5.1 Generalities

Nuclear Magnetic Resonance (NMR) spectra were recorded on Bruker 400 MHz, Varian INOVA 400 MHz and Varian INOVA 600 MHz spectrometers (^1H = 400.08 MHz, 399.77 MHz and 599.32 MHz; ^{13}C {1H} = 100.52 MHz and 150.78 MHz respectively). ^1H and ^{13}C spectra were referenced relative to residual solvent signals. Solvents for NMR spectroscopy (Chloroform-*d*, DMSO-*d*₆, Acetone-*d*₆, CD₃CN, Methylene Chloride-*d*₂, Methanol-*d*₄, Toluene-*d*₈, Benzene-*d*₆) were purchased from Cambridge Isotope Laboratories and Sigma-Aldrich which were referenced according to literature values for residual solvent protons.¹⁶ ^1H NMR photostationary state experiments and ^1H NMR reversion experiments were performed on INOVA 400 MHz and INOVA 600 MHz spectrometers. All photoisomerization experiments utilized a LED light lens at wavelengths 395 nm, 410 nm, 425 nm, 440 nm, 460 nm, 490 nm, 520 nm, 590 nm, 620 nm and 660 nm with a LED Driver IP67 SELV from Chanzon. UV-Vis absorption spectra were obtained with a CARY 300 Ultraviolet-Visible spectrometer employing a quartz cuvette (chamber volume 3.00 mL, pathlength 10 mm, limit 200 – 2500 nm spectral range).

3.5.2 NMR Photochemistry Experiments

3.5.2.1 PSS Experiments

Photostationary State Procedure

In a clean and dry eight-inch NMR tube, 0.7 mL of a 1×10^{-3} M solution of the *Z* isomer in a selected deuterated solvent (Toluene- d_8 , CDCl_3 , CH_2Cl_2) was injected via syringe. The solution in the NMR tube was kept in the dark and purged with nitrogen until an initial ^1H NMR spectrum was taken of pure *Z*. A small piece of Ag foil was added to the NMR tube to prevent any side reactions with the chlorinated solvents. Then the sample was irradiated at various wavelengths (410, 425, 440, 460, 490, 520, 550, 625, 660) for 5 minutes at a distance of 19 cm (~ 7.5 in) from the light source. Immediately afterwards, a ^1H NMR spectrum was taken. The chemical shifts of the N-H protons from *Z* were identified and compared to the N-H protons corresponding to the *E* during the experiment. The maximum *Z* and *E* percentages were obtained from the relative integral values. Photoirradiations were carried out with LEDs (395, 410, 425, 440, 460, 490, 520, 590, 620, 660) to establish the highest %conversions (*Z/E* ratios) of each isomer at each unique wavelength.

3.5.2.2 ^1H NMR Thermal Reversion Experiments

In a clean and dry eight-inch NMR tube, 0.7 mL of a 1×10^{-3} M solution of the *Z* isomer in a selected deuterated solvent (toluene- d_8 , CDCl_3 , CH_2Cl_2) was injected via syringe. The solution in the NMR tube was kept in the dark and purged with nitrogen until an initial ^1H NMR spectrum was taken of pure *Z*. The photoswitch was placed at 19 cm (~ 7.5 in) from the light source and irradiated for 5 minutes at the wavelength where the %*E* conversion was the greatest. After irradiation, the sample was immediately placed into the NMR spectrometer. A ^1H NMR spectrum was recorded every 5 minutes for 4 hours.

3.5.3 UV-Vis Thermal Experiments

Samples were weighed and diluted to volume immediately prior to the UV-Vis experiments. The solution was purged with N_2 to prevent side reaction with O_2 in solution. An initial UV-Vis was taken of the pure *Z* isomer. Then the solution was placed at a distance of 19 cm (~7.5 in) from the light source, irradiated for 5 minutes at room temperature and immediately placed into the spectrometer.

3.5.4 UV-Vis Thermodynamic Reversion Experiments

Samples were weighed and diluted to volume immediately prior to the UV-Vis experiments. The solution was covered, kept in the dark and brought to the UV-Vis spectrometer. A UV-Vis spectrum was taken of the pure *Z* in solution. Then the solution was placed at a distance of 19 cm (~7.5 in) from the light source, irradiated for 5 minutes at room temperature and immediately placed in the spectrometer. A UV-Vis spectrum was recorded every 5 minutes for 4 hours.

3.6 References

1. Bleger, D.; Hecht, S. *Angew. Chem., Int. Ed.*, **2015**, *54*, 11338.
2. Pantuso, E.; Filpo, D., G.; Nicoletta, P., F., *Adv. Opt.Mater.*, **2019**, *7*, 1-35.
3. Stoll, R.S.; Hecht, S., *Angew. Chem.*, **2010**, *49*, 5054–5075.
4. Maerz, B.; Wiedbrauk, S.; Oesterling, S.; Samoylova, E.; Nenov, A.; Mayer, P.; Vivie-Riedle, d., R.; Zinth, W.; Dube, H., *Chem. Eur. J.*, **2014**, *20*, 13984 – 13992.
5. Dongsansuk, A.; Lutz, C.; Neuner, G. *Photosynthetica*, **2013**, *51*, 13-21.
6. Huang, X.; Li, T. *J. Mater. Chem. C.*, **2020**, *8*, 821.
7. Zhao-Yang, Z.; Tao, L., *ChemRxiv*, 2019, Preprint,
<<https://doi.org/10.26434/chemrxiv.9730694.v1>>
8. Frackowiak, D., *J. Photochem. Photobiol. B: Biol.*, **1988**, *2*, 399-408.
9. Jia, S.; Fong, W.-K.; Graham, B.; Boyd, B. J. *Chem. Mater.*, **2018**, *30*, 2873–2887.
10. Merino, E.; Ribagorda, M., *Beilstein J. Org. Chem.*, **2012**, *8*, 1071–1090.
11. Brieke, C.; Heckel, A. *Chem. Eur. J.*, **2013**, *19*, 15726–1573.
12. Radua, A.; Byrne, R.; Alhashimya, N.; Fusaro, M.; Scarmagnani, S.; Diamond, D., *J. Photoch. Photobio. A.*, **2009**, *206*, 109–115.
13. Koeppe, B.; Rompp, F. *Chem. Eur. J.*, **2018**, *24*, 14382-14386.
14. Wiedbrauk, Sandra; Dube, Henry. *Tetrahedron. Lett.*, **2015**, *56*, 4266-4274.
15. Zweig, E. J.; Newhouse, R. T. *J. Am. Chem. Soc.*, **2017**, *139*, 10956-10959.
16. Petermayer, C.; Thumser, S.; Kink, F.; Mayer, P.; Dube, H., *J. Am. Chem. Soc.*, **2017**, *139*, 15060-15067.

Chapter 4

4 Conclusions/Future Work

4.1 Conclusions

Hemithioindigo photoswitches have a promising future as vital components within smart and efficient nanomaterials. The ability of fine tuning their function at the microscale solely on the basis of non-invasive light control allows medical professionals to diagnose and heal inaccessible or inoperable parts of the human body. Changes in these small molecules (via isomerization) lead to alterations in the chemical reactivity of the resulting species impacting the hydrogen bonding toward a substrate which in turn can be amplified in the overall system. From a chemist's standpoint, the opportunity to control molecular systems at the microscale brings insight into many functional applications such as light-controlled catalysts as well as the power to spatially and temporally control a given reagent's activity.³

Hemithioindigo-based hydrogen bond arrays were synthesized with donor and acceptor units between aromatic spacers to establish a self-complementary design. The hydrogen bond arrays differ in the chromophore and alkyl chain substituents and were produced in five to six synthetic steps. The hydrogen bonding of these self-complementary arrays were assessed by ¹H NMR dilution studies. Overall, the dimerization constants ranged from 63 M⁻¹ to 1100 M⁻¹. The weakest dimerization isotherm was of **Z-2b** in toluene-*d*₈ and the strongest was of **Z-3c** in CDCl₃. The Gibbs free energy of the corresponding complexes varied from -10.3 kJ/mol to -17.3 kJ/mol implying that complex formation is indeed a spontaneous process. When comparing **Z-2b**, and **Z-2c**, the addition of the 3,5-bis(trifluoromethyl)phenyl group increased the ΔG of **Z-2c** by 161 kJ/mol. This implies that the hydrogen bond dimerization was stronger

and had greater stability as the electron-withdrawing group pulled electron density away from the urea protons and the hemithioindigo ring. The Gibbs free energies were relatively the same for **Z-3a** and **Z-3b** ($\Delta G = -17$ kJ/mol). The design of **2b** as a hypothetical steric block in the *E* form did not function as planned as **E-2b** was found to dimerize with a $K_d = 210$ M⁻¹ in CDCl₃ and possessed a larger ΔG (-13.3 kJ/mol) than its *Z* counterpart. Nevertheless, in a solution mixture of **Z/E-2b**, the isomers were found to have a greater affinity for complexation with themselves instead of **Z•E**. The X-ray crystal structures of **Z-2a** illustrate solid-state complexation adopting an antiparallel conformation with hydrogen bonds slightly less than ideal with the lowest at 132° (N2B-H2B⋯O1A), and the highest being 161° (N1B-H1B⋯O1A). The crystal structures of **Z-1c** and **Z-3c**, despite being obstructed by DMSO, confirm that the *Z* isomer is the thermodynamic most stable isomer; obtained directly from the reaction.

The hemithioindigo photoswitches synthesized (**2a-c**, **3a,b**) demonstrated moderate photoisomerization in most solvents as well as moderate to strong solution-based complexation in non-polar solvents. These photoswitches incorporated a urea functional group in an **AADD** array to establish a robust self-complementary design. The photoconversion from the *Z* to the *E* and photoreversion (*E* to *Z*) was studied by ¹H NMR and by UV-Vis for **2a-c** and **3a,b**. **Z-2a** and **Z-2b** share similar $\pi \rightarrow \pi^*$ and $n \rightarrow \pi^*$ transitions whereas **Z-2c** is at a slight hypsochromic shift and **Z-2d**, **Z-3a**, **Z-3b** are at a bathochromic shift. The trend found in all photoisomerizations performed is the red-shifted absorption of the *E* isomer when compared to its *Z* counterpart leading to low energy absorptions. The PSS conversions to the *E* isomers varied from 12% to 82%. **Z-2b** in DMSO converted the least (at 12% *E* isomer) when irradiated at 425 nm whereas **Z-2b**

in CHCl_3 and **Z-2c** in acetone showed the largest conversion (at 82% *E* isomer for both) when irradiated at 425 nm. Furthermore, the *E* isomers of the corresponding photoswitches (**2a,b**, **3a,b**) were found to have low metastability at room temperature. Despite the low lifetimes of the *E* isomers, the *Z* isomers were robust with no sign of decomposition or degradation during these photoirradiations. Therefore, these urea-based hemithioindigo photoswitchable hydrogen bond arrays formed moderate to strong hydrogen bond complexes with the *Z* isomeric form of **2a-d** and **3a,b** possessing the qualities to be considered viable as robust photoswitches.

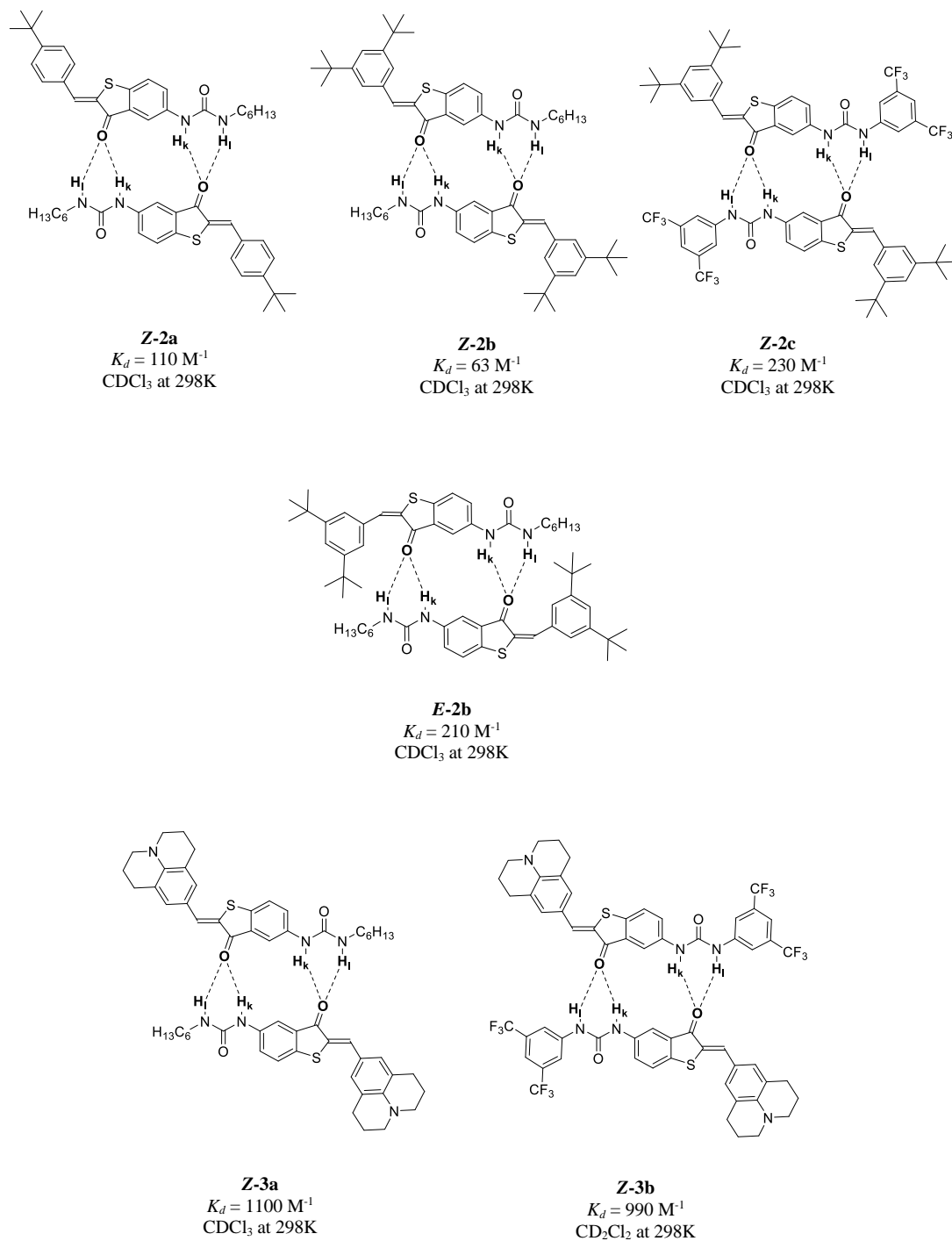


Figure 4.1 Self-complementary hydrogen bond arrays and their dimerization constants (K_d) are illustrated demonstrating the hydrogen bond associations between identical units fashioned in an antiparallel arrangement.

4.2 Future Work

Urea-based photoswitches have a unique binding ability because of their NH group acting as donors and their carbonyl oxygens acting as acceptors despite the fact that they are in close proximity. The 3D spatial rearrangement of these complexes is dependent on the surrounding nearby acceptor and donor atoms. Furthermore, their composure as self-complementary hydrogen bond arrays almost always organize in an alternating fashion with another unit. One major disadvantage and problem that was encountered when working with urea compounds is their insolubility. Substitution of bulky chains and/or long alkyl chains at R₁, R₂, X and Y (Figure 4.2) on the periphery of the complex will counteract this problem whilst having little to no effect on the hemithioindigo fragment both as a hydrogen bond array and a photoswitch. Incorporation of electron rich groups at position X and Y will further add to the electron density deposited on the carbonyl oxygen; thus, contributing to a stronger hydrogen bond. Likewise, installing longer chains (or multiple branching) of electron withdrawing groups at R₁ will pull the electron density away from the NH atoms forcing the protons to lend their electrons to incoming acceptors. Thus, these extrapolations lead to complexes, **A1**, **A2** and **A3**. In designs, **A1** and **A3**, the most thermodynamic stable isomer (which is obtained from the reaction mixture), *Z*, is not the hydrogen binding isomer; thus, their *E* counterpart needs to be obtained to measure the strength of the hydrogen bonding interaction. In contrast, **Z-A2** is obtained straight from the reaction mixture and is the hydrogen bonding isomer. In terms of their photochemistry, **E-A2** should have very low bistability as julolidine chromophores has been known to possess half-lives up to minutes⁶; whereas, **A1** and **A2** contain acenaphthylen-1(2H)-one chromophores with

relatively high lifetimes and exist as extremely stable complexes. These are only predictions based on previous similar designs; however additional modifications to the chromophore will increase the bistability of the individual isomers. The substitution of electron donating and/or electron withdrawing groups will contribute to the rate of photoisomerization and the steady state and change not only the photochemical but also the photophysical properties. Figure 4.2 shows potential designs for future urea-based self-complementary hydrogen bond arrays with unique variations on the chromophore unit.

Photoswitchable polymer-based designs have been a revolving idea in the literature.^{4,5} Incorporation of these photoswitches as linkers between consecutive polymer chains can undoubtedly lead to bifunctional materials with self-healing and stretchable properties via photocontrol. In addition, the affinity of the resulting polymer chains to self-associate will allow for spontaneous pre-assembly after dissolution which will inherently boost the solid-state stability. The combined effect of all electron-rich donating species and/or functional groups to each proposed chromophore (**A1**, **A2**, **A3**) will positively increase the electron push-pull character across the central double bond thereby raising the quantum yield value, photofatigue resistance and photoisomerization kinetics.

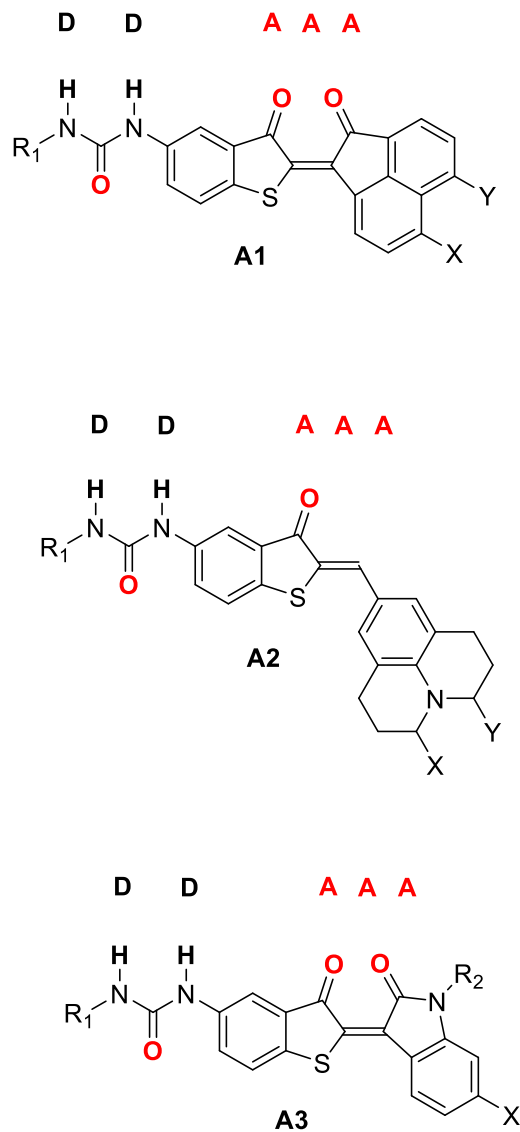


Figure 4.2 Proposed self-complementary hydrogen bond arrays, **A1**, **A2**, and **A3** with substitution of EDG at X and Y and EWG at R₁.

4.3 References

1. Fehrentz, T.; Schönberger, M.; Trauner, D., *Angew. Chem.*, **2011**, *50*, 12156–12182.
2. Samanta, S.; Qin, S.; Lough, A. J.; Woolley, G. A., *Angew. Chem.*, **2012**, *51*, 6452–6455.
3. Stoll, R.S.; Hecht, S., *Angew. Chem.*, **2010**, *49*, 5054–5075.
4. Ihrig, P., S.; Eisenreich, F.; Hecht, S., *Chem. Commun.*, **2019**, *55*, 4290-4298.
5. Yue, Y.; Norikane, Y.; Azumi, R.; Koyama, E., *Nat. Commun.*, **2018**, *9*, 3234.
6. Petermayer, C.; Thumser, S.; Kink, F.; Mayer, P.; Dube, H., *J. Am. Chem. Soc.*, **2017**, *139*, 15060-15067.

A Appendices

A.1 1D NMR Spectra (^1H NMR Spectra)

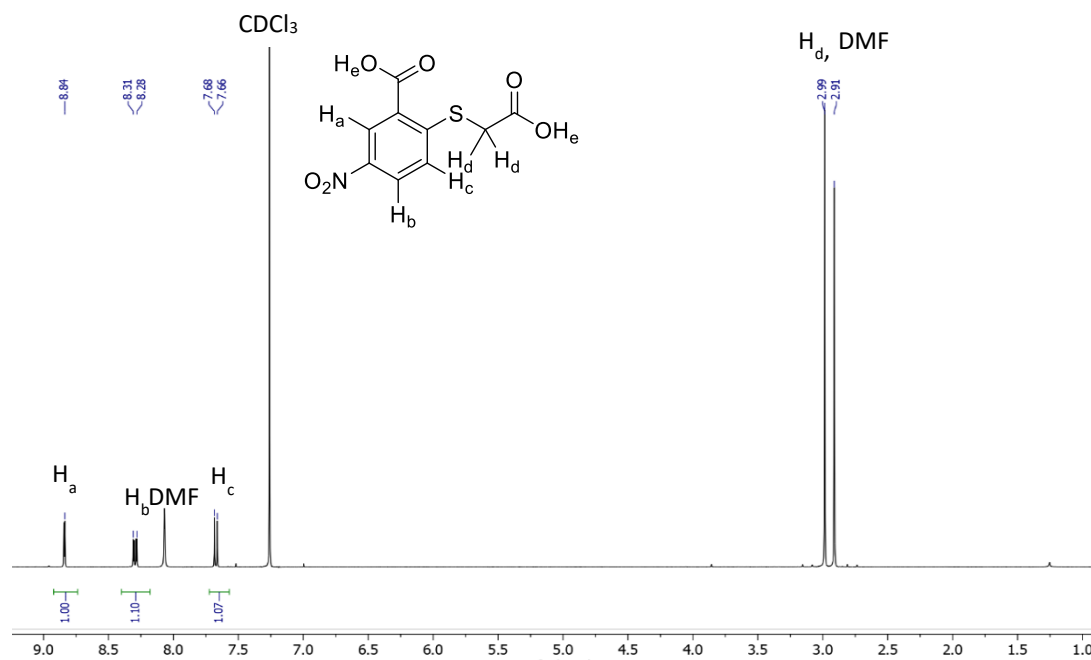


Figure A.1.1 ^1H NMR spectrum of 2-((carboxymethyl)thio)-5-nitrobenzoic acid (5)

in CDCl_3 at 298 K.

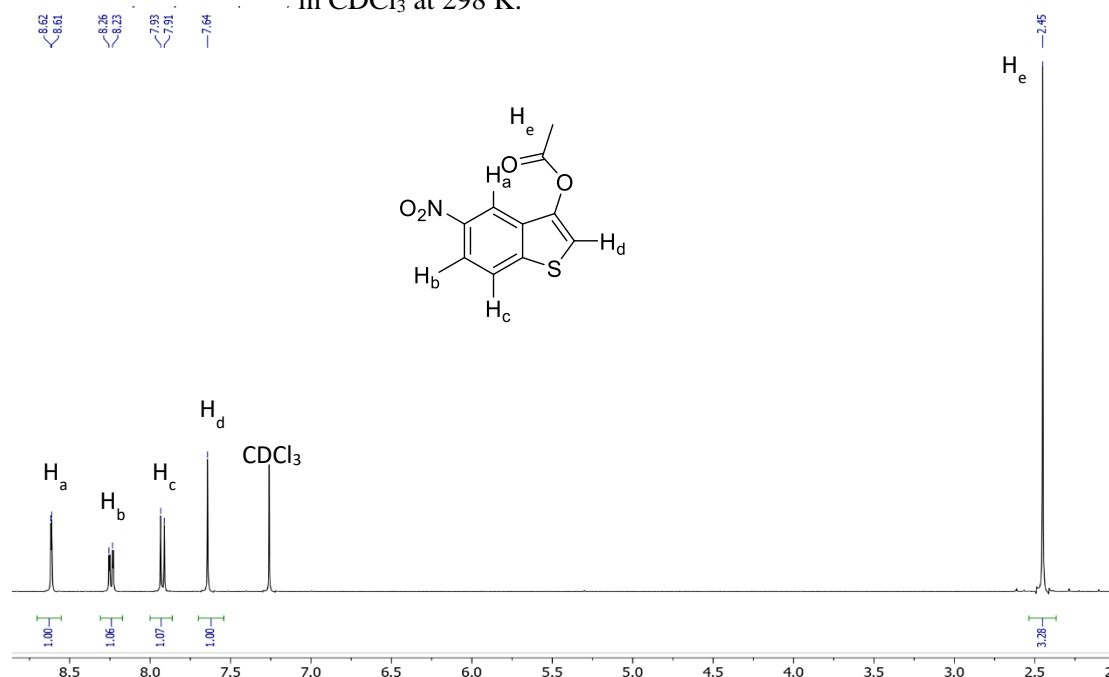


Figure A.1.2 ^1H NMR spectrum of 6-nitrobenzo[b]thiophen-3-yl acetate (6)

in CDCl_3 at 298 K.

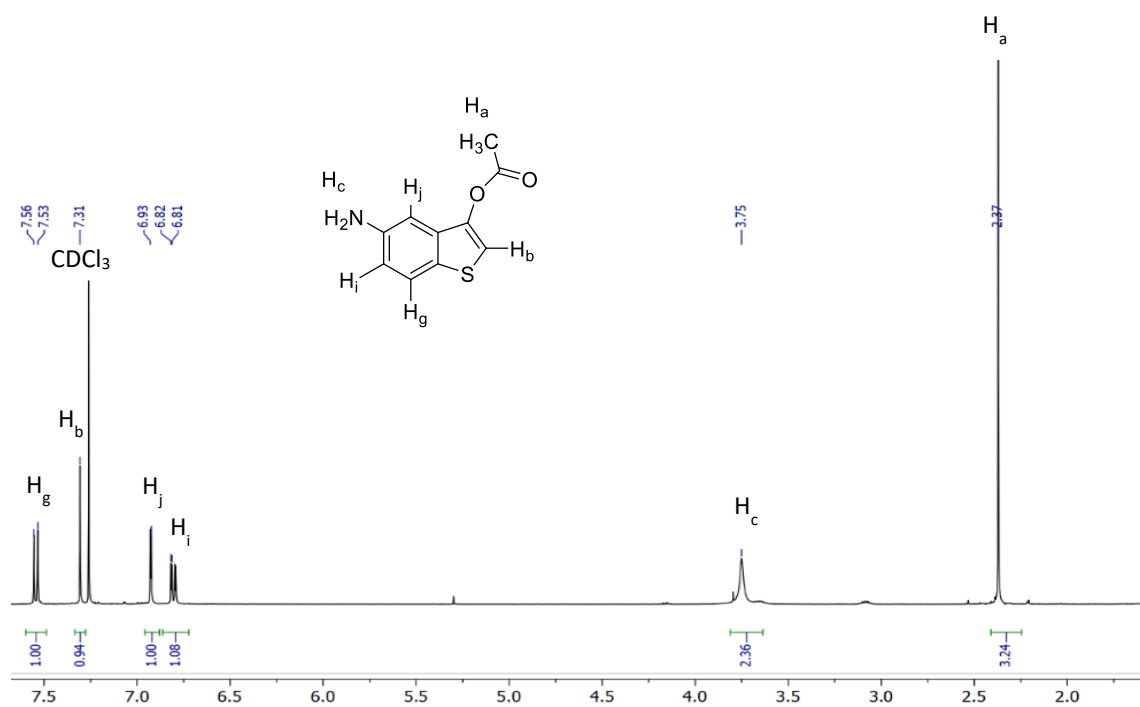


Figure A.1.3 ^1H NMR spectrum of 5-aminobenzo[*b*]thiophen-3-yl acetate (**7**) in CDCl_3 at 298 K.

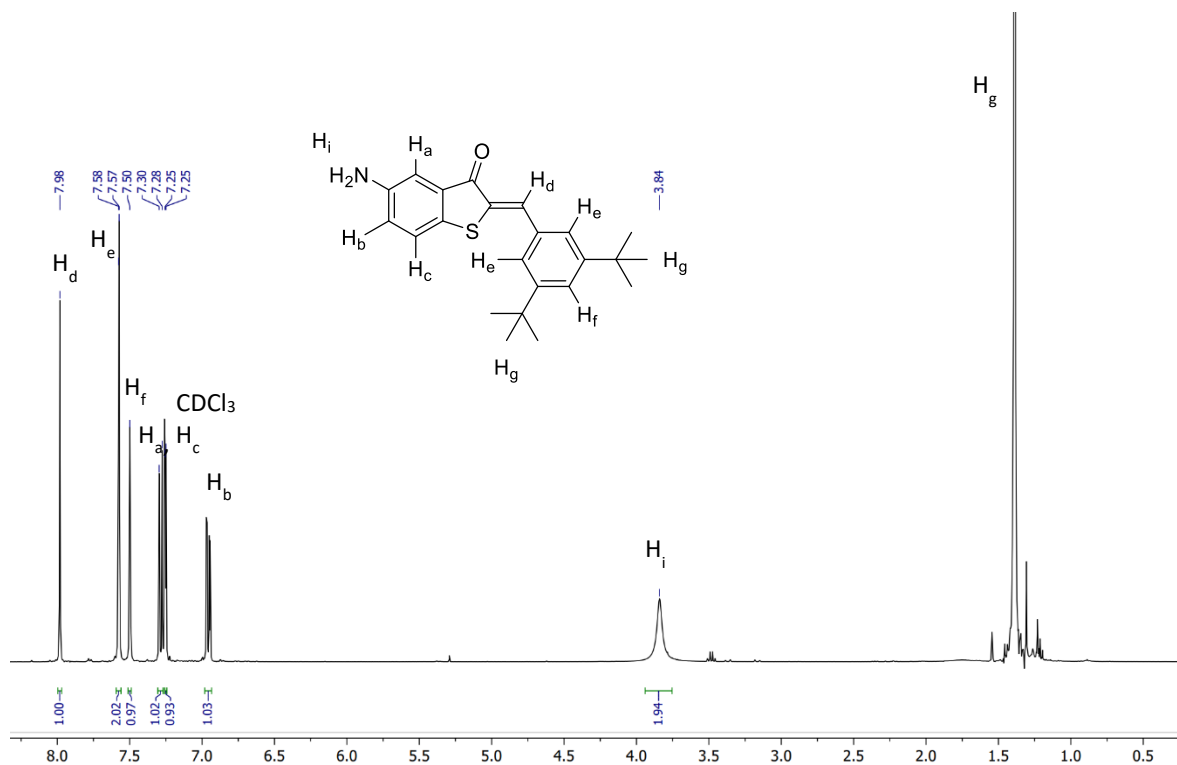


Figure A.1.4 ^1H NMR spectrum of (*Z*)-5-amino-2-(3,5-di-*tert*-butylbenzylidene)benzo[*b*]thiophen-3(2H)-one (**7a**) in CDCl_3 at 298 K.

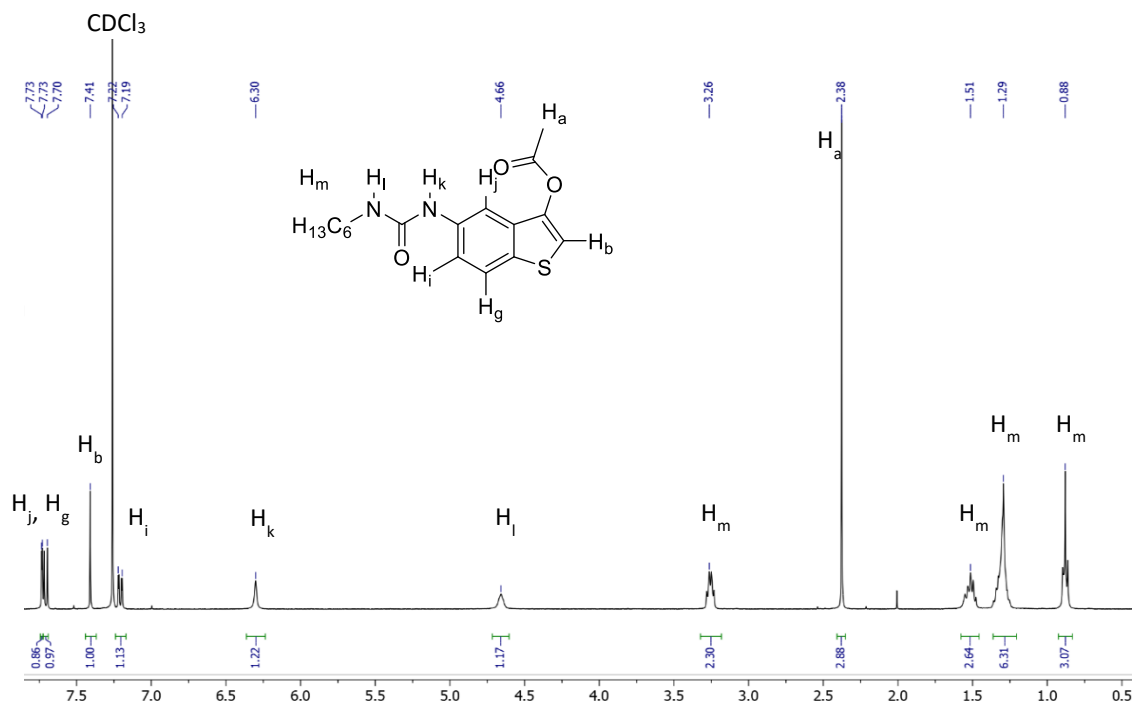


Figure A.1.5 ^1H NMR spectrum of 5-(3-hexylureido)benzo[b]thiophen-3-yl acetate (8a) in CDCl_3 at 298 K.

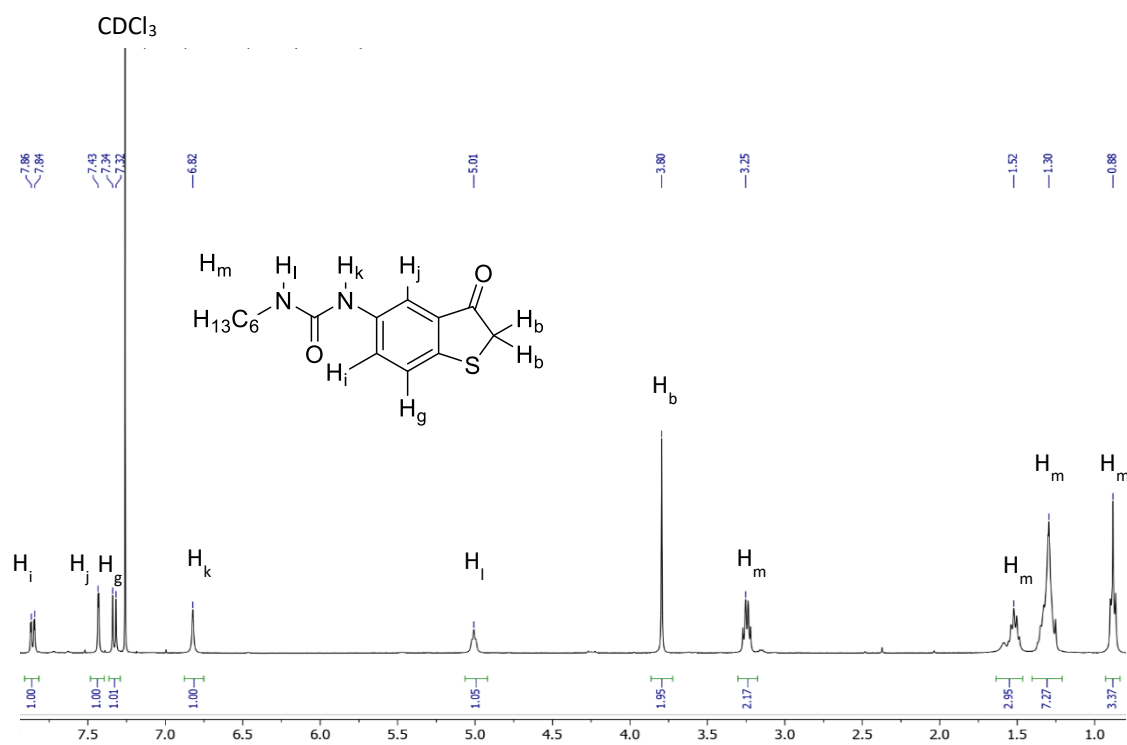


Figure A.1.6 ^1H NMR spectrum of 1-hexyl-3-(3-oxo-2,3-dihydrobenzo[b]thiophen-5-yl)urea (9a) in CDCl_3 at 298 K.

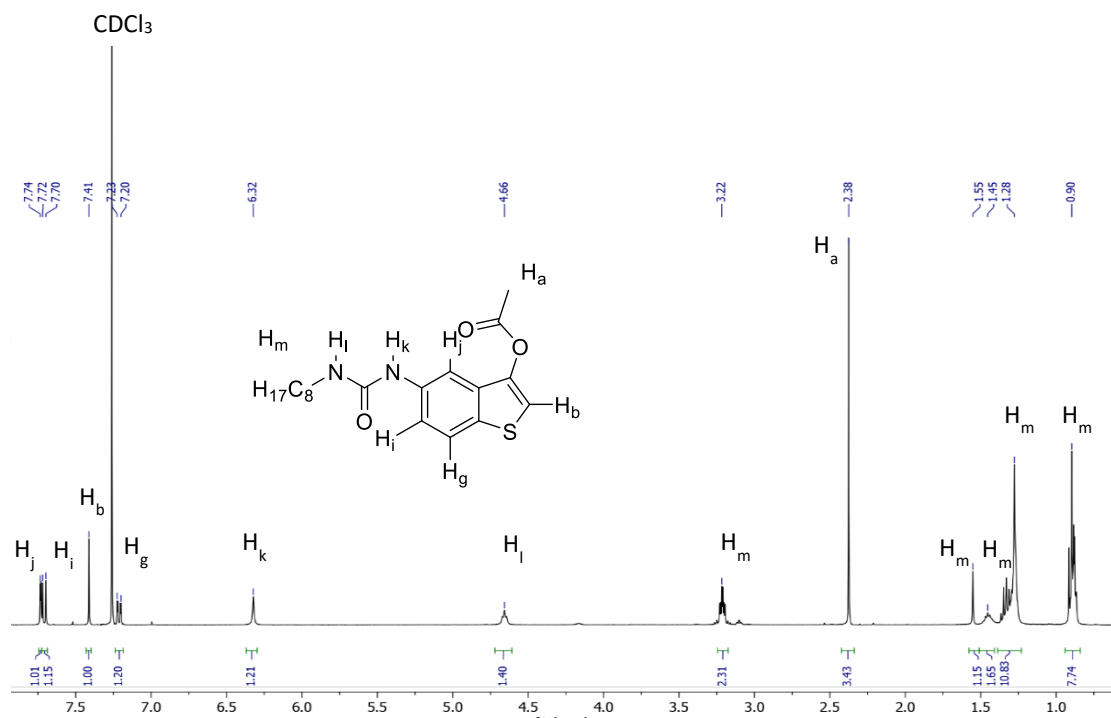


Figure A.1.7 ^1H NMR spectrum of 5-(3-(2-ethylhexyl)ureido)benzo[b]thiophen-3-yl acetate (**8b**) in CDCl_3 at 298 K.

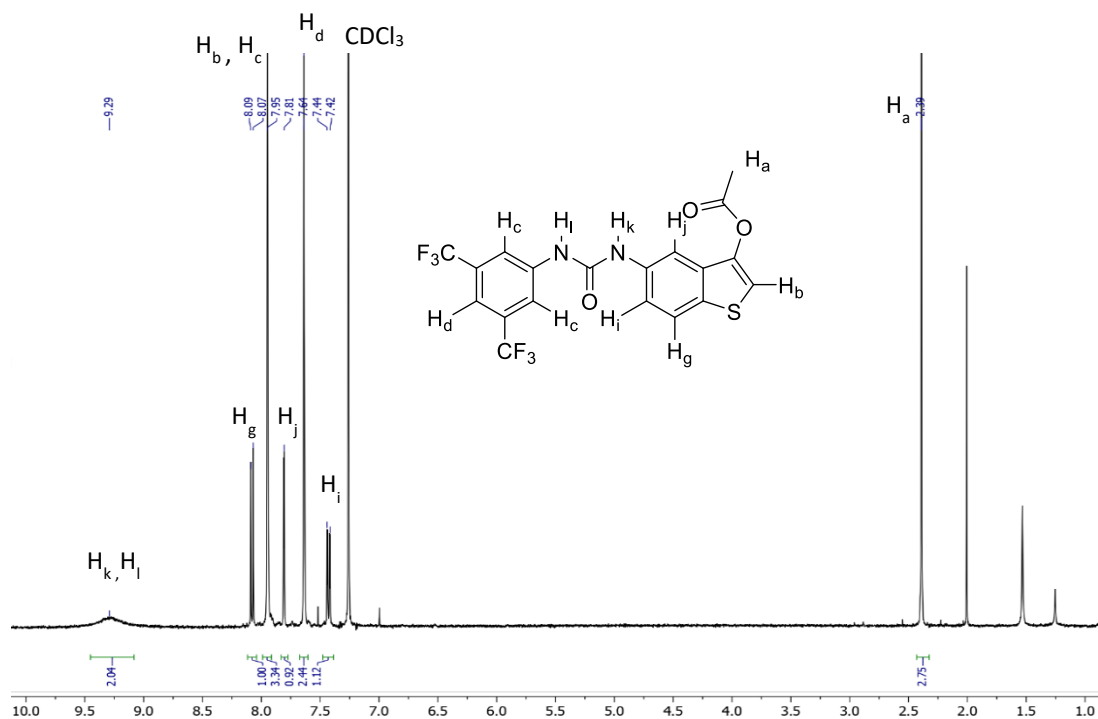


Figure A.1.8 ^1H NMR spectrum of 5-(3-(3,5-bis(trifluoromethyl)phenyl)ureido)benzo[b]thiophen-3-yl acetate (**8c**) in CDCl_3 at 298 K.

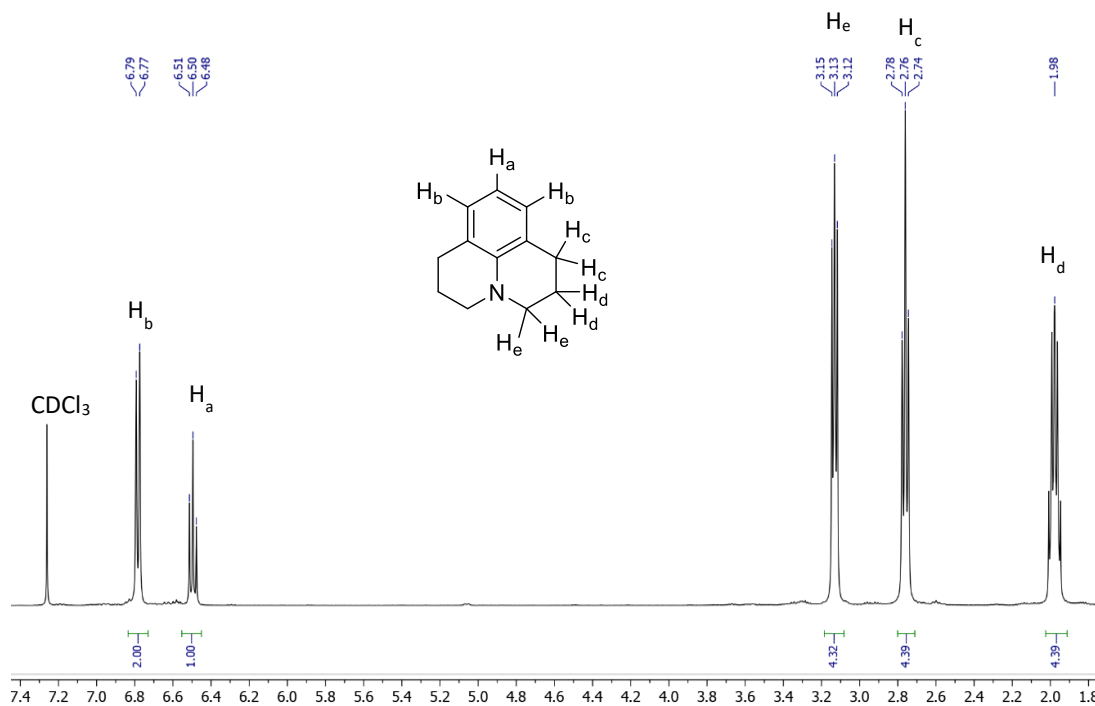


Figure A.1.9 ^1H NMR spectrum of 2,3,6,7-tetrahydro-1H,5H-pyrido[3,2,1-ij]quinoline (**10**) in CDCl_3 at 298 K.

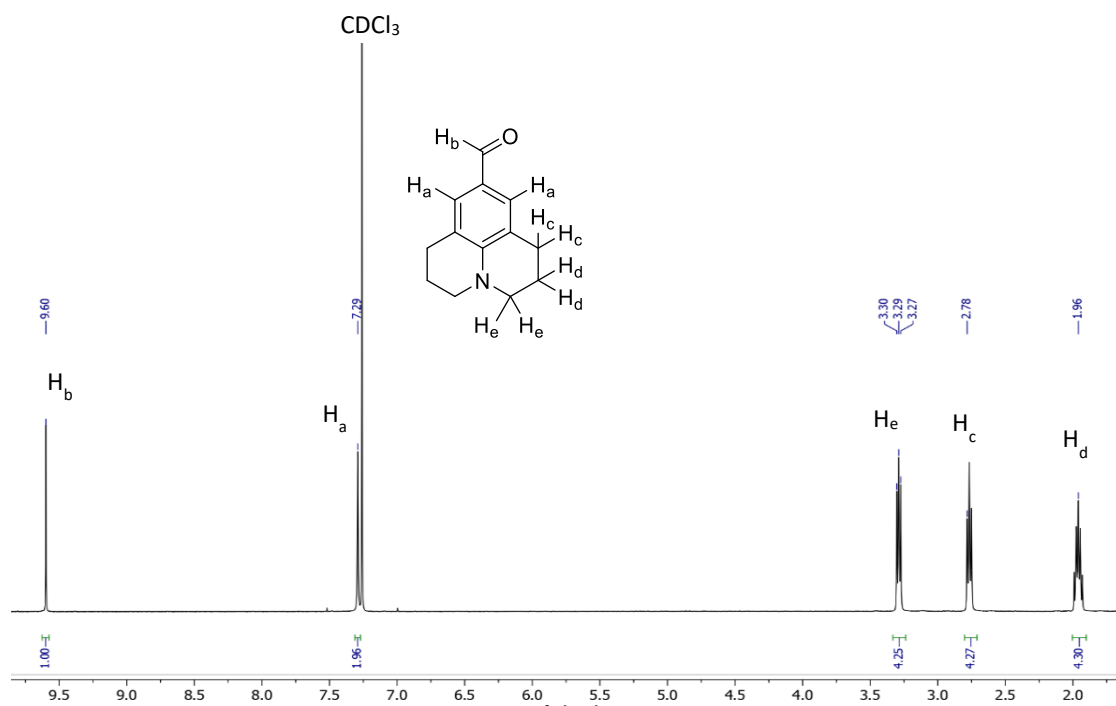


Figure A.1.10 ^1H NMR spectrum of 2,3,6,7-tetrahydro-1H,5H-pyrido[3,2,1-ij]quinoline-9-carbaldehyde (**11**) in CDCl_3 at 298 K.

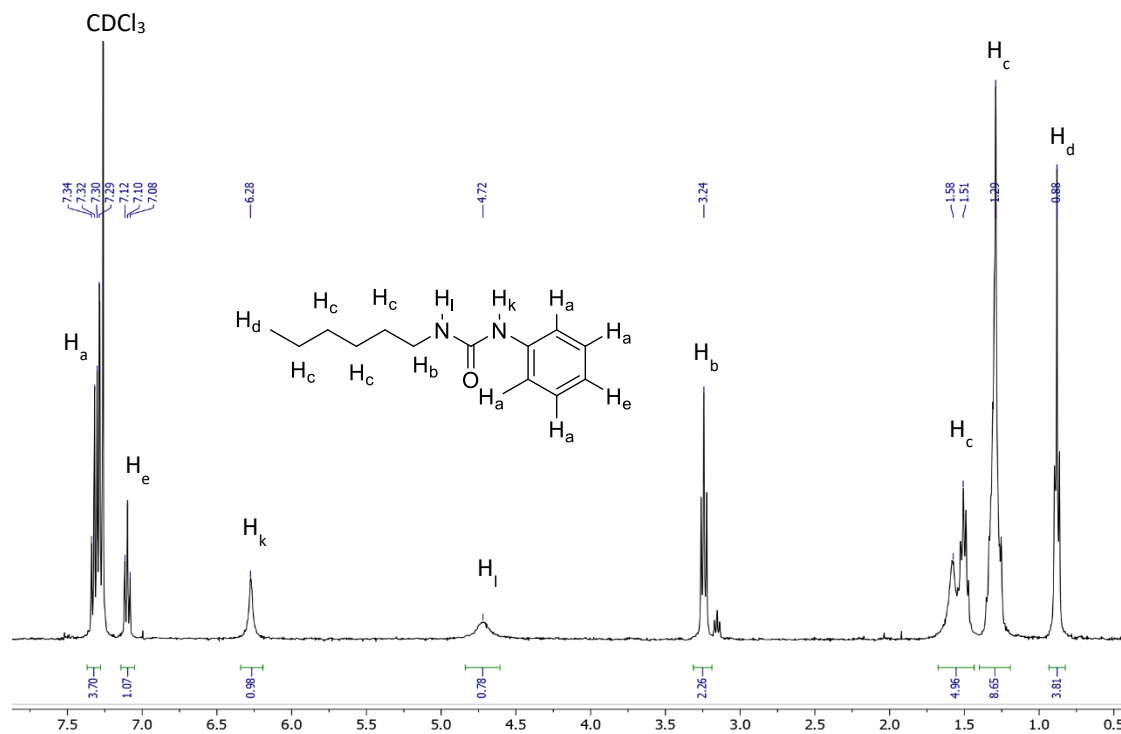


Figure A.1.11 ^1H NMR spectrum of 1-hexyl-3-phenylurea (**13**) in CDCl_3 at 298 K.

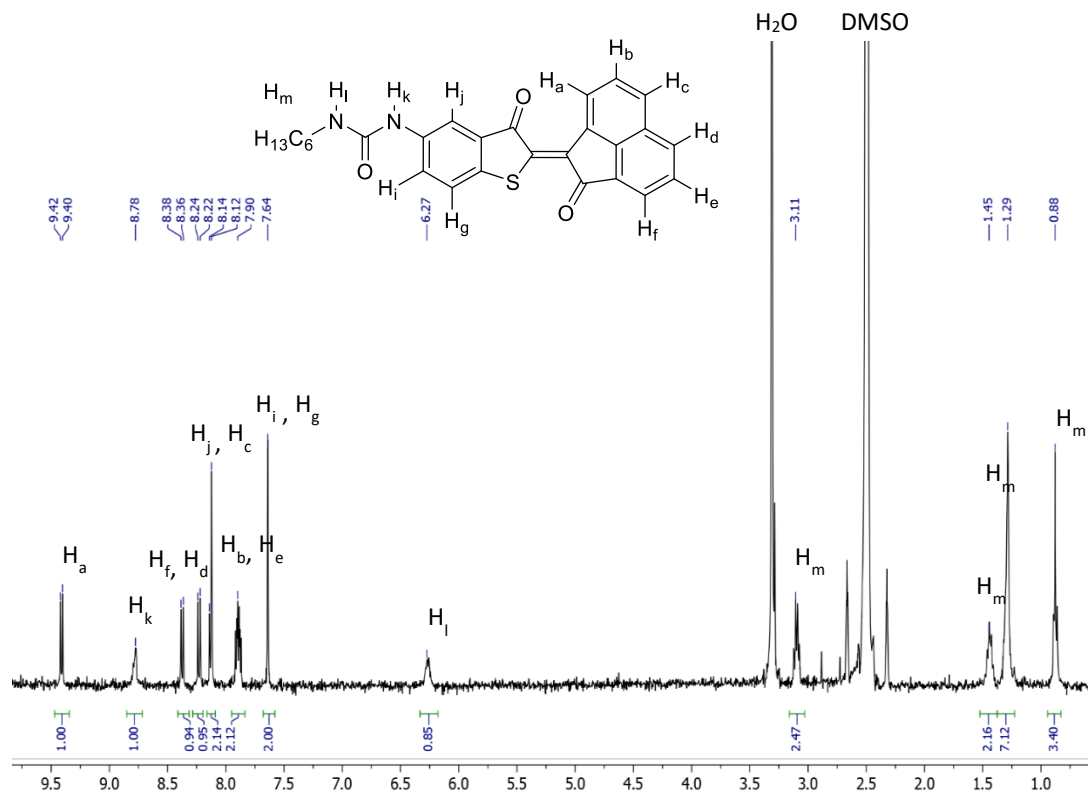


Figure A.1.12 ^1H NMR spectrum of (Z)-1-hexyl-3-(3-oxo-2-(2-oxoacnaphthyl-1(2H)-ylidene)-2,3-dihydrobenzo[b]thiophen-5-yl)urea (**Z-1a**) in DMSO- d_6 at 298 K.

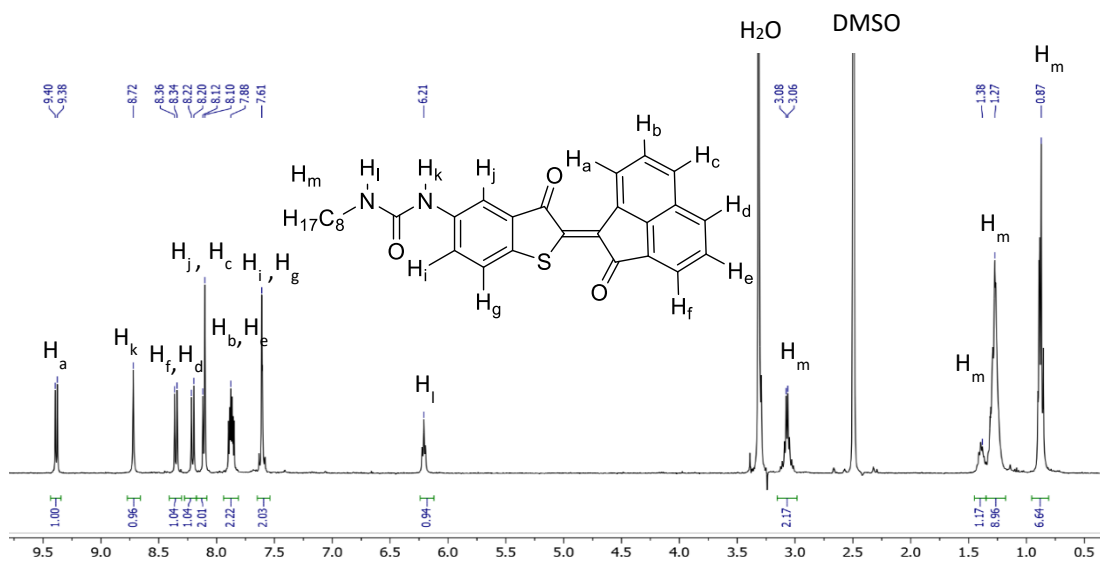


Figure A.1.13 ^1H NMR spectrum of (Z)-1-(2-ethylhexyl)-3-(3-oxo-2-(2-oxoacnaphthyl-1(2H)-ylidene)-2,3-dihydrobenzo[b]thiophen-5-yl)urea (**Z-1b**) in DMSO- d_6 at 298 K.

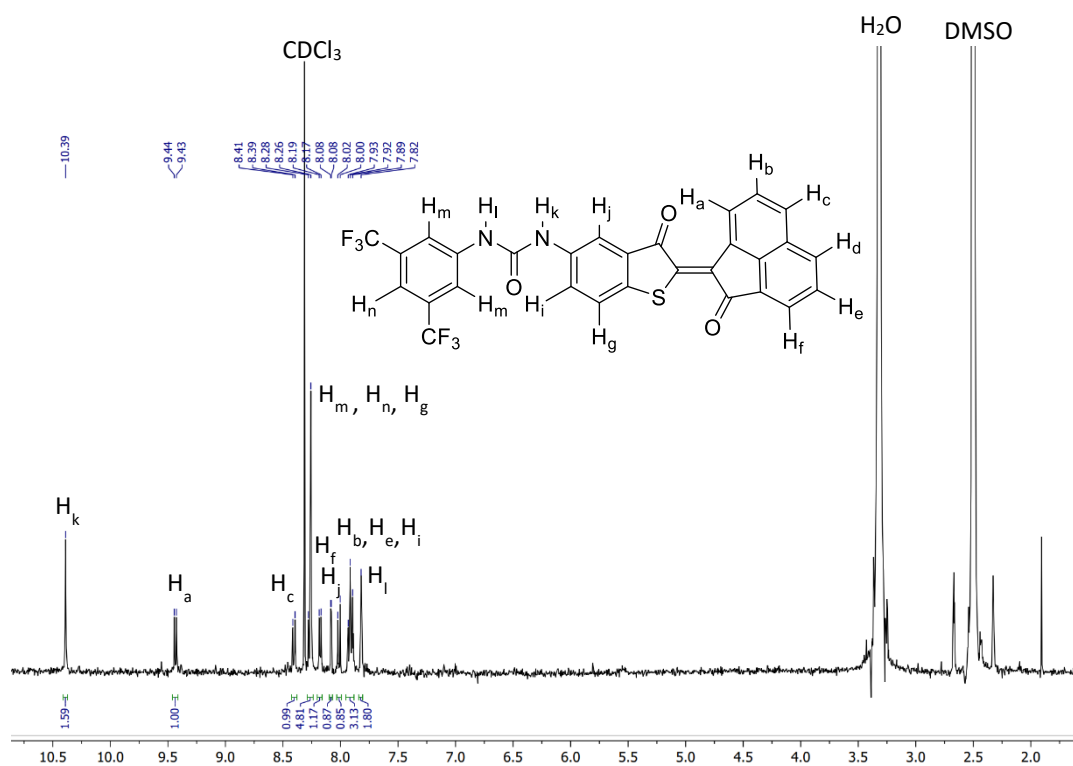


Figure A.1.14 ¹H NMR spectrum of ((Z)-1-(3,5-bis(trifluoromethyl)phenyl)-3-(3-oxo-2-(2-oxoacenaphthylen-1(2H)-ylidene)-2,3-dihydrobenzo[b]thiophen-5-yl)urea (**Z-1c**) in DMSO-*d*₆ at 298 K.

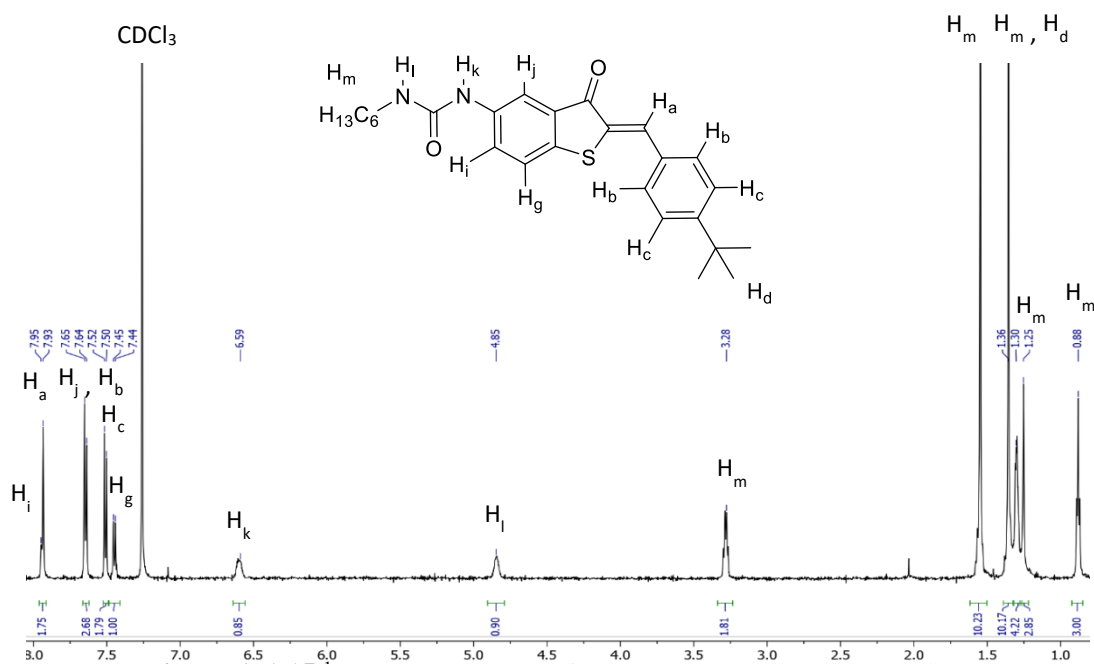


Figure A.1.15 ¹H NMR spectrum of (Z)-1-(2-(4-(tert-butyl)benzylidene)-3-oxo-2,3-dihydrobenzo[b]thiophen-5-yl)-3-hexylurea (**Z-2a**) in CDCl₃ at 298 K.

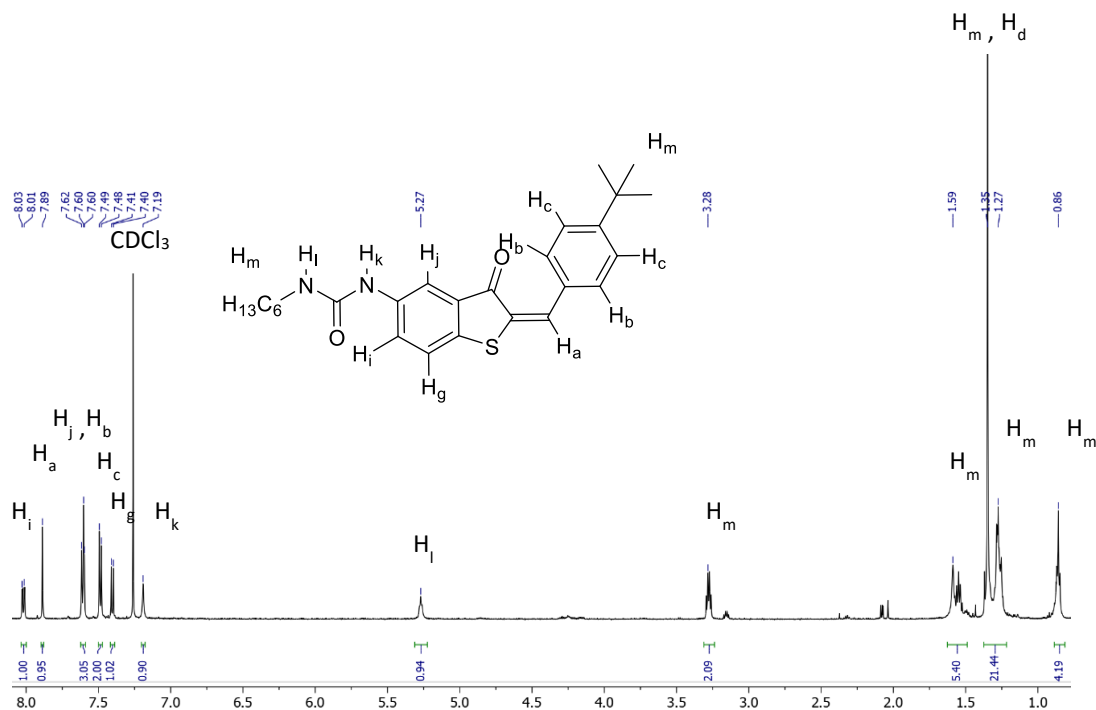


Figure A.1.16 1H NMR spectrum of (*E*)-1-(2-(4-(tert-butyl)benzylidene)-3-oxo-2,3-dihydrobenzo[b]thiophen-5-yl)-3-hexylurea (**E-2a**) in $CDCl_3$ at 298 K.

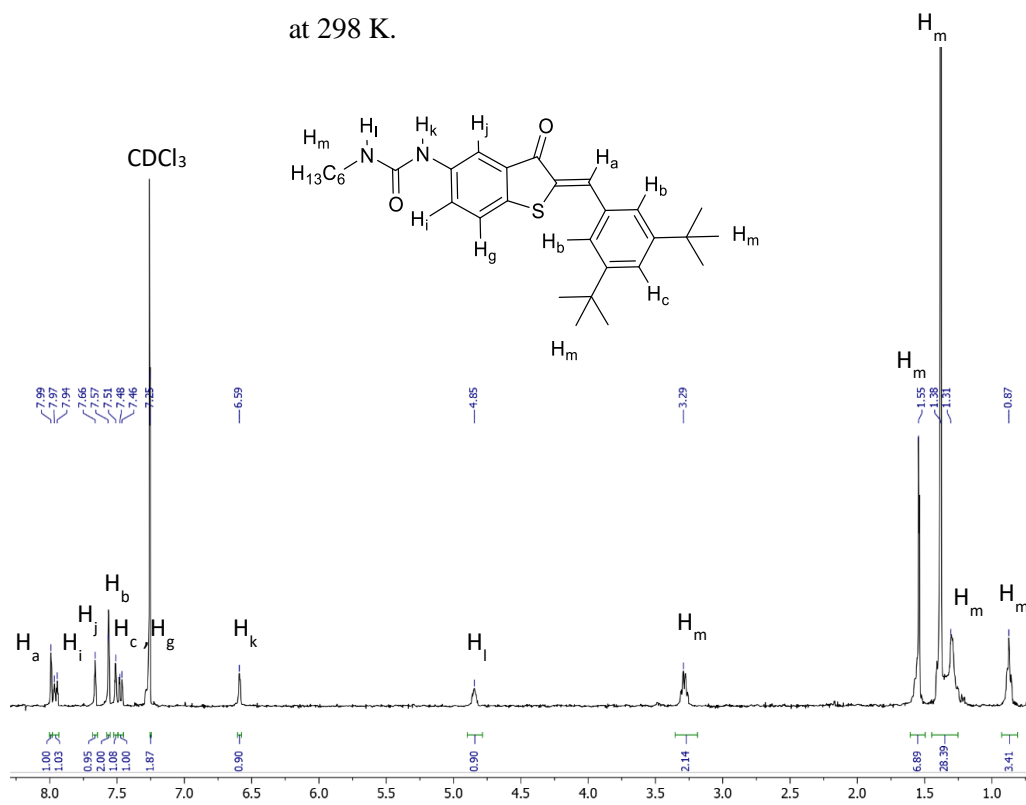


Figure A.1.17 1H NMR spectrum of (*Z*)-1-(2-(3,5-di-tert-butylbenzylidene)-3-oxo-2,3-dihydrobenzo[b]thiophen-5-yl)-3-hexylurea (**Z-2b**) in $CDCl_3$ at 298 K.

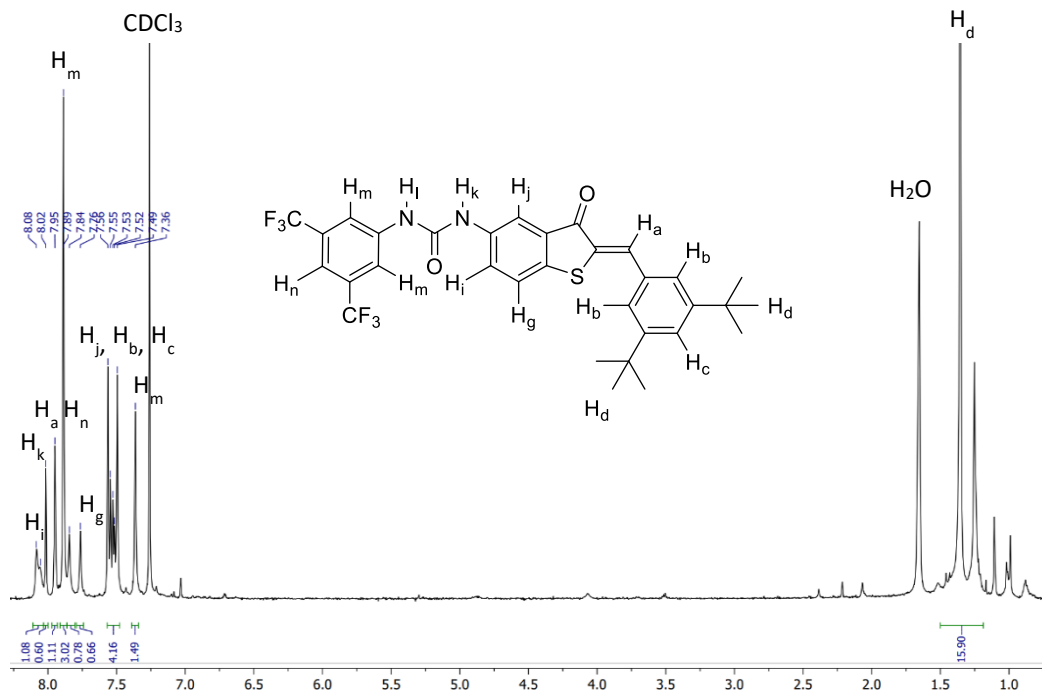


Figure A.1.18 ^1H NMR spectrum of ((Z)-1-(3,5-bis(trifluoromethyl)phenyl)-3-(2-(3,5-di-tert-butylbenzylidene)-3-oxo-2,3-dihydrobenzo[b]thiophen-5-yl)urea (**Z-2c**) in CDCl_3 at 298 K.

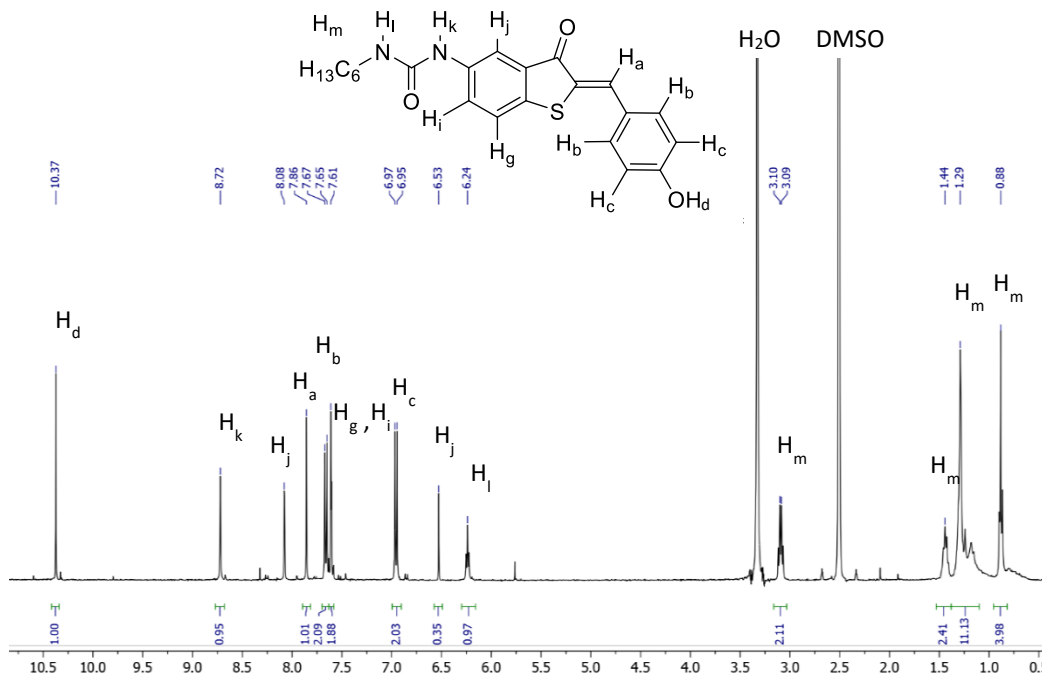


Figure A.1.19 ^1H NMR spectrum of (Z)-1-hexyl-3-(2-(4-hydroxybenzylidene)-3-oxo-2,3-dihydrobenzo[b]thiophen-5-yl)urea (**Z-2d**) in $\text{DMSO}-d_6$ at 298 K.

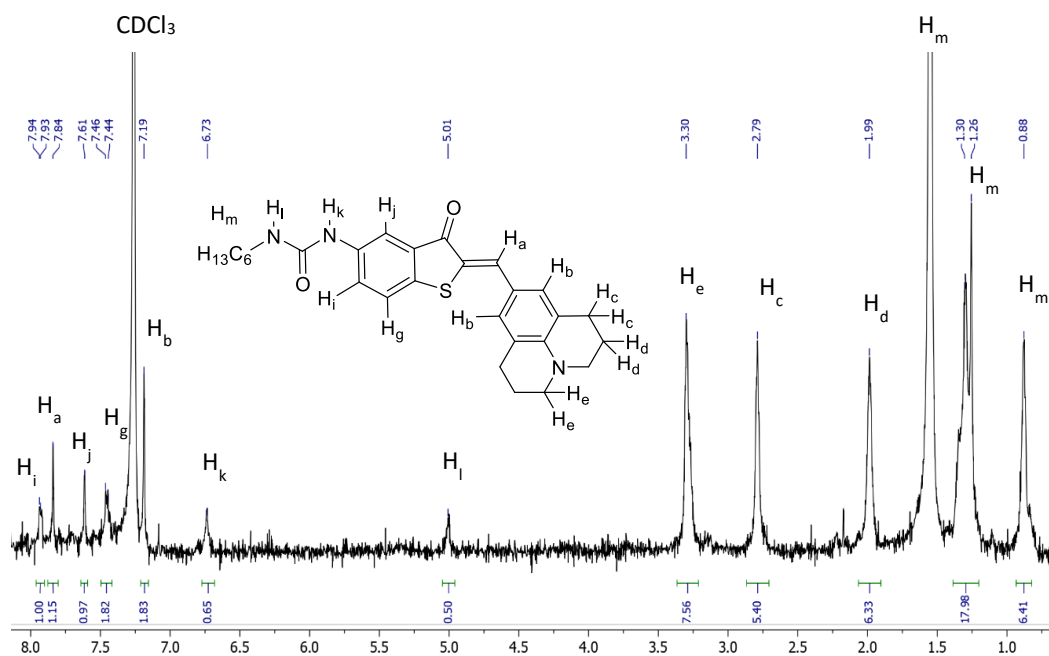


Figure A.1.20 ¹H NMR spectrum of (Z)-1-hexyl-3-(3-oxo-2-((2,3,6,7-tetrahydro-1H, 5H-pyrido[3,2,1-ij]quinoline-9-yl)methylene)-2,3-dihydrobenzo[b]thiophen-5-yl)urea (**Z-3a**) in CDCl₃ at 298 K.

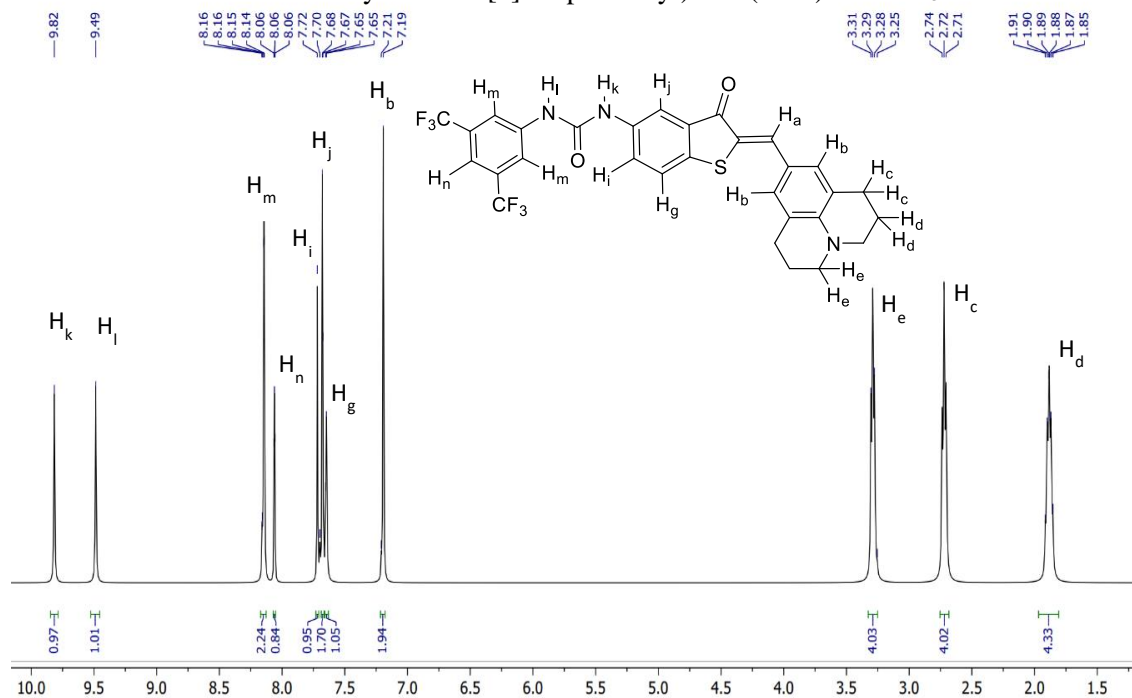


Figure A.1.21 ¹H NMR spectrum of (Z)-1-(3,5-bis(trifluoromethyl)phenyl)-3-(3-oxo-2-((2,3,6,7-tetrahydro-1H, 5H-pyrido[3,2,1-ij]quinolin-9-yl)methylene)-2,3-dihydrobenzo[b]thiophen-5-yl)urea (**Z-3b**) in CDCl₃ at 298 K.

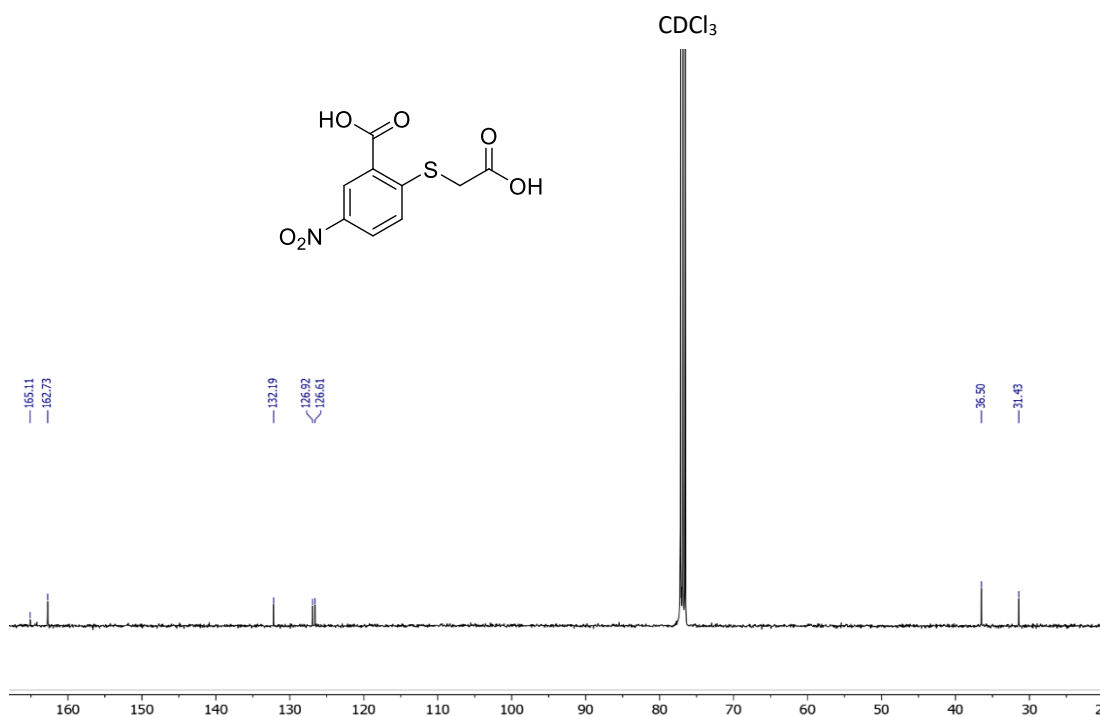
A.2 1D NMR Spectra (^{13}C NMR Spectra)

Figure A.2.1 ^{13}C NMR spectrum of 2-((carboxymethyl)thio)-5-nitrobenzoic acid (5) in CDCl₃ at 298 K.

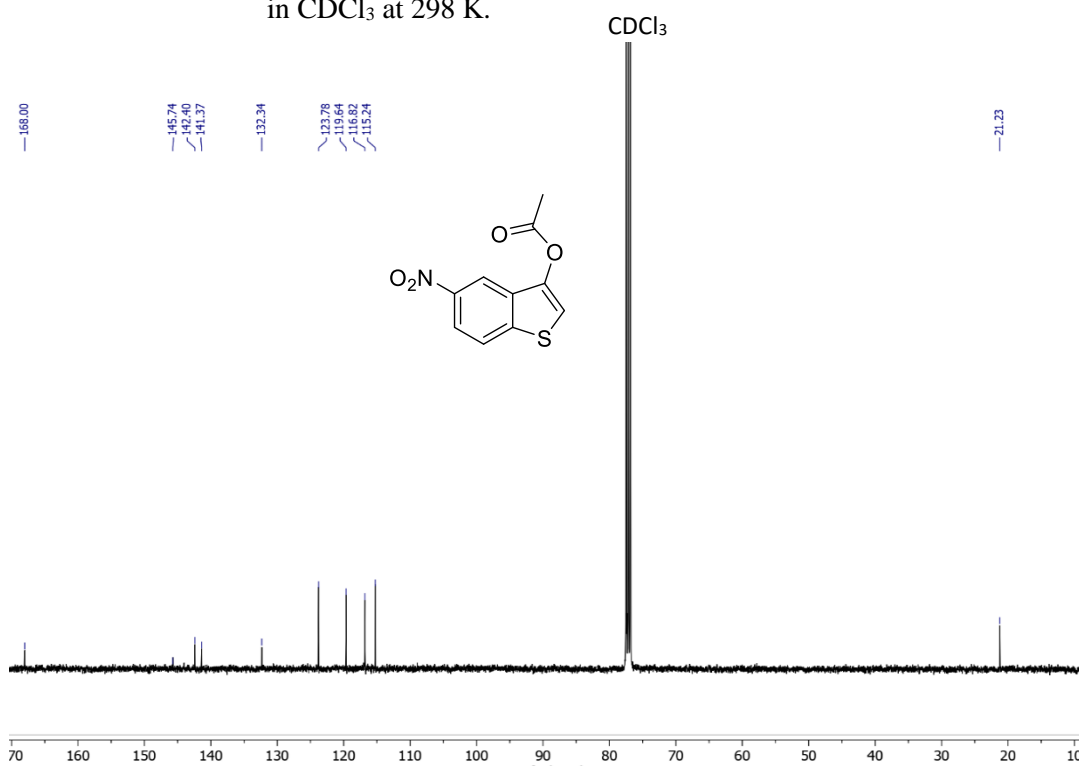


Figure A.2.2 ^{13}C NMR spectrum of 6-nitrobenzo[b]thiophen-3-yl acetate (6) in CDCl₃ at 298 K.

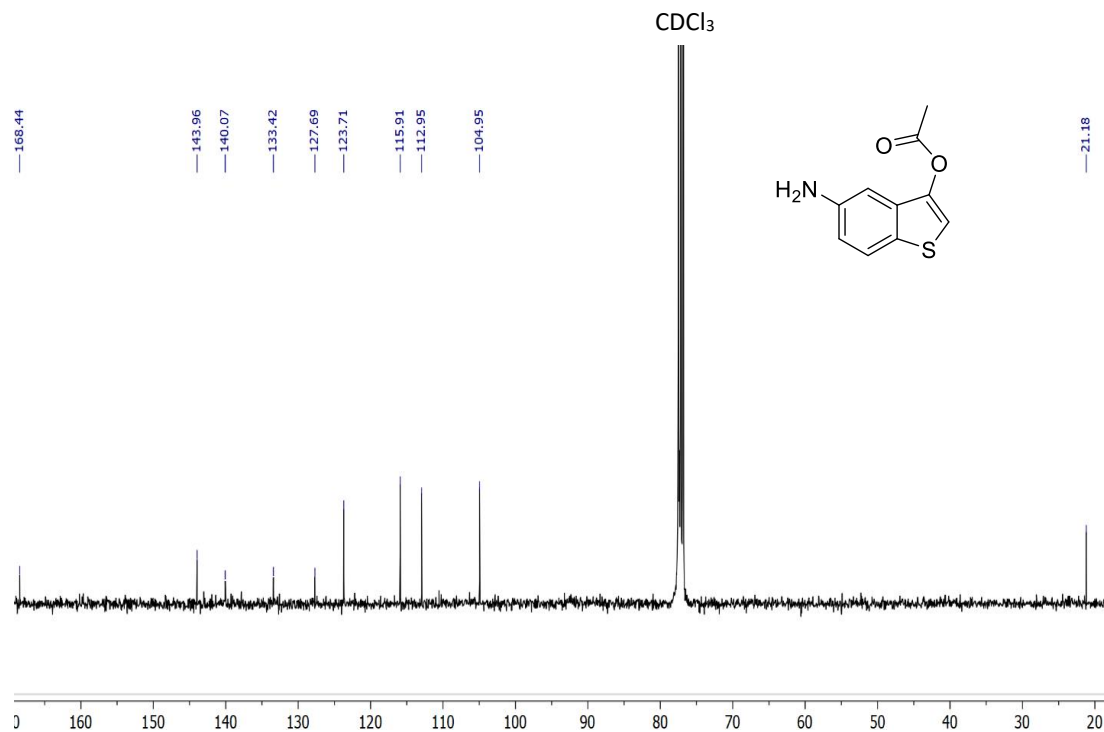


Figure A.2.3 ^{13}C NMR spectrum of 5-aminobenzo[b]thiophen-3-yl acetate (**7**) in CDCl_3 at 298 K.

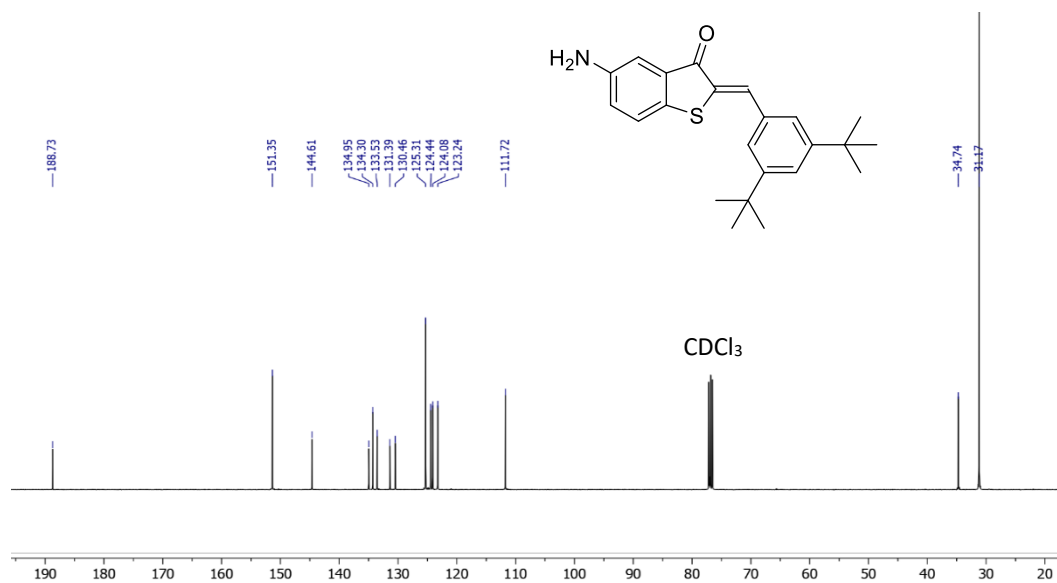


Figure A.2.4 ^{13}C NMR spectrum of (Z)-5-amino-2-(3,5-di-tert-butylbenzylidene)benzo[b]thiophen-3(2H)-one (**7a**) in CDCl_3 at 298 K.

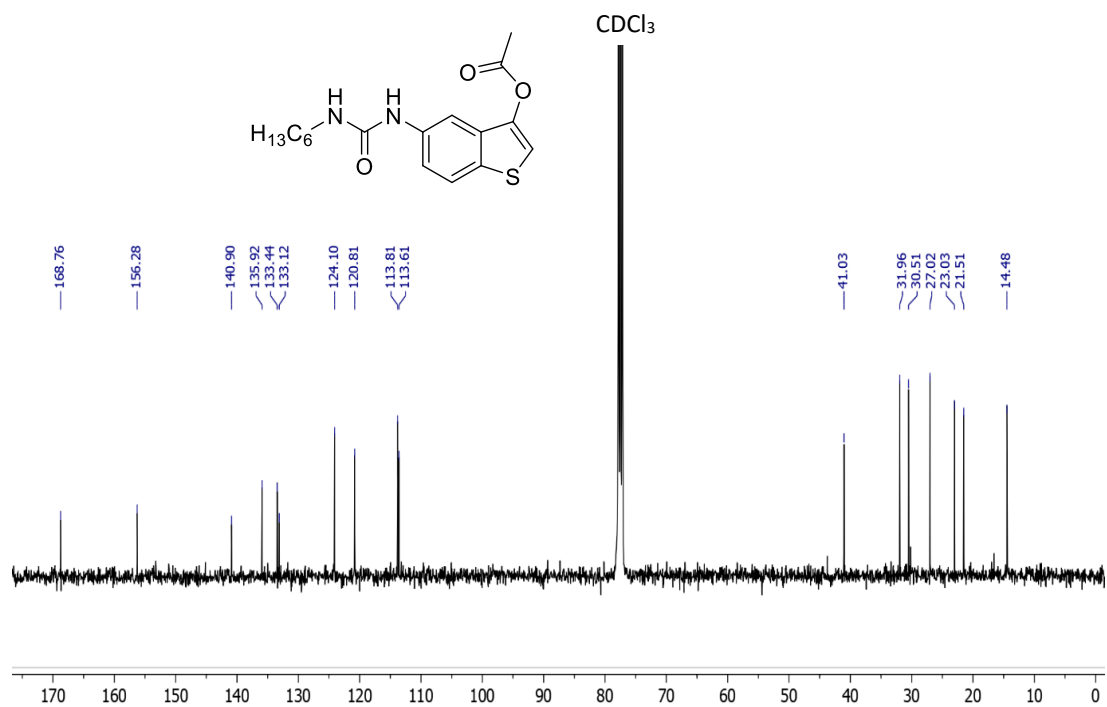


Figure A.2.5 ^{13}C NMR spectrum of 5-(3-hexylureido)benzo[b]thiophen-3-yl acetate (**8a**) in CDCl_3 at 298 K.

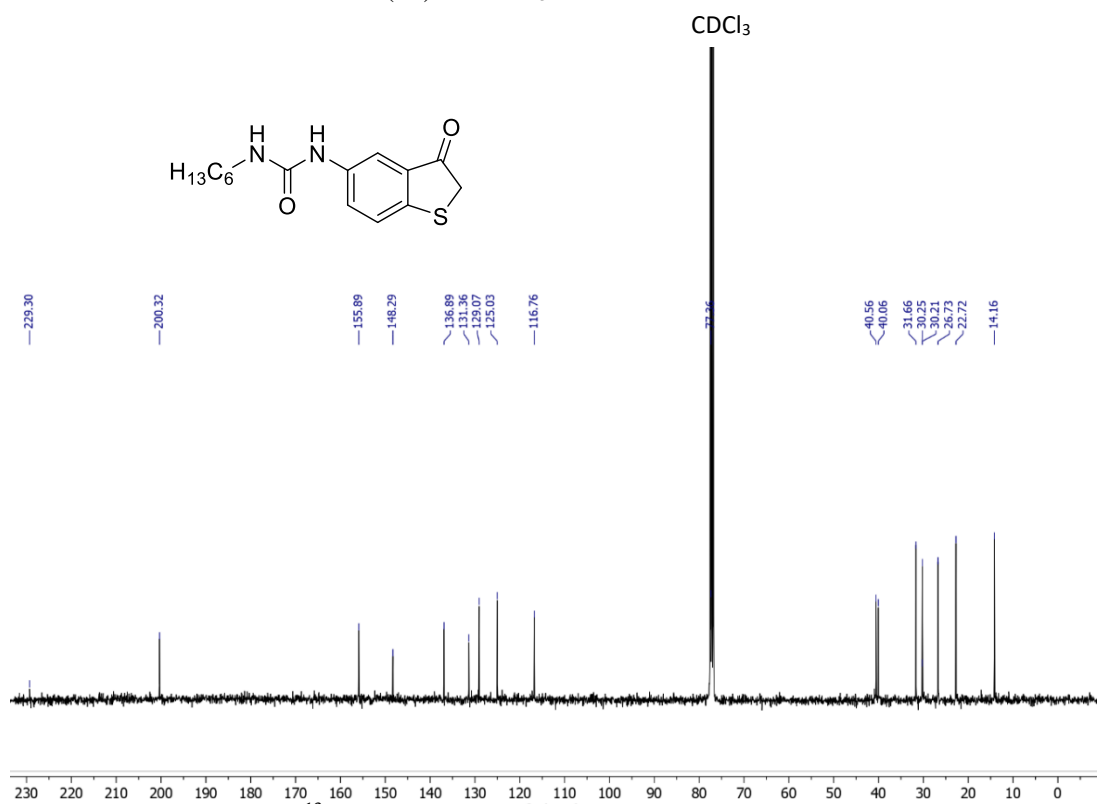


Figure A.2.6 ^{13}C NMR spectrum of 1-hexyl-3-(3-oxo-2,3-dihydrobenzo[b]thiophen-5-yl)urea (**9a**) in CDCl_3 at 298 K.

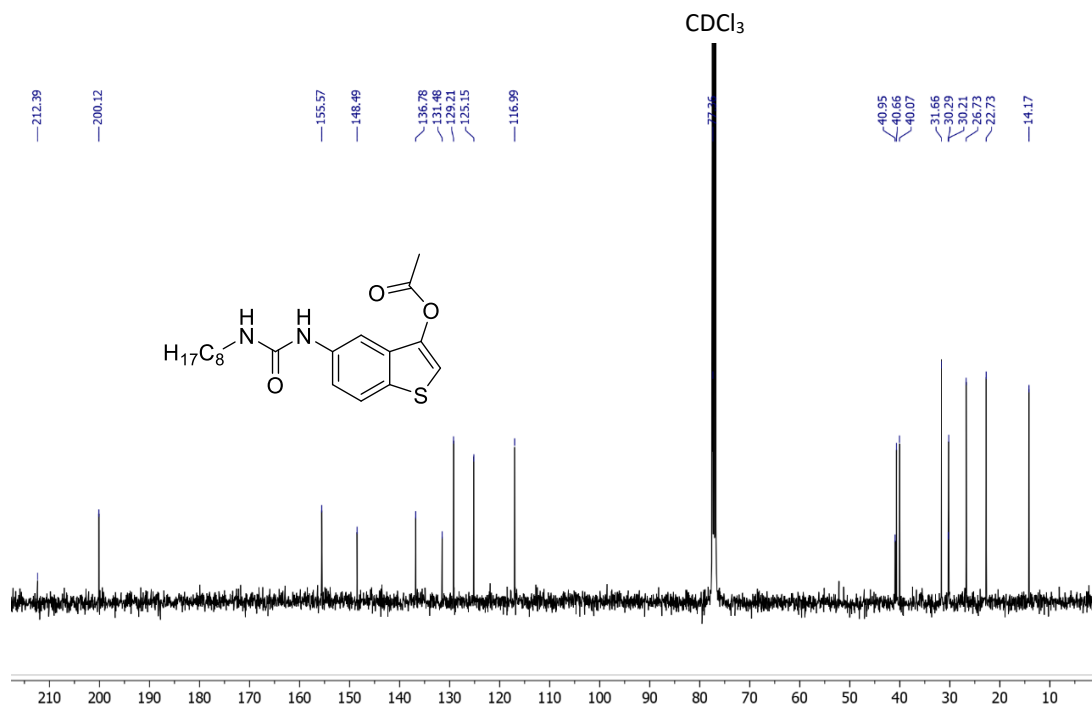


Figure A.2.7 ¹³C NMR spectrum of 5-(3-(2-ethylhexyl)ureido)benzo[b]thiophen-3-yl acetate (**8b**) in CDCl₃ at 298 K.

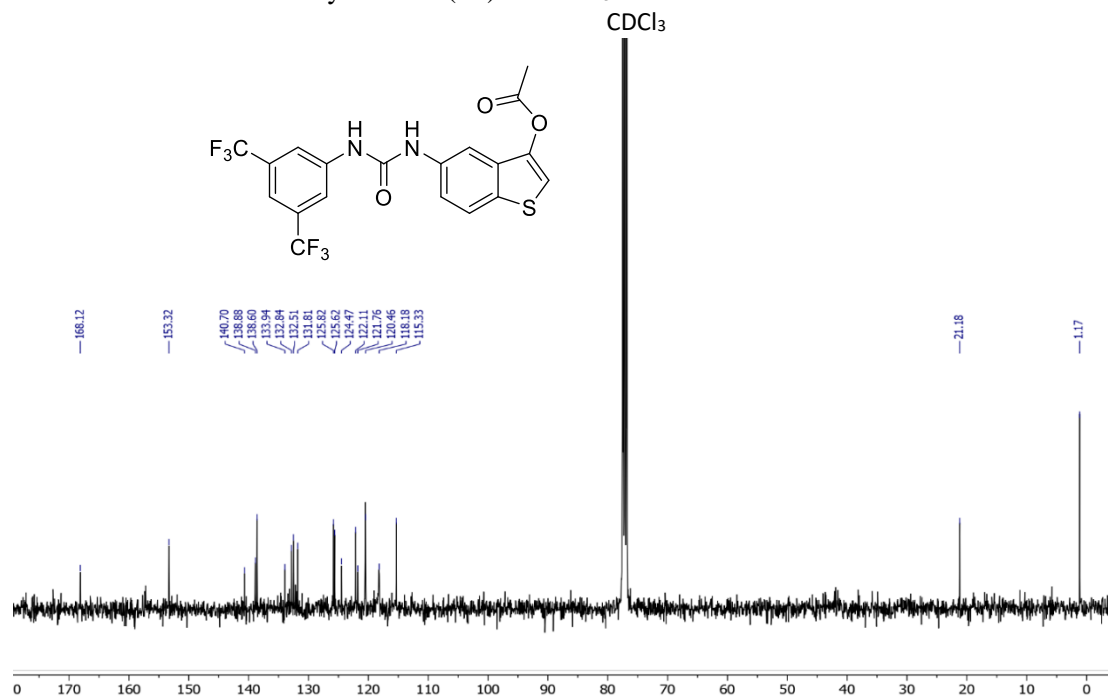


Figure A.2.8 ¹³C NMR spectrum of 5-(3-(3,5-bis(trifluoromethyl)phenyl)ureido)benzo[b]thiophen-3-yl acetate (**8c**) in CDCl₃ at 298 K.

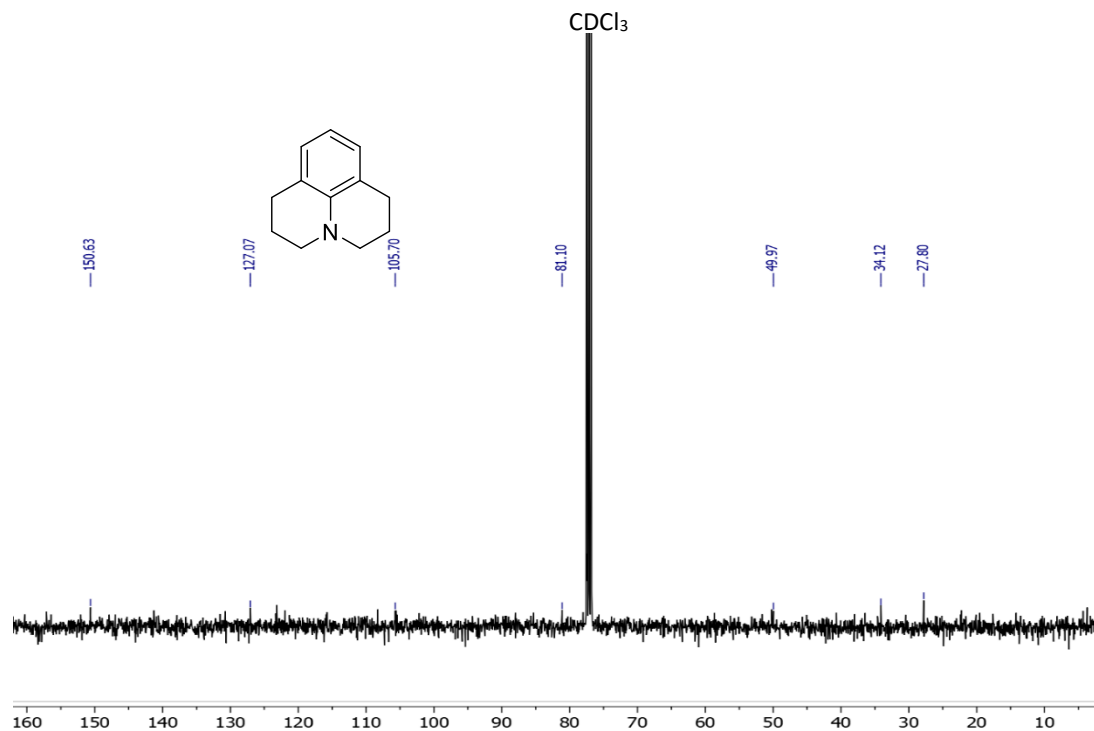


Figure A.2.9 ^{13}C NMR spectrum of 2,3,6,7-tetrahydro-1H,5H-pyrido[3,2,1-ij]quinoline (**10**) in CDCl_3 at 298 K.

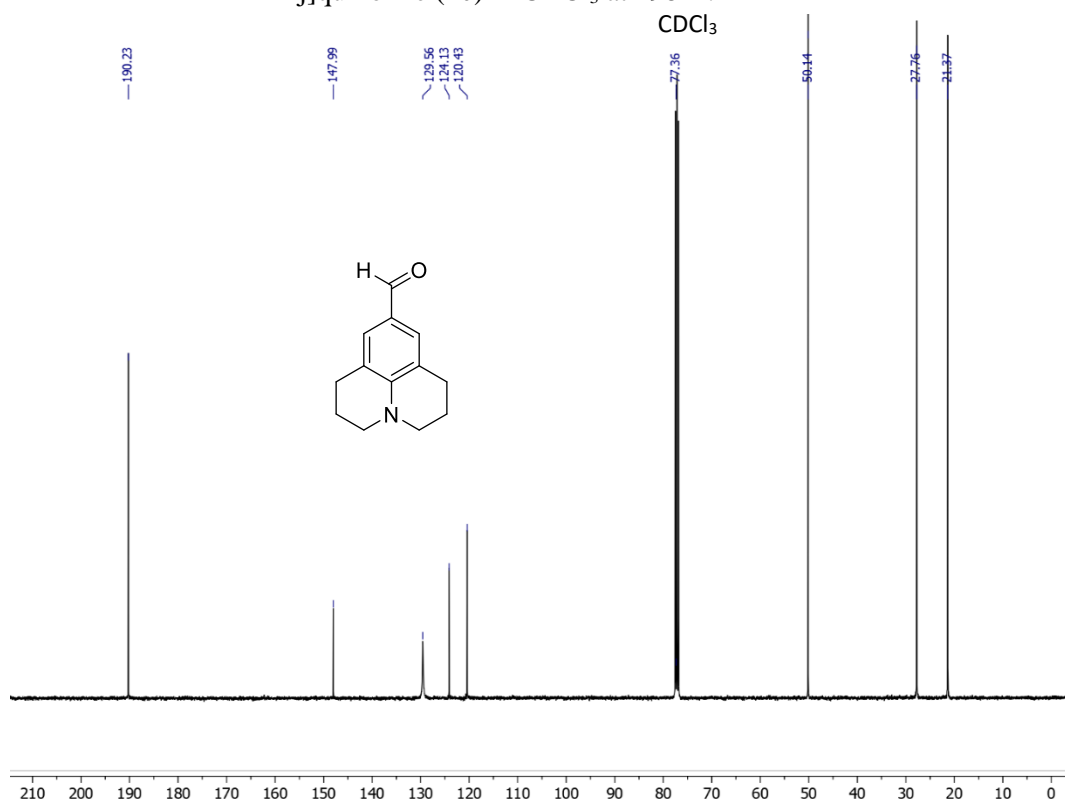


Figure A.2.10 ^{13}C NMR spectrum of 2,3,6,7-tetrahydro-1H,5H-pyrido[3,2,1-ij]quinoline-9-carbaldehyde (**11**) in CDCl_3 at 298 K.

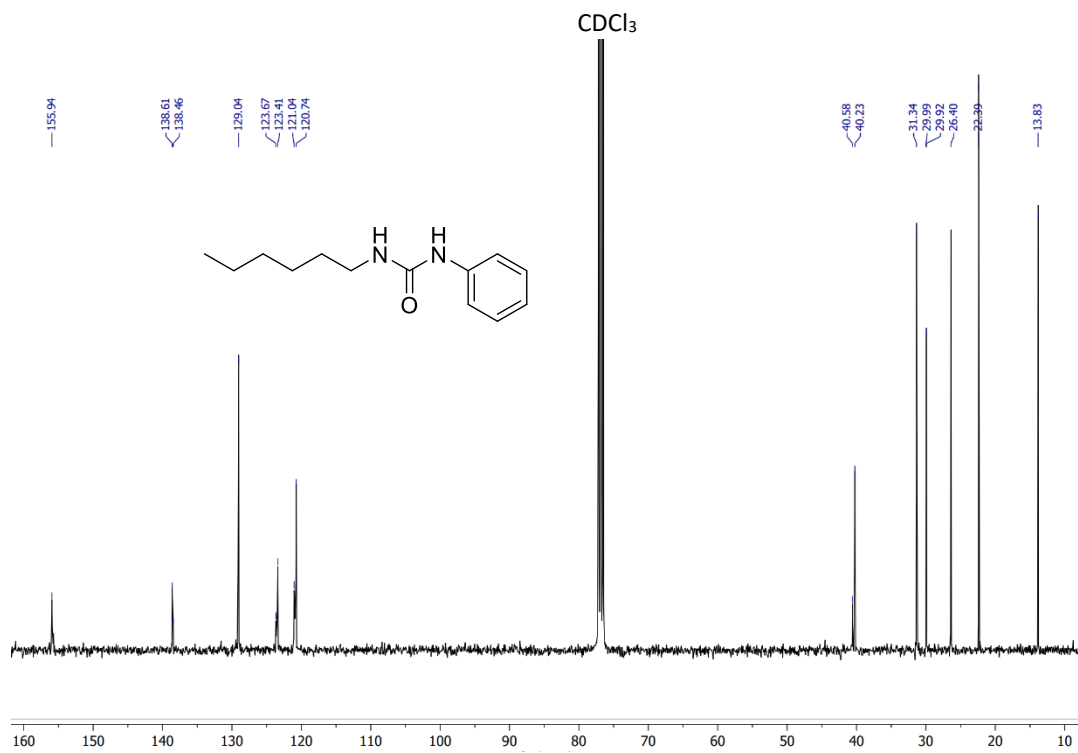


Figure A.2.11 ^{13}C NMR spectrum of 1-hexyl-3-phenylurea (**13**) in CDCl_3 at 298 K.

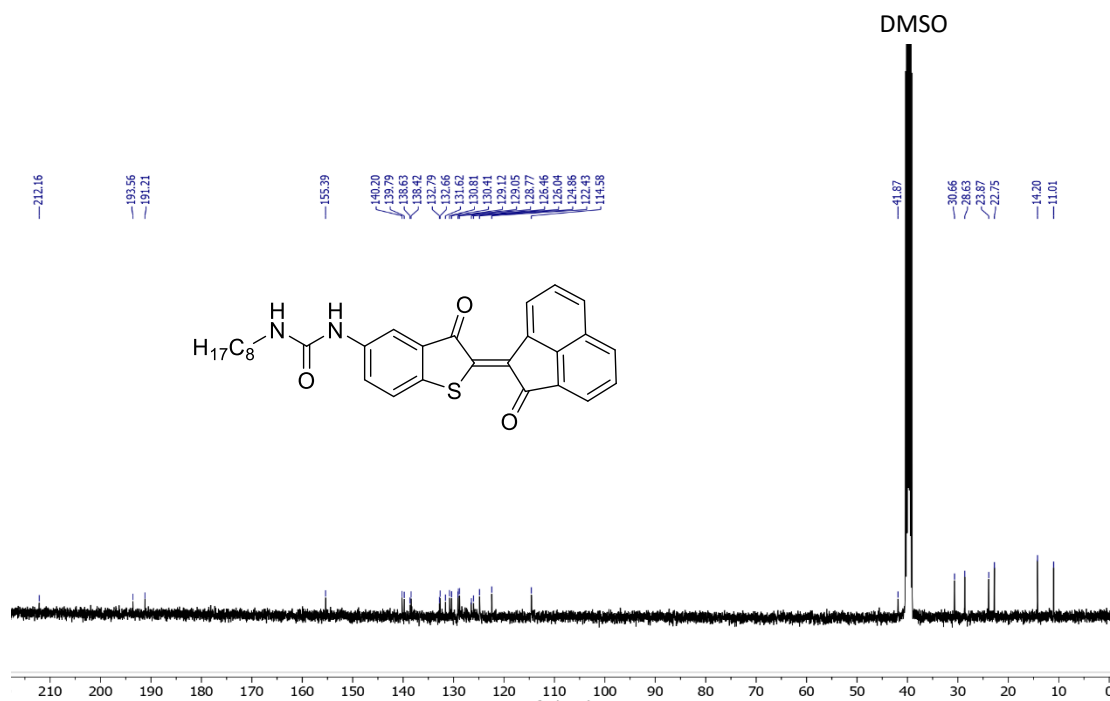


Figure A.2.12 ¹³C NMR spectrum of (*Z*)-1-(2-ethylhexyl)-3-(3-oxo-2-(2-oxoacenaphthylen-1(2H)-ylidene)-2,3-dihydrobenzo[*b*]thiophen-5-yl)urea (**Z-1b**) in DMSO-*d*₆ at 298 K.

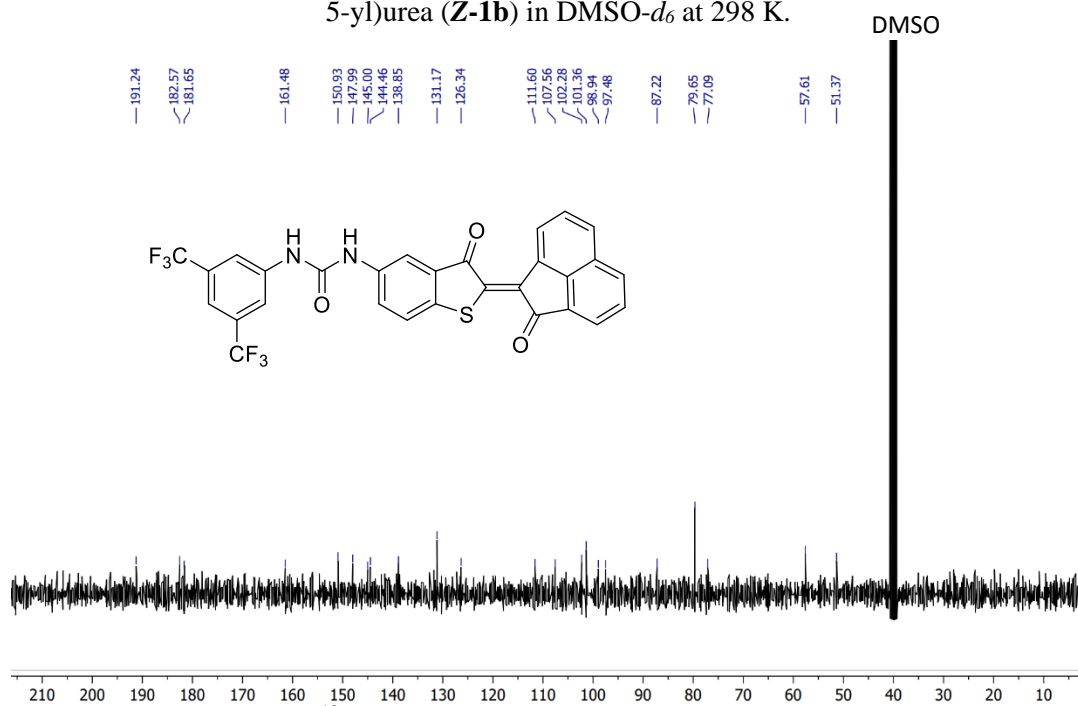
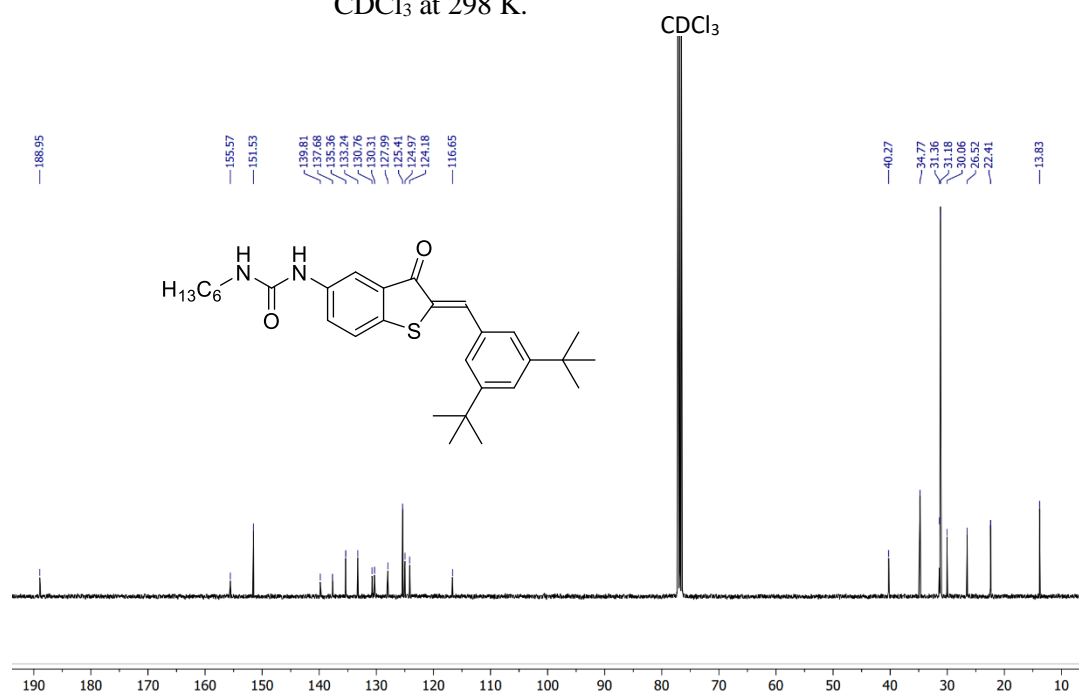
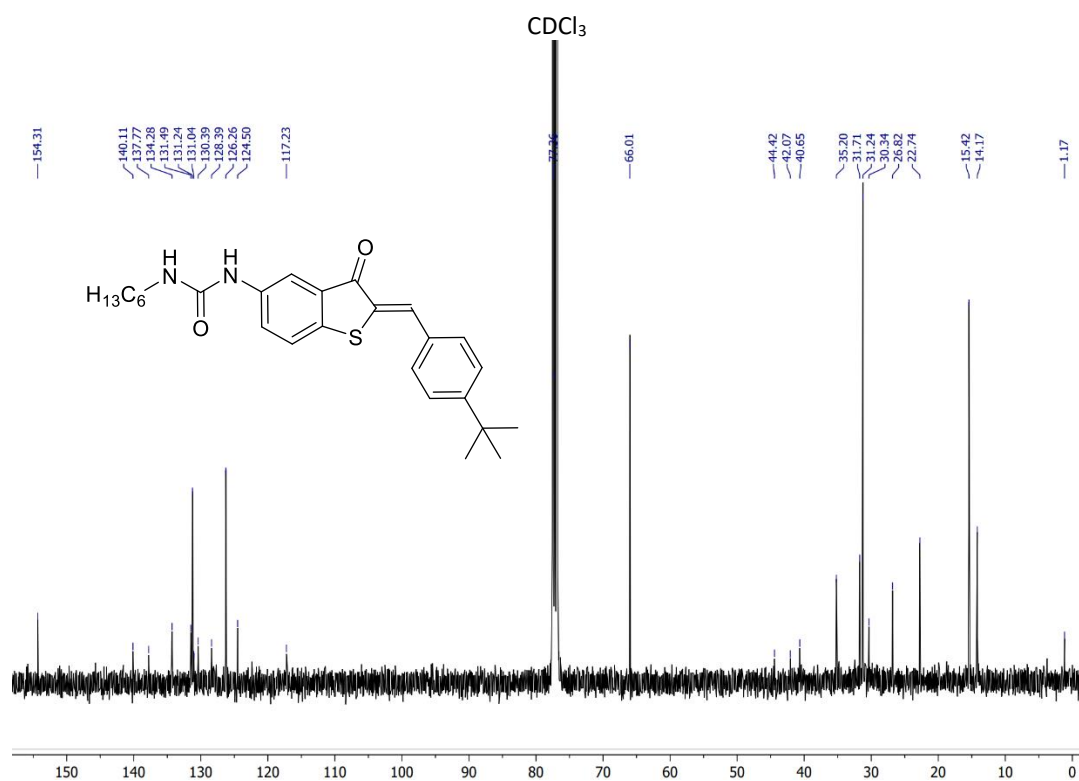


Figure A.2.13 ¹³C NMR spectrum of (*Z*)-1-(3,5-bis(trifluoromethyl)phenyl)-3-(3-oxo-2-(2-oxoacenaphthylen-1(2H)-ylidene)-2,3-dihydrobenzo[*b*]thiophen-5-yl)urea (**Z-1c**) in DMSO-*d*₆ at 298 K.



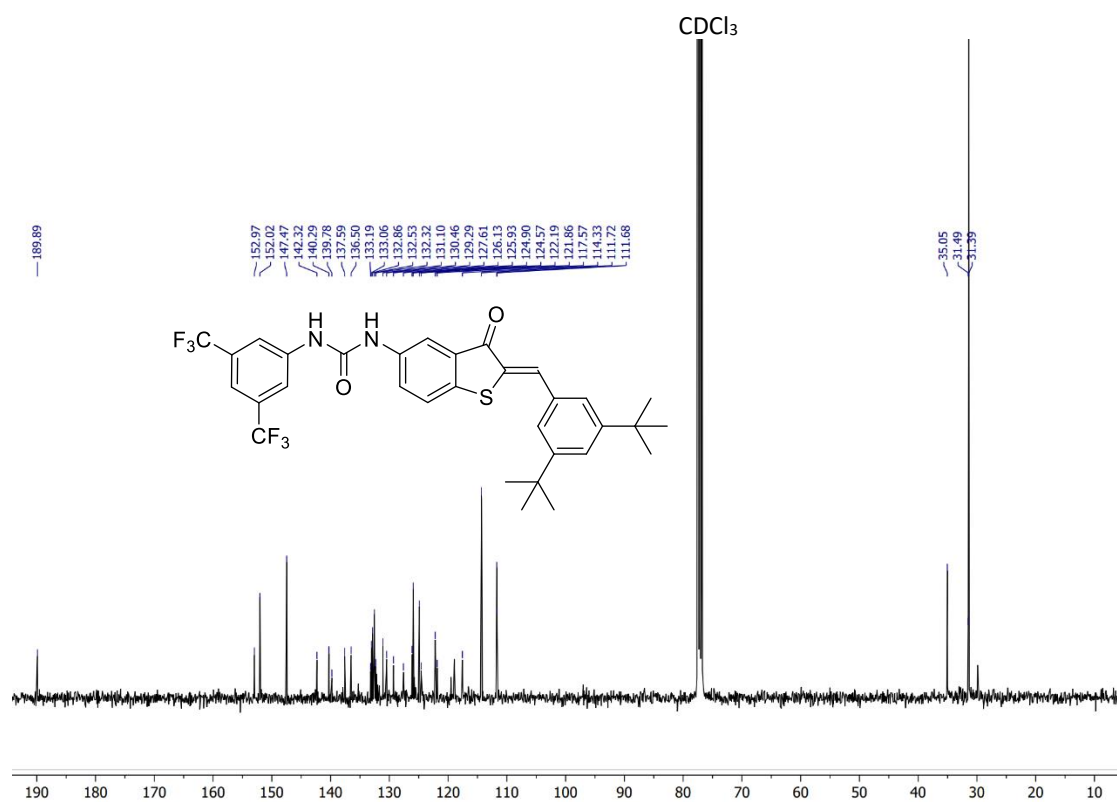


Figure A.2.16 ¹³C NMR spectrum of ((Z)-1-(3,5-bis(trifluoromethyl)phenyl)-3-(2-(3,5-di-tert-butylbenzylidene)-3-oxo-2,3-dihydrobenzo[b]thiophen-5-yl)urea (**Z-2c**) in CDCl₃ at 298 K.

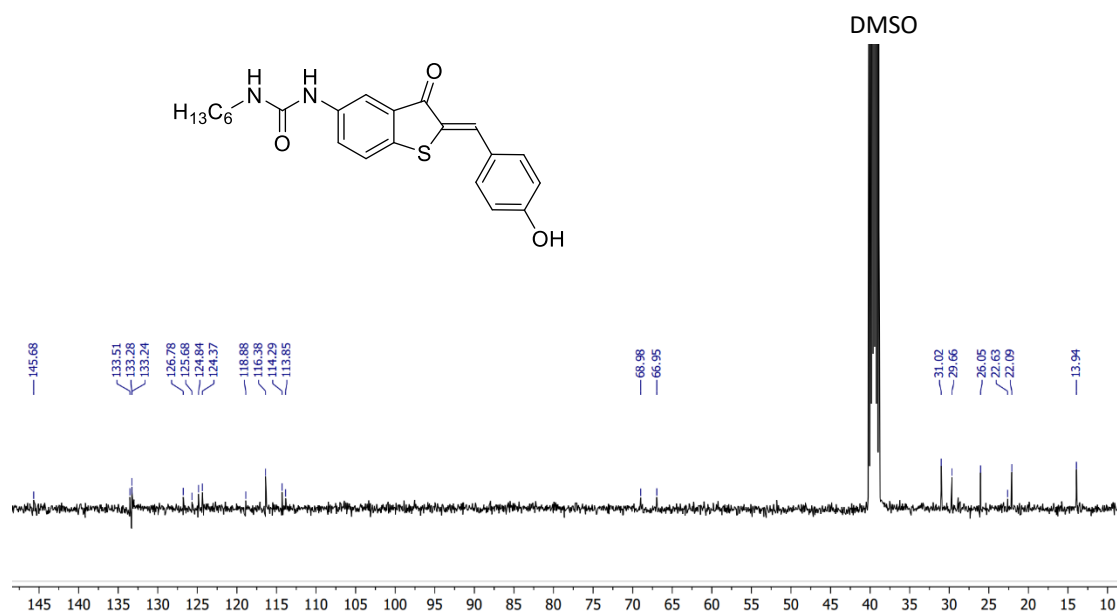


Figure A.2.17 ¹³C NMR spectrum of (Z)-1-hexyl-3-(2-(4-hydroxybenzylidene)-3-oxo-2,3-dihydrobenzo[b]thiophen-5-yl)urea (**Z-2d**) in DMSO-*d*₆ at 298 K.

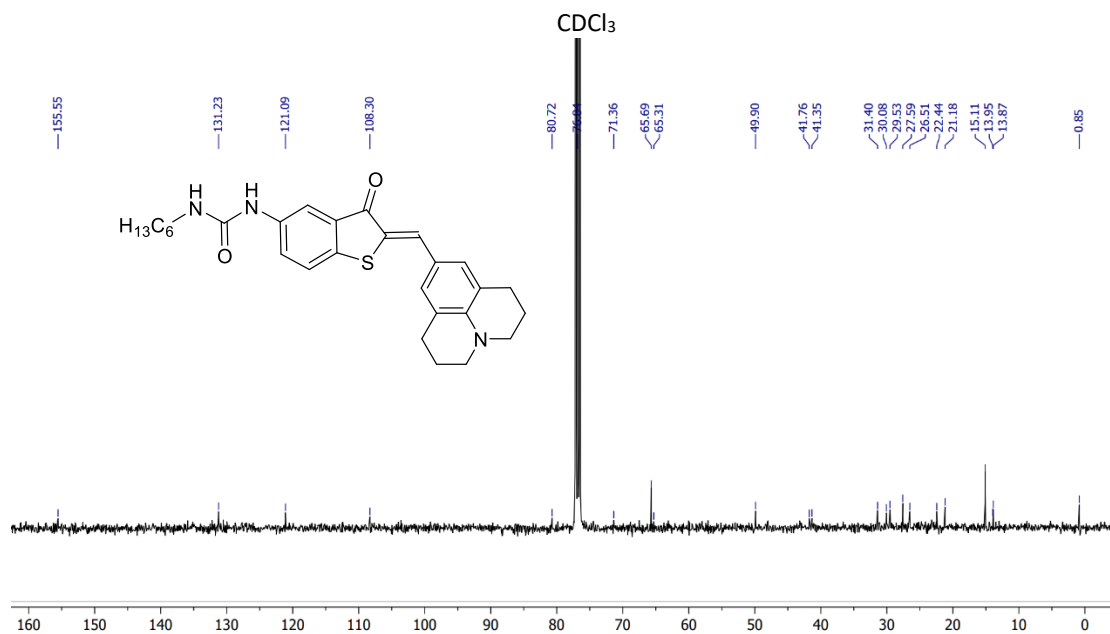


Figure A.2.18 ¹³C NMR spectrum of (Z)-1-hexyl-3-(3-oxo-2-((2,3,6,7-tetrahydro-1H, 5H-pyrido[3,2,1-ij]quinoline-9-yl)methylene)-2,3-dihydrobenzo[b]thiophen-5-yl)urea (**Z-3a**) at 298 K.

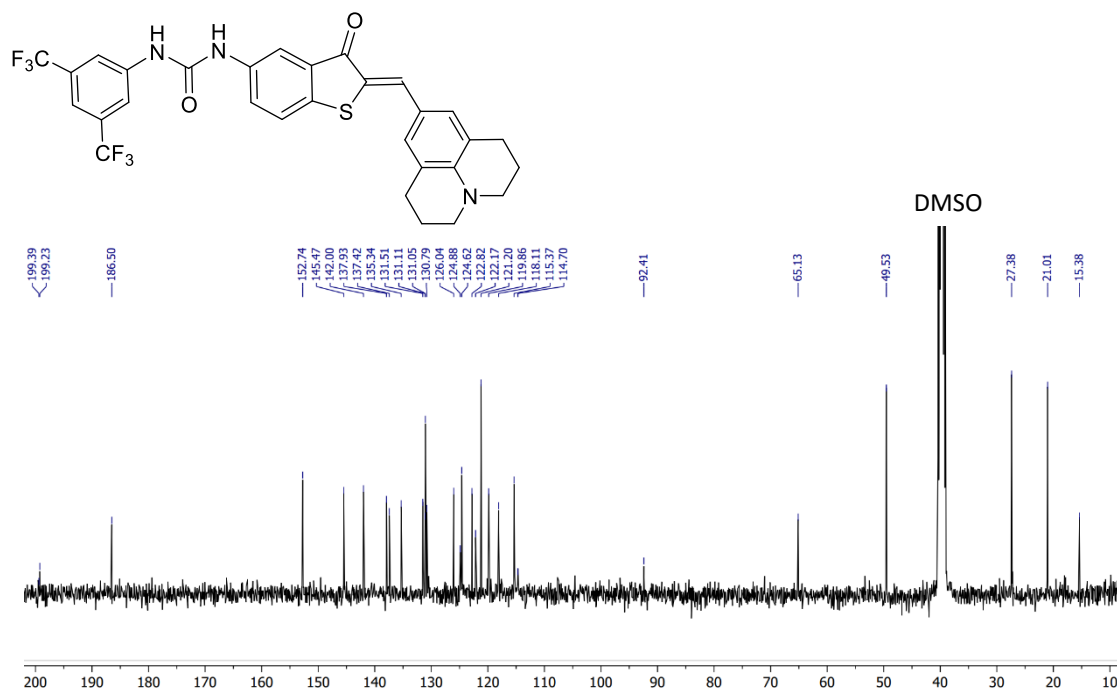


Figure A.2.19 ¹³C NMR spectrum of (Z)-1-(3,5-bis(trifluoromethyl)phenyl)-3-(3-oxo-2-((2,3,6,7-tetrahydro-1H,5H-pyrido[3,2,1-ij]quinolin-9-yl)methylene)-2,3-dihydrobenzo[b]thiophen-5-yl)urea (**Z-3b**) at 298 K.

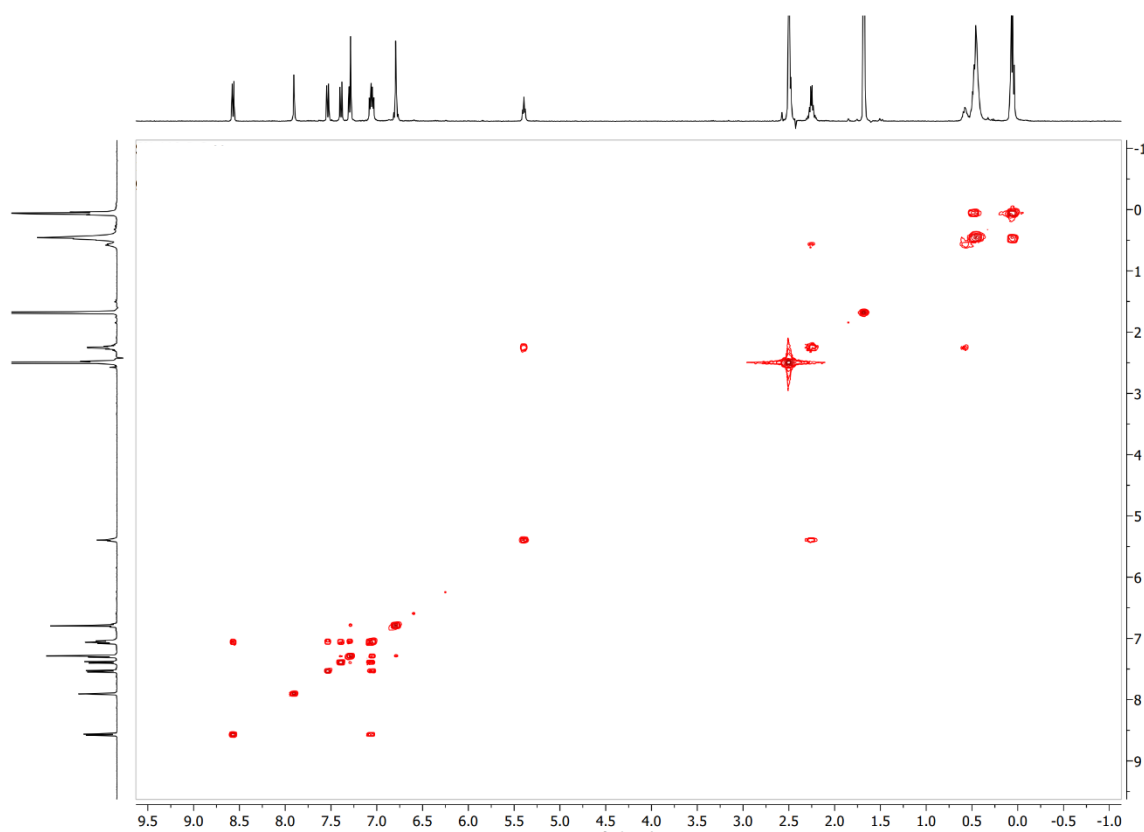
A.3 2D NMR Spectra ($^2\text{COSY}$, HSQC, HMBC)

Figure A.3.1 $^2\text{COSY}$ NMR spectrum of (*Z*)-1-(2-ethylhexyl)-3-(3-oxo-2-(2-oxoacenaophthylen-1(2H)-ylidene)-2,3-dihydrobenzo[*b*]thiophen-5-yl)urea (**Z-1b**) in $\text{DMSO-}d_6$ at 298 K.

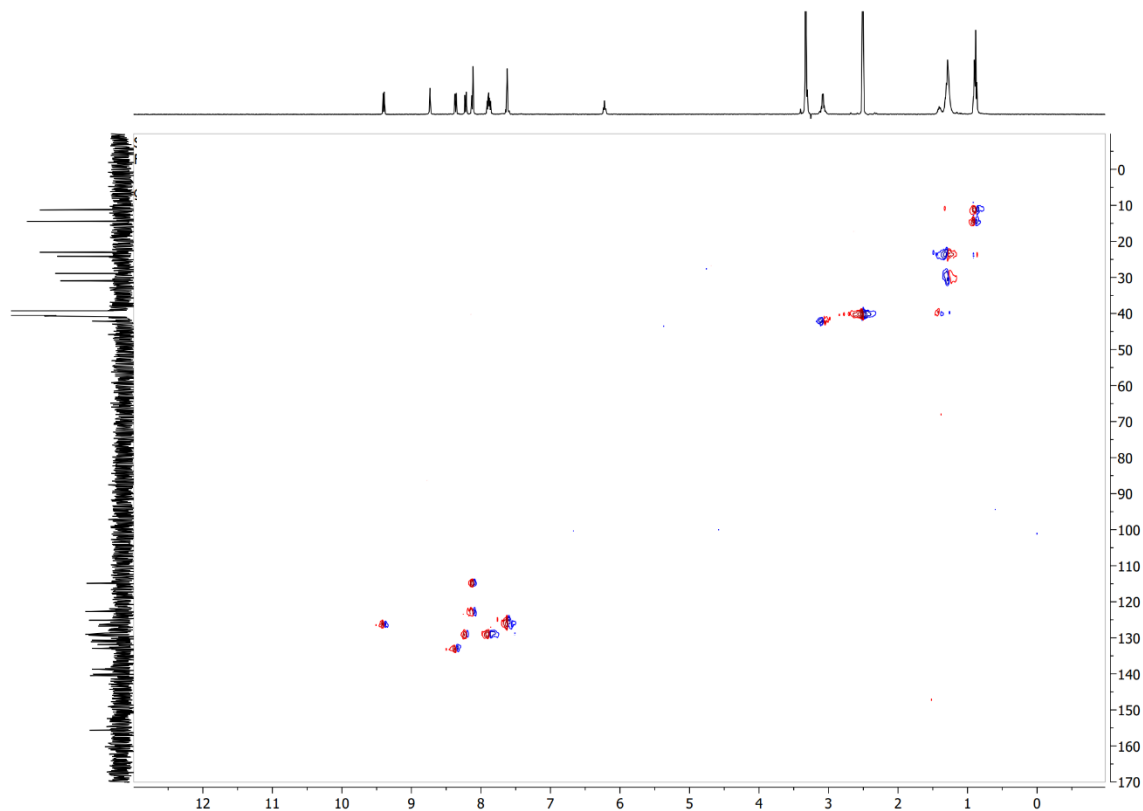


Figure A.3.2 HSQC NMR spectrum of (*Z*)-1-(2-ethylhexyl)-3-(3-oxo-2-(2-oxoacenaophthylen-1(2H)-ylidene)-2,3-dihydrobenzo[b]thiophen-5-yl)urea (**Z-1b**) in DMSO-*d*₆ at 298 K.

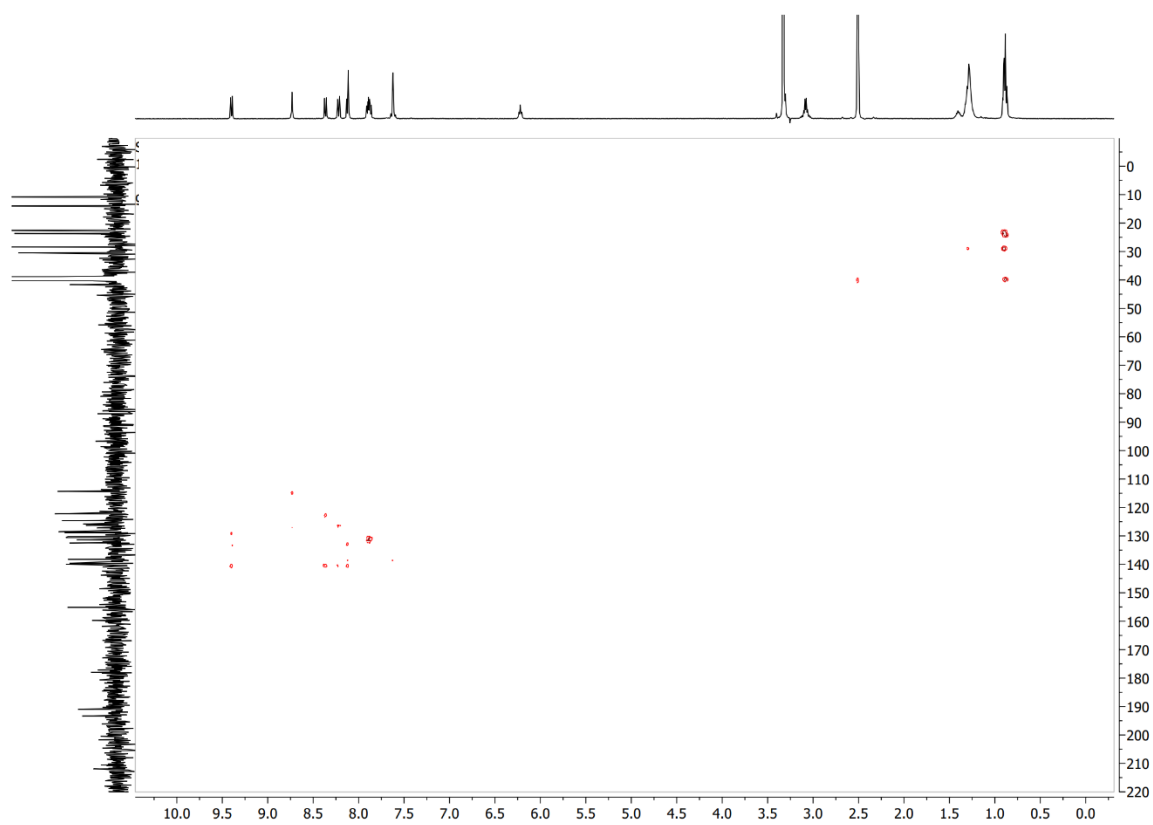


Figure A.3.3 HMBC NMR spectrum of (*Z*)-1-(2-ethylhexyl)-3-(3-oxo-2-(2-oxoacenaophthylen-1(2H)-ylidene)-2,3-dihydrobenzo[*b*]thiophen-5-yl)urea (**Z-1b**) in $\text{DMSO-}d_6$ at 298 K.

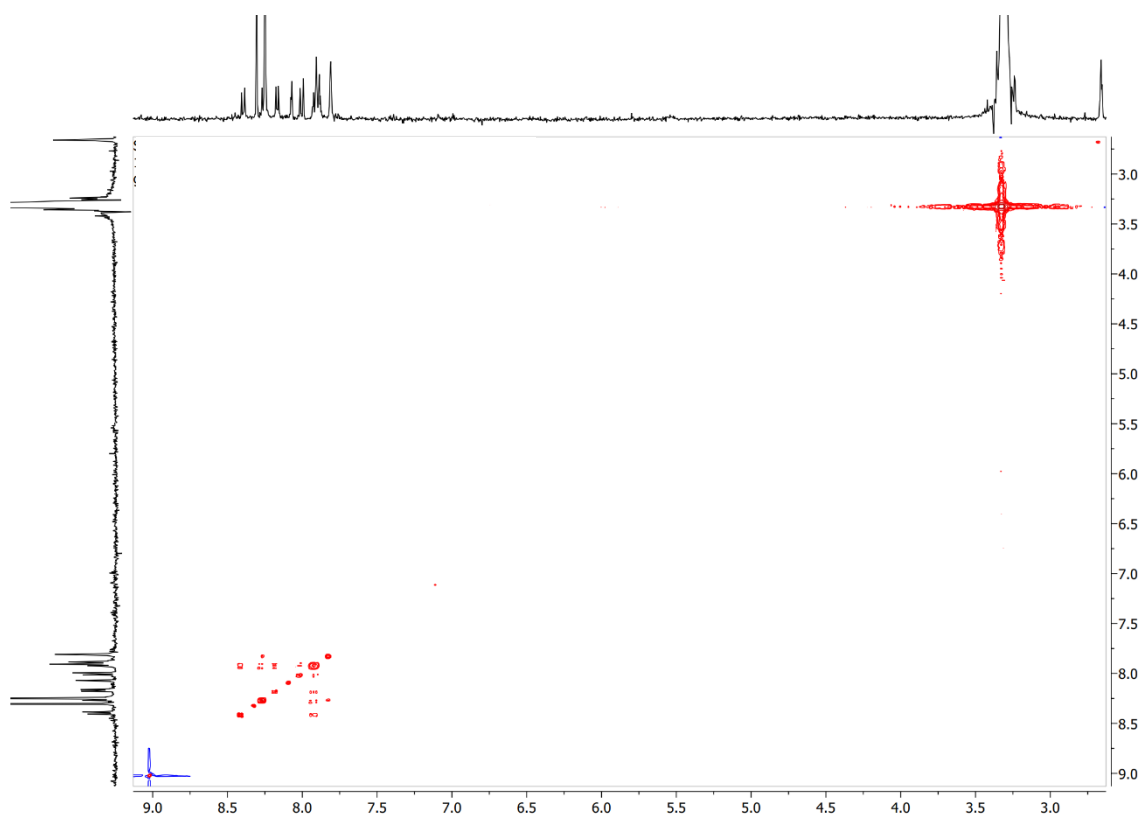


Figure A.3.4 ^{13}C COSY NMR spectrum of (Z)-1-(3,5-bis(trifluoromethyl)phenyl)-3-(3-oxo-2-(2-oxoacenaphthen-1(2H)-ylidene)-2,3-dihydrobenzo[b]thiophen-5-yl)urea (**Z-1c**) in $\text{DMSO-}d_6$ at 298 K.

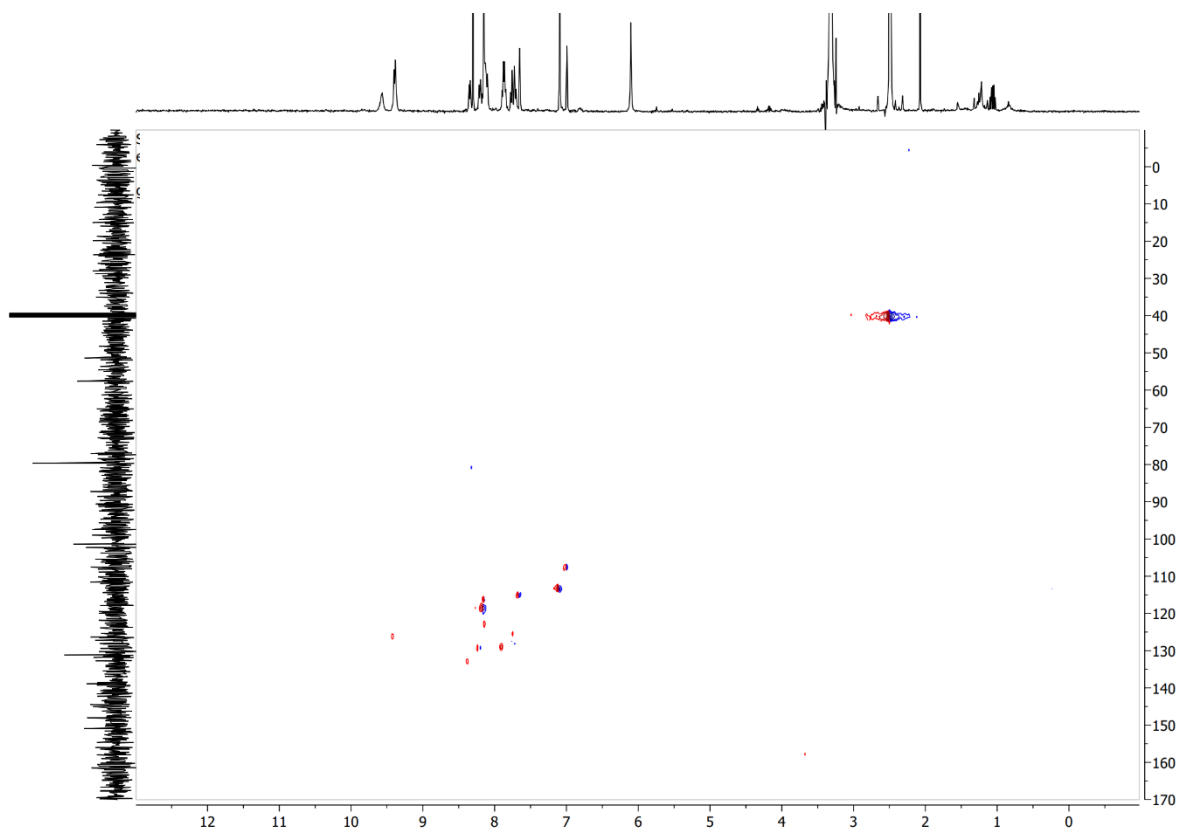


Figure A.3.5 HSQC NMR spectrum of (Z)-1-(3,5-bis(trifluoromethyl)phenyl)-3-(3-oxo-2-(2-oxoacena¹phthyl-1(2H)-ylidene)-2,3-dihydrobenzo[b]thiophen-5-yl)urea (**Z-1c**) in DMSO-*d*₆ at 298 K.

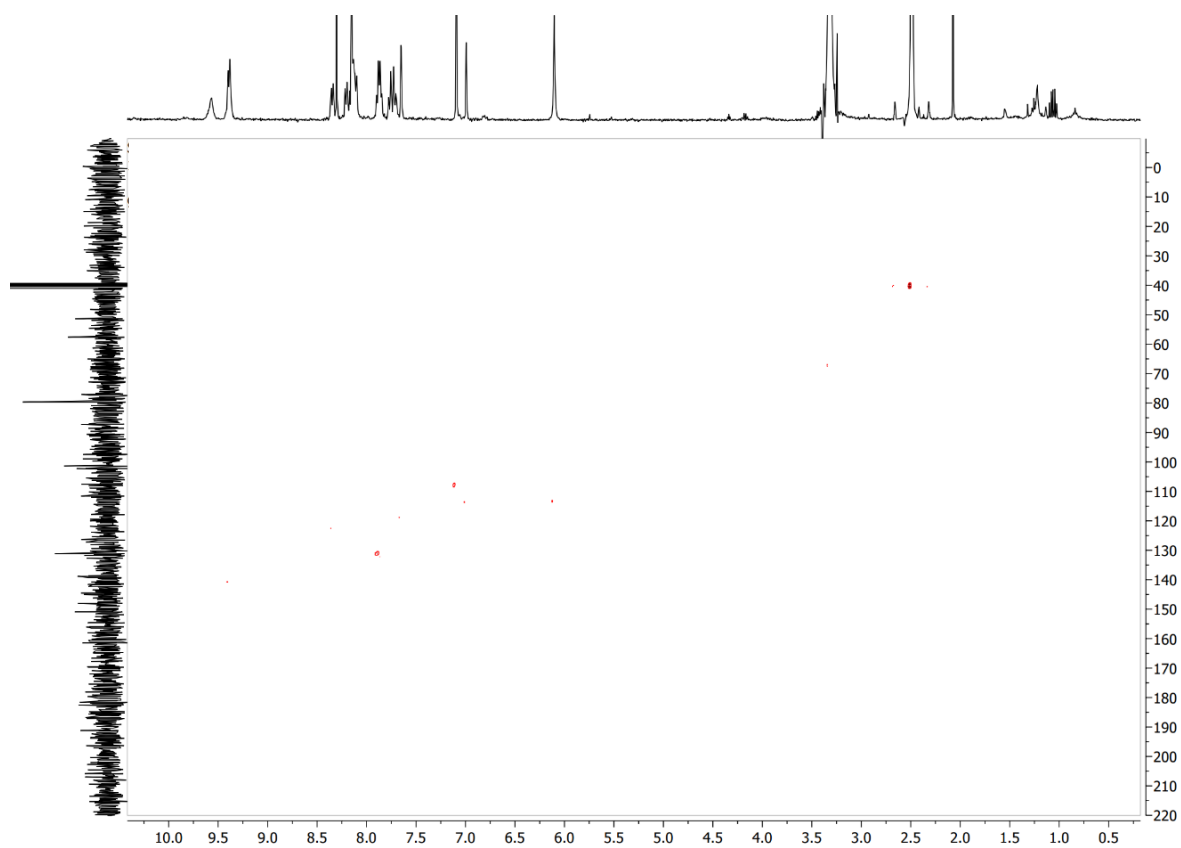


Figure A.3.6 HMBC NMR spectrum of (Z)-1-(3,5-bis(trifluoromethyl)phenyl)-3-(3-oxo-2-(2-oxoacenaophthylen-1(2H)-ylidene)-2,3-dihydrobenzo[b]thiophen-5-yl)urea (**Z-1c**) in DMSO-*d*₆ at 298 K.

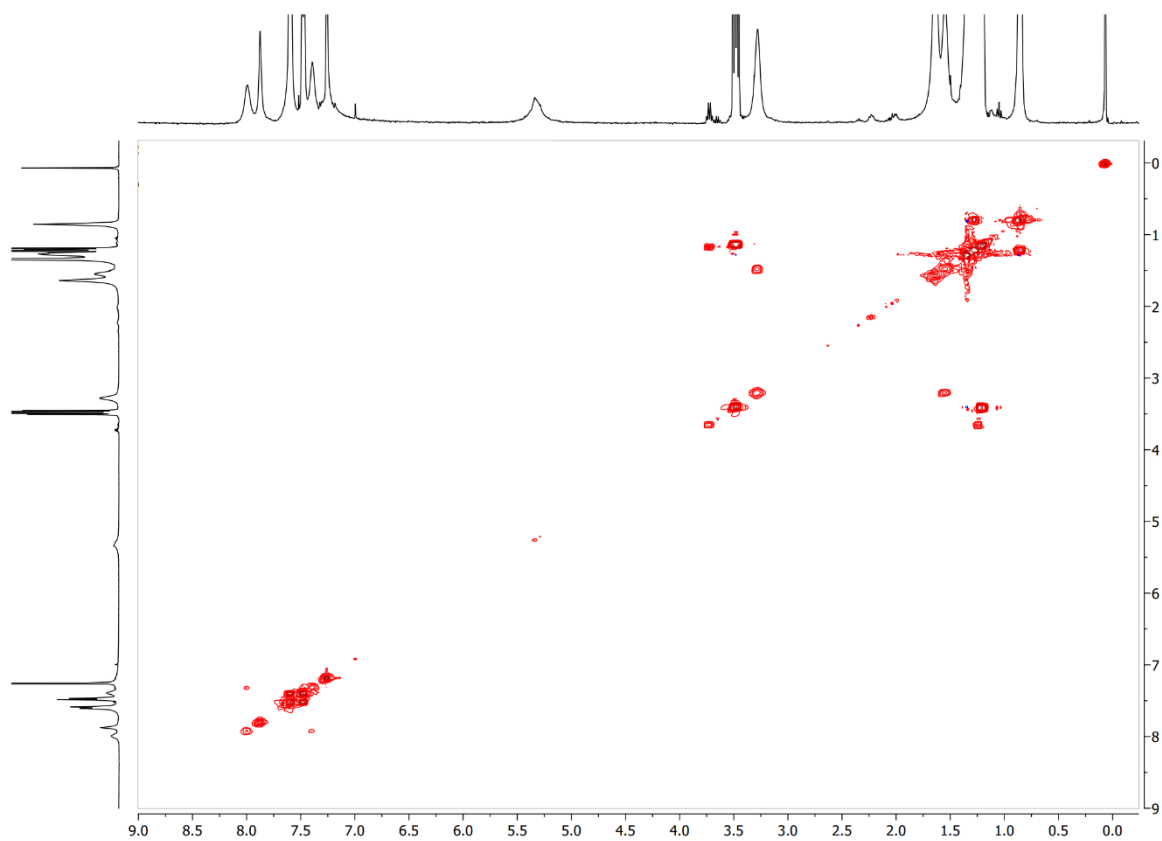


Figure A.3.7 ^{13}C COSY NMR spectrum of (*Z*)-1-(2-(4-(*tert*-butyl)benzylidene)-3-oxo-2,3-dihydrobenzo[*b*]thiophen-5-yl)-3-hexylurea (**Z-2a**) in CDCl_3 at 298 K.

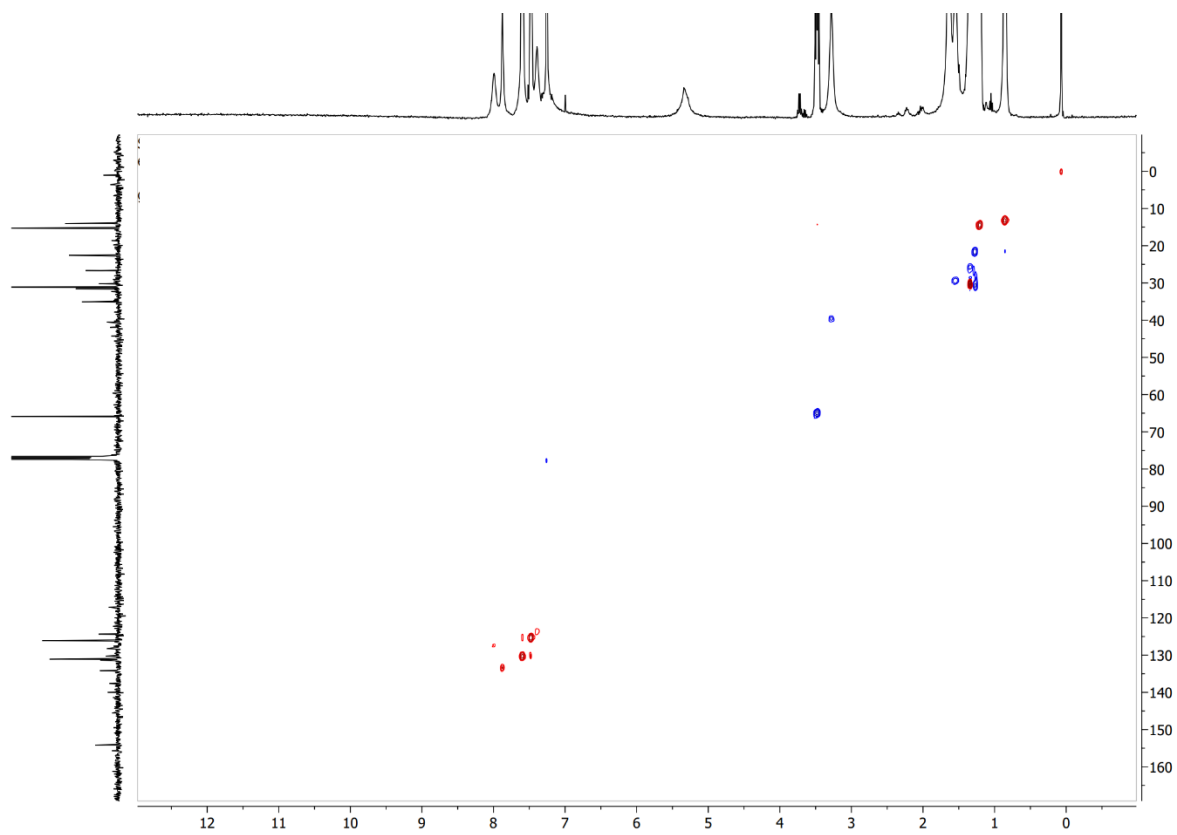


Figure A.3.8 HSQC NMR spectrum of (*Z*)-1-(2-(4-(*tert*-butyl)benzylidene)-3-oxo-2,3-dihydrobenzo[*b*]thiophen-5-yl)-3-hexylurea (**Z-2a**) in CDCl_3 at 298 K.

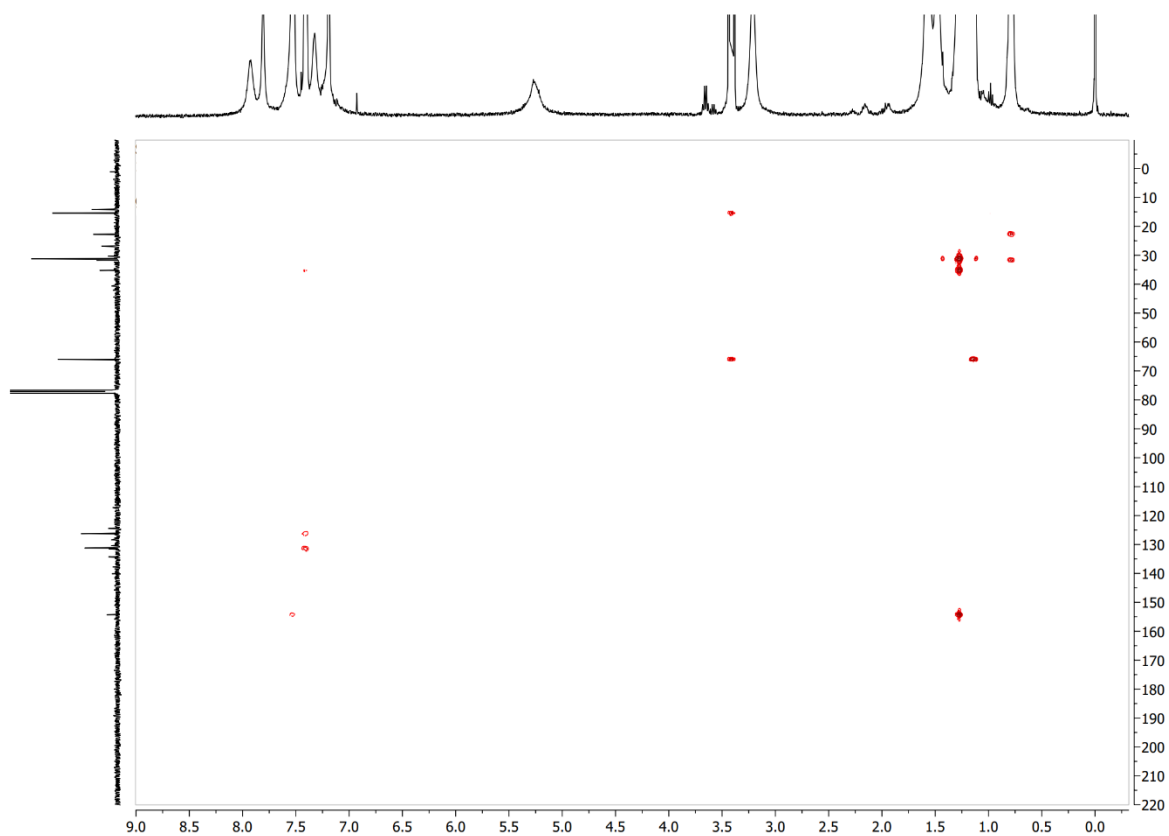


Figure A.3.9 HMBC NMR spectrum of (*Z*)-1-(2-(4-(*tert*-butyl)benzylidene)-3-oxo-2,3-dihydrobenzo[*b*]thiophen-5-yl)-3-hexylurea (**Z-2a**) in CDCl₃ at 298 K.

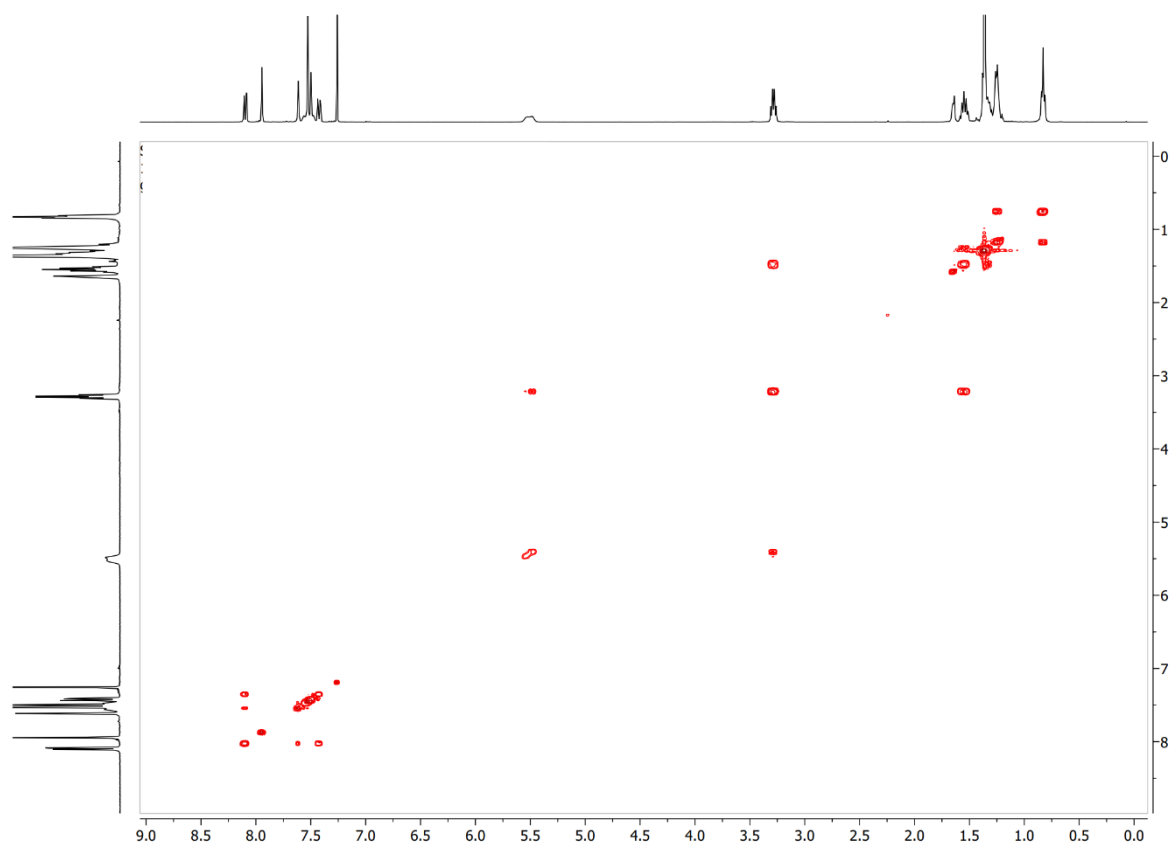


Figure A.3.10 ^{13}C COSY NMR spectrum of (*Z*)-1-(2-(3,5-di-*tert*-butylbenzylidene)-3-oxo-2,3-dihydrobenzo[*b*]thiophen-5-yl)-3-hexylurea (**Z-2b**) in CDCl_3 at 298 K.

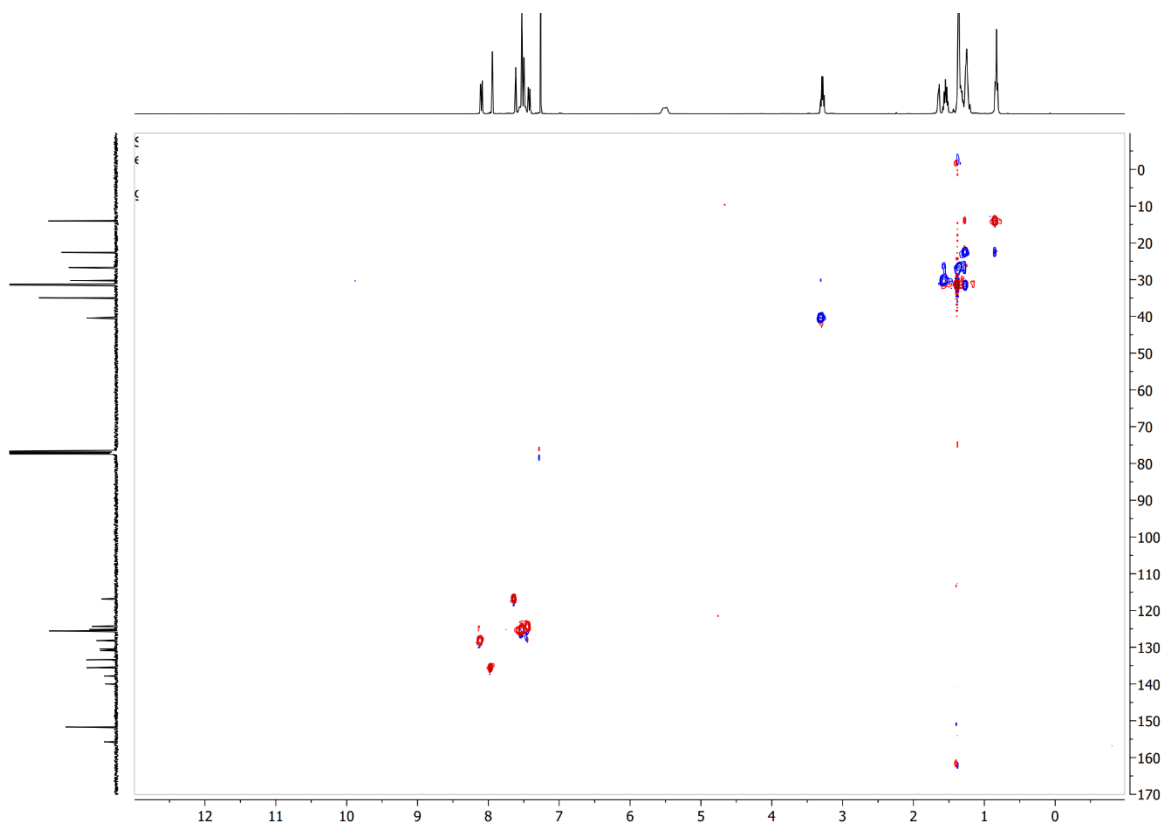


Figure A.3.11 HSQC NMR spectrum of (*Z*)-1-(2-(3,5-di-*tert*-butylbenzylidene)-3-oxo-2,3-dihydrobenzo[*b*]thiophen-5-yl)-3-hexylurea (**Z-2b**) in CDCl₃ at 298 K.

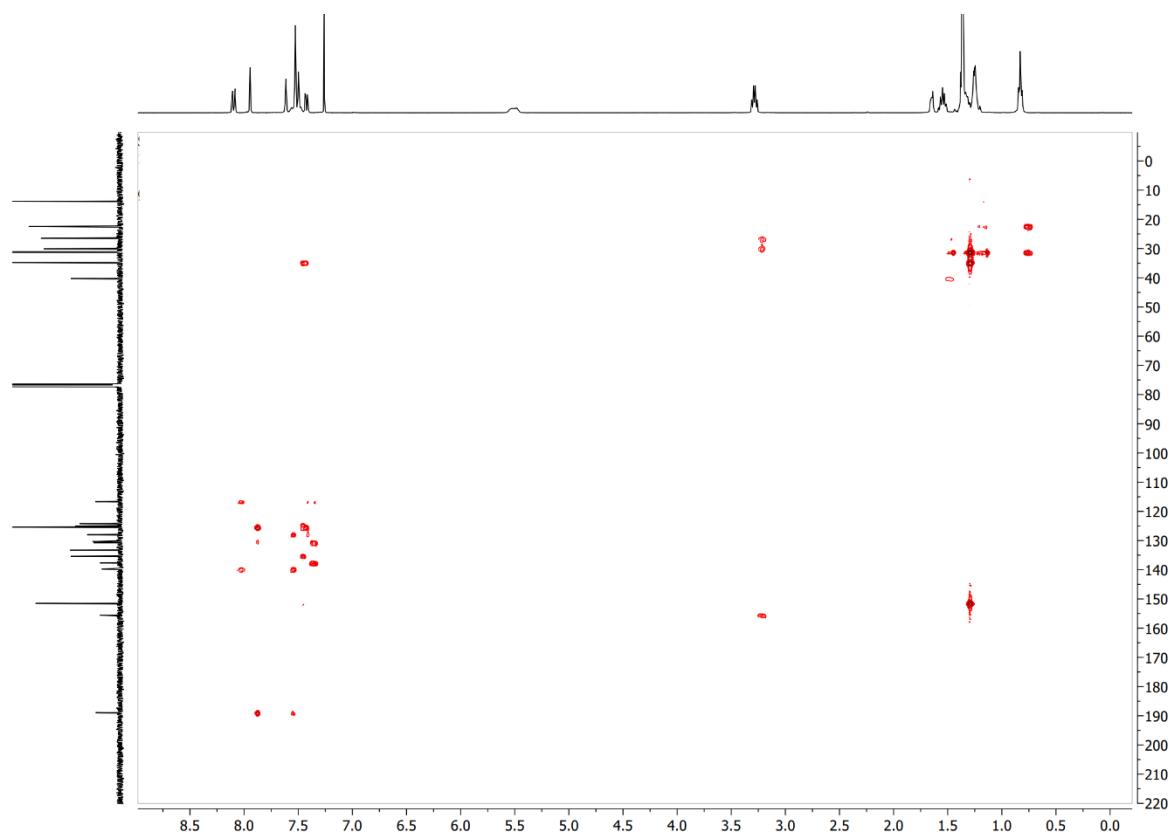


Figure A.3.12 HMBC NMR spectrum of (*Z*)-1-(2-(3,5-di-tert-butylbenzylidene)-3-oxo-2,3-dihydrobenzo[*b*]thiophen-5-yl)-3-hexylurea (**Z-2b**) in CDCl₃ at 298 K.

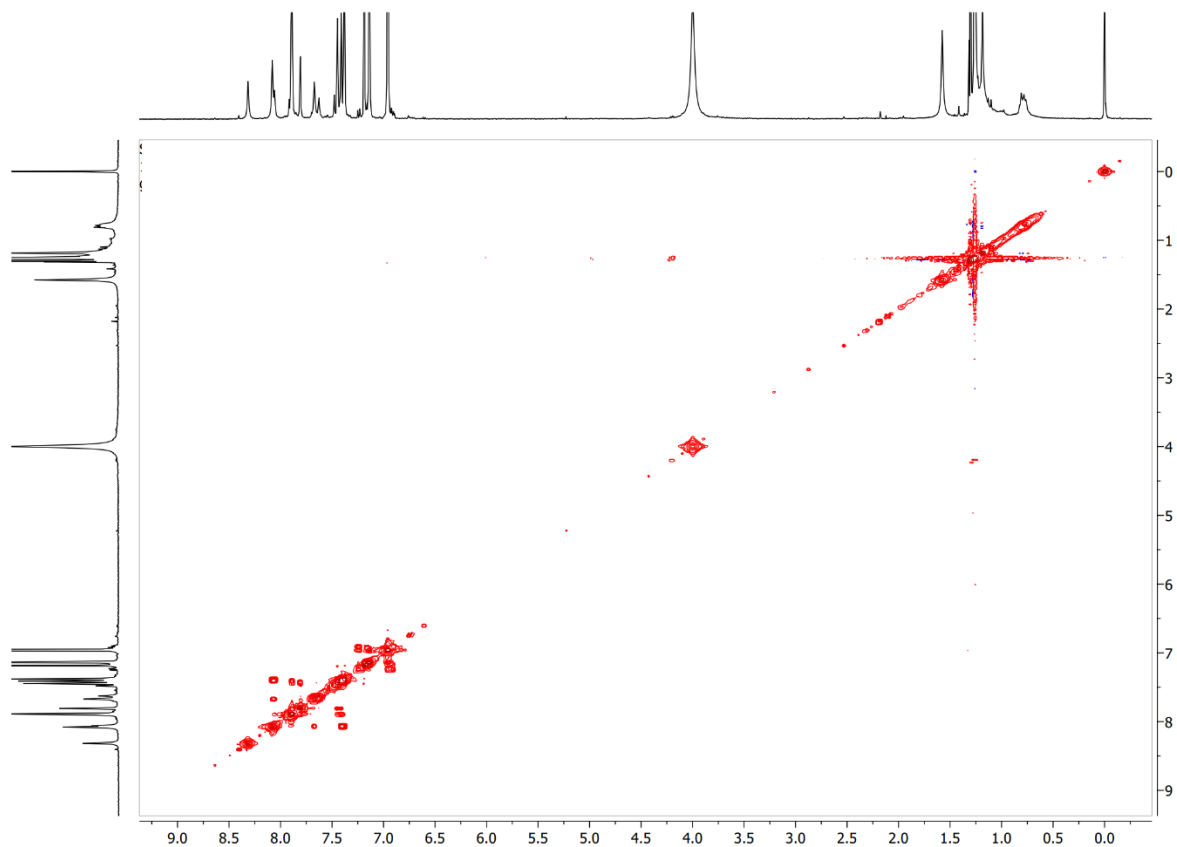


Figure A.3.13 ^{13}C COSY NMR spectrum of (*Z*)-1-(3,5-bis(trifluoromethyl)phenyl)-3-(2-(3,5-di-*tert*-butylbenzylidene)-3-oxo-2,3-dihydrobenzo[*b*]thiophen-5-yl)urea (**Z-2c**) in CDCl_3 at 298 K.

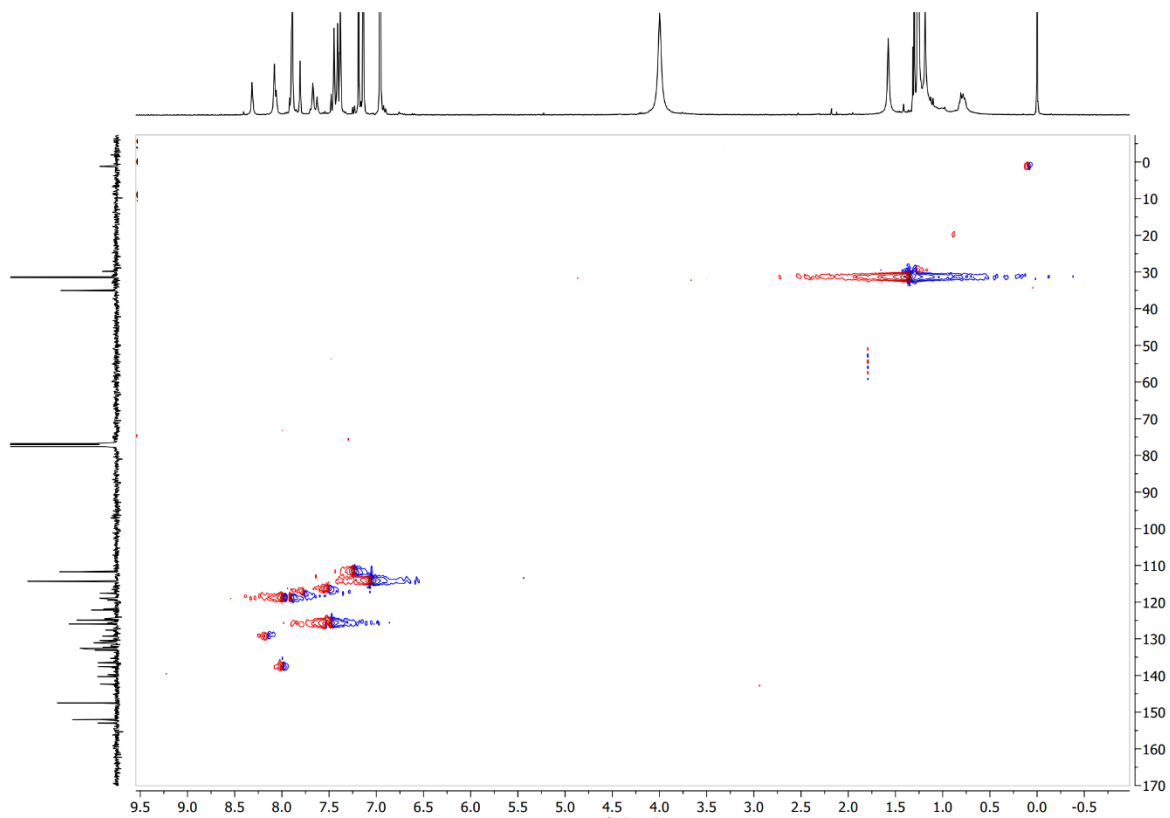


Figure A.3.14 HSQC NMR spectrum of (*Z*)-1-(3,5-bis(trifluoromethyl)phenyl)-3-(2-(3,5-di-*tert*-butylbenzylidene)-3-oxo-2,3-dihydrobenzo[*b*]thiophen-5-yl)urea (**Z-2c**) in CDCl₃ at 298 K.

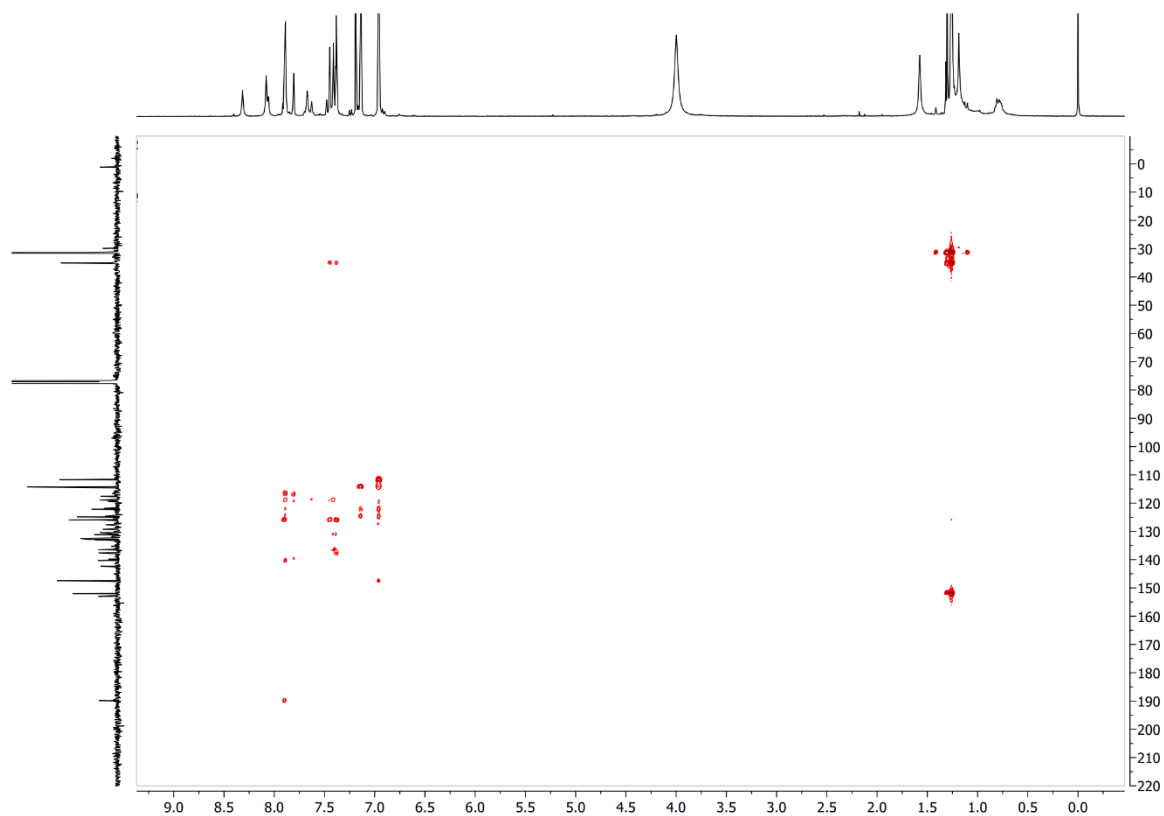


Figure A.3.15 HMBC NMR spectrum of (*Z*)-1-(3,5-bis(trifluoromethyl)phenyl)-3-(2-(3,5-di-tert-butylbenzylidene)-3-oxo-2,3-dihydrobenzo[*b*]thiophen-5-yl)urea (**Z-2c**) in CDCl₃ at 298 K.

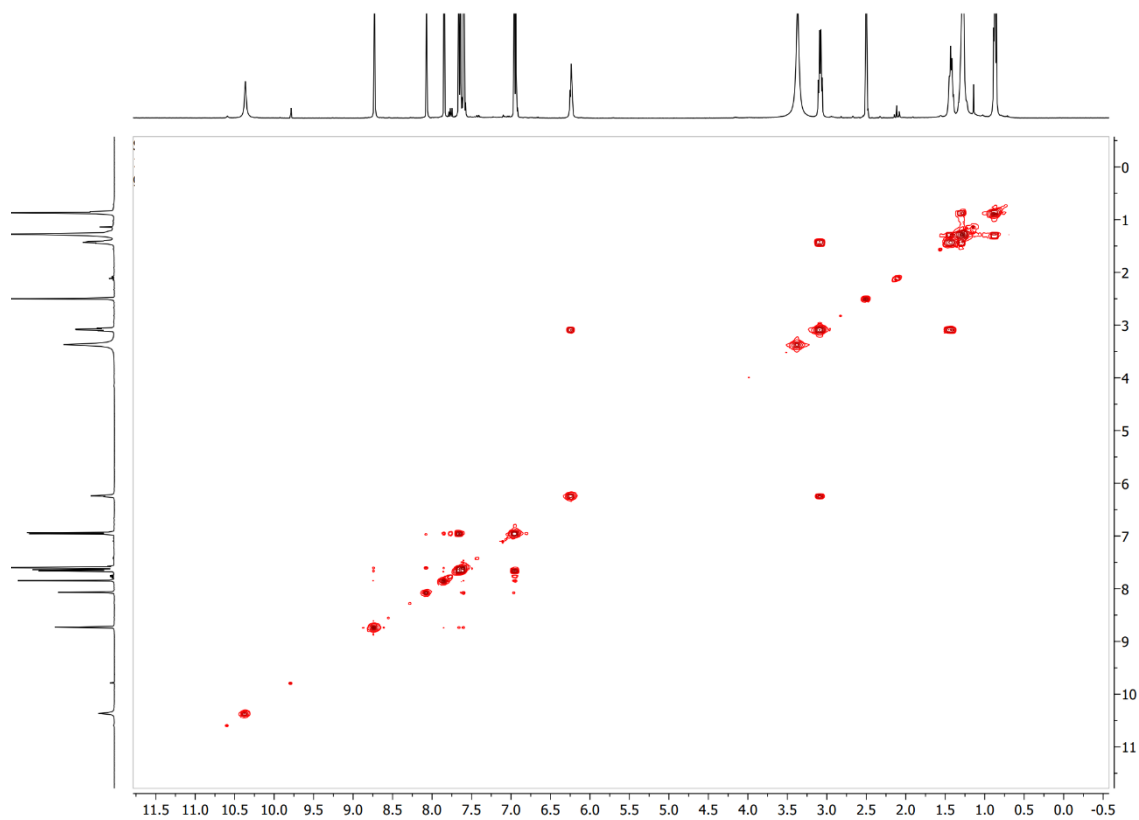


Figure A.3.16 ^{13}C COSY NMR spectrum of (*Z*)-1-hexyl-3-(2-(4-hydroxybenzylidene)-3-oxo-2,3-dihydrobenzo[*b*]thiophen-5-yl)urea (**Z-2d**) in $\text{DMSO-}d_6$ at 298 K.

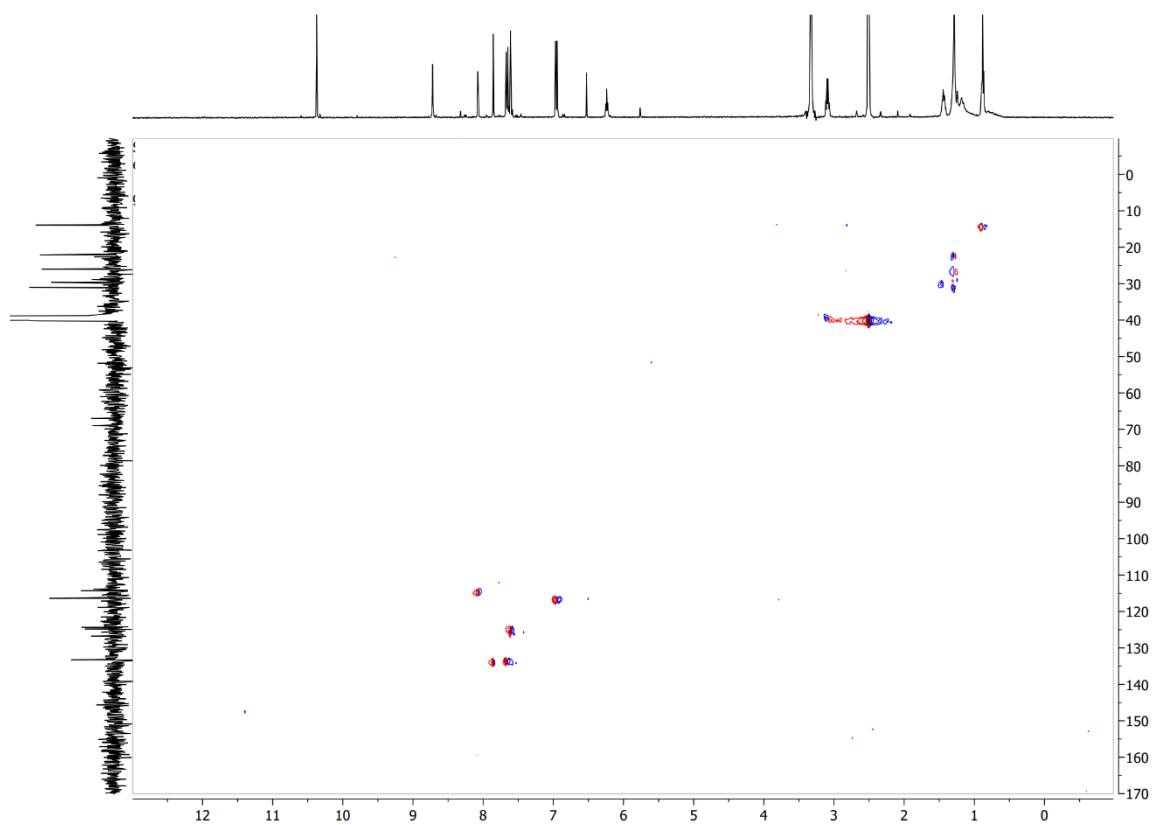


Figure A.3.17 HSQC NMR spectrum of (*Z*)-1-hexyl-3-(2-(4-hydroxybenzylidene)-3-oxo-2,3-dihydrobenzo[*b*]thiophen-5-yl)urea (**Z-2d**) in DMSO-*d*₆ at 298 K.

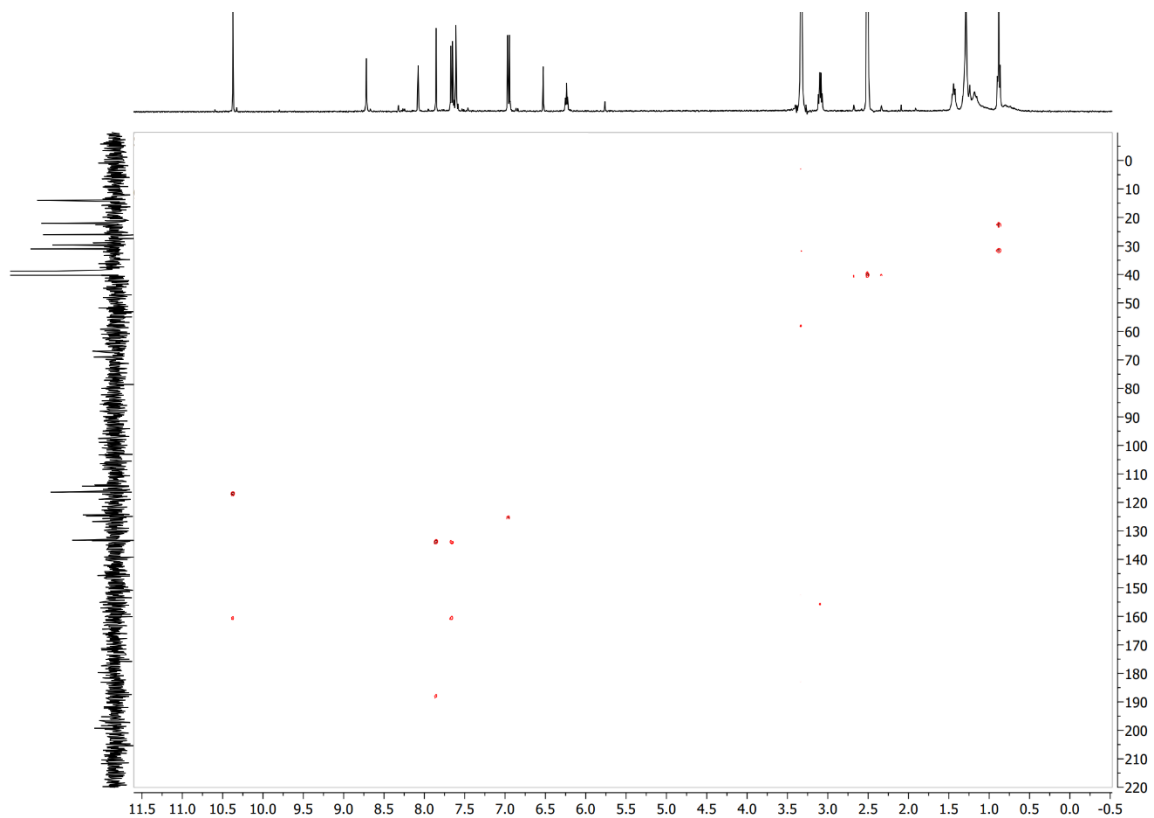


Figure A.3.18 HMBC NMR spectrum of (*Z*)-1-hexyl-3-(2-(4-hydroxybenzylidene)-3-oxo-2,3-dihydrobenzo[*b*]thiophen-5-yl)urea (**Z-2d**) in $\text{DMSO-}d_6$ at 298 K.

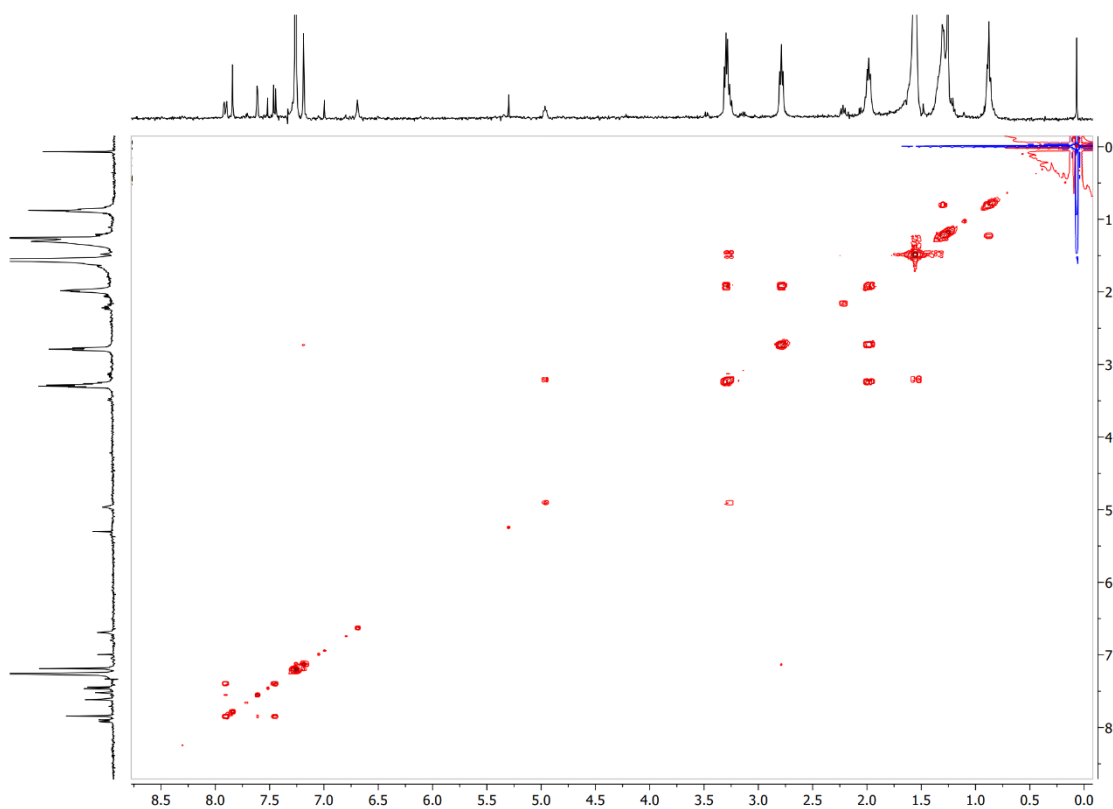


Figure A.3.19 ^{13}C COSY NMR spectrum of (*Z*)-1-hexyl-3-(3-oxo-2-((2,3,6,7-tetrahydro-1*H*, 5*H*-pyrido[3,2,1-*ij*]quinoline-9-yl)methylene)-2,3-dihydrobenzo[*b*]thiophen-5-yl)urea (**Z-3a**) in CDCl_3 at 298 K.

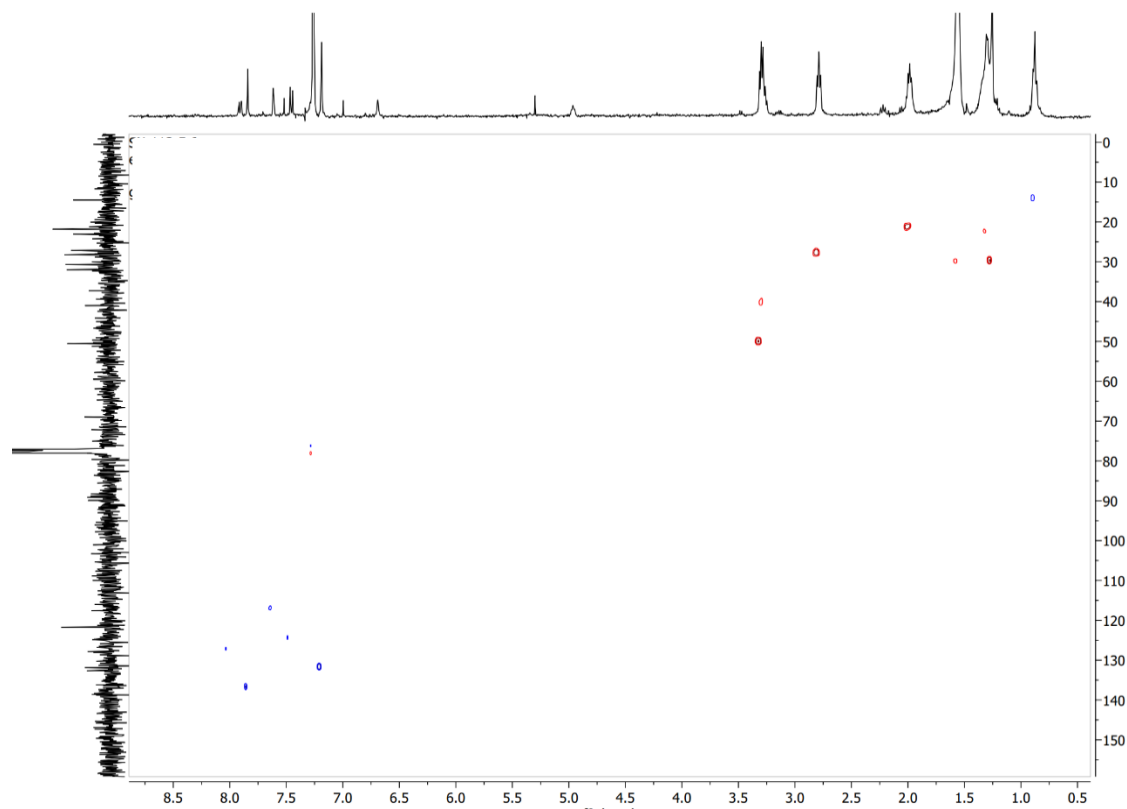


Figure A.3.20 HSQC NMR spectrum of (*Z*)-1-hexyl-3-(3-oxo-2-((2,3,6,7-tetrahydro-1*H*, 5*H*-pyrido[3,2,1-*ij*]quinoline-9-yl)methylene)-2,3-dihydrobenzo[*b*]thiophen-5-yl)urea (**Z-3a**) in CDCl_3 at 298 K.

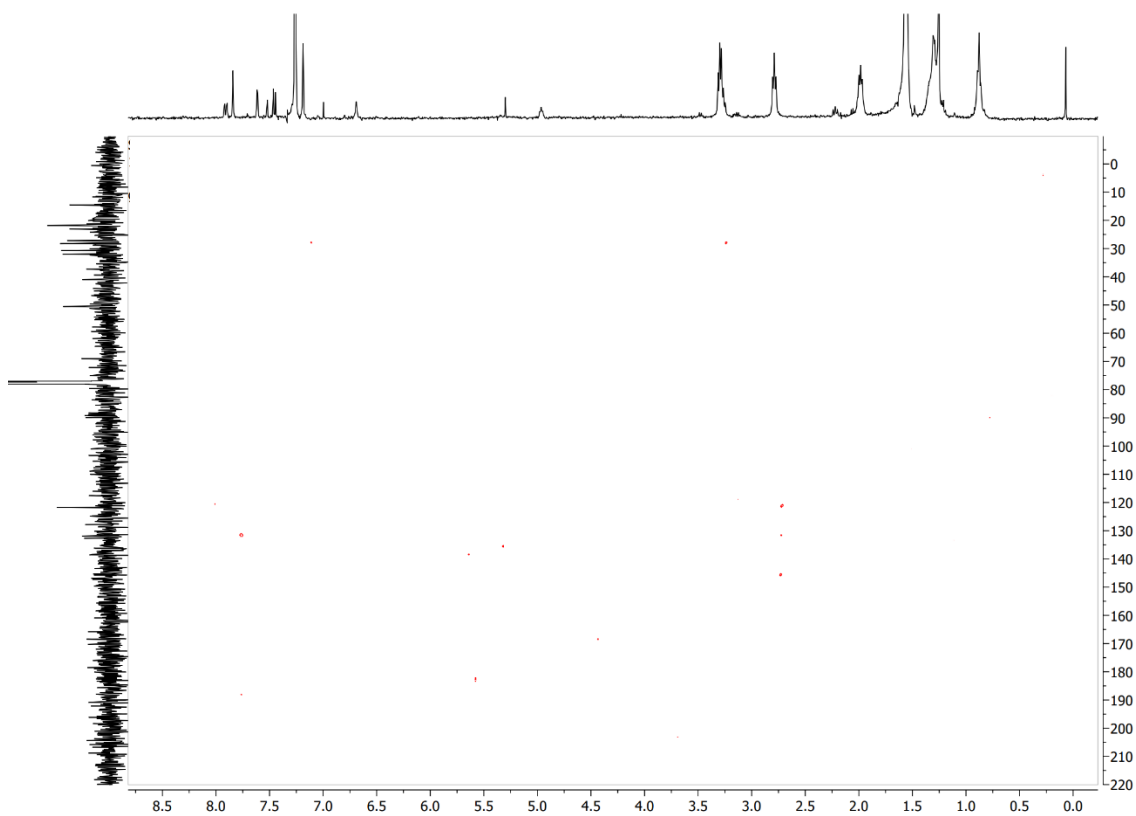


Figure A.3.21 HMBC NMR spectrum of (*Z*)-1-hexyl-3-(3-oxo-2-((2,3,6,7-tetrahydro-1*H*, 5*H*-pyrido[3,2,1-*ij*]quinoline-9-yl)methylene)-2,3-dihydrobenzo[*b*]thiophen-5-yl)urea (**Z-3a**) in CDCl₃ at 298 K.

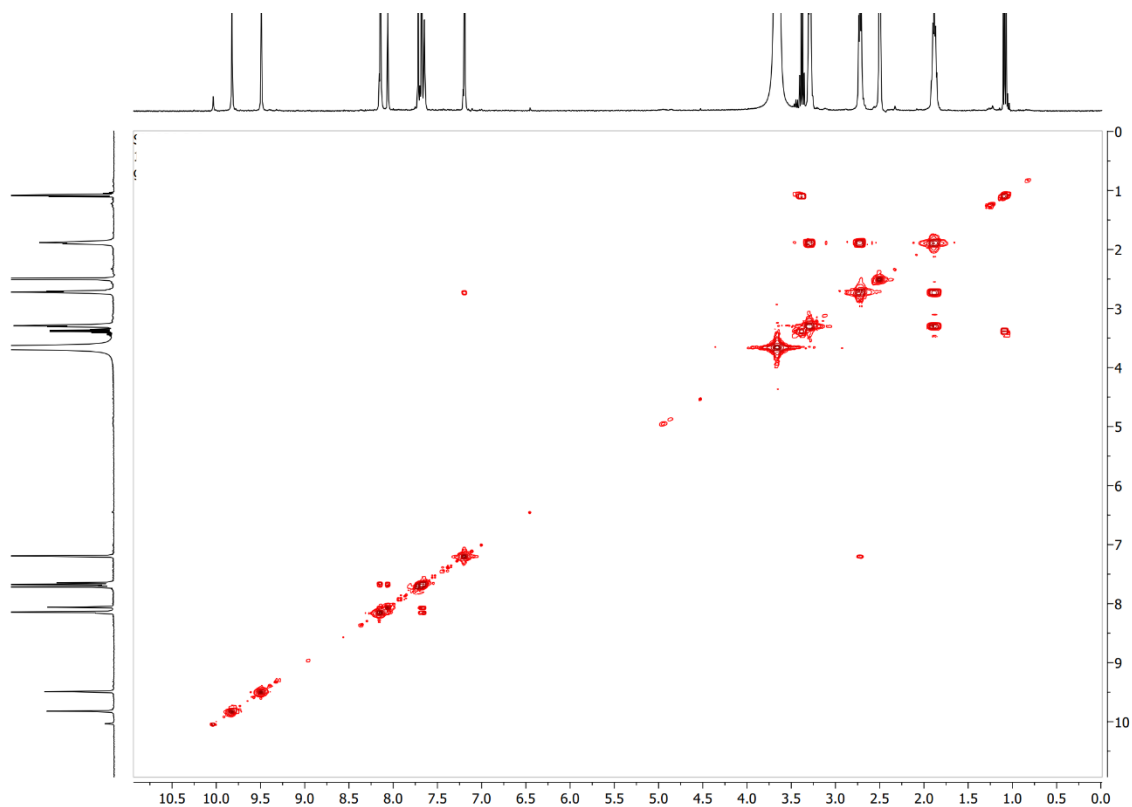


Figure A.3.22 ^2D COSY NMR spectrum of (*Z*)-1-(3,5-bis(trifluoromethyl)phenyl)-3-(3-oxo-2-((2,3,6,7-tetrahydro-1*H*, 5*H*-pyrido[3,2-*i*]quinolin-9-yl)methylene)-2,3-dihydrobenzo[*b*]thiophen-5-yl)urea (**Z-3b**) in $\text{DMSO-}d_6$ at 298 K.

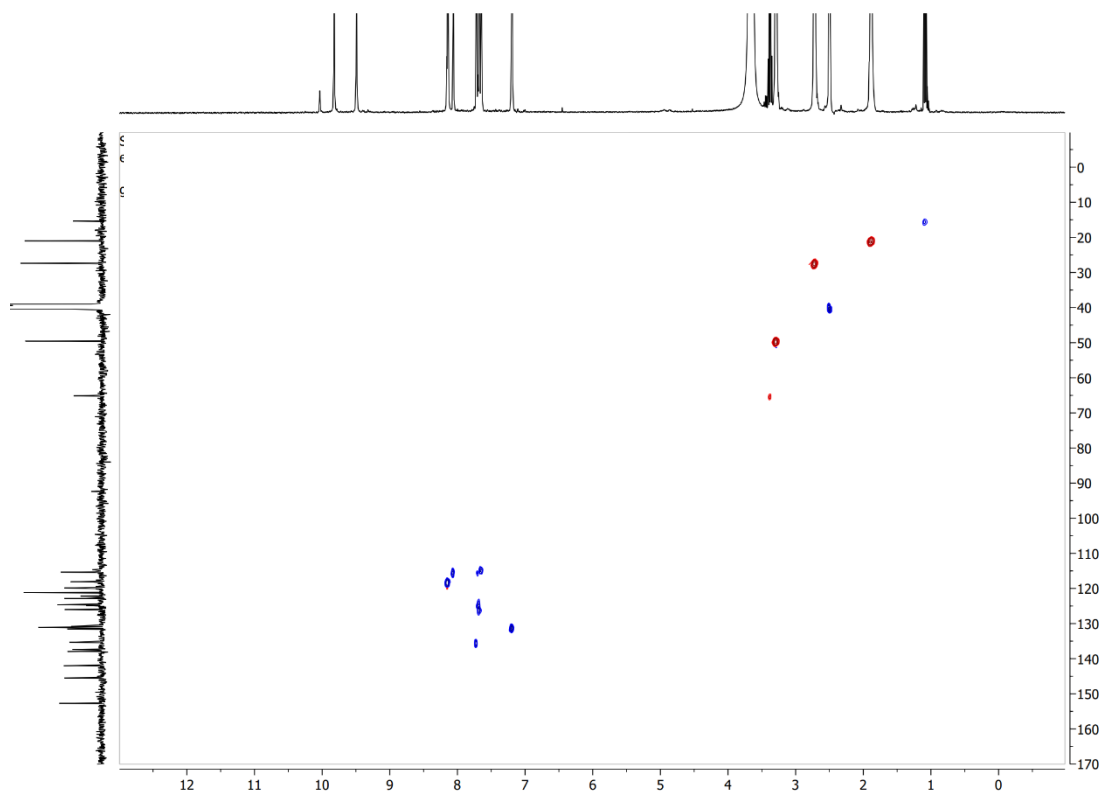


Figure A.3.23 HSQC NMR spectrum of (Z)-1-(3,5-bis(trifluoromethyl)phenyl)-3-(3-oxo-2-((2,3,6,7-tetrahydro-1H, 5H-pyrido[3,2,1-ij]quinolin-9-yl)methylene)-2,3-dihydrobenzo[b]thiophen-5-yl)urea (**Z-3b**) in DMSO-*d*₆ at 298 K.

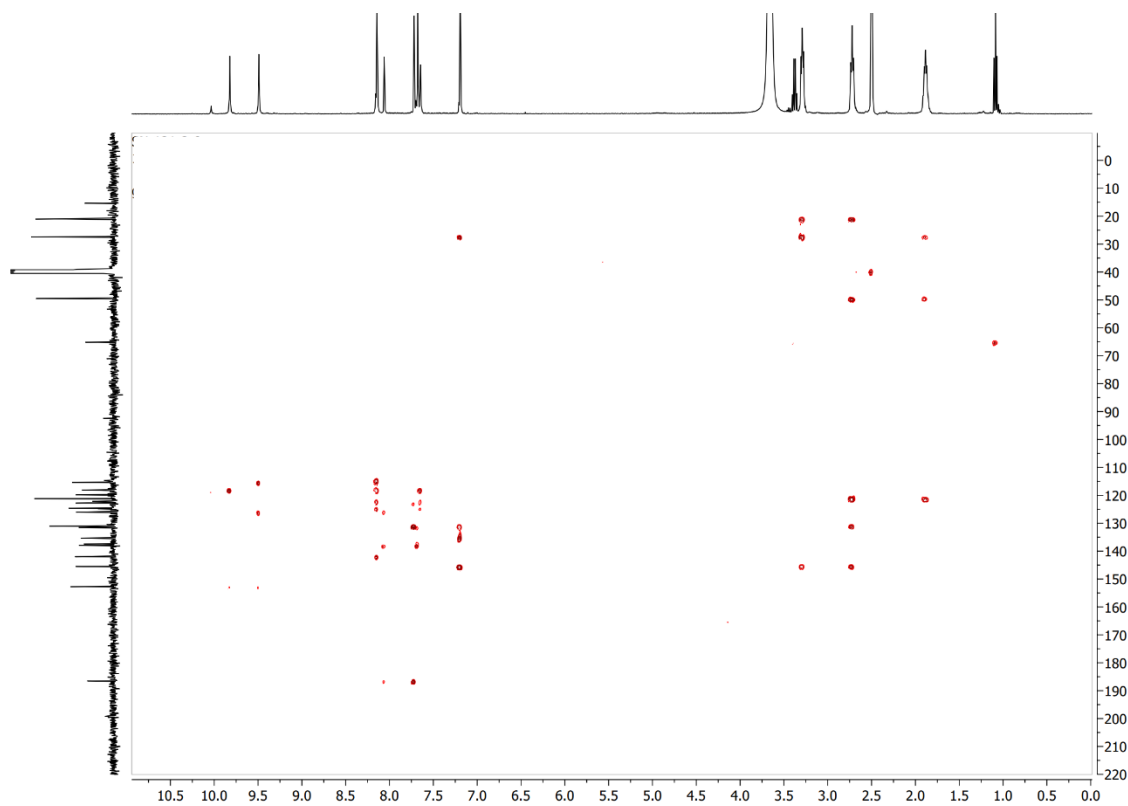


Figure A.3.24 HMBC NMR spectrum of (*Z*)-1-(3,5-bis(trifluoromethyl)phenyl)-3-(3-oxo-2-((2,3,6,7-tetrahydro-1*H*, 5*H*-pyrido[3,2-*i*]quinolin-9-yl)methylene)-2,3-dihydrobenzo[*b*]thiophen-5-yl)urea (**Z-3b**) in DMSO-*d*₆ at 298 K.

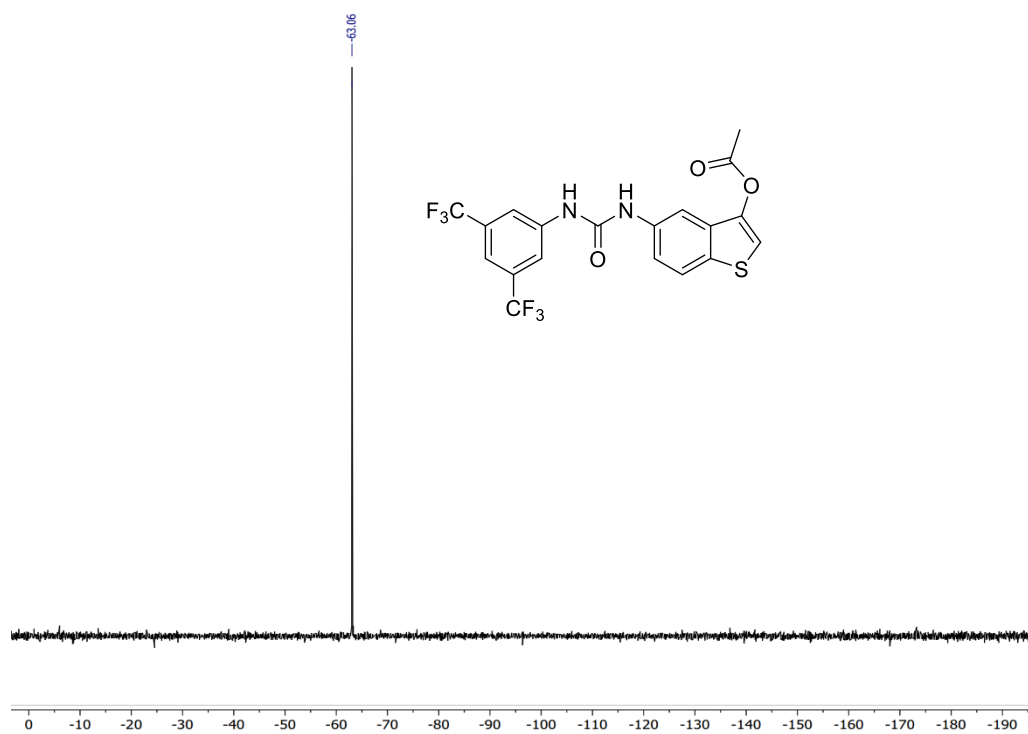
A.4 ^{19}F NMR Spectra

Figure A.4.1 ^{19}F NMR spectrum of 5-(3-(3,5-bis(trifluoromethyl)phenyl)ureido)benzo[b]thiophen-3-yl acetate (**8c**) in CDCl_3 at 298 K.

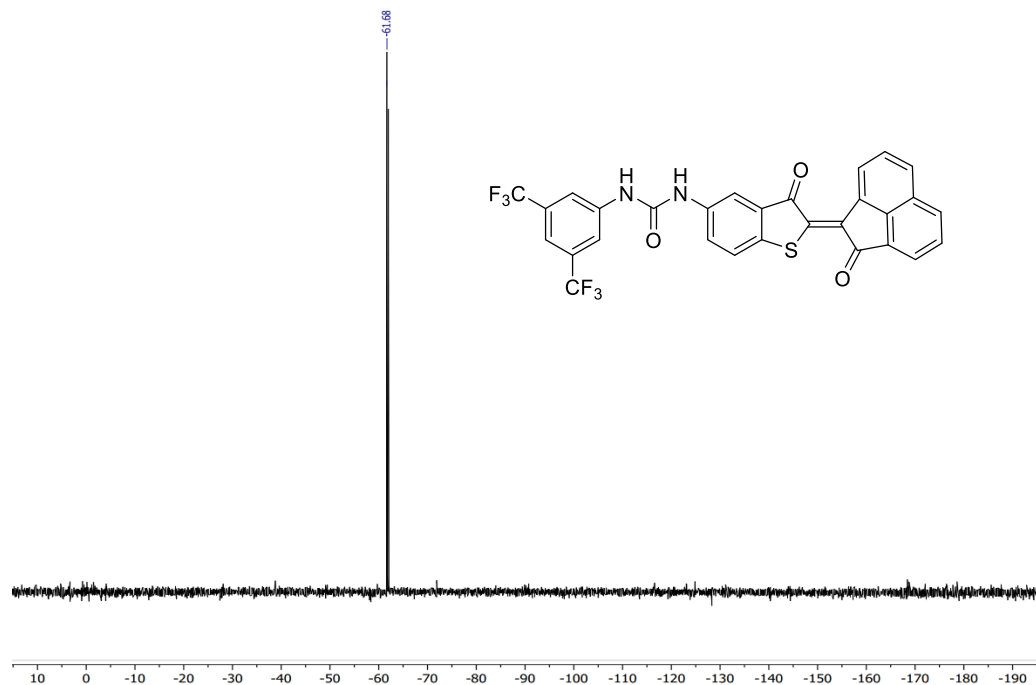


Figure A.4.2 ^{19}F NMR spectrum of (Z)-1-(3,5-bis(trifluoromethyl)phenyl)-3-(3-oxo-2-(2-oxoacenaophthylen-1(2H)-ylidene)-2,3-dihydrobenzo[b]thiophen-5-yl)urea (**Z-1c**) in CDCl_3 at 298 K.

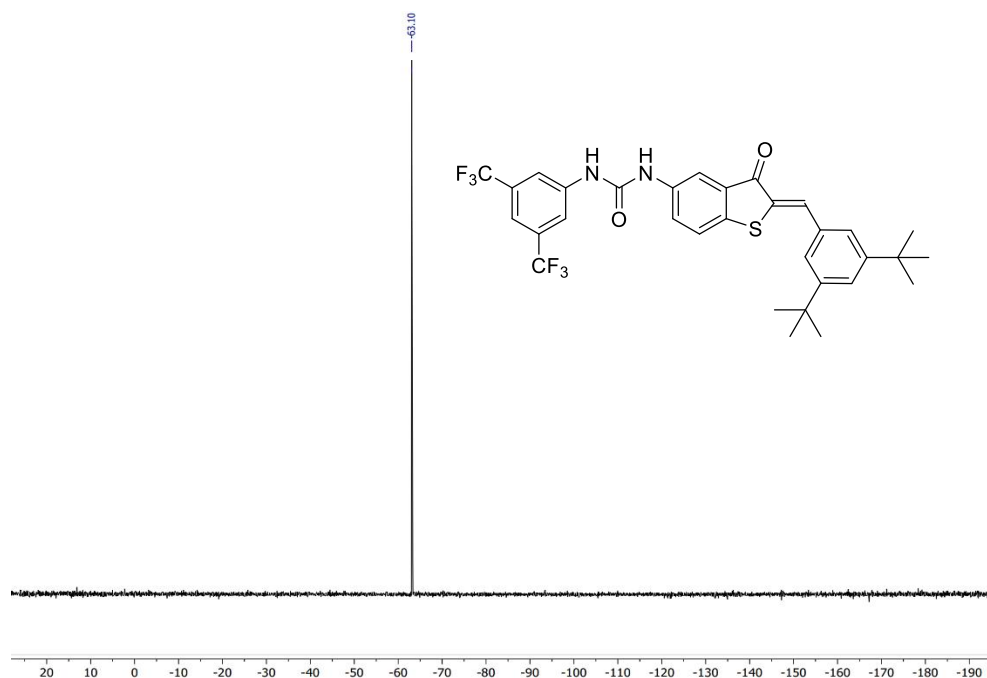


Figure A.4.3 ^{19}F NMR spectrum of (Z)-1-(3,5-bis(trifluoromethyl)phenyl)-3-(2-(3,5-di-tert-butylbenzylidene)-3-oxo-2,3-dihydrobenzo[b]thiophen-5-yl)urea (**Z-2c**) in CDCl_3 at 298 K.

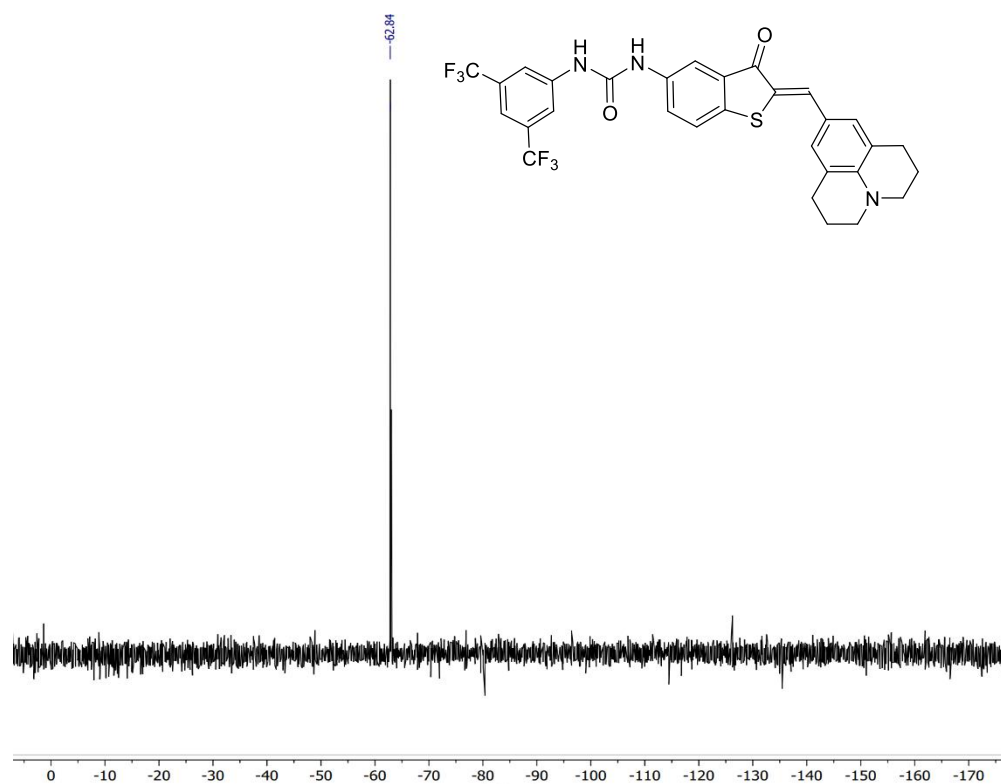


Figure A.4.4 ^{19}F NMR spectrum of (*Z*)-1-(3,5-bis(trifluoromethyl)phenyl)-3-(3-oxo-2-((2,3,6,7-tetrahydro-1H, 5H-pyrido[3,2,1-ij]quinolin-9-yl)methylene)-2,3-dihydrobenzo[b]thiophen-5-yl)urea (**Z-3b**) in CDCl_3 at 298 K.

A.5 Permission to Reproduce Material from the Literature

This Agreement between University of Western Ontario — S. N. ("You") and Elsevier ("Elsevier") consists of your license details and the terms and conditions provided by Elsevier and Copyright Clearance Center.

License Number	4842731145861
License date	Jun 05, 2020
Licensed content publisher	Elsevier
Licensed content publication	Journal of Photochemistry and Photobiology B: Biology
Licensed content title	The Jablonski diagram
Licensed content author	Danuta Frackowiak
Licensed content date	Nov 1, 1988
Licensed Content Volume	2
Licensed Content Issue	3
Licensed Content Pages	1
Start page	399
End page	0
Type of use	Dissertation/Thesis
Requestor type	University/Academic
Format	Electronic
Portion	Figure/tables/illustrations
Number of figures/tables/ illustrations	1
Original Elsevier figure/table number(s)	Figure 1(B)

Curriculum Vitae

Name: Suendues Noori

Education: University of Windsor
Windsor, Ontario, Canada
2014-2018 B.Sc. Honors in Chemistry

University of Western Ontario
London, Ontario, Canada
2018-2020 MSc.

Honors and Awards: Spirol Scholarship Recipient 2014
University of Windsor Entrance Scholarship 2015
University of Windsor Bursary 2017
UWill Discover Conference Award 1st Place 2018
Western Graduate Research Scholarship (WGRS) 2018-2020

Related Work Experience: Undergraduate Teaching Assistant 2018
Graduate Teaching Assistant 2018-2020

Publications:

1. Ocheje, U. M.; Selivanova, M.; Song, Z.; Nguyen, T. H., V.; Charron, P. B.; Ching-Heng, C.; Yu-Hsuan, C.; Billet, B.; **Noori, S.**; Chiu, Y.-C.; Gu, X.; Rondeau-Gagné, S., *Polym. Chem.*, **2018**, *9* (46), 5531-5542.

Conference Presentations:

Noori, S.; **Wisner, J. A.*** Toward A Photoswitchable Self-Complementary Hydrogen Bond Array. 102nd Canadian Chemistry Conference and Exhibition, Quebec, QC. – June 3-7, 2019 (Poster).

Noori, S.; Davoud, F.; Wisner, J. A.* Toward A Photoswitchable Self-Complementary Hydrogen Bond Array. Western Research Forum 2019, London, ON. – March 22, 2019 (Poster).

Noori, S.; Ocheje, U. M.; Rondeau-Gagné, S.* Direct Investigation of the Supramolecular Assembly of Stretchable and Self-healing Conjugated Polymers. UWill Discover 2018, Windsor, ON. – March 22, 2018 (Poster).